



QUEENSLAND UNIVERSITY OF TECHNOLOGY

SCHOOL OF PHYSICAL AND CHEMICAL SCIENCES

VIBRATIONAL SPECTROSCOPY OF KERATIN FIBRES
A FORENSIC APPROACH

Submitted by Helen PANAYIOTOU to the School of Physical and Chemical Sciences, Queensland University of Technology in partial fulfilment of the requirements of the degree of PhD.

March 2004

The work submitted in this thesis has not been previously submitted for a degree or diploma at any other higher education institution. To the best of my knowledge and belief, the thesis contains no material previously published or written by another person except where due reference is made.

Signature: _____

Date: _____

ACKNOWLEDGEMENTS

I would like to take this opportunity to thank all those people who have contributed to the making of this thesis:

My supervisor, Dr Serge Kokot, for his guidance and advice throughout the course of this project.

Dr James Robertson for his advice and help in understanding the complex issues of hair microscopy.

Dr Edeline Wentrup Byrne for her knowledge, motivation and support.

Dr Llew Rintoul for his advice on the many aspects of vibrational spectroscopy.

Dr Azriel Groski for willing to share his knowledge on hair fibres.

The Australian Federal Police for providing funding for this project.

The Queensland University of Technology for providing me with the opportunity to contribute to science.

Umesh for his continuous support and motivation. Last, but certainly not least, mum and dad for all their support and hard work in helping me achieve the most I can.

ABSTRACT

Human hair profiling is an integral part of a forensic investigation but it is one of the most technically difficult subjects in forensic science. This thesis describes the research and development of a novel approach for the rapid identification of unknown human and other related keratin fibres found at a crime scene. The work presented here is developed systematically and considers sample collection, sample preparation, analysis and interpretation of spectral data for the profiling of hair fibres encountered in criminal cases. Spectral comparison of fibres was facilitated with the use of chemometrics methods such as PCA, SIMCA and Fuzzy Clustering, and the less common approach of multi-criteria decision making methodology (MCDM).

The aim of the thesis was to investigate the potential of some vibrational spectroscopy techniques for matching and discrimination of single keratin hair fibres in the context of forensic evidence.

The first objective (chapter 3) of the thesis was to evaluate the use of Raman and FT-IR micro-spectroscopy techniques for the forensic sampling of hair fibres and to propose the preferred technique for future forensic hair comparisons. The selection of the preferred technique was based on criteria such as spectral quality, ease of use, rapid analysis and universal application to different hair samples. FT-IR micro-spectroscopy was found to be the most appropriate technique for hair analysis because it enabled the rapid collection of spectra from a wide variety of hair fibres. Raman micro-spectroscopy, on the other hand, was hindered with fluorescence problems and did not allow the collection of spectra from pigmented fibres. **This objective has therefore shown that FT-IR micro-spectroscopy is the preferable spectroscopic technique for forensic analysis of hair fibres, whilst Raman spectroscopy is the least preferred.**

The second objective (chapter 3) was to investigate, through a series of experiments, the effect of chemical treatment on the micro-environment of human hair fibres. The effect of bleaching agents on the hair fibres was studied with some detail at different treatment times and the results indicate a significant change in the chemical environment of the secondary structure of the hair fibre along with changes in the C-C backbone structure. One of the most important outcomes of this research was the behaviour of the α -helix during chemical treatment. The hydrogen bonding in the α -helix provides for the stable structure of the fibre and therefore any disruption to the α -helix will inevitably damage the molecular structure of the fibre. The results highlighted the behaviour of the α -helix, which undergoes a significant decrease in content during oxidation, and is partly converted to a random-coil structure, whilst the β -sheet component of the secondary structure remains unaffected. The reported investigations show that the combination of FT-IR and Raman micro-spectroscopy can provide an insight and understanding into the complex chemical properties and reactions within a treated hair fibre. Importantly, this work demonstrates that with the aid of chemometrics, it is possible to investigate

simultaneously FT-IR and Raman micro-spectroscopic information from oxidised hair fibres collected from one subject and treated at different times. The discrimination and matching of hair fibres on the basis of treatment has potential forensic applications.

The third objective (chapter 4) attempted to expand the forensic application of FT-IR micro-spectroscopy to other keratin fibres. Animal fibres are commonly encountered in crime scenes and it thus becomes important to establish the origin of those fibres. The aim of this work was to establish the forensic applications of FT-IR micro-spectroscopy to animal fibres and to investigate any fundamental molecular differences between these fibres. The results established a discrimination between fibres consisting predominantly of α -helix and those containing mainly a β -sheet structure. More importantly, it was demonstrated through curve-fitting and chemometrics, that each keratin fibre contains a characteristic secondary structure arrangement. **The work presented here is the first detailed FT-IR micro-spectroscopic study, utilising chemometrics as well as MCDM methods, for a wide range of keratin fibres, which are commonly, found as forensic evidence. Furthermore, it was demonstrated with the aid of the rank ordering MCDM methods PROMETHEE and GAIA, that it is possible to rank and discriminate keratin fibres according to their molecular characteristics obtained from direct measurements together with information sourced from the literature.**

The final objective (chapter 5) of the thesis was to propose an alternative method for the discrimination and matching of single scalp human hair fibres through the use of FT-IR micro-spectroscopy and chemometrics. The work successfully demonstrated, through a number of case scenarios, the application of the technique for the identification of variables such as gender and race for an unknown single hair fibre. In addition, it was also illustrated that known hair fibres (from the suspect or victim) can be readily matched to the unknown hair fibres found at the crime scene. **This is the first time that a substantial, systematic FT-IR study of forensic hair identification has been presented. The research has shown that it is possible to model and correlate individual's characteristics with hair properties at molecular level with the use of chemometrics methods. A number of different, important forensic variables of immediate use to police in a crime scene investigation such as gender, race, treatment, black and white hair fibres were investigated. Blind samples were successfully applied both to validate available experimental data and extend the current database of experimental determinations. Protocols were posed for the application of this methodology in the future.**

The proposed FT-IR methodology presented in this thesis has provided an alternative approach to the characterisation of single scalp human hair fibres. **The technique enables the rapid collection of spectra, followed by the objective analytical capabilities of chemometrics to successfully discriminate animal fibres, human hair fibres from different sources, treated from untreated hair fibres, as well as black and white hair fibres, on the basis of their molecular structure.** The results can be readily produced and explained in the courts of law. Although the proposed relatively fast FT-IR technique is not aimed at displacing the two slower existing methods of hair analysis, namely comparative optical microscopy and DNA analysis, it has given a new dimension to the characterisation of hair fibres at a molecular level, providing a powerful tool for forensic investigations.

CONTENTS

Acknowledgements	i
Abstract	ii
Table of Contents	iv
Table of Figures	xiii
List of Tables	xviii

Chapter 1 – Introduction

1.1 PhD Thesis Outline.....	1
1.1.1. Chemometrics and multi-variate analysis of spectral data.....	3
1.1.2. PhD Thesis objectives.....	6

PART I: Forensic Discussion of Human Hair Fibres

1.2. Literature Review.....	8
1.2.1. A Forensic Investigation into the Matching and Discrimination of Single Human Hair Fibres- A case for Spectroscopic Studies.....	8
1.2.2. Significance of Human Hair Fibres in Forensic Science.....	9
1.2.3. Microscopic and Macroscopic Examination of Hair Fibres.....	11

1.2.4. Application of Microscopic hair examination to forensic cases.....	14
1.2.5. DNA Analysis of Human Hair Fibres.....	15
1.2.6. Summary of Miscellaneous Techniques Proposed for Human Hair Fibres Identification...	19
 <u>PART II: Chemical and Physical Characteristics of</u> <u>Human Hair Fibres</u>	
1.3. Human Hair Fbres.....	22
1.3.1. Morphological Composition	24
1.3.2. Chemical Composition	26
1.3.3. Secondary Structure of Human Hair Fibres.....	29
1.3.4. Physical Characteristics of Hair Fibres.....	30
1.3.5. Variation of Hair Fibre Composition.....	31
1.3.5.(a) Chemical Composition and race.....	31
1.3.5.(b) Chemical Composition and gender, hair colour and age.....	34
1.3.5.(c) Weathering of hair.....	35
1.3.5.(d) Effect of chemical treatment on hair.....	35
1.3.5.(e) Chemical Composition and drugs of abuse.....	36

PART III: Vibrational Spectroscopy

1.4. FT-IR Micro-spectroscopy.....	38
1.5. Raman Micro-spectroscopy.....	43
1.6. Chapter Conclusions.....	47
References.....	48

Chapter 2 – Experimental Methodology

2.1. Hair Sample Collection.....	56
2.2. Hair Sample Treatment.....	56
2.3. Animal Keratin Fibres.....	57
2.4. Sample Preparation for Spectroscopic Analysis...	57
2.5. Spectroscopic Aspects.....	58
2.6. Treatment of Spectral Data.....	59
2.7. Chemometrics Methods of Analysis.....	61
2.7.1. Principal Component Analysis (PCA)...	62
2.7.2. Soft Independent Modelling of Class Analogies (SIMCA).....	64
2.7.3. Fuzzy Clustering (FC).....	65
2.8. PROMETHEE and GAIA.....	66
2.8.1. PROMETHEE.....	70

2.8.2. GAIA.....	74
2.9. Curve-fitting discussion	
2.9.1. Theoretical Aspects of Curve-Fitting.....	75
2.9.2. Curve-Fitting Software.....	77
References.....	78

**Chapter 3 – An FT-IR and Raman Micro-Spectroscopic Comparison Study
of Human Hair Fibres**

3.1. Introduction.....	81
3.2. Vibrational analysis of keratin fibres.....	83
3.2.1. The Peptide Bond.....	83
3.2.2. The Polypeptide Chain.....	85
3.2.3. Amino Acids.....	86
3.3. Chapter Objectives.....	87
3.4. FT-IR and Keratin Fibres.....	88
3.5. Raman Spectroscopy and Keratin Fibres.....	95
3.6. Results and Discussion.....	97
3.6.1. Preliminary Studies.....	97
3.6.2. Comparison of FT-IR and Raman Spectra collected from human hair.....	101

3.6.3. Comparison of Untreated and Chemically Treated human hair fibres through FT-IR and Raman micro-spectroscopy.....	104
3.6.4. Background on hair treatment.....	105
3.6.4.1. Secondary structure (peptide-backbone structure).....	107
3.6.4.2. C-C Skeletal Backbone.....	110
3.6.4.3. Sulfur containing groups.....	111
3.6.4.4. Aromatic hydrocarbon groups.....	113
3.6.4.4.1. Tyrosine.....	113
3.6.4.4.2. Phenylalanine.....	115
3.6.4.4.3. Tryptophan.....	116
3.6.4.5. Basic Amino Acids.....	117
3.6.4.5.1. Histidine.....	117
3.7. Chemometrics Discussion.....	118
3.7.1. FT-IR Micro-spectroscopy.....	118
3.7.1.1. PCA.....	118
3.7.1.2. SIMCA.....	120
3.7.1.3. FC.....	121
3.7.2. Raman Micro-spectroscopy.....	122
3.7.2.1. PCA.....	122
3.7.2.2. SIMCA.....	123

3.7.2.3. FC.....	124
3.8. Chapter Conclusions.....	125
References.....	128

Chapter 4 – Preliminary Investigation of Naturally Occuring Keratin

Fibres by FT-IR Spectroscopy and Chemometrics

4.1. Introduction.....	134
4.2. Application of Vibrational Spectroscopy to Keratin Fibres.....	136
4.3. General Discussion of FT-IR Keratin Spectra.....	138
4.4. Curve-fitting Analysis of Spectra.....	141
4.5. Determination of Secondary Structure through FT-IR Analysis.....	148
4.6. Chemometrics Analysis.....	151
4.6.1. PCA.....	151
4.6.2. SIMCA.....	154
4.6.3. FC.....	155
4.7. PROMETHEE and GAIA background discussion....	157
4.7.1. PROMETHEE and GAIA Analysis of Animal Fibres.....	161

4.7.1.1. Scenario 1.....	162
4.7.1.2. Scenario 2.....	165
4.7.1.3. Scenario 3.....	169
4.7.1.4. Scenario 4.....	171
4.7.2. Conclusions for PROMETHEE and GAIA....	175
4.8. Chapter Conclusions.....	177
References.....	180

**Chapter 5 – A Critical Evaluation of the Forensic Application of FT-IR
Micro-Spectroscopy and Chemometrics for Single Scalp Human Hair Fibres.**

5.1. Introduction.....	183
5.1.1. Variations in Sample Collection and Preparation	
Methods.....	187
5.2. Experimental Design.....	188
5.2.1. Purpose and scope.....	188
5.2.2. Selecting samples from a population.....	190
5.3. Forensic Evaluation of Human Hair – Past studies....	191
5.4. Population Statistics.....	193
5.5. Hair Examination Protocol.....	197
5.6. Validation of methodology.....	199

5.7. Results and Discussion.....	201
5.7.1. Case A. Comparison of untreated hair fibres	
from two different subjects and an unknown source....	201
5.7.1.1. PCA.....	202
5.7.1.2. SIMCA.....	203
5.7.1.3. FC.....	204
5.7.1.4. Conclusions for case A.....	204
5.7.2. Case B. Comparison of chemically treated hair fibres	
from two different subjects and an unknown source.....	205
2.7.2.1. PCA.....	206
2.7.2.2. SIMCA.....	207
2.7.2.3. FC.....	209
2.7.2.4. Conclusion for case B.....	210
5.7.3. Case C. Identification of gender and race variable of	
unknown hair fibres.....	211
5.7.3.1. The Gender Variable.....	212
5.7.3.1.1. PCA.....	212
5.7.3.1.2. SIMCA.....	213
5.7.3.1.3. FC.....	214
5.7.3.1.4. Curve-fit analysis discussion of FT-IR spectra	215
5.7.3.2. The Race Variable.....	220
5.7.3.2.1. PCA.....	221
5.7.3.2.1. SIMCA.....	222

5.7.3.2.3. FC.....	223
5.8. Case D. Discrimination and matching of black and white (unpigmented) hair fibres from the same source and from different sources.....	225
5.8.1. Introduction.....	225
5.8.2. Discussion of results.....	228
5.8.2.1. PCA.....	228
5.8.2.2. SIMCA.....	229
5.8.2.3. FC.....	230
5.8.2.4. FC.....	231
5.9. Chapter conclusions.....	232
References.....	234
<u>Chapter 6 - Thesis Conclusions and Future Work</u>	238
 Appendix I	
 Appendix II	
 Appendix III	

List of Figures (* indicates facing page)

Figure 1.1. A Simplified Schematic representation of nuclear and mtDNA.	16
Figure 1.2. Schematic representation of the growth phase of a hair fibre.	22
Figure 1.3. Schematic of a hair fibre showing the internal structure.	24*
Figure 1.4. Proposed biosynthetic pathway for eumelanin and pheomelanin.	26*
Figure 1.5. Load elongation (stress-strain) curves for hair in water and at 65% relative humidity.	30
Figure 1.6. A schematic diagram of an FT-IR system.	39*
Figure 3.1. Peptide bond formation by a condensation reaction	83
Figure 3.2. Raman spectra of a white untreated hair fibre after exposure to the 633 nm laser at different time intervals	97*
Figure 3.3. Raman spectra collected from a white hair fibre (W), black (B1), and washed (B2) hair using a 633 nm laser power.	98*
Figure 3.4. FT-IR spectra collected from different coloured hair fibres.	99*
Figure 3.5. Raman spectra of a black hair fibre collected after 10 minutes of burning out fluorescence using a 780 nm laser	99*
Figure 3.6. Comparison of an FT-IR and Raman spectrum of a single white human hair fibre.	101
Figure 3.7. FT-IR spectra collected from untreated (U) and treated hair fibres at different time intervals (T1(30 mins), T2 (1 hour), T3 (2 hours) and T4 (5 hours) at 4000-700 cm^{-1}).	104*

- Figure 3.8. Raman spectra collected from untreated (U) and treated hair fibres at different time intervals (T1(30 mins), T2 (1 hour), T3 (2 hours) and T4 (5 hours) at $3400-400\text{ cm}^{-1}$. 104*
- Figure 3.9. Relative areas of S-S and S=O versus treatments times. 112*
- Figure 3.10. Tautomerism of the imidazole ring of histidine. 117
- Figure 3.11. PC1 (45.4%) vs PC3 (9.4%) scores for the FT-IR spectra collected from the untreated and chemically treated hair fibres ($1750-750\text{ cm}^{-1}$). 118*
- Figure 3.12. PC3 loadings plot against the variable for FT-IR spectra collected from the untreated and chemically treated hair fibres ($1750-750\text{ cm}^{-1}$). 119*
- Figure 3.13. PC1 (70.7%) vs PC3 (7.0%) scores for the Raman spectra collected From the untreated and chemically treated hair fibres ($1750-500\text{ cm}^{-1}$). 122*
- Figure 3.14. PC3 loadings plot ($640-500\text{ cm}^{-1}$) 122*
- Figure 4.1. FT-IR spectra of keratin fibres between $4000-700\text{ cm}^{-1}$ spectral region. H; human hair, C; cat, D; dog, W; wool, F; feather, C; cow, Ho; horse. 138*
- Figure 4.2. FT-IR spectra of keratin fibres between $4000-700\text{ cm}^{-1}$ spectral region. H; human hair, C; cat, D; dog, W; wool, F; feather, C; cow, Ho; horse. 138*

Figure 4.3. Fitted FT-IR relative areas of FT-IR spectra.	142*
Figure 4.4. Relative areas of cysteic acid and cysteine of the different keratin fibres.	146*
Figure 4.5. PC1 (86.7%) vs PC3 (3.1%) scores plot for the FT-IR spectra collected from the different types of keratin fibres (1750-750 cm^{-1}).	151*
Figure 4.6. PC3 loadings plot against the variable for FT-IR spectra collected from the different types of keratin fibres (1750-750 cm^{-1}).	152*
Figure 4.7. PC1 (88.8%) vs PC3 (1.7%) scores plot for the FT-IR spectra collected from the different types of keratin fibres (1750-750 cm^{-1}).	153
Figure 4.8. PROMETHEE II Complete ranking for Scenario A.	159*
Figure 4.9. GAIA plane for Scenario A.	160*
Figure 4.10. PROMETHEE II Complete ranking for Scenario B.	160*
Figure 4.11. GAIA plane for Scenario B.	160*
Figure 4.12. PROMETHEE II Complete ranking for Scenario 1.	163*
Figure 4.13. PROMETHEE I Partial Ranking for Scenario 1.	163*
Figure 4.14. GAIA plane for Scenario 1.	164*
Figure 4.15. PROMETHEE II Complete ranking for Scenario 2.	166*
Figure 4.16. PROMETHEE I Partial Ranking for Scenario 2.	166*
Figure 4.17. GAIA plane for Scenario 2.	167*
Figure 4.18. PROMETHEE I Partial Ranking for Scenario 3.	170*
Figure 4.19. PROMETHEE II Complete ranking for Scenario 3.	170*
Figure 4.20. GAIA plane for Scenario 3.	170*
Figure 4.21. PROMETHEE II Complete ranking for Scenario 4.	173*

Figure 4.22. GAIA plane for Scenario 4.	173*
Figure 5.1. A schematic representation of the proposed application of microscopic, FT-IR and DNA techniques for the analysis of unknown hair fibres.	197*
Figure 5.2. A schematic representation of the hypotheses proposed to investigate the origin of an unknown hair fibre found at the crime scene through FT-IR micro-spectroscopy and chemometrics.	198*
Figure 5.3. FT-IR spectra collected from subject V and S and an unknown source from (1750-750 cm^{-1}).	202*
Figure 5.4. PC1 (66.6%) vs PC2 (25.5%) scores plot for the FT-IR spectra collected from subject V, subject S and the two unknown sources.	202*
Figure 5.5. FT-IR spectra collected from subject V and S and an unknown source from (1750-750 cm^{-1}).	206*
Figure 5.6. PC1 (58.8%) vs PC2 (26.6%) scores plot for the FT-IR spectra collected from subject V, subject S and the two unknown sources.	206*
Figure 5.7. FT-IR spectra collected from Female (F), Male (M) and two unknown hair fibres (1750-750 cm^{-1}).	212*
Figure 5.8. PC1 (63.6%) vs PC2 (23.0%) of the reference set (female (F1-9) and Male (M1-9) and validation samples (1750-750 cm^{-1}).	212*
Figure 5.9. PC2 loadings plot (1750-750 cm^{-1}).	212*
Figure 5.10. FT-IR spectra collected from Caucasian (C), Mongoloid (M) and two unknown hair fibres (1750-750 cm^{-1}).	220*

- Figure 5.11. PC1 (70.3%) vs PC2 (23.6%) of the FT-IR spectra collected from Caucasian (C1-3), Mongoloid (M1-3) and validation samples (1750-750 cm^{-1}). 221*
- Figure 5.12. PC1 loadings plot (1750-750 cm^{-1}). 221*
- Figure 5.13. Examples of FT-IR spectra collected from black and white hair fibres. 228*
- Figure 5.14. PC1 (54.9%) vs PC2 (31.0%) scores plot for the black and white hair fibres. 228*
- Figure 5.15. PC2 loadings plot (3100-2800 cm^{-1}). 228*

List of Tables (* indicates facing page)

Table 1.1. Approximate composition of the amino acids found in untreated hair fibres.	28*
Table 1.2. Variation of amino acid composition of human hair of various Racial origin ($\mu\text{M/g}$)	32*
Table 1.3. Summary of FT-IR vs Dispersive IR instrumentation	38*
Table 2.1. List of preference functions	70*
Table 3.1. FT-IR vibrational modes of naturally occurring fibres	84*
Table 3.2. Characteristic band assignments for the different types of protein conformation for Amide I, II and III.	85*
Table 3.3. Background history of hair samples used to collect FT-IR spectra.	99
Table 3.4. Vibrational assignments of cis- and trans- forms.	102
Table 3.5. Summary of results obtained from the curve-fitting of Amide I and II (FT-IR) and Amide III (Raman) for the untreated and chemically treated hair fibres.	108*
Table 3.6. Summary of results obtained from the curve-fitting of CH_2CH_3 for Untreated and chemically treated hair fibres.	110
Table 3.7. Dihedral Angles of the two different proposed theories	111*

Table 3.8. Relative areas of S-S and S=O.	112*
Table 3.9. SIMCA results with $RSD_{crit}=0.106$, $p=0.05$.	120
Table 3.10. FC membership values for a two-cluster model with a soft (2.50) weighting exponent value.	121
Table 3.11. FC membership values for a five-cluster model with a soft (2.50) weighting exponent value.	121
Table 3.12. SIMCA results with $RSD_{crit}=0.164$, $p=0.05$.	123
Table 3.13. FC membership values for a two-cluster model with a soft (2.50) weighting exponent value.	124
Table 3.14. FC membership values for a five-cluster model with a soft (2.50) weighting exponent value.	124
Table 4.1. Error in curve-fitting measurements	142
Table 4.2. Peak positions used in curve-fitting for the keratotic samples of FT-IR spectra and their corresponding relative intensity areas and literature values	142*
Table 4.3. Ratios of the relative areas for the keratotic FT-IR spectra	148*
Table 4.4. SIMCA analysis results with $RSD_{crit}=0.0191$, $p=0.05$	154
Table 4.5. FC clustering membership values for a two-cluster model with a hard (1.50) and soft (2.50) weighting exponent value.	155
Table 4.6. FC membership values for a seven-cluster model with a hard (1.50) and soft (2.50) weighting exponent value.	156
Table 4.7. Simulation data matrix of amide I ratios, cysteine and cysteic acid	159*

Table 4.8. Data matrix of amide I ratios, cysteine and cysteic acid areas and PC1 and PC3 scores for the seven keratotic samples	161*
Table 4.9. Model Parameters	162
Table 4.10. Model Parameters	165
Table 4.11. Model Parameters	169
Table 4.12. Model Parameters	172
Table 5.1. Relationship between sample size and population size.	195
Table 5.2. Success of Validation samples on the basis of treatment, gender and race variables.	199*
Table 5.3 SIMCA results with $RSD_{crit}=0.21$, $p=0.05$.	203
Table 5.4. FC membership values for a two-cluster model with a hard (1.50) and soft (2.50) weighting exponent value.	204*
Table 5.5 SIMCA results with $RSD_{crit}=0.31$, $p=0.05$.	207
Table 5.6. FC membership values for a two-cluster model with a hard (1.50) and soft (2.50) weighting exponent value.	209*
Table 5.7. Background information of the hair fibres used to build the reference and validation set for the gender and race variables.	211*
Table 5.8. SIMCA results with $RSD_{crit}=0.19$, $p=0.05$.	213
Table 5.9. FC membership values for a two-cluster model with a hard (1.50) and soft (2.50) weighting exponent value.	214*
Table 5.10. Summary of the curve-fit measurements obtained from the FT-IR spectra from Case C.	215*
Table 5.11. Background information of the hair samples used to build the reference and validation sets for the race variable.	220

Table 5.12. SIMCA results with RSDcrit=0.2284, p=0.05.	222
Table 5.13. FC membership values for a two-cluster model with a hard (1.50) and soft (2.50) weighting exponent value.	223
Table 5.14. A summary of the structural components of the melanins indicated by the infrared spectra.	226
Table 5.15. SIMCA results with RSDcrit=0.1684, p=0.05.	229
Table 5.16. FC membership values for a two-cluster model with a hard (1.50) and soft (2.50) weighting exponent value.	230
Table 5.17. FC membership values for an eight-cluster model with a hard (1.50) and soft (2.50) weighting exponent value (1750-750 cm ⁻¹).	231*
Table 5.18. FC membership values for an eight-cluster model with a hard (1.50) and soft (2.50) weighting exponent value (3100-2700 cm ⁻¹).	232*

1

INTRODUCTION

1.1 PhD Thesis Outline

“At the present time the evidential value of hair in the forensic context is limited because no reliable means of characterisation has yet been developed which allows the complete individualisation of human hair. This state of affairs is unsatisfactory as human hair are often recovered from crimes of violence and other serious crimes” [1].

“It is not possible...definitely to identify a sample of hair as having come from one individual's head. The probability of identity may grow with every point of resemblance...but the probability should never be stated as a certainty” [2].

“If cases are excluded where hairs possess unusual features, can hair evidence be of so little value, despite the feeling of many experienced scientists that more could be done with hairs?” [3].

The above comments form part of discussions presented in forensic books and journal articles directed towards the significance of hair fibres in forensic cases. The general consensus from the literature and private communications with hair experts in the field has indicated that the significance of hair in criminal cases is grossly underestimated.

When hair is found at the scene of a crime, the most frequently asked question is – does the hair belong to a particular person? Since 1934, the general consensus in the literature is that it is not possible to identify a sample of hair as having come from a particular person's head [4].

Microscopic and macroscopic comparisons have been adopted as basic routine practice for hair identification and are outlined in the hair examination protocols in most of the forensic laboratories around the world. The first use of microscopic techniques were reported as early as 1874 [4]. Since that time there have been no major developments in the area of hair individualisation and microscopic comparison still remains the most common and widely used method of analysis. Some of the disadvantages associated with microscopic comparisons have been related to the subjective measurements often obtained from this type of analysis. The technique can also be time-consuming and requires a high level of expertise from the examiner.

A rapid and simple method of providing a reliable characterisation of human hair fibres that builds an accurate profile of a suspect is highly desirable in forensic cases. Gaudette [5] proposed that *“one approach to hair individualisation would be to obtain enough additional variable characteristics so that when they are added to present macroscopic and microscopic characteristics a statistical analysis would conclusively demonstrate in all instances that the chances of two people having similar hairs would be negligible”*. Seta et al [4] agree with Gaudette and add *“morphological examination should always be considered as the first step of forensic hair comparison.....analytical examination can now be expected to give useful information.....thus, a combination of morphological and analytical data can lead to*

the enhancement of identification probability". Vibrational spectroscopic methods of analysis will often provide discrete qualitative and quantitative information, which can characterise a fibre by replacing or supplementing some of the more subjective measurements made by microscopy. Robbins [6] has indicated a variation in the composition of hair peptides among individuals possibly due to factors such as gender, diet, cosmetic treatment, and weathering effects. Amide vibrations are characteristic of the peptide linkage. Therefore, a variation in the composition of hair peptides will be reflected in the amides. Amide bonds can be readily studied through vibrational spectroscopic methods such as FT-IR and Raman spectroscopy.

1.1.1. Chemometric and multi-variate analysis of Spectral Data

FT-IR and Raman spectroscopy can provide a large amount of analytical data in a short period of time. However, as the number of samples (characterised by many variables) increases, the problems-how to convert raw analytical data into meaningful information and furthermore, how to minimise the subjective factor of interpretation, becomes more and more evident. Obviously, the problem of handling large amounts of data, for purposes such as learning, recognition and prediction, requires the application of special techniques, known as chemometrics techniques.

There are various types of chemometrics techniques some of the most common ones including Principal Component Analysis (PCA), Soft Independent Modeling of Class Analogies (SIMCA) and Fuzzy Clustering (FC). Each technique or a combination of two or more techniques has been successfully applied in the study of cancerous tissues [7], identification of ivory [8], and differentiation of cotton fibres [9].

Chemometrics methods of analysis have been recently applied to the area of forensic science and in particular in the discrimination of forensic soil analysis [10], batch searching of illicit heroin samples [11], and amphetamine sources [12].

The application of chemometrics methods such as PCA, SIMCA and FC for the interpretation of spectra collected from single human scalp hair fibres provide interesting but somewhat limiting information. PCA is a method based on parametric statistics and carries all the advantages and limitations of such models. It is also a qualitative method used for data display. This becomes difficult when dealing with large matrices especially with the use of conventional two-dimensional spectral display. Also, in such circumstances what is viewed in a two-dimensional display may account for only a modest fraction of data variance and there is no easy similar way to assess effects of more PCs. With spectroscopic matrices, which include frequencies as variables, biplots are often unhelpful because an overlay of, for example, 250 points on a score plot produces a diagram that is difficult to interpret. The loadings plot option can be used but however useful such plots may be they are abstract spectra and any conclusions can only be a guide to interpretation and inference of the raw spectra. Sometimes, SIMCA may be a useful tool with which to build a model of several significant PCs; but here one requires at least one well-balanced set of samples on which to build the model before comparisons with spectra from a fibre of interest could be made. Acquisition of suitable samples and the collection of spectra is a time consuming task, which may be difficult to accomplish. Fuzzy clustering is a non-parametric method, which in principle can be used to compare as few as two objects, offers considerable advantages over PCA and SIMCA in that respect, but it does not provide information about the variables controlling the

clustering of objects and as with PCA we must infer from the properties of the objects the meaning of the discrimination into fuzzy clusters on a PC scores plot. Ideally, FC requires a membership function to suit a particular case i.e. there is no universal membership function. Thus, to progress the concept of comparing IR spectra of single human scalp hair fibres for forensic purposes, a new approach is required. This approach preferably should be able to identify each object and provide at least a relative index value to be able to compare it with other objects. It should be able to accomplish this without the need to build reference models for comparison and it should have the facility to compare ideally even just two objects i.e. two fibres. In addition, having obtained the relative comparison indices, it would be useful to have information regarding the influence of the variables on the comparisons.

In a classical forensic case, there is a need to be able to compare different types of keratin fibres such as animal fibres and human hair fibres. A possible solution may lie with the application of multi-criteria decision making (MCDM) methods. These methods have been developed to assist the decision maker (DM) make a choice of the most suitable site for sewage disposal [13] or investigate the performance of competing products [14] etc. There are many such methods that have been developed especially in the operations research field and they have in principle one common objective i.e., to rank objects for comparative purposes to select the preferred or best performing object. A short review of some comparative studies of the better-regarded MCDM methods is presented in chapter 2.

1.1.2. PhD Thesis Objectives

The aim of this thesis was to investigate the potential forensic application of vibrational spectroscopic methods as an identification tool for single human hair fibres. The overall objectives of the research were:

Objective 1: To investigate the forensic application of FT-IR and Raman micro-spectroscopy and some common methods of multivariate methods of analysis such as chemometrics for the investigation of the molecular structure of untreated and chemically treated hair fibres.

Objective 2: To examine the limitations of Raman micro-spectroscopy for the analysis of single human hair directed towards forensic applications.

Objective 3: To examine the limitations of the FT-IR micro-spectroscopy technique for the discrimination of single scalp human hair fibres and to predict some characteristics of blind samples in an effort to understand the limits of FT-IR micro-spectroscopy for application in forensic science.

Objective 4: To investigate the validity of the proposed methodology with some more complex forensic applications which include the matching and discrimination of black and white hair fibres from the same source and from different sources, the matching and discrimination of untreated and treated hair fibres from the same source and from different sources.

Objective 5: To extend the forensic application of the FT-IR micro-spectroscopy to other types of keratin fibres.

The discussion in this thesis is divided into six chapters. The remaining part of chapter 1 focuses on the theory of human hair fibres and its significance in forensic casework. The same chapter also provides a brief outline of the vibrational

techniques employed for the experimental work in this thesis. Chapter 2 describes the materials, procedures and spectroscopic aspects presented in this work. The same chapter also provides background theory into some common methods of multivariate analysis such as chemometrics, MCDM methods and curve fitting. Chapter 3 provides a comparative study of FT-IR and Raman micro-spectroscopy for the analysis of untreated and chemically treated hair fibres. Discussion in the chapter focuses on the chemical modification of the secondary structure, C-C skeletal backbone and some of the amino acids during oxidation of the hair fibres. Chapter 3 also provides a detailed study of the potential application of FT-IR and Raman micro-spectroscopy to the forensic analysis of hair fibres. Chapter 4 discusses the application of FT-IR micro-spectroscopy to various types of natural hard keratin fibres, such as mammalian and feather keratins, and attempts to discriminate the fibres on the basis of their characteristic molecular structures. Chapter 5 presents a detailed systematic study of the forensic application of FT-IR micro-spectroscopy to the discrimination and matching of single scalp human hair fibres. The same chapter also explores some of the fundamental chemical reasons for the discrimination of the hair fibres. The limitations of the technique are also highlighted and presented through a series of validation studies. Finally, chapter 6 provides conclusions and suggestions for further work.

PART I: FORENSIC DISCUSSION OF HUMAN HAIR FIBRES

1.2. Literature Review

.....Inside the death sack, Smith found the cinders and a small amount of household fluff, containing a few human and animals hairs.....but the hairs were of far greater interest. They (hair) showed a remarkable irregularity of contour and had many definite twists. This peculiarity was caused by rather careless artificial waving. As far as I could judge by examination in a comparison microscope, the hairs from the sack and those from Mrs. Donald were identical in every detail. [7]

Sir Sydney Smith (Sherlock Holmes)

1.2.1. A Forensic Investigation into the Matching and Discrimination of Single Human Hair Fibres – A Case for Spectroscopic Studies

The Oxford dictionary defines the word “forensic”, from the Latin forensis (forum), as “ of or used in courts of law” [15]. To the general community, forensic science refers to “the application of sciences to matters of law” [16]. Forensic science is an extensive area with specialised fields some of which include document examination, firearms, explosives, fingerprints and footprints, and the analysis of trace and biological evidence. **This thesis is concerned with the analysis of trace evidence, in particular human hair fibres.**

In 1910, Edmond Locard formulated the ‘exchange principle’, which states that the criminal always leaves something at the scene of a crime or takes something away [17]. The exchange principle—which today is referred to as ‘contact traces’—is the very basis of physical evidence in forensic science. Contact traces include among

others, footprints, fingerprints, fibres, blood, semen, saliva, hair, drugs, explosives, paint, glass, petroleum products, firearms and soil [17]. During crimes of violence, specifically against people, certain trace materials such as hair or fibres will be transferred between the victim and the perpetrator or left at the scene of the crime.

It is often observed that every human being is unique. Our superficial differences, however, scarcely hint at the differences found at the genic and cellular level. With respect to human hair, David Stoney [18] states; *“Each hair is a piece of tissue which could conceivably possess the biochemical individuality of blood or the structural individuality of fingerprints”*.

1.2.2. Significance of human hair in forensic science

Literature, from the fictional stories of Sherlock Holmes to real-life cases, has illustrated repeatedly the frequent occurrence of human hair fibres in criminal offences, in particular rape and homicide. The importance of human hair as useful associative evidence is related to the fact that hair originates directly from an individual. Hairs growing out of the skin are essentially dead strands of protein, and as each portion of scalp hair grows out from the scalp, it incorporates some chemicals that are present in the body. Therefore, as such chemicals in the hair change, one has a record of the changing chemical composition of the body over a period of time. Discussions in the literature have indicated that every person loses approximately 100 hair fibres per day [19, 20]. This makes hair a readily accessible material, and it is frequently present at the crime scene or on the clothing of the participants. Hair is resistant to chemical decomposition and can retain structural features over a long

period of time. A hair fibre is difficult to destroy-except by fire- and will remain in a grave long after the body has decomposed [20].

The purpose of hair analysis in a forensic investigation is to provide or add to trace evidence that may convict a suspect in a court hearing. Even though hair analysis has been used in the courtroom to help solve crimes for over 150 years, it is still considered as a subjective science [22]. This is because hair is considered as a general material, and over the years, forensic scientists have tried to find a way to isolate the physical and chemical properties that could serve as individual characteristics of identity.

1.2.3. Microscopic and Macroscopic Examination of Hair Fibres

At present, examination of hair relies heavily upon morphological characterisation with the use of macroscopic and microscopic techniques. Prof. Rudolf Virchow reported the first forensic investigation of human hair in 1861 [23]. In 1910, Dr Victor Balthazard with Marcelle Lambert described a method closely resembling the techniques used today by forensic scientists, namely, a reliance on microscopic techniques to observe and compare morphological features of hair [23]. In 1940, Kirk [24], published a series of papers entitled “Human Hair Studies”, which examined the potential of utilisation of various physical and chemical properties of hair with the purpose of individualising human hair. It was proposed that to solve the problem of hair individualisation scientists would have to extend their abilities beyond the microscopic examination of hair. However, the general methods, philosophy and significance of forensic hair examination have not changed significantly since that time [4].

Various examination protocols have been published for the comparison of human hair by a number of different authors. Dr James Robertson an international accredited hair examiner, presently employed at the Australian Federal Police has developed a microscopic protocol for hair examination [25]. In summary, the examination of hair fibres begins with the **collection of samples of both known** (known hairs are hairs from all relevant individuals in a case) **and recovered hairs**. Thirty to forty known hairs is considered to be a satisfactory sample. The second step is the **examination of hairs under a stereomicroscope** (magnification 10x). The selection of known hairs – usually 5 to 10 hairs – is dependent upon the length and colour of the fibre. If there is a large variation between these samples, then a larger number of known samples

must be examined. A checklist is used to record the macroscopic features such as *length* of the hair fibre, *shaft profile* (for example whether it is straight, wavy or curly), the *colour of the hair fibre*, whether *the root is present or absent* and the *appearance of the tip* (for example whether it is cut, split etc.). Once the known hairs have been investigated, then examination of the recovered hairs proceeds in a similar way. However, in the case of the recovered hairs all the hairs have to be examined. In addition, it is important to study the variation of features along the hair shaft as hair examination involves pattern recognition.

The next step is the **examination of hairs by light compound microscopy** (magnification powers 50x, 100x, 250x and 400x), where further microscopic features are recorded such as the *pigment density and distribution*, *the type of medulla* (opaque or translucent) and *distribution, cortical texture, thickness of cuticle and colour*. The above two microscopes; stereomicroscope and light compound microscope, allow for the exclusion of structurally different hairs and the inclusion of similar hairs.

The final decision however, as to whether or not the known and the recovered hair could have a common origin is made when the hairs are examined under a **comparison microscope**. The comparison microscope is a useful instrument because it enables two specimens to be viewed side-by-side and subsequently compared detail for detail.

Even though microscopic techniques of human hair comparison are widely being used in laboratories around the world, the acceptance of such methods in forensic circles remains a subject of debate. Many of the characteristics in the hair examination

protocol are subjective (for example colour and texture). Even though every hair examiner claims to use reliable and consistent criteria it is not possible to obtain reproducibility between 2 or more hair examiners analysing the same hair [26]. This is due to the inability to place a numerical value or probability on the experience of the hair examiner and each case is treated on its own merits [27].

The need for further independent, scientific and controlled studies to validate microscopic hair analysis as a forensic technique are vital [28]. Since it is not possible to assess the reliability of forensic hair comparison analysis based solely on the experience that examiners have in their day-to-day work, empirical studies performed in a controlled environment become critical. As stated in the dictionary of science and technology [29], a scientific method is *“an organized approach to problem-solving that includes testing [data] objectively, interpreting results, and stating conclusions that can later be evaluated independently by others”*. To ensure objectivity, it is necessary to design ‘blind’ tests to ascertain whether a given result is produced by the expected combination of indicators, or by chance [30]. **This thesis will focus in isolating relevant chemical information of human hair fibres through vibrational spectroscopic methods. Two sets of samples; known and unknown (blind) will be used in the study. The application of blind trials will assist in providing an objective measure for hair identification using the proposed technique.**

1.2.4. Application of Microscopic Hair Examination to Forensic Cases

Most forensic scientists agree that examination of hair fibres with optical microscopy is useful in cases where two hairs are structurally dissimilar to the degree that an individual can be readily excluded [23]. However, when comparisons are made between two hair fibres of similar colour and/or hair fibres that lack detailed features, exclusion is not readily possible and the examination can provide equivocal results.

The Federal Bureau of Investigation (FBI), concludes hair comparison reports with the following statement; *“It is noted that hair does not possess a sufficient number of unique individual microscopic characteristics to be positively associated with a particular person to the exclusion of all other”* [31].

Even though microscopic examination of human hair has been the subject of debates in the forensic field, this does not imply that microscopic analysis is of no value. On the contrary, cases reported in the literature are indicative of the significance of such examinations and it has assisted in many criminal investigations such as in the famous William’s case *State v. Williams* [32], and other cases such as *Mcgreew v. State* [33], *People v. Linscott* [34], *State v. Fukusaku* [35], *Suggs v. State* [36], and *People v. Sutherland* [37]. The offences in these cases ranged from criminal deviate conduct to murder and aggravated kidnapping, which illustrate the widespread occurrence of hair fibres in criminal offences.

1.2.5. DNA Analysis of Human Hair Fibres

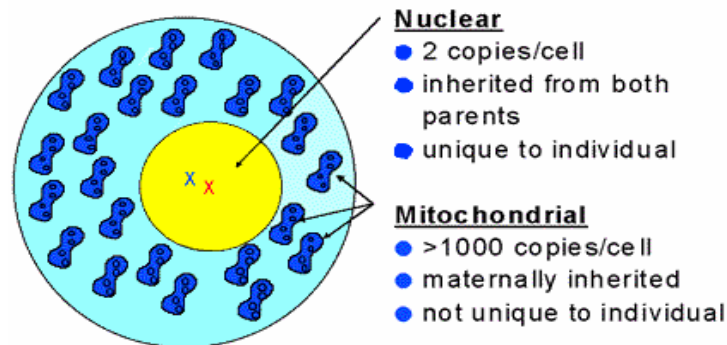
Miescher [38] first discovered deoxyribonucleic acid (DNA) in 1869, but scientists were slow to comprehend the significance of the findings. Not until 1953, with the help of James Watson, Francis Crick and Maurice Wilkins [38], was the structure and composition of the DNA molecule finally revealed. By 1962, Watson, Crick and Wilkins had received the Nobel Prize in Medicine, and science was well on the road to discovering what these “building blocks of life” could do.

DNA (and its close relative ribonucleic acid, RNA) is actually a polymer of molecules [39] meaning that they are made of many repeating units, commonly referred to as nucleotides. These nucleotides are made up of a sugar and a phosphate backbone, plus a ‘base’ of a heterocyclic amine. Both the phosphoric acid and the ribose sugar are structural, while the nitrogenous bases are informational. The sugar component is either β -D-ribofuranose (RNA) or β -D-2-deoxyribofuranose (DNA).

Recent advances in genetic grouping have led to DNA analysis, which has been regarded by many as a promising technique for hair identification. It is not within the scope of this thesis to present an extensive discussion on DNA analysis, however it is necessary to provide a general introduction on this subject in order to highlight its application to hair analysis. Deoxyribonucleic acid (DNA), is the genetic material found in all human cells that carries the coded messages of heredity unique (with the exception of identical twins) to each individual. In criminal cases, DNA can be extracted from samples of blood, semen, saliva, skin, or hair follicles found at a crime scene and then compared to DNA drawn from a suspect to determine if there is a “match”. The actual DNA typing success rate for single hairs has been shown to be in

the area of 34 percent for case samples [21]. The inheritable traits that are controlled by DNA arise out of its ability to direct the production of proteins.

There are two types of DNA tests that can be performed and include nuclear DNA and mt- DNA (mitochondrial DNA) (Figure 1.1).



1

Figure 1.1. A simplified schematic representation of nuclear and mt-DNA.

Single shed hairs and hair shafts contain only minute amounts of undegraded DNA and analysis of nuclear DNA markers is mostly unsuccessful. In a 1998 study by Linch et al. [40], entitled “Evaluation of the human hair root for DNA typing subsequent to microscopic comparison” 15 telogen² head hairs from 15 different individuals were analysed. The results indicated that no telogen hairs were correctly typed for gender identification by the Fluorescence In Situ Hybridization (FISH) method. FISH uses nonradioactive fluorescently labelled chromosome specific DNA probes that can rapidly identify the presence of a chromosome, chromosome region, or a gene in cells. Most cells and cell remnants exhibited no signals, while a few cells exhibited more than two signals and in these cases some male hair root materials exhibited female signals and some female hair root materials exhibited male signals.

² Telogen is the final stage of hair growth and is commonly referred to as the resting phase.

The authors concluded by stating that these findings strongly indicate nuclear DNA degradation. Another study by Prahlow and co-workers [41] using FISH showed that the gender of the individual could be correctly identified from at least two of the four collection sites in each case. Overall, successful gender identification was available in 65% of the collection.

Since the majority of hairs (90%) found at crime scenes are in the telogen phase, mtDNA offers a more suitable target for analysis, as it is present in more than 1000 copies per cell [42, 43]. Human mtDNA is an extrachromosomal, closed circular, organelle-specific genome consisting of approximately 16.5kb. The mtDNA genome consists of coding sequences for 2 ribosomal RNAs, 22 transfer RNAs, 13 proteins and a noncoding region approximately 1,100 base pairs long, called the displacement loop or control region [43]. Most of the sequence variation between individuals is found within the control region. There are three major drawbacks to this technique; firstly it is maternally inherited; the mtDNA sequence is identical for siblings and all their maternal relatives and thus is not unique to an individual, secondly given the fact that it is quite new it is relatively expensive, and thirdly it is time consuming. In addition, in cases where the hair has been heavily degraded, there is the problem of contamination and thus the reliability of the results has been questioned [44]. If more than one individual's DNA is extracted and amplified, the sequencing results will reflect this mixture. In some cases, the contaminating DNA can greatly exceed the DNA from the donor and thereby yield a false positive result. In addition, due to the high sensitivity level of this method, it results in an increased possibility of contamination, which necessitates additional controls. In a paper by Allen et al [45], the authors proposed a new mtDNA technique for the analysis of shed hair. The

authors discussed the problems associated with carrying out mtDNA from specimens with low yields, which involve several labor-intensive steps due to the possibility for introducing contamination.

DNA profiling promised reliable individual identification, but as with any new technology controversies abound. *People v. Castro* was the first reported case to successfully challenge the validity of DNA evidence [46]. The deficiencies in the DNA procedures were by no means minor or technical. The court wrote: “In a piercing attack upon each molecule of evidence presented, the defence was successful in demonstrating to this court that the testing laboratory failed in its responsibility to perform the accepted scientific techniques and experiments” [47]. Significantly, the prosecution and defence experts met out-of-court and issued a joint statement, including the following: “[T]he DNA data in this case are not scientifically reliable enough to support the assertion that the sample...do or do not match. If this data were submitted to a peer review journal in support of a conclusion, it would not be accepted. Further experimentation would be required” [47]. The probability statistics that follow DNA results can easily mislead Judges and juries, in particular when they are presented with statistics such as ‘1 in 37 million’ to mean what it appears to say. Such statistics are quite impressive but the question is do they reliably represent the true value of the evidence. Lewontin and Hartl [48] stated that the estimates of the probability of a matching DNA profile “as currently calculated and unjustified and generally unreliable”.

1.2.6. Summary of Miscellaneous Techniques Proposed for Human Hair Fibres Identification

Apart from the traditional microscopic examination techniques and the most recent developments of DNA analysis, numerous other techniques have been developed and applied in an aim to individualise of human hair and include:

1. *Pyrolysis gas chromatography*. This technique does not provide an effective means of hair discrimination. Studies have shown that the pyrograms of different individuals were essentially the same and any small differences between individuals were attributed to experimental error [49].
2. *Trace element analysis*. Trace element analysis was initially regarded as a promising technique for hair characterization. However, various problems associated with the interpretation of the results mainly the correlation between elements, the variation of the elemental composition over the head, along the length of the fibre, and also across the hair diameter have proven the technique unreliable [50].
3. *ABO blood grouping*. ABO blood groupings are still regarded with some skepticism. Most forensic scientists in the West regard the ABO groupings of Caucasian hair, as being unreliable and prone to error and therefore unsuitable as a routine method of analysis. However, the ABO system has been applied as a potential useful forensic marker in Chinese populations. Successful groupings of both head and pubic hair from local Chinese population in Hong Kong have been carried out and the results have been accepted by the courts of law [51].

5. *Isoelectric Focusing of Human Hair Keratins (IEF)*. There is no conclusive evidence that this technique discriminates individuals from different races, and different individuals within the same race [52].

6. *FT-IR spectroscopy*. Two papers published in the Journal of Forensic Sciences illustrate the application of FT-IR micro-spectroscopy, using a diamond anvil cell- for forensic purposes [53, 54]. The spectra were compared from female and male subjects and the authors concluded that conventional methods of interpretation are not sufficient to differentiate single hair fibres on the basis of gender and hair colour. Chemical treatments such as bleaching, dyeing and perming, was the only variables that could be discriminated. The authors concluded that if differences to gender, age, hair colour and chemical treatment could be detected through infrared spectroscopy, they must be more subtle than the simplistic technique used in their study. Initial studies obtained as part of a Masters degree by this thesis' author [55] using FT-IR microscopy indicated the possibility of matching and discriminating single hair fibres. The spectra collected were interpreted by the use of chemometrics methods of analysis such as Principal Component Analysis (PCA), Soft Independent Modeling of Class Analogies (SIMCA) and Fuzzy Clustering (FC). *This application of chemometrics constitutes a significant difference between past and present approaches. The significant conclusion drawn from this pilot study was that FT-IR micro-spectroscopy followed by chemometrics is a possible technique for the discrimination of human hair single fibres.*

The discussion in this chapter has shown that microscopic hair analysis is an involved and tedious procedure with much of the difficulty arising from the lack of discrete numerical and quantifiable features in human hairs. The proposed research in this thesis assumes that court evidence pertaining to hair comparison and individualisation can be made less judgmental by the application of vibrational spectroscopy for data collection and the various chemometrics methods such as pattern recognition to facilitate interpretation of the spectral data. Any new method arising from this research is not intended to replace microscopical comparisons of hair but rather to generate scientific data in a manner that could assist and strengthen microscopic hair identification comparisons.

PART II: CHEMICAL AND PHYSICAL CHARACTERISTICS OF HUMAN HAIR FIBRES

1.3. Human Hair Fibres

To the casual observer, hair appears to be a fairly uniform structure, differing in individuals only in colour and amount. However, hair is a physically and chemically complex multicellular structure whose biology is only partially understood. In order to interpret the results of hair analysis tests accurately, some rudimentary understanding of the biology of hair is necessary. Thus, the discussion presented in the sections forming part II of this chapter will offer a brief review of the physical and chemical composition retained by hair.

Hair is produced by specialised organs in the skin known as hair follicles (figure 1.2). Deep within an active follicle, the cells making up the hair shaft in its formative stages are alive and active, however, once the hair reaches the skin surface, these cells become keratinised.

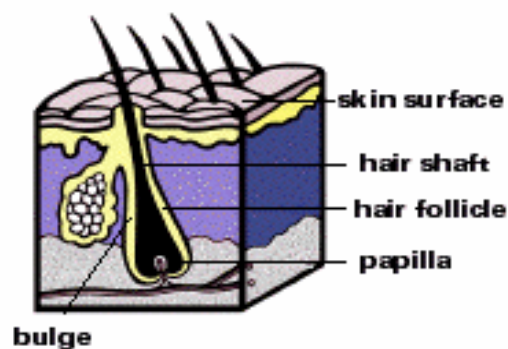


Figure 1.2. Schematic representation of the growth phase of a hair fibre.

The schematic diagram in Figure 1.2 illustrates an active human hair bulb and fibre inside a follicle, which originates in the subcutaneous tissues of the skin. The dermal papilla, located near the centre of the bulb is important for the growth of hairs. Melanocytes, which produce hair pigments, and basal layers, which produce hair cells, are also located within the bulb. Blood vessels carrying nourishment to the growing hair fibre are located deep within the skin at the base of the bulb [56].

The formation of human hair fibres can be divided into three distinct zones. Firstly there is the zone of biological synthesis and orientation. This is found at and around the bulb of the hair. It is also known as the growth phase or anagen. At any given time, about 90% of scalp hair are in the growth stage. The next zone is called keratinisation or transition stage (catagen) and this is where stability is built into the hair structure through the formation of cystine linkages, which form through a mild oxidative process. The metabolic activity slows down, and the base of the follicle migrates upward in the skin toward the epidermal surface. The final zone (telogen) that eventually emerges through the skin surface is the permanent region of a hair fibre, which consists of the cuticle, cortical and sometimes medullary cells as well as intercellular cement. Once the rest phase is over, the hair strand falls out and a new growth begins.

The major emphasis in the first part of this chapter is on the chemistry and structure of the permanent zone of human hair. The primary focus is on human scalp hair as opposed to hair from other parts of the body.

This image is not available online. Please consult the hardcopy thesis available from the QUT library

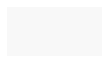


Figure 1.3. Schematic diagram of a hair fibre showing the internal structure [56].

1.3.1. Morphological composition

A hair fibre consists of three main morphological components (Figure 1.3): the outer layer known as the cuticle, the cortex that contains the bulk of the fibre, and the medulla.

The cuticle is the outer layer of the fibre and serves as a chemically resistant region surrounding the cortex. The thickness of the cuticle varies between 5 to 10 scales with each scale approximately 0.5 μm to 1.0 μm thick and 45 μm long [56]. Each cuticular cell consists of a number of intracellular lamellar subcomponents: the A-layer, exocuticle and endocuticle as shown in Figure 1.3. The A-layer is very rich in cystine (30%), and is characterised as a biochemically stable layer, which strongly resists physical and chemical forces. The exocuticle is also cystine-rich (15%) representing about two-thirds of the cuticle structure. The endocuticle is the least cystine-rich component (~ 3%).

The cell membrane complex (CMC) (Figure 1.3) or intercellular cement contains very little protein, and it is believed to consist mainly of lipids and polysaccharides [56]. The function of the CMC is to provide intercellular connections between the main types of the cell components such as cuticle/cuticle, cuticle/cortical, cortical/cortical and if the medulla is present cortical/medulla. These intercellular regions contribute both mechanically and chemically to the function of the fibre.

The cortex constitutes the major part of the hair fibre and is largely responsible for the mechanical properties of the fibre. The cortical cells consist of long uniform filaments, which are complex protein networks. There are two types of cortical cells;

the paracortex and the orthocortex, and these are most easily demonstrable in wool fibres. The chief components of the cortical cells as shown by high-resolution electron microscopy are the fibrous (low-sulfur) and matrix (high-sulfur) proteins. The matrix proteins are packed around the aligned, oriented, α fibrous proteins. Amino acid analysis of the fibrous and matrix proteins shows considerable differences. The most striking is the cystine content, which is much higher in the matrix compared to the fibrous protein. It has been suggested that the fibrous proteins contain approximately 40% sulfur-rich protein and are devoid of α -helix, while the matrix proteins contain 60% low-sulfur and a significant α -helical protein content.

The molecular weight of low-sulfur proteins has been estimated to be between 53 000 and 45 000, while for the sulfur-rich proteins it ranges between 10 000 to 28 000. The sulfur-rich proteins constitute an extremely heterogenous group with regard to molecular weight and composition and variations have been reported from species to species and with changes to nutritional status. The sulfur-rich proteins are found, in their native state, to be basic in character, while the low-sulfur proteins are found to be acidic [56].

The coiled coils of the low sulfur α -keratin are believed to be closely associated in a group of two or three to form a twisted rope called a protofibril. A still controversial number of protofibrils (believed to be nine) forms the microfibril (crystalline - α), which is embedded in the sulfur-rich amorphous keratin matrix [56-59]. Some authors propose that approximately 10 protofibrils constitute the microfibril [59], while others propose that groups of eight protofibrils assemble together to form microfibrils [60]. The microfibrils are arranged in a larger structural unit called a

This image is not available online. Please consult the hardcopy thesis available from the QUT library

Figure 1.4. Proposed biosynthetic pathway for eumelanin and pheomelanin.

macrofibril, which is tightly bound to the surrounding amorphous matrix by cystine linkages [56]. This matrix comprises the largest structural subunits of the cortex in human hair fibres. It contains the highest concentration of disulfide bonds, most of which are thought to be intrachain rather than interchain bonds because the matrix swells considerably when wet with water and mechanically resembles a lightly cross-linked gel rather than a highly cross-linked polymer. Cortical cells also contain pigment granules and nuclear remnants [56]. In human hair, the medulla occurs intermittently along a fibre and may be totally absent, suggesting that it no longer has any functional significance [59].

1.3.2. Chemical composition

The chemical composition of human hair consists of four different types of components:

1. Elements – the elements found in hair are mainly C, H, O, N, and S and at trace level include Ca, Mg, Sr, B, Al, Na, K, Zn, Cu, Fe, Ag, Au, Hg, Pb, Sb, Sn, W, Mo, I, P, and Se. The primary sources of the trace elements are from metabolic irregularities, sweat deposits and the environment [56].
2. Pigments – The colour of hair is derived from the secretory products of melanocytes. These products consist of a range of melanin pigments with different structures and compositions. There is substantial evidence to suggest that all pigments are biochemically related, arising from a common metabolic pathway in which dopaquinone is the key intermediate as shown in Figure 1.4. Two types of biogenetically related pigments are involved: eumelanin, giving dark

colour and pheomelanin giving light colours. The structure of eumelanins is still unclear, while pheomelanins are thought to consist mainly of benzothiazine and benzothiazole units derived from cysteinyl dopas [56, 59]. The graying of hair appears to be the result of gradual loss of tyrosinase activity during the anagen stage. Hair pigments will be further discussed in chapter 5.

3. Lipids – lipids exist in human hair either as free components or structural lipids. The latter are generally associated with the CMC and they still have not been fully characterised. The free lipid of human hair is primarily of sebaceous origin and its concentration is governed by several factors including androgens (which control the sebaceous gland activity), shampooing frequency, and by rubbing against objects such as combs, brushes and pillows. Free lipids exist both on the surface of hair and inside fibres and shampoos generally remove only surface lipids. The free lipid of human hair is chemically complex and it is primarily responsible for the condition known as oily hair. Free lipids consist of about 50% free fatty acids (saturated and unsaturated) and neutral lipids including triglycerides, free cholesterol, wax esters, paraffin and squalene [56].

4. Proteins - depending on its moisture content (up to 32% by weight), human hair consists of approximately 65% to 95% proteins [56]. There are 20 different alpha-amino acids commonly found in proteins and a representation of each is listed in Appendix I. All of these amino acids, except for proline, contain a free carboxyl group and a free unsubstituted amino group on the alpha-carbon.

This table is not available online. Please consult the hardcopy thesis available from the QUT library

Table 1.1 : Approximate composition of the amino acids found in untreated human hair

Table 1.1 shows the approximate composition of the amino acids found in untreated human hair fibres. The amino acids are divided into 6 different groups; (1) Hydrocarbon, (2) Hydroxyl, (3) Carboxylic acid, (4) Basic amino acids, (5) Sulfur containing group, and (6) Aromatic hydrocarbon group. The high amount of hydrocarbon-containing amino acids confirms that hydrophobic interactions are important controlling factors in the reactivity of hair towards cosmetic ingredients. Hydroxyl and amide groups interact through hydrogen bonding interactions, and the basic groups interact through hydrogen bonding and ion-exchange type interactions.

1.3.3. Secondary Structure of Human Hair Fibres

All mammalian keratins consist of filaments about 7 nm in diameter, embedded in a nonfilamentous matrix. Studies have shown that the filaments are composed of helical proteins (approximately 10 Å in diameter) of comparatively low cystine content (low-sulfur proteins) and are responsible for the characteristic α X-ray pattern as first proposed by Pauling and Corey [56]. Wide-angle X-ray diffractions (up to approximately 15 Å repeating units) of unstretched human hair and other keratin fibres (wool and porcupine quill) show several spacings, among which are equatorial spacing (perpendicular to the fibre axis) of 9.8 Å and meridional spacing (parallel to the fibre axis) of 5.1 and 1.5 Å. Pauling and Corey interpreted the 1.5 Å spacing to represent the distance between each amino acid residue, the 5.1 Å spacing to represent the repeat distance for coiling, corresponding to 3.6 amino acids residues and the 9.8 Å spacing to represent the centre-to-centre distance between each α -helix (approximately the diameter of the α -helix). A linear polypeptide α -helix would have a repeat distance of 5.4 Å units, so coiling of each helix was proposed to account for the shorter 5.1 Å meridional spacing. Further, it was suggested that 2 or 3 strands of polypeptides were coiled about each other analogous to a twisted rope. The structure has been routinely referred to as the “coiled coil” model. The model that is accepted for animal hair is the two-strand lope polypeptide, however the precise coiled coil is still unclear for human hair.

The right-handed α -helix is favoured by hydrogen bonding and Van der Waals forces while the left-handed form is less stable because the C α and carbonyl-oxygen atoms approach one another quite closely. Therefore the right-handed α -helix is the principal conformation of the polypeptide chains in α -keratin.

1.3.4. Physical Characteristics of Hair Fibres

The stress-strain behaviour of human hair was better understood after X-ray studies were carried out. It can be explained as the process of conversion of α -keratin, where the chains are arranged in compact pattern, to β -keratin, where the chains are completely unfolded.

This image is not available online. Please consult the hardcopy thesis available from the QUT library

A B C

Figure 1.5. Load elongation (stress-strain) curves for hair in water and at 65% relative humidity [56].

The A zone of the extension curve shown in figure 1.5 represents the α -form, which is homogeneously resistant to stretching. This resistance is mainly provided by hydrogen bonds that are present between the turns of the α -helix. The B zone represents the transition from α -keratin to β -keratin where the chains unfold without offering any resistance (Figure 1.5). The C zone shows the β -configuration's resistance to stretching. Stretching hair can produce splits and cracks in the

endocuticle and transverse cracks in the cuticle layers as well as damage in the cortex. The load value marking the start of the B section of the curve depends on the α -keratin. All factors diminishing this cohesion decrease the load value. For example, when hair is wet, the *yield region* begins at approximately half the load value for dry hair, as a result of the weaker hydrogen bonds and Coulombic interactions. Once the hair has been subjected to chemical treatments, the extent of stretching for both the A and B zones is increased and the load value for the transition from A to B is lowered [56].

1.3.5. Variation of hair fibre composition

The literature provides some evidence to suggest that genetically related factors, diet, cosmetic treatment and weathering may produce variation in either the actual contents or the determined contents of certain amino acids in whole human-hair fibres. Simmonds [61] has provided evidence to suggest that Merino wools differ in chemical composition among different sheep. A number of authors have extended this observation to human hair fibres [62, 63]. The following will provide a comprehensive discussion of the research carried out on human hairs.

1.3.5. (a) Chemical composition and race

Several attempts have been made to investigate whether there is any relationship between the chemical composition of human hair and race. Dekio and Jodi [63] estimated the concentration of fibrous and matrix proteins in Africoid, Caucasoid and Mongoloid hair. Head hair samples were collected from five male and female volunteers from each ethnic group and the hair samples were treated with urea and

TABLE 1.2

Ranges of amino acid composition of human hair of various racial origin ($\mu\text{mol/g}$) [61]

This table is not available online. Please consult the hardcopy thesis available from the QUT library

mercaptoethanol to reduce the disulphide bonds. Hair was then homogenized, and iodoacetic acid was added to homogenates which yielded S-carboxymethylated (SCM) protein derivatives. Finally, the SCM matrix and the SCM fibrous proteins were separated by centrifugation. The mean concentration of fibrous proteins was greater in Mongoloid hair (14.3 ± 0.8) in comparison to Caucasoid (9.2 ± 0.7) and Africoid (8.6 ± 0.8). However, the mean concentration of matrix proteins was highest for Africoid hair (46.0 ± 2.7) in comparison to Caucasoid (31.9 ± 1.3) and Mongoloid hair (32.9 ± 2.7). The ratio of fibrous to matrix proteins differed considerably between Africoid (0.18 ± 0.02), Caucasoid (0.29 ± 0.02) and Mongoloid (0.45 ± 0.03).

For years the elemental analysis of sulfur and nitrogen, supplemented later by the determination of cystine content, served as the only measure of human hair comparisons. Pioneering the field were Rutherford and Hawk [61] who carried out a comparative study of hair of different racial origins. Their work has suggested subtle differences in the relative percentages of various amino acids found in the hydrolysates of hair from African sources as compared to Caucasian ones. Wolfram [61] has compiled a more complete set of data from the literature of whole-fibre amino acid analysis that show a general overlap in the amounts of all the amino acids from the scalp hair for the three major racial groups; Caucasoid, Africoid and Mongoloid. Table 1.2 shows the ranges of the amino acid composition of human hair of the three major racial groups. The results include six separate studies by Simmonds (1955), Menakrt et al. (1966), Robbins and Kelly (1969), Wolfram and Lindemann (1971), Gold and Scriver (1971) and Wolfram and Yare (1978) [61]. Overall the authors suggested that even though there is a general overlap in the concentrations of the different amino acids between the three racial groups there are

some apparent differences for the concentrations of cysteic acid, half-cystine, glutamic acid, histidine, lysine, methionine and possibly tyrosine as illustrated in the highlighted region of Table 1.2.

In another study [56], the amino acid variance between samples of hair from five different female Caucasians was analysed. In total, 18 amino acids were analysed and nine of these indicated significant variance at the $\alpha=0.01$ level (Proline, Glycine, Alanine, Valine, Tyrosine, Phenylalanine, Cysteic acid, Histidine, and Arginine) and three amino acids at the $\alpha=0.05$ level (Half Cystine, Isoleucine, and Leucine). The authors concluded that a larger number of samples would show larger deviations. The differences found in these samples were attributed to weathering effects and other factors that control the relative ratios of the different proteins of the fibres. The study concluded that there is a possible variation of amino acids in the hairs from different individuals.

Elsewhere, it has been suggested [53] that studies based on the peptide bonds of the hair fibre will provide the best means of determining with certainty if any differences exist in the proteins of different races. Vibrational spectroscopic techniques enable the investigation of the amide peptide bonds and thus are a fundamental option for this type of analysis.

1.3.5. (b) Chemical composition and gender, colour and age

In a study by Clay et al. [56], hair from 120 different subjects were quantitatively analysed for cystine and cysteine. The hair in this study was selected from both males and females of varying age and pigmentation. Analysis was achieved by the hydrolytic method of Shinohara. The authors claimed that male hair contained slightly more cystine than female, and dark hair generally contained more cystine than light coloured hair. A similar relationship between the cystine content and hair colour has been reported by Ogura et al. [56]. Clay et al., have suggested that factors such as diet (malnutrition), cosmetic treatment, and environmental effects (sunlight degradation) may contribute to variations among these samples but they were not considered for this study. However, given the traditionally longer hairstyles for the female population, the potential for environmental factors affecting the results should not be overlooked. The weathering, or resistance to it, might also reflect in the positive correlation found between the intensity of fibre pigmentation and the cystine content of hair. No consistent relationship was found between age and cystine content.

1.3.5. (c) Weathering of hair

Weathering effects in human hair may be explored by comparing tip ends, which have been exposed longer to photochemical degradation than root ends. The photochemical degradation of cystine provides a major cause for variation in this amino acid found among individual samples. In a study by Tadokuro et al [56] the cystine and cysteine contents of tip ends were shown to be lower than in root ends. Complementary to these results, larger amounts of cysteic acid have been reported in hydrolysates of tip ends of human hair than in root ends clearly suggesting a conversion of the cystinyl groups in human hair to higher oxidation states by the elements.

1.3.5. (d) Effect of chemical treatment on hair

During the course of its cosmetic manipulations, hair often comes in contact with hydrogen peroxide (H_2O_2). This oxidant is the principal ingredient in bleaches, serves as an indispensable aid in oxidative hair colouring, and performs the disulfide rebuilding task in permanent waving.

With regards to protein and amino acid reactions, conventional bleaching products utilise hydrogen peroxide in alkaline media (pH 10 and above) and under such conditions the perhydroxy anion (HO_2^-) is the predominant reactive species and its attack on keratin appears to be centred on the disulfide bond. An estimate of the number of disulfide bonds broken by oxidising agents would indicate the extent of these reactions with the hair fibre. On average, 10-20% loss of cystine is likely to occur during bleaching, although in the case of hair frostings, as much as 50% of

disulfide bonds might undergo oxidative cleavage [56]. However, much less oxidation of cystine has been reported to take place during oxidative dyeing. In such cases, dye precursors take part to compete for available peroxide with the result that little of the agent is left to cleave the disulfide bonds. During bleaching, some of the keratin dissolves in the reaction medium. The weight losses are, however, small and even for extended treatment do not exceed 1% of the fibre weight.

Apart from cystine several other amino acids can also react under severe treatment conditions resulting in a decrease or increase of the concentration of the amino acids. In another study, wool fibres were oxidised for 24, 48 and 72 hours. There was a significant increase to the concentrations of cysteic acid from $19 \mu\text{mol g}^{-1}$ (untreated) to $321 \mu\text{mol g}^{-1}$ after 72 hours of treatment, with a corresponding decrease in the concentration of the disulfide bond from $486 \mu\text{mol g}^{-1}$ (untreated) to $292 \mu\text{mol g}^{-1}$. Other amino acids affected by oxidation included; alanine, arginine, half-cystine, glutamic acid, glycine, histidine, lysine, proline, serine, threonine, tryptophan, tyrosine and valine [56].

1.3.5. (e) Chemical composition and drugs of abuse

The most significant advantage of hair testing for drugs appears to be its unusually long detection window in comparison to other biological samples i.e., once drug is deposited in hair, it remains detectable for a period of months to years. However, a primary concern in hair testing is that the methodology should provide an objective means for assessing drug use by an individual [64]. Drug testing methods are biased if particular ethnic groups are predisposed to test positive more often in comparison to other groups. Presently, there is mounting evidence, which suggests that bias exist in

hair testing for drugs of abuse due to selective accumulation of drugs by particular hair types. Evidence indicates that the binding of drugs to Africoid and Mongoloid hair is substantially greater in comparison to Caucasoid hair [64, 65]. In addition, hair colour and cosmetic treatment also affect the binding of drugs to different hair types. Present data indicates that black hair binds more drug in comparison to brown and blond hair and that bleached hair binds more drug in comparison to untreated hair [64].

Table 1.3

FT-IR vs Dispersive IR

Advantages	FT-IR	Dispersive IR
Multiplex (Fellgett)	All frequencies are measured simultaneously i.e., all the wavenumbers of light are detected at once.	All frequencies are measured successively i.e., only a small wavenumber range at a time is measured.
Throughput (Jacquinot)	For the same resolution, energy throughput is higher than in a dispersive instrument. All the Infrared radiation passes through the sample and strikes the detector at once in an FTIR spectrometer. There are no slits to restrict the wavenumber range and reduce the intensity of infrared radiation that strikes the detector. Therefore, the detector sees the maximum amount of light at all points during a scan.	For the same resolution, energy throughput is lower than in a FT-IR instrument.
Connes advantage	He-Ne laser acts as an internal reference for each scan. The frequency of the laser accurately known and it is very stable. Therefore, the frequency calibration of the interferometer is much more accurate and has much better long term stability than that of dispersive instruments.	-----
Negligible stray light	Stray light is greatly reduced when compared to that of a dispersive instrument. This is because it is not modulated by the interferometer and thus does not contribute to the interferogram.	-----

PART III: VIBRATIONAL SPECTROSCOPY

The ability to perform non-destructive analysis on small and often unique samples by vibrational micro-spectroscopy has been utilised successfully by forensic scientist. The term vibrational spectroscopy is one that is becoming more frequently used to determine collectively the techniques of FT-IR, NIR and FT-Raman. All of which allow vibrational spectra (i.e. Raman or IR) to be obtained from small samples through adapted light microscopes. Sections 1.4 and 1.5 are an introduction to the theoretical aspects of FT-IR and Raman micro-spectroscopy, respectively.

1.4. FT-IR micro-spectroscopy

Fourier transform infrared microscope systems are becoming standard instrumentation in forensic laboratories around the world. The instrumental aspects of IR microscopes have been comprehensively discussed by Batrick [66] and Kirkbride [67].

The development of FT-IR spectroscopy in the late 1960's almost totally supplanted dispersive instruments, that were considered the bedrock of infrared analysis in the 1950's. Comparisons of FT-IR versus dispersive instruments have been discussed in the given references [66, 67] and a summary is presented in Table 1.3.

Since the introduction of FT-IR techniques coupled with microscope accessories, IR analysis has found new applications in the analysis of single fibres. FT-IR microscopy allows for rapid scan rates, multiplexing capabilities, and minimal sample preparation which have greatly reduced the time and effort required to obtain IR spectra of single fibres. In addition, the technique is essentially non-destructive

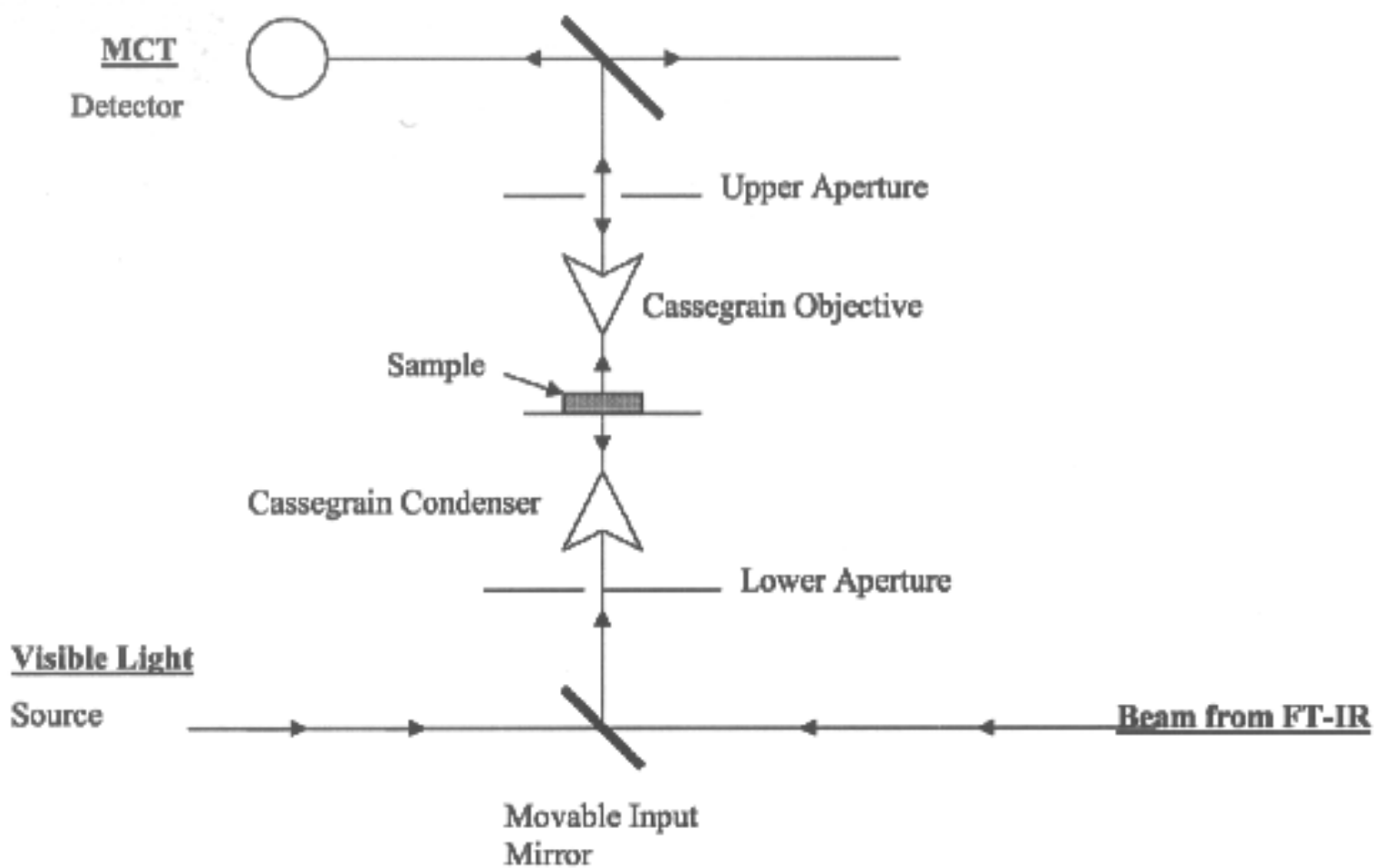


Figure 1.6. A schematic diagram of an FT-IR system.

because only a small portion of the fibre needs to be flattened. The components of an infrared microscope compare closely with those of the visual microscope. Both microscopes contain an illumination source, an aperture, a condenser, a specimen stage, an objective, an eyepiece and a detector. A schematic diagram of an infrared microscope is shown in Figure 1.6 and is not intended to represent any manufacturer's specific offering.

In basic terms infrared spectroscopy is the study of the interaction of infrared light with matter. When infrared radiation interacts with matter it can be absorbed, causing the chemical bonds in the material to vibrate.

The process begins with the infrared beam collected by a mirror after leaving the interferometer and is directed through a hole in the side of the spectrometer into the microscope. This beam allows the IR spectrum of the sample to be obtained. The condenser is the optic used in a microscope to focus light on the sample and the objective is used to collect light after it has interacted with the sample. These two optics are usually Cassegrain mirrors as shown in the diagram. After the objective there is an aperture, which is used to define the area whose infrared spectrum is going to be obtained. For many samples, as it is in the case of hair fibres, the size of the infrared beam is usually greater than the diameter of the sample. As a result some of the infrared beam is lost and thus does not interact with the sample. The upper aperture prevents spurious bands by keeping stray light away from the detector.

The infrared beam is brought to a focus by appropriate optics onto a detector. Two principle detectors are commonly employed in FT-IR spectroscopy. The first one is known as DTGS (deuterated triglycine sulphate) detector. This detector has a wide frequency range application and is suitable for most normal applications. The second detector is a liquid nitrogen cooled MCT (mercury cadmium telluride). This detector has faster response, higher sensitivity allowing faster scanning and considerably lower noise levels. In the current study, the detector of choice was the MCT detector.

The infrared microscope can be used in the reflectance or transmittance mode. Transmission samples suffer from what is known as the “thickness problem” [67, 68]. To let the right amount of light pass through, the ideal thickness of a sample needs to be adjusted between 1 and 20 microns. The advantage of collecting spectra in the reflectance mode is that the reflectance samples suffer less from a thickness problem and as such it is not necessary to flatten the fibre to quite the same degree as that when using the transmission mode [68]. However a disadvantage of collecting spectra in reflectance as opposed to transmittance is that a lot of the infrared beam is scattered by the sample and thus is not collected by the Cassegrain and never reaches the detector [69]. As a result the spectra are usually noisier than spectra collected in the transmission mode but an increase to the number of scans offers a reasonable signal-to-noise ratio that can usually eliminate this problem. In this work, the samples were collected in the transreflection mode so as to eliminate as much as possible the thickness problem of the hair fibre. In a study by Paris [70] the optimum number of scans for single human hair fibres was found to be 256. During reflectance, the sample is mounted on to a gold mirror, and the infrared beam is

bounced off the sample. The background sample is obtained by reflecting the light off a clean portion of the gold mirror.

Flattening the fibres prior to analysis offers several advantages [68]. Firstly, deviations from Beer's law are reduced because samples are more uniform in thickness, secondly the reduction in pathlength is important for fibres possessing high absorptivity, and finally the flattening increases the surface area of the sample available for analysis. This enhances the signal to noise ratio while reducing diffraction effects at the fibre edges. Thus, fibres may be flattened by any of the three following methods:

(1) Diamond Anvil Cell (DAC)

The DAC consists of two diamond windows (anvils), each embedded in the centre of a cylindrical piston used to stabilise the anvils until they are pressed together. The two anvil samples faces are of different sizes so as to facilitate the alignment of the sample. The smaller anvil sample with an approximate diameter of 0.5 to 1.0 mm is the effective aperture of the cell.

(2) Attenuated Total Reflectance (ATR) ZnSe crystal

ATR normally requires a considerable amount of sample, but spectra of quite small quantities have been obtained using the recent development of micro-ATR systems on an FT-IR. The internal reflectance element (IRE) usually used is made of ZnSe, with a penetration depth of 1 to 5 μm .

(3) Metallic hand-held roller.

One of the main disadvantages of the DAC and the ATR is that the transmission spectra obtained give an average picture of multiple fibres. Since more than two hair fibres are usually required, this can cause problems in forensic cases, where only very small amounts of sample are available. In a study, by Signori and Lewis [71] the three above methods for flattening the hair fibre were compared. The results showed that the ZnSe crystal technique is not particularly effective, because it provided results with poor reproducibility as only poor sample-crystal contact was achieved and the level of noise recorded was too high to allow accurate detection. The DAC enabled better sample-crystal contact and thus higher levels of transmittance were obtained. However, it was found to give sensitive and reproducible spectra only when seven to nine hair fibres were analysed at one time but did not provide reproducible spectra of single fibres. Another disadvantage of using the ATR and DAC cells is that the sample needs to cover the whole of the cell, otherwise spectra with the transmittance of the baselines greater than 100% may be obtained. This arises from the greater reflectance losses from the anvil faces when the cell is empty compared to that which occurs when a sample is present (due to a greater difference in index of refraction between air and diamond vs sample and diamond).

It has been suggested that the process of flattening the fibre in a DAC as well as in a ZnSe crystal can be sufficient enough to destroy any points of comparison arising from the secondary structure of the polymer [67, 68]. Although no major spectral differences have been reported as a result of applying pressure to the fibre samples, minor changes in peak frequencies, intensities and shapes do occur for certain fibres.

Hair is a soft enough sample to be flattened using a metallic hand-held roller so that we can eliminate to a certain degree the distortion of the secondary structure of the hair due to high pressure flattening methods such as ATR and DAC.

1.5. Raman micro-spectroscopy

Raman spectroscopy is a complementary technique to IR in terms of the spectral information each provides. Raman micro-spectroscopy, like FT-IR micro-spectroscopy is a technique whereby a conventional microscope is coupled to the Raman spectrometer, and permits analysis of very small fragments and particles. The optical layout of Raman microscopy is schematically very similar to the infrared microscope, the main difference being that there are two light sources, which have to be co-linear, and parfocal at the sample.

Like dispersive and Fourier Transform Infrared Spectrometers, Raman spectrometers have evolved in two different main technological paths; dispersive systems, which employ a monochromator for processing the signal, and FT system, which employ an interferometer with an analogous purpose. An excellent recent review on instrumentation for dispersive systems is given by McCreery [72] and for FT systems is provided by Hendra [73].

In the Raman experiment, the Raman shifted wavelength is usually backscattered 180° to the incident laser radiation. For this reason, virtually no sample preparation is required for many samples. Sample thickness and opaqueness for Raman measurements are irrelevant and those samples which are difficult to study by FT-IR

microscopy pose few problems for the Raman micro-spectroscopy. Similarly, samples containing water or in contact with glass can be measured readily by Raman micro-spectroscopy.

The source of light used in micro-Raman spectrometers is the laser, which enters the microscope through the epilluminator, and is then directed by a beamsplitter down the objective lens. The collection optics is composed of appropriate lenses configured to optimise signal detection. The objective lens of the microscope is used to focus the laser onto the sample so that the maximum intensity signal passes through the monochromator and also an aid to avoid laser-heating effects that may produce changes in the sample. The laser is focused by the microscope lenses to a diffraction-limited spot, which has a diameter of about 1 μm and a focal depth of about 1 μm . The signal analyser processor may be defined as an optical arrangement that allows making a frequency, or energy, decomposition of the signal. In the case of FT systems, the signal processor consists of a Michelson interferometer and a FT processor, while in the case of dispersive system the signal processor in a monochromator. After, this step, the processed signal reaches the detector. In the case of the dispersive systems, the detectors of choice are photomultiplier tubes (PMT) or charge coupled devices (CCD). PMTs are less sensitive but provide a very useful tool when the interest is focused on details of the peak line shape. CCD detectors, on the other hand, represent the modern technology in mutlichannel detection due to their low dark-noise signal and high-quantum efficiency which being wavelength dependent, may reach more than 80% in the case of thinned CCD detectors [74].

Raman spectroscopy is based on the inelastic scattering of monochromatic light from a material. When a material is illuminated with monochromatic light, most of the light is elastically scattered (Rayleigh scattering) at the same wavelength as the incident light. The interaction of light with vibrational/rotational motion of molecules causes a very small proportion of the incident light to be inelastically scattered (Raman scattered) at different wavelengths to that of the incident light. The vibrational spectrum obtained from Raman spectroscopy is complementary to that obtained from infrared spectroscopy, because of the different selection rules. IR absorption spectroscopy is based on changes in the dipole moment during molecular vibrations, whereas Raman spectroscopy involves a change in the polarisability.

The Raman band in a spectrum is separated from the Rayleigh band by the frequency of modulation of exciting photon by the molecule oscillator $\pm\nu$. The ratio of Stokes to Rayleigh can be expressed as $I_{St}/I_{Rayl} \approx 10^{-5}$. Therefore the Stokes Raman band is about 100 times weaker than the Rayleigh band [75]. The ratio of Anti-Stokes to Stokes can be expressed by the following equation:

$$I_{St}/I_{anti-St} = (\nu_0 - \nu)^4 / (\nu_0 + \nu)^4 \approx e^{-h\nu/kT} \approx 10/1 \quad \text{Equation 1.1}$$

According to equation 1.1 the intensity ratio $I_{St}/I_{anti-St}$ is determined by the ratio of populations of the vibrational energy levels, and strongly depends on temperature. Therefore, the anti-Stokes-line intensity increases (or the Stokes-line intensity decreases) as the temperature is elevated. At low temperatures (or room temperature), more of the molecules are at a lower vibrational-energy level than higher vibrational-energy levels. Thus, a large fraction of molecules will have Stokes-type transitions

than anti-Stokes transitions, and as a result the Stokes line will have higher intensity than the anti-stokes line [75, 76]. A conventional vibrational Raman spectrum therefore, consists of a series of Stokes emissions separated in frequency from the exciting radiation by the various vibration frequencies of the sample.

The selection rules for Raman activity of vibrations require that the molecular polarizability must change during the vibration, and the intensity of the Raman band is a function of the magnitude of the change in polarizability [77].

$$(\Delta\alpha/\Delta q)_0 \neq 0$$

Equation 1.2

where α = molecular polarisability,

q = the normal co-ordinates describing the motion of an atom.

The polarizability is related to the distortion of the electron cloud of a molecule in the presence of an electric field and is represented by the following equation [77]:

$$\alpha = \mu/E$$

Equation 1.3

where μ = induced dipole moment,

E = strength of electric field.

1.6. Conclusions

The current chapter aimed to review the chemistry and structure of hair keratin fibres. The literature indicates a certain degree of variation between hair fibres from different individuals within the same race and different races. It has been suggested that genetics, weathering (primarily sunlight exposure), cosmetic treatment, and diet (not the normal diets of healthy individuals, but protein-deficient diets) have a direct affect on the composition of the amino acids. Hair fibres are frequently encountered in crime scenes, and they are usually examined by microscopic methods of analysis. However, there are cases where such analysis can provide equivocal results. Since there is a varying composition of hair peptides, it may be possible to study such variation using vibrational spectroscopic methods. The results and discussion presented in this thesis will examine the possibility of matching and discriminating single scalp human hair fibres by FT-IR and Raman micro-spectroscopy.

REFERENCES –CHAPTER 1

1. Porter, J and Fouweather, C., An Appraisal of Human Hair as Forensic Evidence, *Journal of the Society of Cosmetic Chemists*, **26**, pp. 299-313, (1975).
2. Jones, D. N., The Study of Human Hair as an Aid to the Investigation of Crime, *Journal of Forensic Medicine*, **3**, pp. 55-63, (1956).
3. Robertson, J. An Appraisal of the Use of Microscopic Data in the Examination of Human Head Hair, *Journal of the Forensic Science Society News*, **22**, pp. 890-895, (1982).
4. Seta, S., Sato, H., and Miyake, B., Forensic Hair investigation, *Forensic Science Progress*, **2**, pp. 147-166, (1988).
5. Gaudette, B. D., Some Further Thoughts on Probabilities and Human hair Comparisons, *Journal of Forensic Sciences*, **23**, pp. 758-763, (1978).
6. Robbins, C. R., and Kelly, C. H., Amino Acid Composition of Human Hair, *Textile Research Journal*, pp. 891-896, (1970).
7. Wentrup-Byrne, E., Rintoul, L., Gentner, J. M., and Fredericks, P. M., *Mikrochim Acta*, **14**, pp. 615-616, (1997).
8. Brody, R. H., Edwards, H. G., and Pollard, A. M., Chemometric methods applied to the differentiation of Fourier-transform Raman spectra of ivories, *Analytica Chimica Acta*, **427**, pp. 223-232, [2001].
9. Gilbert, C., Kokot, S., and Meyer, U., Application of DRIFT Spectroscopy and Chemometrics for the Comparison of Cotton Fabrics, *Applied Spectroscopy*, **47**, pp. 741-747, (1993).
10. Thanasoulas, N. C., Piliouris, E., Kotti, M-S., Evrimidis, N., Application of multivariate chemometrics in forensic soil discrimination based on the UV-Vis

- spectrum of the acid fraction of humus, *Forensic Science International*, **130**, pp. 73-82, [2002].
11. Klemenc, S., In common batch searching of illicit heroin samples-evaluation of data by chemometrics methods, *Forensic Science International*, **115**, pp. 43-52, [2001].
 12. Krawczyk, W., Parczewski, A., Application of chemometric methods in searching for illicit Leuckart amphetamine sources, *Analytica Chimica Acta*, **446**, pp. 107-114, [2001].
 13. Khalil, W. A-S., Goonetilleke, A., Kokot, S., and Carroll, S., Use of Chemometrics methods and multicriteria decision making for site selection for sustainable on-sit sewage effluent disposal, *Analytical Chimica Acta*, in print [2003].
 14. Olson, D. L., Comparison of three multicriteria methods to predict known outcomes, *European Journal of Operational Research*, **130**, pp. 576-587, [2001].
 15. Smyth, F., *Cause of Death; The Story of Forensic Science*, Orbis Publishing, London, (1980).
 16. Martin, E. A., (ed), *A Dictionary of Law*, Oxford University Press, N.Y., 4th edition, (1997).
 17. Peterson, J. L., *Forensic Science: Scientific Investigation in Criminal Justice*, in **“Forensic Science a Symposium at the 168th Meeting of the American Chemical Society”** edited by Gould, R. F., American Chemical Society, U.S.A., pp. 127-136, (1975).
 18. Marriner, B., *On Death’s Bloody Rail*, St Martin’s Press, U.S.A., (1991).

19. Bisbing, R.E., Human Hair in a Forensic Perspective, Michigan State Police, Bridgeport Laboratory, Bridgeport. Washington University, Masters in Forensic Science-Lecture Materials, (1997).
20. DeForest, P. R., and Gaensslen, R. E., and Lee, H. C., **Forensic Science: An introduction to Criminalistics**, McGraw-Hill Book Company, U.S.A., (1983).
21. Saferstein, R., **Criminalistics: An Introduction to Forensic Science**, Prentice Hall, U.S.A., (1998).
22. Kirk, P.L., DeForest, P. R., Forensic Individualisation of Hair, *Criminologist*, **8**, pp. 35-45, (1973).
23. Bisbing, R. E., The Forensic Identification and Association of Human Hair, in Forensic Science Handbook, edited by Saferstein, R., Prentice Hall Regents Inc, U.S.A., (1982).
24. Kirk, P. L., Gamble, L. H., Human Hair Studies. Part II, *J. Crim. Law*, 31, pp. 627, (1940).
25. Robertson, J., Forensic Examination of Fibres: Protocols and Approaches – An Overview in “**Forensic Examination of Fibres**” edited by Robertson, J., Ellis Horwood Ltd, U.K., (1992).
26. Stafford Smith, C. A., and Goodman, P. D., Forensic Hair Comparison analysis: Nineteenth Century Science or Twentieth Century Snake Oil? *Columbia Human Rights Law Review*, 27, pp. 227-291, (1996).
27. Smith, S., and Linch, C., A Review of Major Factors Contributing to Errors in Human Hair Association by Microscopy, *American Journal of Forensic Medicine and Pathology*, **20**, pp. 269-273, (1999).

28. Lalonde, S. A., An Attempt at Determining Probabilities in Human Scalp Hair Comparison, *J. Forensic Sci.*, 33, pp. 884, (1988).
29. Dictionary of Science and Technology, Academic Press, (1992).
30. Hammond Barnhart Dictionary of Science, (1986).
31. Federal Bureau of Investigation (FBI), web page <http://www.fbi.gov/>, (2000).
32. State v. Williams, 1995 WL 324021 (Tenn.Crim.App. 1995)
33. McGrew v. State, 682 N.E.2d 1289 (Indiana Sp. Ct. 1997)
34. People v. Linscott, 142 Ill. 2d 22, 566 N.E.2d 1355 (1991)
35. State v. Fukusaku, 85 Hawai'i Sp. Ct. 462, 946 P.2d 32 (1997)
36. Suggs V State, 322 Ark. 40, 907 S.W.2d 124 (1995)
37. People v. Sutherland, 155 Ill.2d 1, 610 N.E.2d 1 (1993)
38. Bettelheim, F. A., March, J., Organic and Biochemistry, 3rd edition, Saunders College Publishing, (1998).
39. Kobilinsky, L., "Deoxyribonucleic acid structure and function – A Review" in *Criminalistics: An Introduction to Forensic Science*, edited by Saferstein, R., Prentice Hall, (1990).
40. Linch, C. A., Smith, S. L., Prahlow, J. A., Evaluation of the Human Hair Root for the DNA Typing Subsequent to Microscopic Comparison, *J. Forensic Sci.*, **43**, pp. 305-314, (1998).
41. Prahlow, J. A., Lantz, P. E., Cox-Jones, K., Nagesh Rao, P., and Pettenati, M. J., *Journal of Forensic Sciences*, **41**, pp. 1035-1038, (1996).
42. Isenberg, A. R., Moore, J. M., Mitochondrial DNA Analysis at the FBI Laboratory, *Forensic Science Communication*, **1**, pp. 1-9, (1999).

43. Wilson, M. R., Stoneking, M., Holland, M. M., DiZinno, J. A., Budowle, B., Guidelines for the Use of Mitochondrial DNA Sequencing in Forensic Science, *Crime Laboratory Digest*, **20**, pp. 68-77, (1993).
44. Allen, M., Engstrom, A-S., Meyers, S., Handt, O., Saldeen, T., Haeseler, A., Paabo, S., and Gyllensten, U., Mitochondrial DNA Sequencing of Shed Hairs and Saliva on Robbery Caps: Sensitivity and Matching Probabilities, *J. Forensic Sci.*, 43, (3), pp. 453-464, (1998).
45. People v. Castro, 545 N.Y.S.2d 985 (N.Y. Sup. Ct. 1989)
46. Castro, 545 N.Y.S.2d at 996.
47. Eric Lander, DNA Fingerprinting on Trial, 339, *Nature*, 501, 504 (1989)
48. Lewontin R. C. and Hartl D. L., Population genetics in forensic DNA typing, *Science*, **254**, pp. 1745, (1991).
49. Porter, J., Fauweather, C., Appraisal of Human Head Hair as Forensic Evidence, *J. Soc. Cosmet. Chem.*, **26**, pp.299-313, (1975).
50. Goulding, J., Elemental Analysis of Hair for Forensic Application – A Personal Journey in “Forensic Examination of Hair Fibres”, new edition Robertson.
51. Ballantyne, J., Tsui, P., and Yim, C. W., The ABO Groupings of the Hair Shaft as a Routine Casework Method presented at the “*International Association of the Forensic Sciences 10th Triennial Meeting*” in Oxford, UK., (1984).
52. Rodriguez-Calvo, M. S., Carracedo, A., Munoz, I., and Concheiro, L., Isoelectric Focusing of Human Hair Keratins: Correlation with Sodium Dodecyl Sulfate – Polyacrylamide Gel Electrophoresis (SDS-PAGE) Patterns and Effect of Cosmetic Treatments, *Journal of Forensic Sciences*, **37**, pp. 425-431, (1992).

53. Hopkins, J., Brenner, L., and Tumosa, C. S., Variation of the Amide I and Amide II Peak Absorbance Ratio in Human Hair as Measured by Fourier Transform Infrared Spectroscopy, *Forensic Science International*, **50**, pp. 61-65, (1991).
54. Brenner, L., Squires, P.L., Garry, M., and Tumosa, C.S., A Measurement of Human Hair Oxidation by Fourier Transform Infrared Spectroscopy, *Journal of Forensic Sciences*, 13, pp. 420-426, (1985).
55. Panayiotou, H., Masters Thesis, Vibrational Spectroscopy of Human Hair Fibres, Queensland University of Technology, (1998).
56. Robbins, C. R., **Chemical and Physical Behaviour of Human Hair**, Springer-Verlag, New York, (1994).
57. Fraser, R. D. B., MacRae, T. P., Conformation in Fibrous Proteins and Related Synthetic polypeptides, Academic Press, N.Y., (1975).
58. Zviak, C., *The Science of Hair Care*, Marcel Dekker, Inc, U.S.A., (1986).
59. Ryder, M. L., *Hair*, Edward Arnold, London, (1973).
60. Bolinski, R.C., *Modern Concepts in Biochemistry*, 5th edition, Allyn and Bacon, Boston (1987).
61. Wolfram, L. J., The Reactivity of Human Hair. A Review, in *Hair Research, Status and Future Aspects*, edited by Orfanos, C. E., Montagna, W., and Stüttgen, G., Springer-Verlag, Germany, (1981).
62. Jollès, P., Zahn, H., Höcker, H., *Formation and Structure of Human Hair*, Birkhäuser Verlag, Germany, (1997).
63. Dekio, S., and Jodi, J., Amounts of Fibrous Proteins and Matrix Substances in Hairs of Different Races, *J. Dermatol.*, 17, pp. 62, (1990).

64. Cone, E.J., and Joseph, R.E., The Potential for Bias in Hair Testing for Drugs of Abuse, in “Drug Testing in Hair” edited by Kiantz, P., CRC Press, U.S.A., (1996).
65. Kidwell, D.A., and Blank, D.L., Hair Analysis: Techniques and Potential Problems”, in “Recent Developments in Therapeutic Drug and Clinical Toxicology”, edited by Sunshine, I., Marcel Dekker, N.Y., (1992).
66. Batrick, E.G., and Tungol, M.W., Infrared Microscopy and its Forensic Applications in “Criminalistics: An Introduction to Forensic Science”, Prentice Hall, edited by Saferstein, R., U.S.A., (1998).
67. Kirkbride, K.P., The Application of Infrared Microspectroscopy to the Analysis of Single Fibres, in “Forensic Examination of Fibres”, edited by Robertson, J., Ellis Horwood, U.K., (1992).
68. Humecki, H.J., Practical Guide to Infrared Microspectroscopy, Marcel Dekker, U.S.A., (1995).
69. Smith, B.C., Fundamentals of Fourier Transform Infrared Spectroscopy, CRC Press, U.S.A., (1996).
70. Paris, B., Vibrational Spectroscopy of Human Hair with Forensic Applications, Honours Thesis, Queensland University of Technology, (1998).
71. Signori, V., Lewis, D.M., FTIR Investigation of the Damage Produced on Human Hair by Weathering and Bleaching Processes: Implementation of Different Sampling Techniques and Data Processing, 19, pp. 1-13, (1997).
72. McCreery, R.L., Instrumentation for Dispersive Raman Spectroscopy in “Modern Techniques in Raman Spectroscopy”, edited by Laserna, J.J., Wiley Publishing, U.K., (1996).

73. Hendra, P.J., Fourier Transform Raman Spectroscopy in “Modern Techniques in Raman Spectroscopy”, edited by Laserna, J.J., Wiley Publishing, U.K., (1996).
74. Jimenez-Sandoval, S., Micro-Raman Spectroscopy: A Powerful Technique for Material Research, *Microelectronics Journal*, 31, pp. 419-427, (2000).
75. Tu, A.T., Raman Spectroscopy in Biology: Principles and Applications, Wiley Publishing, U.S.A., (1982).
76. Hendra, P., Jones, C., and Warnes, G., Fourier Transform Raman Spectroscopy: Instrumentation and Chemical Applications, Ellis Horwood, England, (1991).
77. Schraefer, B., Infrared and Raman Spectroscopy: Methods and Applications, VCH, N.Y., (1995).

2

EXPERIMENTAL METHODOLOGY

2.1. Hair Sample Collection

Scalp hair fibres were randomly selected from different volunteers, whose general particulars such as gender, racial background, hair treatments and age were recorded. In total 136 different hair fibre samples were collected and a complete reference list is presented in Appendix II.

2.2. Hair Sample Treatment

The chemical treatment performed on the hair fibres studied in chapter 3 was done using a commercial hair bleaching crème (WELLA)¹. The hair samples were examined as received and not pre-treated (i.e., washed or cleaned) prior to dyeing. The portion of the hair closest to the middle of the hair fibre was used to prepare the tresses for bleaching.

Approximately one to two grams of hair was weighted on an analytical balance (Mettler PM400) to make each tress. The bleaching was performed at room temperature for 30 minutes, 1 hour, 2 hours and 5 hours in order to study the effect that normal (salon treatment times of 30 minutes) and extreme treatment times have on the secondary structure and amino acids of the hair fibres.

Initially, each tress was clipped onto an aluminium foil. The bleaching solution was applied on to the hair fibres by the use of a commercial hair brush. The brush was dipped into the bleaching solution and the excess crème was brushed on the side of the bowl. The crème left on the brush was then applied on to the hair tress in a downward direction with one stroke. The same procedure was repeated on the other side of the hair tress.

The hair tresses were then covered with aluminium foil and left depending on the time limit. The tresses were rinsed for one minute in warm distilled water (500 ml, 30°C) and were finally left to air dry for one week.

2.3. Animal Keratin Fibres

Animal keratin fibres were obtained from *cat's fur*, and *bird's feather (parrot)* represented the softer tissues, *cow* and *horse hair* represented the harder ones, while *human hair*, *wool* and *dog hair* represented tissues of intermediate thickness.

2.4. Sample Preparation for Spectroscopic Analysis

Prior to any experimental work, the hair fibres were pre-conditioned under standard conditions of humidity (65%RH) and temperature (22.2°C) for one week (Clayson IM1000R incubator).

FT-IR analysis of a single hair fibre begins by placing the fibre on a white laminated board and rolling it with a hand-held, stainless steel roller (ca. 5 mm diameter). The approximate diameter of the fibre prior to flattening was 34 µm. Once flattened the

¹ “Welloxon Special” (9% Creme peroxide) Ingredients; water purified, H₂O₂, Cetearyl alcohol and sodium lauryl sulphate, sodium phosphate, fragnace, phosphoroc acid, paracetamol.

long diameter of the now ellipsoid hair increases to greater than 100 μm so that a 100 μm aperture is sufficient for spectral collection.

Once flattened, the fibre was placed on a gold mirror and both ends of the fibre were secured on to the mirror with a double-sided adhesive tape. In this study a hand-held metallic roller was sufficient to flatten the fibres. In a study by Paris [1], Scanning Electron Microscopy (SEM) and FT-IR microscopy were employed to investigate the effect that different number of rolls have on the fibre sample. The results indicated that in order to produce spectra of good resolution with minimal damage to the fibre 10 rolls of the hair with a steel roller is satisfactory for obtaining the required thickness with minimal damage to the hair.

Raman spectroscopy does not require any specific sample preparation. A single hair fibre was placed on an aluminium slide and both ends of the fibre were secured on to the slide with a double-sided adhesive tape.

2.5. Spectroscopic aspects

A Perkin-Elmer FT-IR 2000 System spectrometer was equipped with a PE *i*-series infrared microscope and a mercury-cadmium-telluride detector (MCT), cooled with liquid nitrogen. A round aperture was used to obtain a spatial resolution of 100 μm . A spectrum of the gold mirror was collected as background and reflectance spectra (4000-400 cm^{-1}) were collected from one mounting of the sample, each spectrum being sampled from a different spot on the sample within the 100 μm aperture. Prior to collecting the spectra the sample was purged with helium for approximately 10

minutes. Others specification for sample collection included a spectral resolution of 8 cm^{-1} , 256 scans and a mirror velocity of 2 cm/s .

A Renishaw Raman system 1000 Microprobe equipped with 633nm and 780 nm lasers was used to collect spectra in the range between 4000 to 400 cm^{-1} . Spectra were accumulated for 8 scans with 60 seconds acquisition time for each scan.

2.6. Treatment of spectral data

The collected spectra were transferred to a floppy disc and converted into ASCII format using GRAMS_32, which baseline corrects (linear algorithm) the spectra, and samples the spectral intensity every four wavenumbers.

Prior to submitting the collected spectra for chemometrics, a number of pre-treatment techniques were employed. Pre-treatment refers to any mathematical transformation of the original data and the type of pre-treatment performed on a data set is dependent upon the context of the problem, the origin of the data, i.e. if the data is single source (coming from the same instrument) or multi-source (coming from a variety of instruments). In the current work, data is collected from a single source; the spectrometer. Therefore, the data pre-treatment techniques commonly employed in this case are:

1. The spectral data is systematically sampled every 4 cm^{-1} so as to fit into the 256 data column matrix available in Excel 5.0 for further work, and
2. Transformations of variables (standardisation) so as to make the variable (wavenumbers) of equal weight in an analysis.

The spectral region of 1750-750 cm^{-1} was selected because it contains the majority of typical FT-IR absorption bands for human hair-keratin. The spectral regions between 1750-750 cm^{-1} and 750 to 400 cm^{-1} were studied for the Raman experiments. The 251 spectral data points from the ASCII file were imported into an Excel 5.0 spreadsheet (256 column limit), and this matrix was double centred (y- and x-mean scaled). The double centred matrix was imported into SIRIUS (Version 2.3), for processing by chemometrics. This procedure aims to remove the effect of the 'size' component reflected by the first PC of the unpretreated data set.

2.7. Chemometrics methods of analysis

Several efforts have been made to reach an acceptable definition of chemometrics- often something along the lines of “how to get chemically relevant information out of measured chemical data, how to represent and display this information, and how to get such information into data” [2]. There are numerous methods for analysing chemical data, the most common ones include;

- (a) multivariate calibration,
- (b) structure-(re)activity modelling,
- (c) pattern recognition, classification, and discrimination, and
- (d) multivariate process modelling and monitoring.

Detailed theory of these methods has been discussed elsewhere [3]. Chemometrics has been applied in a wide range of investigations and some examples are given in the following references [4-7].

The following forms a discussion on the different types of chemometrics applied in the current study.

2.7.1. Principal component analysis (PCA)

PCA is a well-known pattern recognition method for data reduction and exploratory analysis of high-dimensional data [8]. The aim of PCA is to obtain a relatively small set of new latent variables, or principal components (PCs), that describe most of the variability in the data with minimal loss of information [9]. This can be achieved by transforming the original variables into orthogonal components, which are linear combinations of the original variables. Each component is characterised by scores that are projections of the objects (i.e. spectra) onto a particular component, and loadings, which reflect the contribution of a particular variable to a particular component. PCs are calculated such that the first component accounts for the greatest variation in the data while subsequent components describe progressively decreasing amount of variance. The loadings of PC1 commonly resemble the mean spectrum of all spectra, while loadings of subsequent PCs can indicate or highlight variations between the various spectra, but in all cases loadings plots should be regarded only as abstract spectra.

The number of PCs that can be extracted from a data set is the same as the number of original variables. However, not all of the PCs are significant. An approach to identifying the significant PCs is achieved by cross-validation which aims to estimate the parameters of the PC model after removing a single object from the data set and calculating a partial sum of squares error. This process is repeated for all the objects in the data set and the partial sums of squares for the prediction errors are summed to give a total prediction error. It is this error that determines the significance of the given PC, with significant PCs improving the prediction of the model.

PCA is particularly useful for visually displaying 2-dimensional information, the data being transformed into principal components by the following equation [10]:

$$PC^{rs} = a_{r1}x_{s1} + a_{r2}x_{s2} + \dots + a_{rn}x_{sn} \quad \dots\dots\dots\text{Equation 2.1}$$

Where PC^{rs} = score for object s on component r;

a_{r1} = loadings or weighting of variable 1 on component r;

x_{s1} = measured value of variable 1 on component s; and

n = total number of original variables

There are two main advantages associated with the application of PCA and these include [9]

- (i) no prior knowledge about the sample or variables, and
- (ii) the data structure is represented on as few latent variables as possible.

2.7.2. Soft independent modeling of class analogies (SIMCA)

SIMCA is a common supervised method of data classification method. Each selected class of objects is separately modelled by PCA, and the significant number of components for each model is extracted by methods such as leave-one-object-out-cross-validation. Residual standard deviations (RSD) are computed for a class as a whole and for each object. The former measures the mean distance between the objects of a class model, and the latter measures the orthogonal distance between the object and the class model. Assuming the residuals to be normally distributed, a critical F ratio for a selected level of significance may be estimated and this yields a critical distance (RSD), which defines the class boundaries. The RSD is computed for a class as a whole and for each object. The former measures the mean distance between the object of a class, and the latter measures the orthogonal distance between the object and the class model.

This RSD indicates how well an object is explained by a class [11]:

$$RSD_{|c|} = \left[\sum_{i=1}^{i=x_c} (e_{x|c|})^2 / (N_c - P - 1) \right]^{1/2} \dots\dots\dots \text{Equation 2.2}$$

Where $e_{x|c|}$ is the error of object x fitted to class model C;

N_c is the number of samples or objects of class C;

P is the number of principal components ; and

$RSD_{|c|}$ is the Residual Standard Deviation of class C

A model class is selected and the requirement for this is to contain a substantial number of objects. The objects of other classes are then fitted to the model class. A class distance can be obtained and it is an indication of the separation between the two classes. Values of less than one indicate a very small degree of difference, while values greater than three indicate that the classes are quite different [8]. In this work, the quantitative description of the visual differences observed during PCA, was further investigated using SIMCA.

2.7.3. Fuzzy clustering (FC)

Fuzzy clustering (FC) is a non-hierarchical classification method, which is well described by Adams [11]. Its application is relatively uncommon, and its properties as available through the SIRIUS (Version 2.3) will be outlined here. The aim of FC is to highlight similar objects as well as to provide information regarding the relationship of each object to each cluster [10]. With FC, the classification is performed with a membership function e.g. $m(x) = 1 - c|x-a|^p$ (a, c and p are constants). The user nominates the number of classes, and on processing the data, a membership value of 1 or less is assigned to each object. Membership values close to 1 indicate strong belonging to a class but those less than 1/n (where n is the number of clusters) have low or no association with a class. In addition, the exponent p may be varied between 1 and 3. Higher values of the exponent favour the fuzzy state of object membership, and if an object has a high membership value when p is large, then this object has a strong association with the class, i.e. robust membership. Conversely, if an object's membership is spread over several classes when p is low, then the object has what is commonly referred to as fuzzy class membership, i.e. the object has

properties of several classes [3, 11]. In contrast to PCA and SIMCA, where a reasonable number of objects are required for robust modelling, FC can compare as few as two objects. An advantage of a low p value (i.e. 1) is that it facilitates the distinction between the objects that clearly belong to one cluster and those that are members of several clusters.

2.8. PROMETHEE and GAIA

In the hair experiments carried out in this thesis, it becomes important to be able to investigate the response² of a given procedure. The above chemometrics methods PCA, SIMCA and FC although useful in the information they each provide, they do not allow selection and analysis of specific criteria.

Hair analysis is complex, and generally, there is a large amount of data generated which makes it difficult to evaluate. This problem can be overcome by the use of multivariate methods of analysis whereby large volumes of data can be processed for exploring and understanding relationships between different parameters. Multivariate ranking analysis can be used to evaluate the selected hair fibres with the aid of multicriteria decision-making methods (MCDM) such as PROMETHEE (The Preference Ranking Organisation METHod for Enrichment Evaluations) and GAIA (Geometrical Analysis for Interactive Aid), SMART (Simple Multiattribute Rating Technique) and ELECTRE III. The literature [12, 13] generally underlines the fact that ultimately the choice of methodology especially of procedures, which perform roughly comparably, rests with the decision maker. There are specific strengths and

² Response refers to the criterion used to evaluate the procedure.

weakness associated with each of the MCDM methods and it is therefore necessary to exercise care and judgement in selecting an appropriate method for a specific application. Researchers have investigated the problem of choosing a model to best suit a decision problem and there are a number of models to assist both the analyst and the decision maker to select the best method to be used. The following discussion presents some of the most current literature comparative papers dealing with multicriteria methods.

Salminen et al [14] compared three different types of MCDM methods, ELECTREE III, PROMETHEE II and SMART, specifically because of their suitability in the context of environmental decision-making. The authors found little difference in performance between SMART and PROMETHEE, with ELECTRE III proving to be the method of choice. The authors supported their decision by stating that ELECTRE III allows the possibility to have partially non-compensatory treatment of the problem and proportional thresholds for imprecise data in comparison to SMART and PROMETHEE. In a study presented by Oslon [13], three methods of multicriteria analysis, SMART, PROMETHEE and a centroid method (which is a version of SMART using swing weighting) were compared to statistically recording detailed performance characteristics of major league professional baseball. The study was intended to demonstrate how these methods of preference modeling work on data with precise measures and known outcomes. Olson suggested that all the methods have value in support human decision making and concluded by proposing that the relative accuracy of these three methods in a case of known outcomes results in PROMETHEE II and SMART to be equally accurate. Lerche et al [15], compared the partial order Hasse Diagram Technique (HDT) with some multi-criteria methods

including PROMETHEE, on the basis of external input i.e., on subjectivity and transparency. The authors presented a useful diagrammatic comparison of a number of different multi-criteria methods, including HDT, PROMETHEE, AHP and different versions of Monte Carlo methods for scientific based and public participation comparisons. On the basis of scientifically based analysis, the authors regarded HDT as best performing but placed PROMETHEE close to this method, and well above its possible alternatives such as NAIADE and ORESTE. Based on public participation, the authors rated AHP as the preferred method followed by the Monte Carlo version of AHP.

In this thesis, PROMETHEE (partial and complete) and GAIA were the selected multi-criteria methods for the analysis of the hair experiments, namely due to the availability of the Decision Lab software and also because both methods allow the optimisation of a number of different criteria which enables the analyst to investigate and evaluate the multi-variate data. It is of particular interest to note that PROMETHEE and GAIA have been discussed and developed [16] in detail for decades in the operation of research, but have only recently been introduced in the field of chemometrics [17, 18].

In this thesis, PROMETHEE and GAIA were applied for the analysis of three matrices consisting of animal and human keratin fibres. The primary aims of the PROMETHEE and GAIA work presented here are;

- (i) to provide ranking information necessary to discriminate between different types of keratin fibres (animal and human).

- (ii) to assess the parameters influencing the differentiation of the different types listed above;
- (iii) to explore the use of GAIA in the identification of the important criteria influencing the differentiation of the fibres.

Additionally, it was hoped to demonstrate how the combination of the well-regarded MCDM methods, PROMETHEE and GAIA, can contribute to the development of a methodology specifically designed for the study of keratin fibres.

Table 2.1

List of Preference Functions [19]

This table is not available online. Please consult the hardcopy thesis available from the QUT library.

2.8.1. PROMETHEE

PROMETHEE is a non-parametric multi-criteria decision making method which ranks a number of objects (or actions, in this thesis- keratin fibres) on the basis of a range of variables or criteria. For each variable, the user must indicate [16]:

- A preference function. A preference function $P(a, b)$ defines how much outcome a has to be preferred to outcome b .
- A global preference index (or ordering) $\Pi(a, b)$. The global preference index calculates the preference of experiment a over experiment b for all the criteria, i.e. top down (maximised) or top-down minimised.
- A weighting value.

The PROMETHEE procedure involves:

1. Transformation of the raw data matrix to a difference matrix.

For each criterion, the column entries, y , of the raw data matrix are subtracted from each other to create a difference, d , matrix.

2. Application of the preference function

For each criterion, the selected preference function $P(a, b)$ is applied to decide how much the outcome a is preferred to b . In the Decision Lab software (which is the chosen software in this study [19]), six choices for preference functions are available and are described in Table 2.1.

3. Calculation of an overall or global preference index, π

$$\pi(a, b) = \sum_{j=1}^k w_j * P_j(a, b) \dots\dots\dots \text{Equation 2.3.}$$

w_j = weightings

This relationship provides an overall or global index, π , for comparison of preference of object a over b .

4. Calculation of outranking flows

$$\varphi^+(a) = \sum \pi(a, x) \dots\dots\dots \text{Equation 2.4.}$$

$$\varphi^-(a) = \sum \pi(x, a) \dots\dots\dots \text{Equation 2.5.}$$

Positive outranking flow $\Phi^+(a)$ which expresses how each object outranks all other objects, and a negative outranking flow $\Phi^-(a)$ which states how each object is outranked by all other objects.

5. Comparison of outranking flows

PROMETHEE consists in pairwise comparisons of all the experimental results and leads to a partial preorder [16, 20]:

1. a outranks b if

$$\Phi^+(a) > \Phi^+(b) \text{ and } \Phi^-(a) < \Phi^-(b)$$

or

$$\Phi^+(a) > \Phi^+(b) \text{ and } \Phi^-(a) = \Phi^-(b)$$

or

$$\Phi^+(a) = \Phi^+(b) \text{ and } \Phi^-(a) < \Phi^-(b)$$

2. a is indifferent to b if

$$\Phi^+(a) = \Phi^+(b) \text{ and } \Phi^-(a) < \Phi^-(b)$$

3. a cannot be compared with b :

in all other cases where b does not outrank a (using rule similar to those in 1 above)

6. Calculation of net outranking flow

$$\Phi(a) = \Phi^+(a) - \Phi^-(a) \quad \dots\dots\dots \text{Equation 2.6.}$$

To establish a complete order, one calculates the net outranking flow Φ by subtracting Φ^- from Φ^+ . This full ranking eliminates incomparability and is therefore more efficient, however it becomes less reliable [16].

An outranking line diagram can be drawn for both the partial (PROMETHEE I) and complete (PROMETHEE II) pre-order to visualise the information and to support the decision maker.

2.8.2. GAIA

The geometrical analysis for interactive aid (GAIA) biplot plane displays graphically the relative position of the alternatives in terms of contributions to the various criteria. The GAIA plane is a powerful tool to identify conflicts between criteria and to group the alternatives. Both the criteria and the objects are projected on the principal components plane in a similar way to PCA. The longer a projector vector for a criterion, the more variance it contains. The aim of a criterion is to differentiate the objects, for example if the criteria vectors are oriented approximately in the same direction, they are correlated i.e. the preferences are similar. On the other hand, independent criteria are characterised by almost orthogonal vectors, and conflicting criteria have vectors in opposite directions. The decision vector, π , is composed of the weights, normalised to one, of the different criteria. This weight is considered to be the mean of the vectors of the different criteria. The projections on that vector follow the order of the complete ranking of PROMETHEE. It can therefore be interpreted as a decision axis for the complete ranking. If this axis is short the criteria are in conflict, the decision vector is nearly orthogonal to the principal components plane, and a good compromise is found near the origin. The decision power of the axis is therefore small in such situations. If the axis is long, the best locations will be those that are found in this direction and as far from the origin as possible [16].

The GAIA plane provides a δ ratio, which is expressed in percentage of the quantity of information preserved. In all cases, the plan chosen for the projection is the one, which maximises its pertinence. The plan is qualified as 'perfect' if it preserved

100% of the data during projection. Espinasse et al [20] proposed that all plans preserving at least 80% of information are usable.

2.9. Curve fitting discussion

2.9.1. Theoretical aspects

Curve fitting analysis is often used for the analysis of underlying peaks of vibrational spectra for both quantitative and qualitative investigations [21, 22].

Curve-fitting in this work was performed through a Gaussian-Lorentzian model. It is not within the scope of this thesis to present a detailed theory on the Gaussian-Lorentzian model. However, a brief introduction into the subject is discussed in the following part of this section.

Since the development of the Michelson interferometer, the theoretical basis for the shift and shape of spectral lines has been the subject of investigation [22]. Breene [23] discussed several physical reasons for the shift and shape of spectral lines including what is known as the Doppler effect, as well as natural and collision broadening. In low pressure gas-phase spectra, the shape of the absorption band is governed by the Doppler effect which leads to spectral peaks having a Gaussian profile given by:

$$I_G(\omega, \gamma) = h \exp - (\omega/\gamma)^2 \quad \dots\dots\dots \text{Equation 2.7.}$$

Where I is the absorbance intensity;

h is the peak height;

γ is the Gaussian width parameter;

ω is the centralised wavenumber ($\omega = \sigma - \sigma_0$);

σ is the wavenumber; and

σ_0 is the wavenumber at peak maximum.

As the pressure of the system is increased collision effects become important. In turn, collision broadening may exceed Doppler broadening and the shape of the spectral curve changes [22, 23]. Collision broadening gives rise to a Cauchy function, which is commonly referred to as the Lorentzian profile:

$$I_L(\omega, \lambda) = \frac{h}{1 + (\omega/\lambda)^2} \dots\dots\dots \text{Equation 2.8.}$$

Where λ is the Lorentzian width parameter and the remaining parameters (I , h , ω , σ , and σ_0) are defined above.

Prior to any curve-fitting analysis of the spectral data, it is important to consider two vital points:

- (1) Number of peaks, and
- (2) two other sets of parameters relating to these peaks; band shapes and half-widths.

The two latter parameters can be established either by assumption or by an optimisation procedure during the course of the calculations [22]. In the present instance, fitting was done with Gaussian-Lorentzian profiles of equal width. Maddams [22] has indicated that a goodness of fit criterion is required to assess the overall success of the curve-fitting and, hence, to show if any of the assumptions are

seriously in error. The goodness of fit criterion is presented in each of the discussion chapters (chapter 3-5).

Prior to any analysis of spectra, estimates of the number of peaks and their corresponding peak position were obtained from the literature [24, 25]. These parameters are optimised so that the differences between the fitted and measured spectra are minimised [21].

The following equation represents the optimisation used in the PEAKFIT software. This equation is referred to as the Least Squares Optimisation method and is aimed to minimise a function so as to obtain the best-fit [21]:

$$B = \sum_{i=1}^n W_i (E - M_i)^2 \quad \dots\dots\dots \text{Equation 2.9}$$

where B = minimum for best fit;

W = statistical weight;

E = experimental values; and

M= calculated values at the ith point.

Curve fitting has been previously applied to the study of keratin fibres [24]. A discussion of this paper is presented in chapter 3.

2.9.2. Curve fitting software

The collected FT-IR and Raman spectra from untreated and chemically treated hair fibres in chapter 4 (30 min., 1, 2, and 5 hours) were converted from spc files to prn files using GRAMS32. Curve-fitting was performed using PEAKFIT version 4.0 software.

REFERENCES – CHAPTER 2

1. Paris, B., **Vibrational Spectroscopy of Human Hair with Forensic Application**, Honours Thesis, Queensland University of Technology, (1998).
2. Beebe, K. R., Pell, J., and Seasholtz, M. B., Chemometrics: A Practical Guide, *Technometrics*, **41**, pp. 375-376, (1999).
3. Brereton, R. G., Chemometrics: **Application of Mathematics and Statistics to Laboratory Systems**, Ellis Horwood Ltd., London, (1990).
4. Gilbert, C., Kokot, S., and Meyer, U., Application of DRIFT Spectroscopy and Chemometrics for the Comparison of Cotton Fabrics, *Applied Spectroscopy*, **47**, pp. 741-747, (1993).
5. Wentrup-Byrne, E., Rintoul, L., Gentner, J. M., and Fredericks, P. M., *Mikrochim Acta*, **14**, pp. 615-616, (1997).
6. Panayiotou, H., and Kokot, S., Matching and Discrimination of Single Human-Scalp Hairs by FT-IR Microspectroscopy and Chemometrics, *Analytica Chimica Acta*, **392**, pp. 223-235, (1999).
7. Church J. S., and O'Neil J. A., NIR and Chemometrics: An Application in the Wool Industry, Contributed Article in *The Internet Journal of Vibrational Spectroscopy*, **3**, 1st edition, (1999).
8. Meglen, R. R., Chemometrics: Its role in Chemistry and Measurement Sciences, *Chemometrics and Intelligent Laboratory Systems*, **3**, pp. 17-29, (1988).

9. Albano, C., Dunn, W., Edlund, U., Johansson, E., Norden, B., Sjostrom, M., and Wold, S., Four Levels of Pattern recognition, *Analytica Chimica Acta*, **103**, pp. 429-443, (1978).
10. Adams, M. J., **Chemometrics in Analytical Spectroscopy**, The Royal Society of Chemistry, Cambridge, (1995).
11. Massart, D. L., Vandeginste, B. G. M., Deming S. N., Michotte, Y., and Kaufman, L., **Chemometrics: A Textbook**, Elsevier, New York, (1988).
12. Al-Shemmeri, T., Al-Kloub, B., Pearman, A., Model choice in multicriteria decision aid, *European Journal of Operational Research*, **97**, pp. 550-560, [1997].
13. Oslon, D. L., Comparison of three multicriteria methods to predict known outcomes, *European Journal of Operational Research*, **130**, pp. 576-587, [2001].
14. Salminen, P., Hokkanen, J., Lahdelma, R., Comparing multicriteria methods in the context of environmental problems, *European Journal of Operational Research*, **104**, pp. 485-496, [1998].
15. Lerche, D., Bruggemann, R., Sorensen, P., Carlsen, L., and Nielsen, O. J., A Comparison of partial order technique with three methods of mutli-criteria analysis for ranking of chemical substances, *J. Chem. Inf. Comput. Sci*, **42**, pp. 1086-1098, [2002].
16. Keller, H. R., Massart, D. L., and Brans, J. P., Mutlicriteria decision making: a case study, *Chemometrics and Intelligent Laboratory Systems*, **11**, pp. 175-189, (1991).
17. Kokot, S., Phuong, T. D., *Analyst*, **124**, pp. 561-569, (1999).

18. Kokot, S., King, G., Keller, H. R., and Massart, D. L., *Anal. Chim. Acta*, **268**, pp. 81-94, (1992).
19. Brans, J-P., and Marecshal, B., **How to Decide with PROMETHEE**, ULB and VUB Brussels Free Universities, pp. 1-5, (2000).
20. Espinasse, B., Picolet, G., and Chouraqui, E., Negotiation support systems: A multi-criteria and multi-agent approach, *European Journal of Operation Research*, **103**, pp. 389-409, (1997).
21. Vendeginste, B. G. M., and De Galan, L., Critical Evaluation of Curve Fitting in Infrared Spectrometry, *Analytical Chemistry*, **47**, pp. 2124-2132, (1975).
22. Maddams, W. F., The Scope and Limitations of Curve Fitting, *Appl. Spectr.*, **34**, pp. 245-267, (1980).
23. Breene, R. G., The Shift and Shape of Spectral Lines, Pergamon Press, N.Y., (1961).
24. Joy, M., Lewis, O. M., The Use of Fourier Transform Infrared Spectroscopy in the Study of the Surface Chemistry of Keratin Fibres, *J. Soc. Cosmet. Chem.*, **13**, pp. 249-261, (1991).
25. Akhtar, W., Edwards, H. G. M., Farwell, D. W., Nutbrown, M., Fourier-Transform Raman Spectroscopic Study of Human Hair, *Spectrochimica Acta Part A.*, **53**, pp. 1021-1031, (1997).
26. Hsu, S.L., Moore, W.H., and Krimm, S., Vibrational Spectrum of the Unordered Polypeptide Chain: A Raman Study of Feather Keratin, *Biopolymers*, **15**, pp. 1513-1528, (1976).

3

AN FT-IR AND RAMAN MICRO-SPECTROSCOPIC COMPARISON STUDY OF HUMAN HAIR FIBRES

The objective of this chapter is twofold; (1) To evaluate the use of Raman and FT-IR micro-spectroscopy techniques for the forensic sampling of hair fibres and to propose the preferred technique for future forensic hair comparisons, (2) To investigate, through a series of experiments, the effect of chemical treatment on the micro-environment of human hair fibres. Spectral data will be interpreted through the use of chemometrics and curve-fitting analysis of relevant spectroscopic bands. The research presented in this chapter will provide the foundation for the work leading to chapters 4 and 5.

3.1. Introduction

Infrared and Raman micro-spectroscopy are commonly employed vibrational techniques. Though complementary - in terms of the spectral information each provide – they are governed by different selection rules which often result in different complementary spectra for a given sample. While IR spectra are the result of absorption of radiation, Raman spectra arise from an inelastic scattering energy [1]. When a photon is scattered inelastically by a molecule, it may gain or lose energy and hence scattering is recorded at higher or lower frequencies. The frequency displacement from the exciting radiation corresponds to a characteristic molecular mode of vibration. Thus, bands that appear weak in the IR spectrum will be strong in the Raman spectrum and vice versa.

In order to make detailed vibrational band assignments, it is valuable to have both IR and Raman data. In the case of keratin fibres, the main-chain skeletal bands dominate the IR spectra, while the side-chain bands are the prominent features in the Raman spectra. References [2-7] illustrate the application of FT-IR to keratin fibres, while Raman studies have been sparse. This is mainly attributed to high spectral backgrounds encountered in the Raman spectra of most keratin samples due to factors such as impurities, fluorescence, difficult adjustments of sample position and alignment of optics, as well as the length of the experimental procedure [8, 9]. Fluorescence can often be avoided by using FT-Raman systems with 1064 or 780 nm lasers to irradiate the sample. However, sensitivity at these wavelengths is reduced but can be improved by the use of an excitation wavelength of 633 or 514 nm. Pigmented fibres have been found to suffer from fluorescence which is the dominant spectral feature [8, 9, 10].

Eventhough fluorescence can often be a major drawback when using Raman spectroscopy, the technique offers a number of distinct advantages over IR spectroscopy, some of which include:

- (i) in the Raman experiment, the Raman shifted wavelength are backscattered 180° to the incident laser radiation, and as a result no sample preparation is required for many samples, and
- (ii) Raman offers access to a lower range of vibrational frequencies compared to the mid-IR instruments.

3.2. Vibrational analysis of keratin fibres

In general, vibrational spectroscopy enables an assessment of the protein-polypeptide structure. The vibrations of these proteins can be categorized into three groups; the peptide bond, the polypeptide chain and amino acids. Certain groups can be studied through FT-IR and others by Raman spectroscopy, while some groups can be studied by either of the methods. A combination of the two techniques can provide a great amount of information with regards to the protein-polypeptide structure of the keratin being investigated. Sections 3.2.1.-3.2.3. provide a discussion of the peptide bond, the polypeptide chain and amino acids of the keratin fibres.

3.2.1. The peptide bond

The peptide bond is the most abundant bond within a keratin protein. It is formed by a condensation/dehydration reaction between the carboxy group of the first amino acids with the amino group of the second amino acids (figure 3.1).

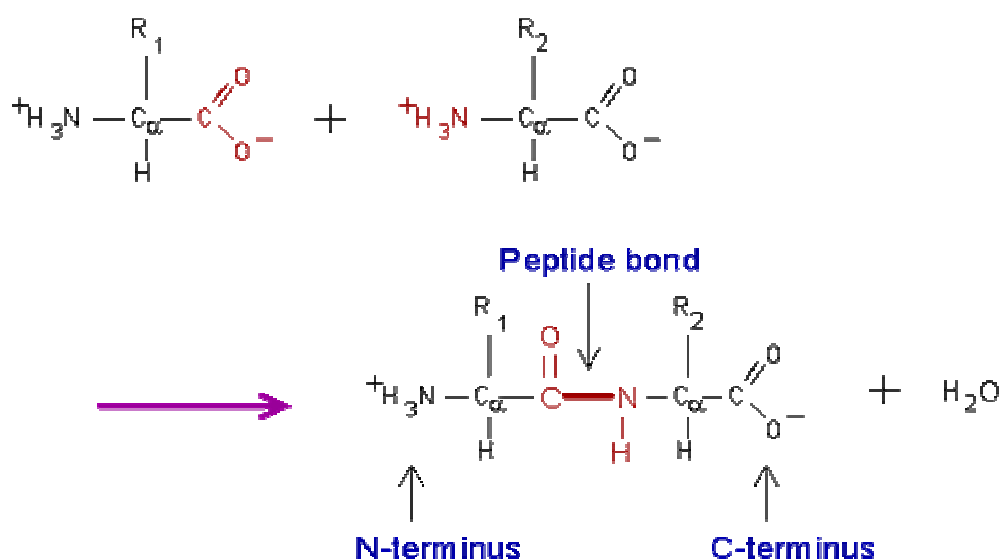
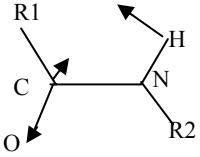
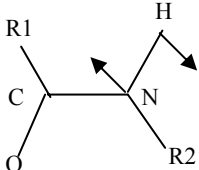
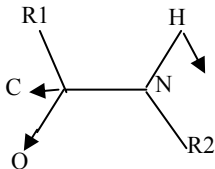


Figure 3.1. Peptide bond formation by a condensation reaction.

Table 3.1**FT-IR vibrational modes of naturally occurring keratin fibres**

		FT-IR Vibrations
Amide I		$\nu(\text{C}=\text{O})$ β -pleated sheet 1670 cm^{-1} $\nu(\text{C}=\text{O})$ random coil 1665 cm^{-1} $\nu(\text{C}=\text{O})$ α -helix 1655 cm^{-1} $\nu(\text{C}=\text{O})$ β -pleated sheet 1624 cm^{-1}
Amide II		$\delta(\text{N-H}) \nu(\text{C-N})$ α -helix 1550 cm^{-1} $\delta(\text{N-H}) \nu(\text{C-N})$ β -pleated sheet 1531 cm^{-1}
Amide III		$\nu(\text{C-N}) \delta(\text{N-H})$ random coil 1249 cm^{-1}
$\delta(\text{CH}_2)(\text{CH}_3)$		1454 cm^{-1}
Cystine oxides		$\nu_a(\text{S-O})$ cysteic acid 1170 cm^{-1} $\nu_s(\text{S-O})$ cystine dioxide 1125 cm^{-1} $\nu_s(\text{S-O})$ cystine monoxide 1075 cm^{-1} $\nu_s(\text{S-O})$ cysteic acid 1040 cm^{-1} $\nu_s(\text{S-O})$ cysteine-s-sulphonate 1024 cm^{-1}

The bond has an unusual property that has a marked effect on the rigidity of a polypeptide chain and consequently on the folding of the polypeptide chain. It has partial double bond character, which is caused by the resonance of electrons rapidly moving between the oxygen and nitrogen to make the C-N bond a partial double bond C=N. The consequence of this arrangement is that the peptide bond is very rigid because C=N is much less flexible than a C-N bond [11].

The vibrations of the atoms in this bond give rise to a number of distinctive vibrational bands and the frequencies of each bond depend on specific properties of its environment. Since the frequencies of these modes of vibration are sensitive to peptide conformation and the type of hydrogen bonding, they are often used in characterising the secondary structure of the peptide backbone [11]. Table 3.1 provides the band assignments for the characteristic modes of vibration of the keratin proteins in the FT-IR spectral region between 1750-750 cm^{-1} . This region is often referred to as the “fingerprint region” of the keratin fibre mainly because it contains the major amide bands, CH deformations and cystine oxides. The first amide band is referred to as amide I and represents primarily the C=O stretching vibration coupled to the in-plane bending of the N-H and stretching of C-N bonds. Amide I is a complex band and it can be either due to the coupling between two or more similar carbonyl stretching modes or the heterogeneity among the backbone carbonyl groups [11]. Such heterogeneity can arise either from intrinsic basic differences among carbonyls and/or from conformationally related differences in the strengths of the hydrogen bonds associated with the carbonyls [11]. Amide II, due to the coupled N-H in-plane bending and C-N stretching vibrations is strongly overlapped by bands originating from amino acid side chain vibrations and is a strong feature in the IR

Table 3.2

Characteristic band assignments for the different types of protein conformations for Amide I, II, and III [11]

This table is not available online. Please consult the hardcopy thesis available in the QUT library

Table 3.2.

Characteristic band assignments for the different types of protein conformation
for Amide I, II and III [12].

This table is not available online. Please consult the hardcopy
thesis available from the QUT library

while is weaker in the Raman spectra. The amide III mode is the in-plane combination of CN stretching and NH in-plane bending with contributions from the CC stretch and CO in-plane bend. The amide III band although highly sensitive to secondary structure, is weak in the infrared spectrum but strong in the Raman.

3.2.2. The polypeptide chain

The polypeptide chain is considered to be the backbone of keratin proteins. Keratin proteins are frequently classified on the basis of their x-ray diffraction patterns as α -, β -, feather and random coil. Such hard mammalian keratins are commonly found to give a characteristic α -pattern [12]. In contrast, hard avian and reptilian tissues give a characteristic pattern of reflections, which is quite different and is referred to as the feather pattern [12]. In some respects the feather-pattern resembles that obtained from the stretched mammalian keratin which Astbury designated the β -pattern [12]. The fourth pattern, given for example by the cuticle from animal hairs, is often described as random coil (or amorphous) [12]. Table 3.2 presents the FT-IR and Raman characteristic vibrations for the different types of protein conformations for amide I, II and III. In general, these structures are formed through intramolecular hydrogen bonding between the carbonyl oxygen of one peptide bond and the hydrogen atom of another. It has been reported [11, 13] that in the α -helical conformation, the interactions between amide groups are intrachain. The situation is quite different with β -sheets where the vibrations of the amide groups in adjacent chains are coupled through interchain hydrogen bonds.

The C-C skeletal backbone vibration is conformationally sensitive and is found at approximately 1448 cm^{-1} in both IR and Raman spectra. This band can be used in

conjunction with the amide bands for identification of various secondary structures [14]. Jurdana et al [14] calculated the ratio of Amide III (β sheet)/(CH₂)(CH₃) in an attempt to estimate the relative β -sheet structure of wool, hair and feather. This ratio will be discussed in greater detail in chapter 4.

3.2.3. Amino acids

In addition to the amide bands, vibrations associated with some of the amino acids can also be investigated through the use of Raman spectroscopy. The vibrations of these amino acids can be classified into two groups: the C-H vibrations, which originate from the CH₂/CH₃ groups and the vibrations, which originate from the aromatic rings of phenylalanine, tyrosine and tryptophan. A list of the amino acids and their structures appears in Appendix I. The present study will focus on the amino acids tyrosine, phenylalanine, tryptophan, histidine and cystine. Each of these amino acids will be discussed in greater detail in a later part of this chapter. It is important to note that this is the first time a detailed study of the behaviour of the above-mentioned amino acids during chemical bleaching of human hair has been carried out.

3.3. Chapter Objectives

The aim of the work presented in this chapter is twofold:

(a) To collect FT-IR and Raman spectra of untreated and chemically treated (at different time intervals) human hair fibres and to compare the spectral information obtained from each of the above-mentioned techniques; and

(c) To evaluate the use of Raman and FT-IR micro-spectroscopy techniques for the forensic analysis of hair fibres and to propose the preferred technique for forensic hair comparisons. The selection of the preferred technique will be based on criteria such as ease of use of the technique, sample preparation and universal application to different hair samples.

In this chapter, the spectra were initially interpreted visually and later through chemometrics methods of analysis and MCDM methods. Curve-fitting of the relative intensity areas of the major bands such as amide I, II, III (α -helix and β -sheet), CH_2CH_3 , and various amino acids such as cysteine, cysteic acid, phenylalanine, tyrosine, histidine and tryptophan, was also applied in an attempt to quantitatively monitor the changes during chemical treatment of hair fibres.

3.4. FT-IR Spectroscopy and Keratin Fibres

The following discussion presented in this section relates to the work published in the area of IR and FT-IR spectroscopy. As the research in this study is directly related to human hair fibres, the discussion will focus on the application of IR and FT-IR to human hair fibres. However given the chemical and morphological similarities between hair and wool keratin, reference will also be made to work published in the literature discussing wool fibres.

Two initial IR studies of keratin fibres were carried out by Weston [15] and Bit-Alkhas et al [16], who employed the KBr pellet technique to study the oxidation of human hair and wool. These authors were the first to report the formation of the 1040 cm^{-1} band due to the oxidation of cysteine to cysteic acid as a result of chemical treatment.

Baddiel [17] employed ATR to study the changes in the chemical composition of hair keratin with cuticle and cuticle-free hair fibres. Using a refractive index for hair of 1.55, the depth of penetration into the hair was calculated to be about $3.5\text{ }\mu\text{m}$ and thus the majority of the signal originated from the cuticle. The spectra of the hair containing the cuticle showed a band at 3470 cm^{-1} , which the author assigned to the H-bonded OH stretch of water residing in keratin. Cuticle-free hair contained the same band 40 cm^{-1} lower thus indicating a more tightly bound water structure in the cortex. Baddiel suggested that with the exception of arginine, side chains are unlikely to significantly contribute to the N-H vibrations in hair and the absorptions represent a mixed protein consisting, to a large extent, of helical and amorphous configurations. Therefore at 1578 cm^{-1} (COO^-), the absorption of hair containing the cuticle is less

than the cuticle-free hair. The cuticle was concluded to be composed primarily of α -keratin with a significant amount of β -keratin present, while the cortex was found to consist of α -keratin plus random coil or amorphous forms.

In 1983, Low and Severdia [18] employed FT-IR photothermal beam deflection spectroscopy (PBDS) to study the spectra of single human hair fibres. The hair was initially washed in an aqueous solution of soap and household cleaners, and then in water. The spectrum displayed several minor changes, which the authors attributed to the removal of body oils. The application of hydrogen peroxide to hair resulted in the formation of a relatively prominent absorption band near 1730 cm^{-1} , which appeared as a weak shoulder on the high frequency side of the 1750 cm^{-1} band. Fifteen years ago, Baddiel [17] had attributed the 1730 cm^{-1} band to the carbonyl-stretching band of free carboxyl groups belonging to glutamic and aspartic acids. Low and Severdia proposed that the presence of the 1730 cm^{-1} band indicates that treatment of hair by hydrogen peroxide results in the formation of some free carboxyl groups.

In 1985, Strassburger [19] employed FT-IR (DAC), to estimate quantitatively the oxidative damage of treated human hair by normalising the cysteic acid band against various keratin band intensities. The author supported the use of amide III as the internal standard due to its stability, while they found the amide I absorption to be less stable and often out of linear range. A linear relationship was found between the bleach concentration and the percent of sulfur oxidised to cysteic acid. The oxidative attack was proposed to be concentrated in the cuticle and outer cortical cells because cystine is more concentrated in the cuticle than in the cortex with very little found in the medulla. The author emphasised that a surface analysis method, such as internal

reflectance could determine the oxidation of sulfur in the entire hair and probably show higher levels of oxidation with more reproducible results.

In the same year, Hilterhaus and Zahn [20] employed the KBr technique to study the influence of permanent waving on the chemistry and structure of human hair. The spectra were normalised to amide I, which Strassburger [19] argued to be a sensitive band, due to the fact that it is influenced by the water deformation band, and should thus be used with great caution. In the untreated hair fibres an increase in oxidation of a hair fibre from the root to the tip was noticed, and was attributed to the photo-oxidative attack on the amino acid side chains. The authors noted the same behaviour in wool fibres and concluded that treated hair contained higher levels of cysteic acid than untreated hair.

Comparisons of IR microscopy, diffuse reflectance and ATR for examining oxidative hair damage was made by Joy and Lewis [5]. In this study, ATR/KRS-5 was found to be the least reproducible method, while diffuse reflectance spectra of fibres mixed with KBr produced very noisy spectra. Collection of spectra by IR microscopy in transmission mode allowed sampling of specific locations in a fibre whilst giving better spectra and was considered the best method of analysis by the authors. Six years later, Signori and Lewis [21], re-visited the affect that different methods of flattening have on the reproducibility of the spectra. Chemically treated hair fibres were flattened using ATR, Diamond Anvil Cell (DAC) and a metallic roller. IR spectra of hair were collected using the three different flattening methods and the spectra were compared. The authors proposed that the flattening of the fibres by a metallic roller yields reproducible spectra, whilst ATR was found to be non-

reproducible. DAC using 7-9 fibres yielded better results than the ATR, however the spectra were not as reproducible as those obtained from the metallic roller.

Bramanti et al [6], employed FT-IR micro-spectroscopy (DAC) in an attempt to distinguish between hairs in the three different phases; anagen, catagen and telogen. FT-IR micro-spectroscopy enables information to be obtained at the molecular level both with respect to the degree of hair ageing and alterations of cell differentiation due to exogenous and endogenous chemical and physical agents. The spectra showed remarkable differences in the bulb region near the root, possibly due to a major DNA content with respect to protein components. The authors investigated the 1080 cm^{-1} band, which is related to the DNA, and 1540 cm^{-1} band, which is related to the protein of the hair fibre, both of which are known to be of particular interest especially in the case of pathology samples. The conclusion was that the ratio of $A_{1080\text{ cm}^{-1}}/A_{1540\text{ cm}^{-1}}$ and the $A_{1080\text{ cm}^{-1}}/A_{1238\text{ cm}^{-1}}$ offer significant reproducible parameters for differentiating between the three growth stages of hair and thus providing an estimate of the degree of hair aging. The variations of these values are related to the structural changes accompanying the cellular differentiation proceeding from the bulb matrix to the shaft and also to modifications that occur in the different periods of a hair cycle.

Douthwaite et al [7] employed ATR spectroscopy to study the reaction of cystine residues in wool with peroxy compounds. The main product identified was cysteic acid, the presence of which highlights the instability of intermediate disulphide oxides under the peroxy treatment conditions. Four year later, Bradley and Mathieson [2] applied FT-IR spectroscopy to investigate the surface chemistry of wool during

different types of treatment. The authors concluded that wool fibres which have been subjected to either wet chlorine treatment or UV exposure have very strong intensity bands at 1040 and 1170 cm^{-1} due to S-O and SO_2 respectively, which are of much lower intensity in the spectrum from the untreated material.

FT-IR microscopy has been applied to cross and lateral sections of hair fibres, in an attempt to analyse for drugs of abuse [22]. By spectrally mapping infrared functional groups related to the various drugs, a three-dimensional image of the drug location could be obtained. This sample preparation technique eliminates the question of externally contaminated hair by analysing only that portion of the fibre that is formed within the root where ingested material would be transported. The results indicate a direct correlation between drug and medulla presence in the hair. Two theories of drug incorporation into the hair have been proposed; the more prominent one suggests that the drugs are taken up through the hair root, where the hair shaft is formed, with the drug binding to the medulla material. The second theory is less prevalent and states that the drugs are taken up from the exterior through the cuticle via perspiration, as in spiking. The spectral data has also shown that different drugs bind differently to the various hair materials.

Gniadecka et al [23], obtained near-infrared Fourier Transform Raman spectra of intact human skin, nail and stratum corneum. The authors suggested that the location of the amide I and III bands indicate that the majority of proteins in all keratin samples have the same secondary alpha-helical structure. It was further suggested that the position of the cystine band revealed a higher stability of the disulfide bonds in the hair and nail. The analysis of vibrations of CH groups showed that in hair and

nail, the proteins are highly folded and interact with the surroundings only to a small degree. The position of lipid specific peaks in the spectra of hair, nail and stratum corneum suggested a highly ordered, lamellar crystalline lipid structure.

FT-IR spectroscopy has also found applications to the forensic analysis of human scalp hair fibres. In 1985, Brenner et al [3] using FT-IR spectroscopy (DAC) monitored the cysteic acid absorption peak at 1044 cm^{-1} in hair samples from 135 Caucasian subjects. The authors stated that given the controversial nature of the current methods employed in the analysis of human hair, FT-IR spectroscopy might provide an alternative. This study suggested that a degree of discrimination between treated and untreated hair fibres is possible however variables such as normal hair colour, moisture, and age of hair sample were found to have little or no apparent effect on the results. Six years later, Hopkins et al [4], examined human scalp hair samples by FT-IR spectroscopy and the ratio of the amide I to amide II band absorbances was determined. The authors suggested that since amide I and II are characteristic of the peptide linkage and since there is a varying composition of hair peptides, the absorption ratio could be used to monitor variations that may arise in the hair fibres. Three to four sections were removed from the midpoint of the hair shaft and placed across the diamond window (2 mm diameter) and flattened. The authors concluded that the spectra showed little or no difference in the amide I/II band ratio that could be correlated to gender, age, hair colour or chemical treatment. The authors suggested that “if such differences do exist and can be detected by infrared spectroscopy, they must be more subtle than the simplistic technique used in this study”.

In 1994, Batrick et al [24] proposed that even though the IR spectra of hairs from different individuals are not readily distinguishable, the presence of hair spray or other coatings on hair can significantly increase the value of the evidence. ATR spectra were collected from cleaned hair and that coated with hair spray, and the difference spectrum of the two closely resembled that of the spectrum collected from hair spray. The authors concluded that further work is required to determine the compositional variation of hair sprays and thus to establish the capability to discriminate the spectra of different hair products.

3.5. Raman Spectroscopy and Keratin Fibres

The pioneers in the field of Raman spectroscopy and keratins were Lin and Koenig [25] who in 1975, published Raman spectra of wool in its natural state and that equilibrated in heavy water (D_2O). The spectra however, were not clearly resolved and no spectral information was provided in the $\nu(C-H)$ stretching region ($3400-2700\text{ cm}^{-1}$).

Raman spectroscopy is particularly useful in identifying natural textile fibres such as wool and cotton and synthetic fibres such as polyester and nylon [26, 27]. The technique has also been successfully used to determine the configuration of polypeptide chains of constituent proteins in feather keratin [28] and to investigate structural changes in wool fibres due to annealing [29].

Pande [30] obtained FT-Raman spectra of unpigmented hair and monitored the decrease in the disulphide band intensity at 510 cm^{-1} , upon weathering, bleaching and reduction with thioglycolate with a corresponding increase in cysteic acid at 1045 cm^{-1} .

In 1994, Hogg et al [8], employed FT-Raman spectroscopy to investigate the structure of scoured wool cloth and fibres subjected to hydrogen peroxide bleaching. The study indicated that FT-Raman spectroscopy could show structural changes in the fibres that are caused by chemical oxidative treatments. In the same year, Williams et al [9] published a paper, which discussed the different FT-Raman spectra of human keratotic biopolymers such as skin, callus, hair and nail. The principal structural dissimilarities were in the sulfur content of tissues containing hard keratin (hair and nail) and soft keratin (stratum corneum and callus). The authors concluded that the

hard keratins are rich in the sulphur-containing amino acid cysteine (ca. 7-8%), while the soft keratins contain little cystine (ca. 0.5%), but are glycine rich (ca. 23%) compared to hard keratins (ca. 5-7%).

A year later, Jurdana et al [14] employed a confocal laser Raman microprobe to monitor the degree of order/disorder in the secondary structure of wool, human hair and feather keratin. The amide III band at 1248 cm^{-1} was used as a marker for disordered protein along with bands at 1338 and 1313 cm^{-1} . The occurrence of the amide I band at 1656 was concluded to be consistent with a predominantly α -helical secondary structure. The authors used the ratio of the intensity of 1248 cm^{-1} band (amide III, β -sheet) to that of the relatively stable CH_2CH_3 bending mode (1447 cm^{-1}) to determine the secondary structure of wool, hair and feather keratin. The results indicated that feather samples mainly exhibit a β -sheet orientation, while wool and human hair showed an α -helical structure.

Akhtar et al [10] applied FT-Raman spectroscopy to study hair fibres before and after bleaching. In addition to changes in the disulfide and cysteic acid intensities, the authors also supported the view of a decrease in tyrosine for bleached hair along with changes in the relative intensities of the amide I and III bands, the methylene (CH_2) bending modes and deformation modes at $1300\text{-}1460\text{ cm}^{-1}$.

Rintoul et al [31] determined the orientation of the structures in the wool and feather samples using polarised Raman spectroscopy. The authors proposed an alpha helix orientation for the amide I band of the wool structure, while the feather samples displayed a β -sheet conformation.

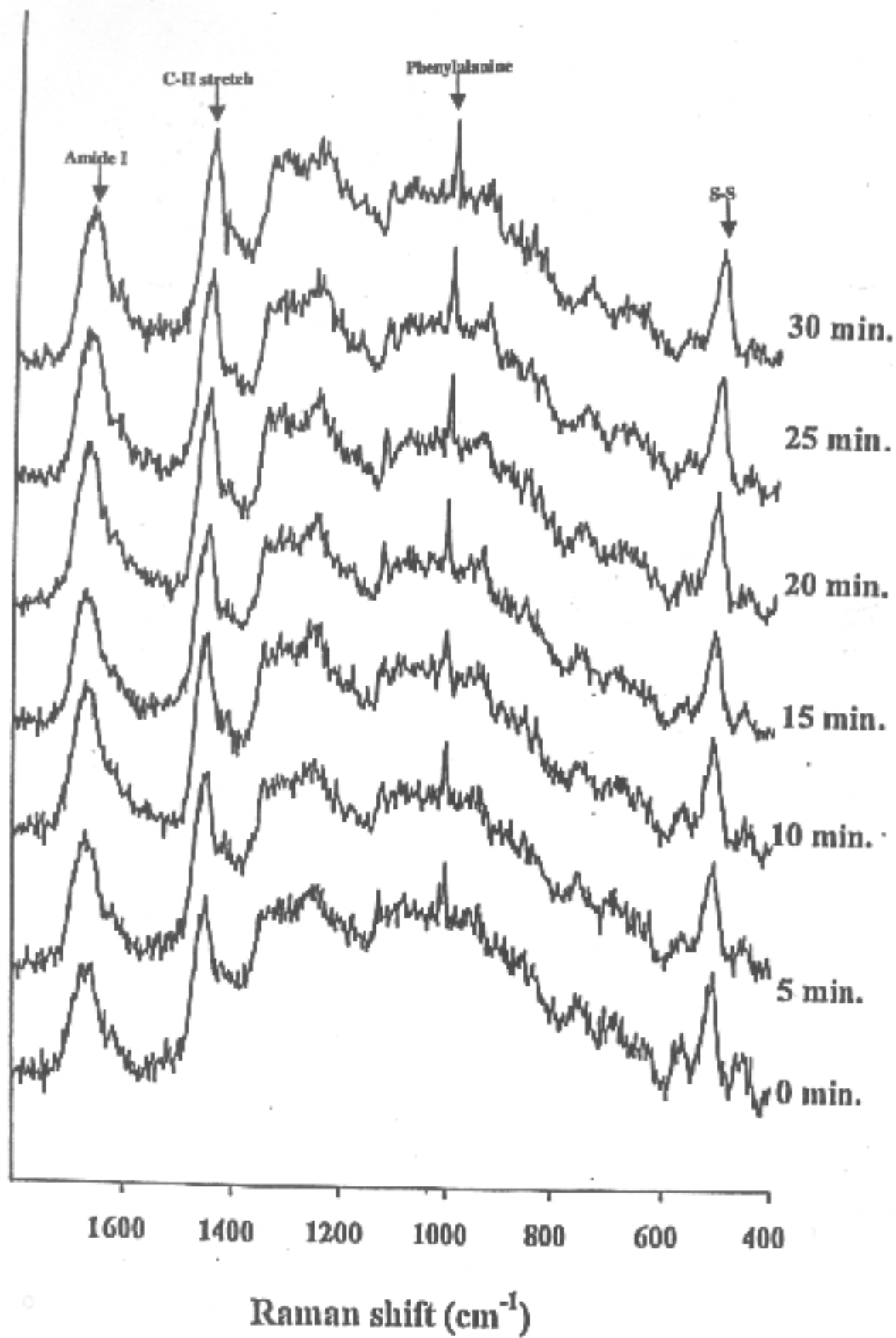


Figure 3.2. Raman spectra of a white untreated hair fibre after exposure to the 633 nm laser at different time intervals.

3.6. Results and discussion

3.6.1. Preliminary Studies

A major problem encountered in the conventional Raman technique is that of fluorescence which can totally swamp the weak Raman signal. This is particularly a common phenomenon when analysing biological materials such as in this case human hair.

Even though hair fibres are weak Raman scatterers [14], there are a number of possible ways of improving the signal to noise ratio of the spectra. These include increasing laser power and increasing measurement time. This is also known as ‘fluorescence quenching’ and involves the sample being irradiated with the excitation laser for a long period of time before collecting the spectra. After that, the fluorescence signal is eliminated or reduced to a tolerable level. However both increase in laser power and measurement time, can lead to an increase in the possibility of photodegradation. One of the objectives in this work was to investigate the stability of hair fibres to different types and amounts of laser irradiation and therefore establish the optimum spectral collection parameters for future work.

The initial investigation involved exposing a single white (non-pigmented) hair fibres from a male subject to the 633 nm laser source at different time intervals (Figure 3.2). On initial exposure certain characteristic Raman bands are visible, and include amide I (1670 cm^{-1}), C-H stretch (1448 cm^{-1}), aromatic ring breathing (1002 cm^{-1}) and S-S stretch (508 cm^{-1}). There is a slight decrease in fluorescence with increase in exposure time. The intensities of the vibrations associated with the aromatic amino acids (such as tyrosine (850 cm^{-1} and 830 cm^{-1}), phenylalanine (1005 cm^{-1}) and

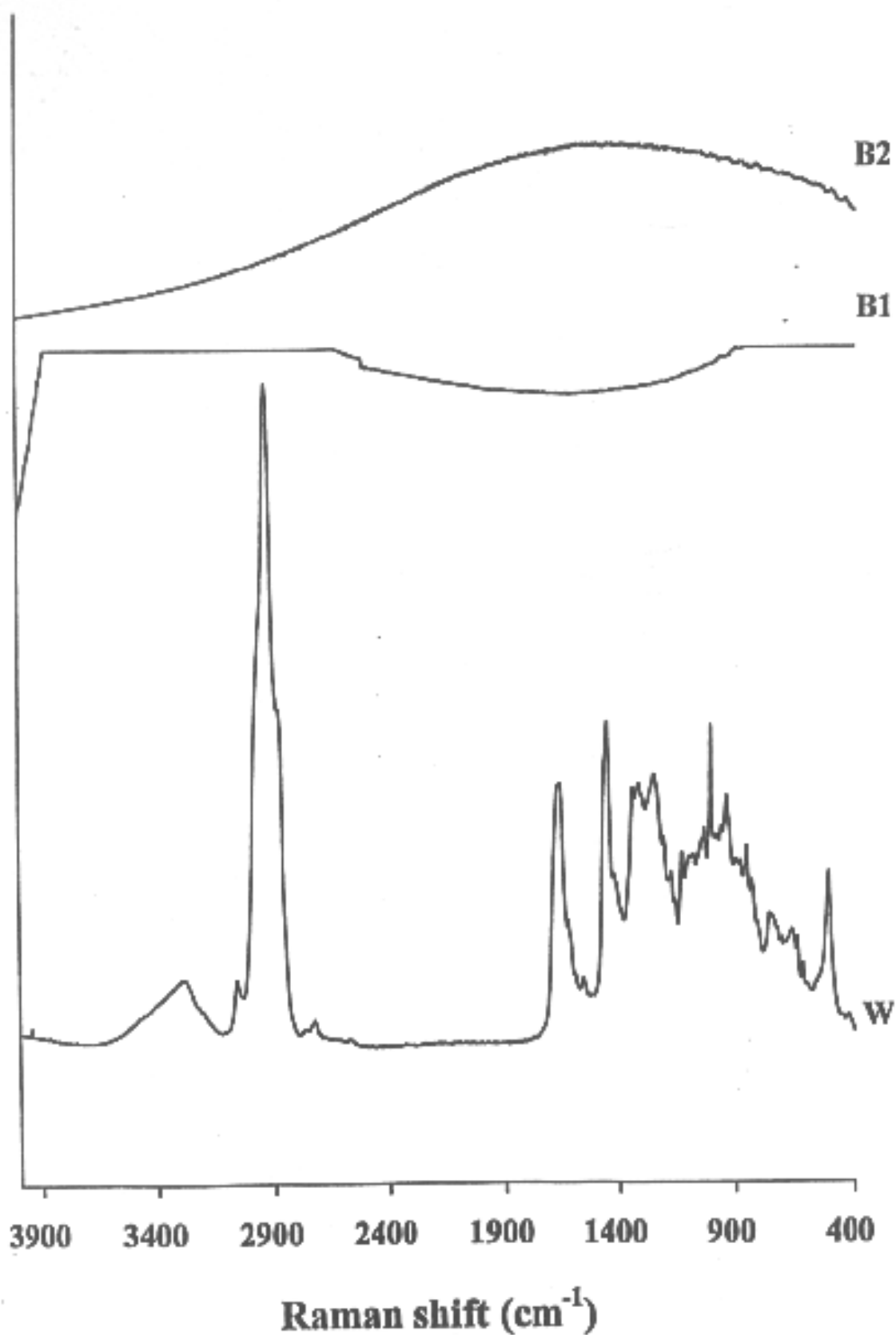


Figure 3.3. Raman spectra collected from white hair fibres (W), and black (B1) hair fibre using a 633 nm laser power. The B1 fibre was washed in a water/acetone mixture and the Raman spectra of thae fibre are shown as B2.

tryptophan (1340 cm^{-1}) do not decrease with increasing exposure time, indicating that the quenching of fluorescence is not due to degradation of the aromatic amino acids. The present experiment has shown that exposure of a hair fibre to the laser source for a period of 15 minutes is sufficient to produce Raman spectra of improved signal to noise ratio.

The next step was to establish the optimum experimental conditions for the collection of the Raman spectra. A number of different scans were used and a good signal to noise ratio was obtained at 8 scans accumulated for 60 seconds using a 633 nm laser power.

Reasonable Raman spectra (Figure 3.3) were obtained from non-pigmented hair (W). However, large background fluorescence did not allow spectral collection from pigmented hair fibres (B1). The hair was washed with a water/acetone (50:50) mixture so as to reduce the amount of lipids and/or other substances formed on the surface of the pigmented fibres, that might be contributing to the fluorescence of the hair. The spectra marked as B2 in figure 3.3 relates to the washed hair fibre. Comparison of this spectra with that of the unwashed fibre shown as B1 does not indicate any significant reduction in fluorescence. It thus appears that since the lipids and other substances formed on the surface of the hair have been eliminated as contributing factors to the fluorescence of the fibre in the Raman, the melanin pigment of the hair is the only remaining significant contributor in the fluorescence of the fibre.

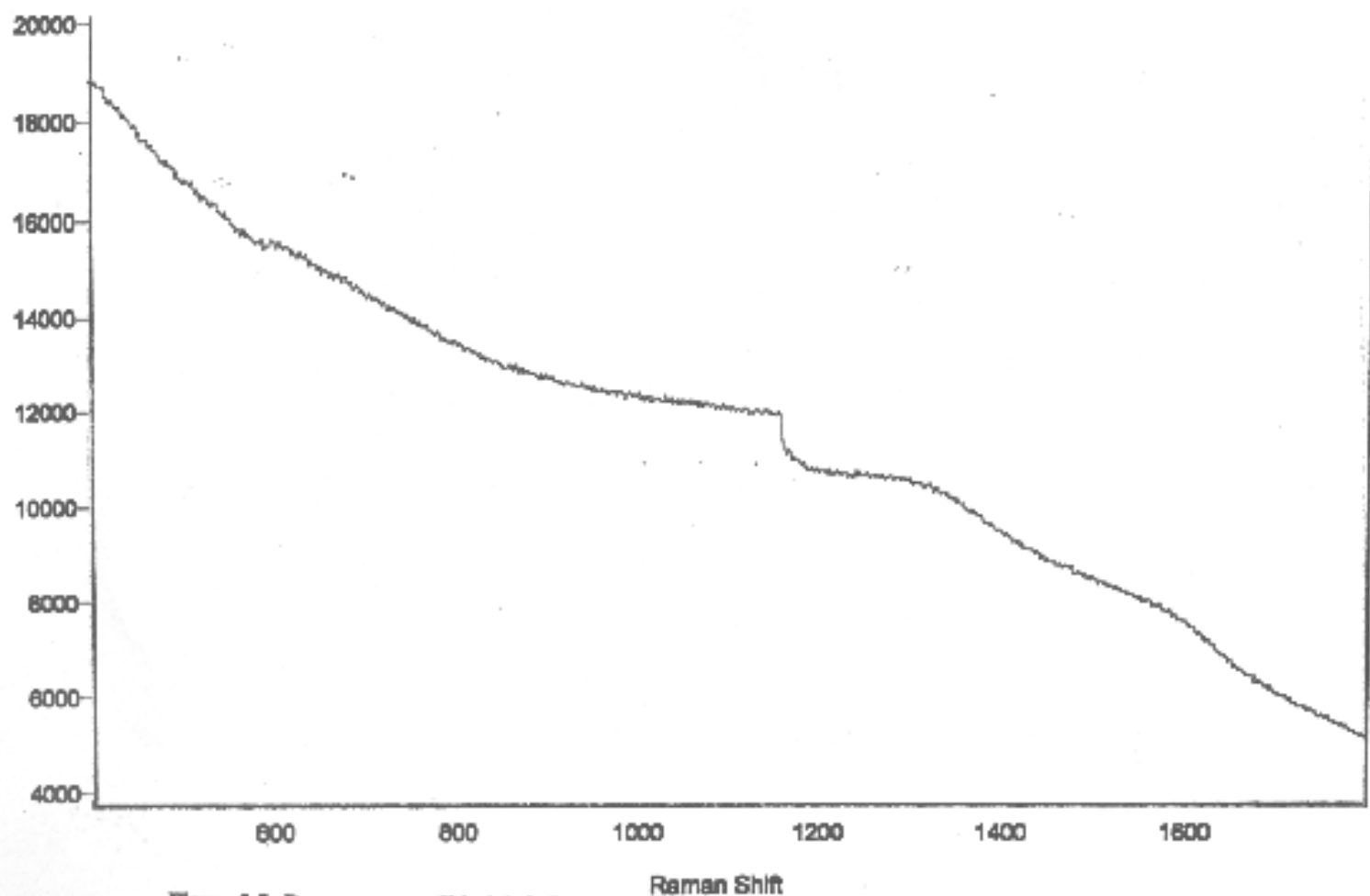


Figure 3.5. Raman spectra of black hair fibre collected after 10 minutes of burning out fluorescence using a 780 nm laser.

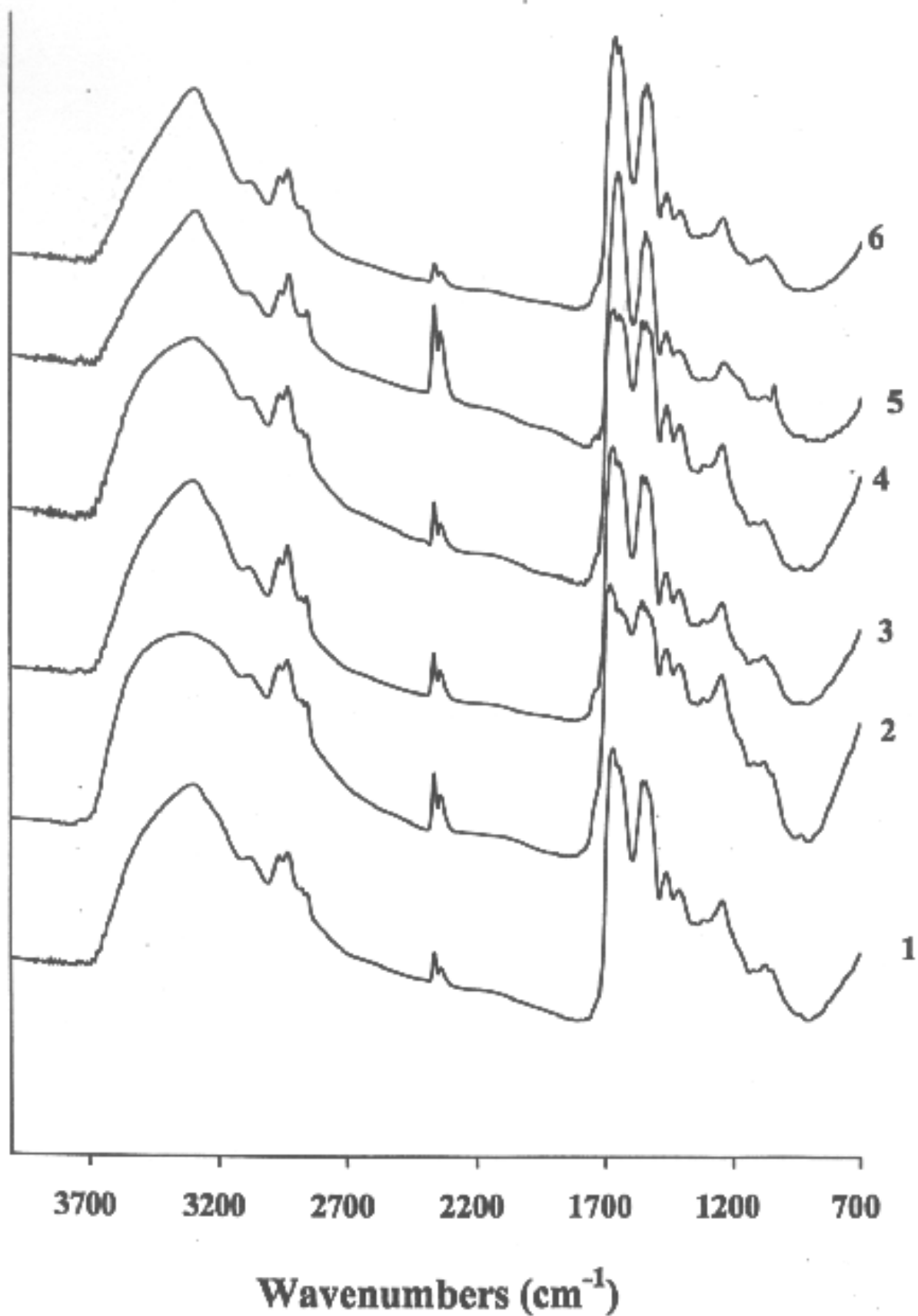


Figure 3.4. FT-IR spectra collected from subjects shown in table 3.3 in absorbance (4000-700 cm^{-1}).

FT-IR spectra, on the other hand, could be readily obtained from a wide range of pigmented hair fibres (Table 3.3) as shown in Figure 3.4.

Table 3.3

Background history of hair fibres used to collect FT-IR spectra

Subject	Gender	Race	Colour of Hair	Treatment
1	Female	Caucasian	Dark Brown	No
2	Female	Caucasian	Blonde	No
3	Female	Caucasian	Red	No
4	Female	Mongoloid	Black	No
5	Female	Caucasian	Blonde	Permanent Dyed and Permed
6	Male	Caucasian	Brown	No

Fluorescence in the Raman spectra can often be avoided by using a 780 nm laser to irradiate the sample. In the case of hair fibres the 780 nm laser resulted in spectra with slightly less fluorescence (Figure 3.5) than the 633 nm laser. However the spectral sensitivity at higher wavelengths was poor and it was still impossible to obtain spectra from anything else other than white hair fibres. It is therefore proposed that the suitable laser wavelength to obtain a Raman spectrum of a non-pigmented (white) hair fibre is 633 nm.

Overall, 40 different white hair fibres (2 different hair fibres from each subject) were examined from 20 different subjects (10 females and 10 males in the age groups of 30-65). It was observed that the time required to burn out the fluorescence varied between hair fibres collected from different subjects. In particular, it was found that age and gender influence the amount of time required to burn out the fluorescence. It was noted that white fibres collected from younger subjects (in the 30-35 age group)

took approximately double the time to burn out the fluorescence than older subjects (in the 50's and above age group). The appearance of gray and white hair fibres suggests an age-related exhaustion of the pigmentary potential of each individual hair follicle [32]. The transition of pigmented hair to non-pigmented (white) hair involves a dilution of the pigment over a period of time [32]. It thus follows that the white hair fibres from younger subjects still retain a certain amount of pigment (even though not visible), and thus require more time to burn out the fluorescence in comparison to the white hair fibres from the older subjects.

Spectral collection of white hair fibres from female subjects required more time to burn out fluorescence than white hair fibres from male subjects of the same age group. This could be related to the fact that the dilution of the pigments in the male hair fibres occurs in a faster rate than that of the female fibres [32]. These results are only preliminary and further research, using a larger number of samples, is required to establish the fundamental chemical reasons for the variation in the pigments and their relation to age and gender.

Work so far has established that the fluorescence associated with a pigmented hair fibre is a major limitation of Raman micro-spectroscopy and it thus limits the technique to the analysis of non-pigmented (white) hair fibres. As a result of the work presented so far, further Raman work presented in this thesis will be carried out on non-pigmented hair fibres only.

3.6.2. Comparison of FT-IR and Raman spectra collected from human hair

An example of an FT-IR and a Raman spectrum obtained from the same single hair fibre is shown in figure 3.6.

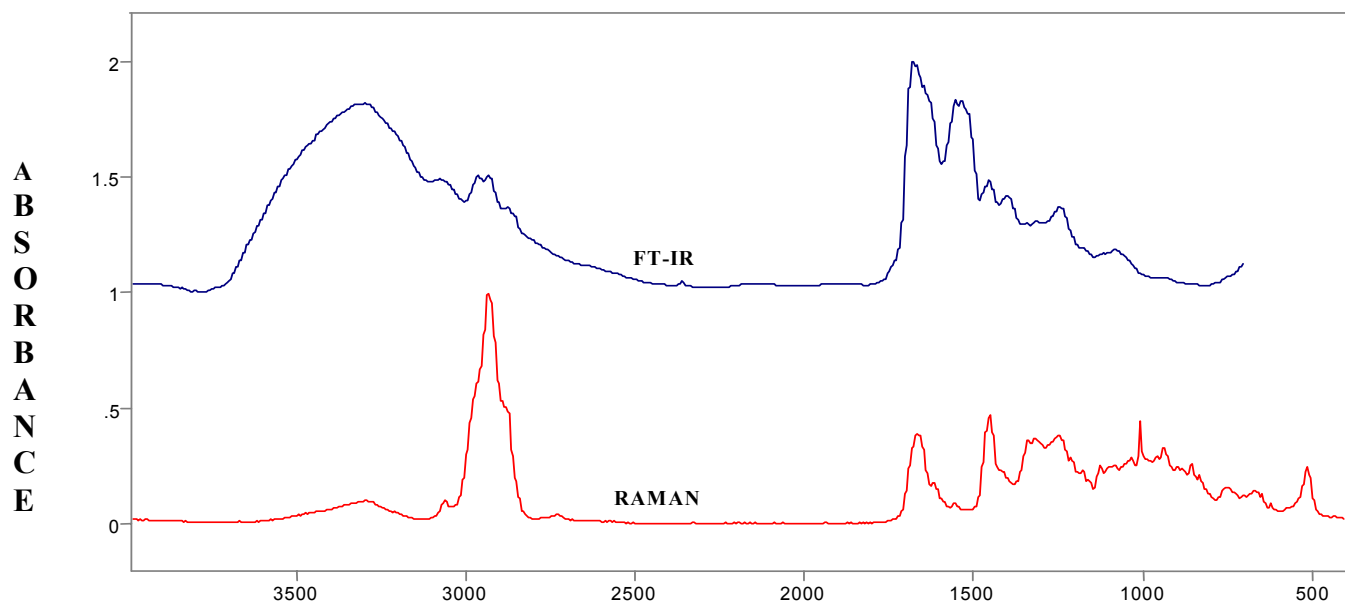


Figure 3.6. Comparison of an FT-IR and Raman spectrum of a single white human hair fibre.

In the FT-IR spectra the peak at approximately 3400 cm^{-1} is due to water and appears as a broad band that masks less intense features in this region. Amides A and B are found in the $3300\text{-}3050\text{ cm}^{-1}$ region as a Fermi resonance doublet and appear as very weak bands in both FT-IR and Raman. Spectral features in the $3100\text{-}2700\text{ cm}^{-1}$ region are assigned to the stretching modes of the C-H lipid alkyl chains. The methyl (CH_3) asymmetric and symmetric modes are observed at 2955 and 2933 cm^{-1} , respectively, and the methylene (CH_2) asymmetric and symmetric modes at 2875 and 2855 cm^{-1} .

The wavenumber region between $1700\text{-}1500\text{ cm}^{-1}$ contains the most intense features in the IR spectrum, arising from the -CONH- grouping, predominantly from protein

structures such as amide I and II bands at 1657 and 1547 cm^{-1} , respectively. The amide II band is much weaker at approximately 1540 cm^{-1} . Amide III appears as a weak band in the IR spectrum, while is more prominent in the Raman spectrum at approximately 1266 cm^{-1} .

Cis and trans amide bonds have different frequencies. In proteins all peptide bonds are in the trans form. In the case of human hair fibres, the presence of the amide I at ca. 1657 cm^{-1} (Table 3.4) indicates that the peptide bonds are in trans form.

Table 3.4

Vibrational Assignments of Cis- and trans-forms [34]

This table is not available online. Please consult the hardcopy thesis available from the QUT library

The region between 1500-1200 cm^{-1} contains several bands of medium and strong intensity in the IR and weaker in the Raman. Here, the bands have been assigned as $\delta(\text{CH}_3)$ modes around 1470-1350 cm^{-1} and $\delta(\text{CH}_2)$ wagging modes at 1250 cm^{-1} . Lipid material extracted from the surface of wool and hair fibres is known to consist of a considerable proportion made up of free fatty acids. Internal lipids in wool and hair fibres consist mainly of free fatty acids, cholesterol, triglycerides and other wax esters. It has been suggested that the cell membrane complex in hair and wool consists on average of 15% lipids (based on total fibre weight) [33]. The major lipids present in the cell membrane complex of wool and hair are similar to those found in

membranes of keratinised human stratum corneum. In the former, multiple lipid bilayer structures have been found, whereas in the cell membrane complex of wool and hair only two lipid bilayers are present; lipid $\nu(\text{C-C})$ at 1128 cm^{-1} which broadens between 1031 and 1126 cm^{-1} , and indicates the presence of several spectral features of different conformation in this region.

In the FT-IR spectra, the region between 1200 - 400 cm^{-1} contains one of the most important bands, which is attributed to the cysteic acid vibrations at 1040 cm^{-1} . This band has been extensively studied in the literature [3, 5, 7] to monitor the degree of chemical oxidation of the fibre during chemical treatment. This region also contains other bands such as the cysteic monoxide and cysteic dioxide vibrations at 1071 and 1121 cm^{-1} , respectively.

For the Raman spectrum some critically important skeletal molecular information is contained in the spectral region between 1200 - 400 cm^{-1} and bands attributable to cis-, trans-, and random conformation of the CCC backbone of lipids are identifiable [34]. A relatively weak feature in the Raman spectrum that is absent in the IR spectrum is the $827/850\text{ cm}^{-1}$ doublet, which is attributed to CCH deformations. The weak C-S stretching bands at 621 and 643 cm^{-1} are due to phenylalanine (624 cm^{-1}) and tyrosine (644 cm^{-1}) aromatic side chains, which are two of the amino acids constituting the polypeptides of hair fibres. It has been suggested that these two Raman vibrations together with the position of the amide I (1652 cm^{-1}) and amide III (1274 cm^{-1}) bands indicate that hair proteins exist predominantly in the α -helix conformation but may also contain some unordered protein element [23]. In the lower wavenumbers of this

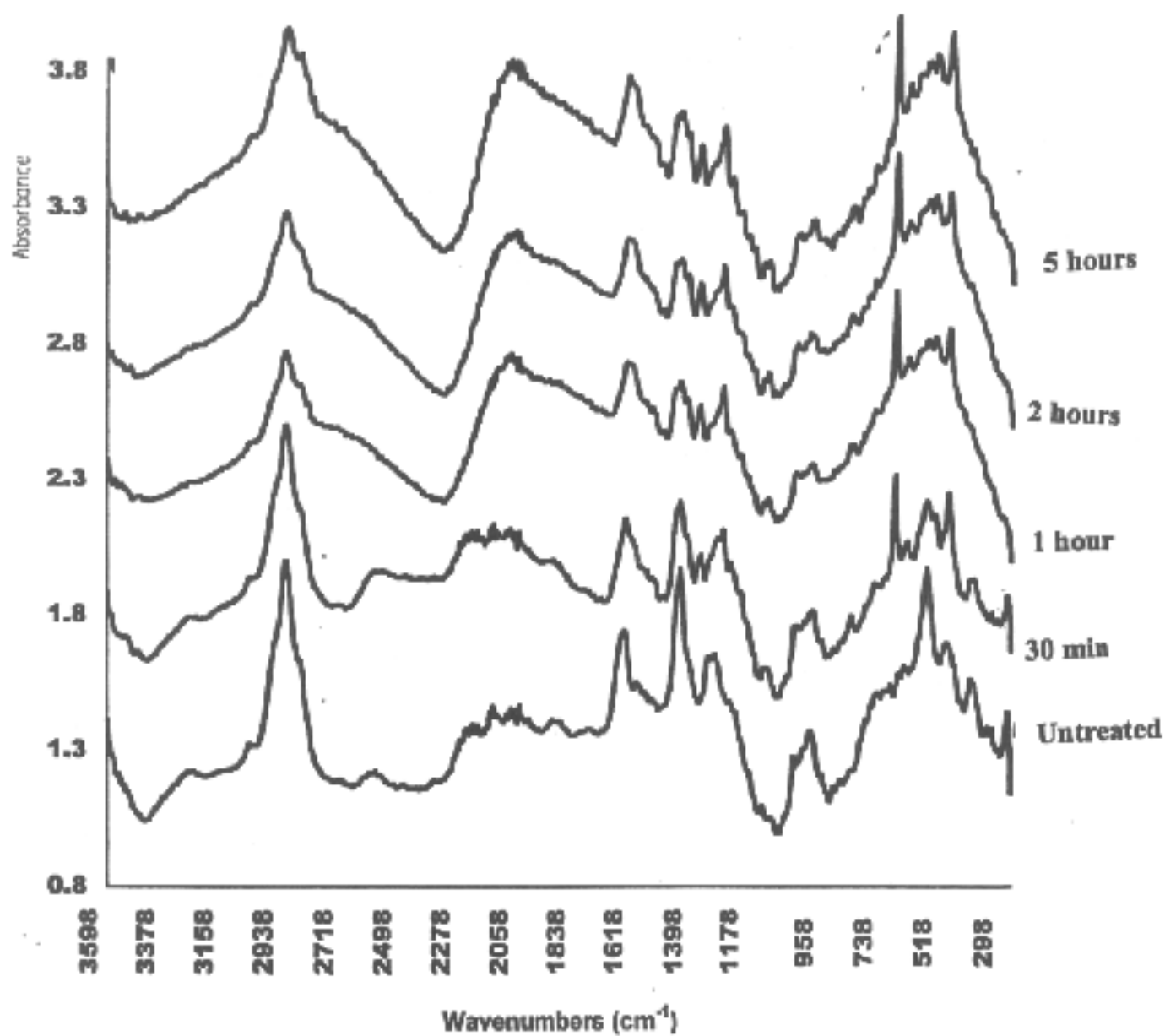


Figure 3.8. Raman spectra for human hair fibres treated at different time intervals ($3400\text{-}400\text{ cm}^{-1}$)

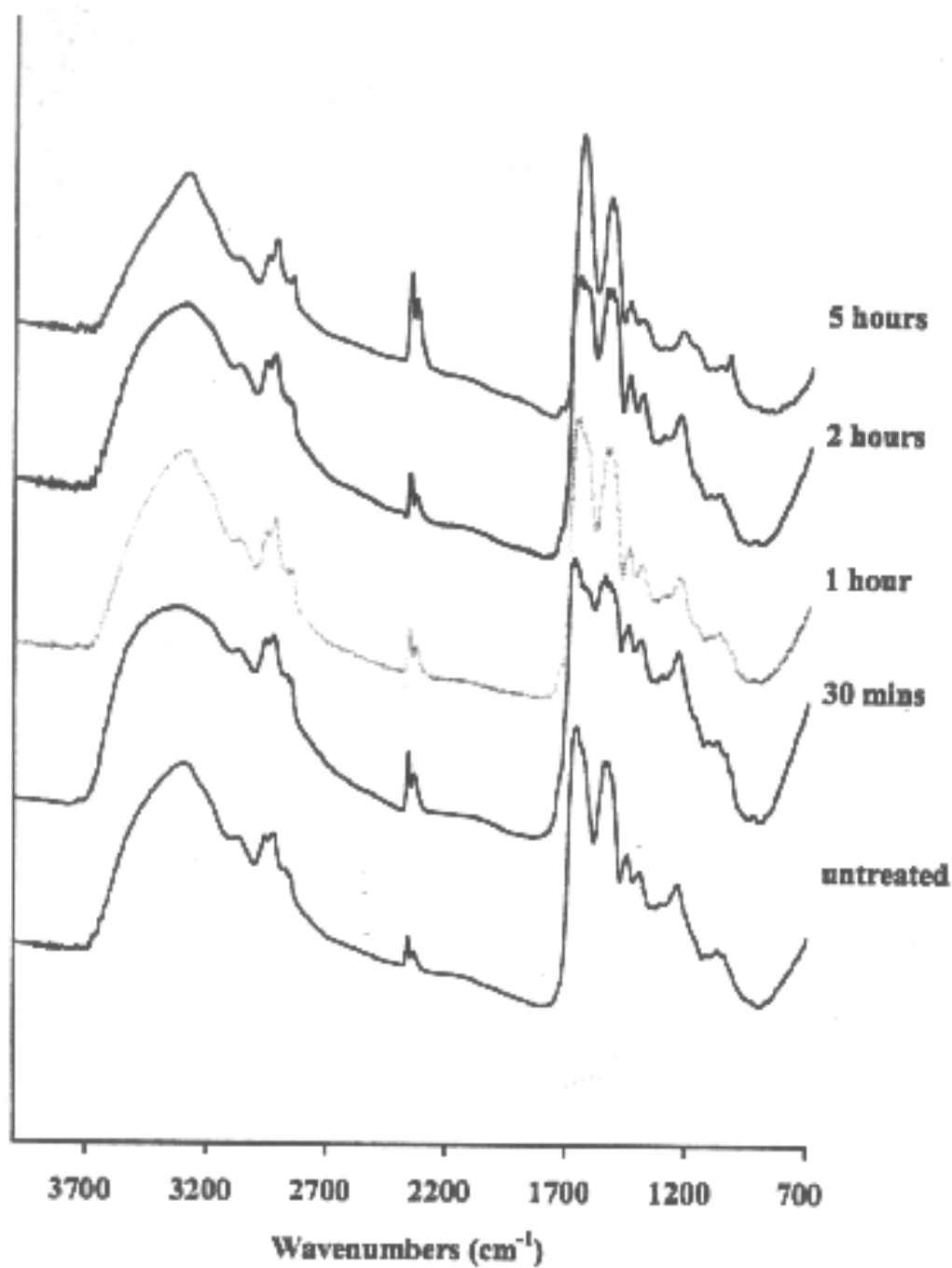


Figure 3.7. FT-IR spectra of human hair fibres treated at different time intervals (4000-700 cm^{-1}) in absorbance.

spectral region a broad feature at 510 cm^{-1} is assigned to the $\nu(\text{SS})$ stretching mode of sulfur bridges in the keratin protein.

3.6.3. Comparison of untreated and chemically treated human hair fibres by FT-IR and Raman micro-spectroscopy

The FT-IR and Raman spectra shown in Figures 3.7 and 3.8 respectively are those obtained from untreated and chemically modified hair fibres. The most significant change in the FT-IR spectra is the appearance of a new band at 1042 cm^{-1} , which is related to the cysteic acid vibrations. In the Raman spectra, the most significant change is observed in the $\nu(\text{S-S})$ stretching mode at approximately 510 cm^{-1} . The above spectroscopic evidence can be correlated with the production of cysteic acid groups in place of cystine linkages attributable to the hydrogen peroxide treatment. There are also changes in the $\delta(\text{CH}_2\text{CH}_3)$ region ($800\text{-}850\text{ cm}^{-1}$) of the spectra and these can be related to the altered conformations of the skeletal backbone of the keratin, owing to the scission of the disulphide linkages. This region will be further investigated using curve-fitting methods of analysis.

As previously discussed due to the fluorescence of the pigmented hair fibres during Raman analysis, only non-pigmented hair fibres were used for future work. The literature suggests that the resulting oxidation product is not a function of the lack of pigment in gray hair [3]. A gray and natural coloured hair from an individual showed similar absorbance profiles whether they were taken from individuals who have treated or not subjected their hair to any chemical treatment [3].

3.6.4. Background on Hair Treatment

The chemical treatment of the hair fibres has been described in chapter 2, section 1.2. In the cosmetic treatment of hair, bleaching is carried out by the oxidation of melanin pigments. This oxidation can lead, if carried to extremes, to total solubilisation and elimination of the melanin pigment.

In practice, all bleaching treatments are oxidative alkaline treatments capable of acting on the keratin itself. The literature [33] suggests that hair lightening can be achieved by bleaching hair fibres for a maximum of 1 hour. It therefore becomes important to examine the reactions occurring in the chemical structure of the hair fibre, because in addition to bleaching the pigment, they will also cause a whole series of modifications in hair properties.

Alkaline oxidizing compositions will thus act on the melanin itself as well as on the hair keratin's accessible reaction sites. These include hydrogen bonds, cystine linkages, side chain amino or free amino groups, e.g. lysine, arginine, hydroxyl groups of certain amino acids such as serine, threonine and tyrosine and finally amide groups in the polypeptide chain. The hydrolytic attack on the amide bonds can give rise to oligopeptides, which are soluble in water and can therefore be removed by rinsing [33, 34].

The literature [33] has shown that the major chemical differences between bleached hair and normal hairs are the lower percentage contents of cysteine, tyrosine and methionine along with a higher cysteic acid content found in bleached hair. Since hydrogen bonding is also affected by oxidation, changes to the intensities of the bands

Table 3.5

Summary of results obtained from the curve-fitting of Amide I and II (both in the FT-IR) and Amide III (Raman) for untreated and chemically treated hair fibres.

Treatment Times	Amide I (random coil) 1665 cm ⁻¹	Amide I (α -helix) 1655 cm ⁻¹	Amide I (β -sheet) 1624 cm ⁻¹	Amide II (α -helix) 1550 cm ⁻¹	Amide II (β -sheet) 1531 cm ⁻¹	Amide III (β -sheet) 1249 cm ⁻¹
Untreated	4.8	14.1	5.6	26.6	13.5	10.3
½ hour	5.3	10.8	5.8	21.4	13.4	10.6
1 hour	5.7	10.6	5.9	13.5	13.2	10.5
2 hours	5.6	10.5	5.9	20.8	13.4	10.4
5 hours	5.5	10.3	5.8	26.3	13.3	10.5

associated with the secondary structure of the fibre may also be expected. It was therefore proposed that the regions between 1750-750 cm^{-1} for FT-IR and 1750-450 cm^{-1} for Raman will be analysed through curve-fit so as to monitor any changes that might be taking place in the keratin fibre as a result of chemical oxidation. The position of the bands selected for curve-fitting in the FT-IR spectra and Raman spectra was selected according to the band positions obtained from the literature [5, 10].

3.6.4.1. Secondary structure (peptide-backbone structure)

Amide I, II and III vibrations are affected by hydrogen bonding and by the rotational angles ψ and ϕ involved in α -helices, β -sheets and disordered structures [11, 12, 13]. In general, these structures are formed through intramolecular hydrogen bonding between the carbonyl oxygen of one peptide bond and the hydrogen atom of another. The role of the hydrogen bond is particularly important in stabilising and forming the α -helix of the coiled chain. Hydrogen bonds can be broken by water molecules inserting themselves between the polypeptide chain and along with the cystine linkages can also be affected during oxidation of the fibre.

The amide I, II and III (amide III can be better observed in Raman, amide I and II in FT-IR) are the most sensitive probes for the conformational changes in the protein [36]. Table 3.5 presents the results obtained from the relative intensity areas for the amide I, II and III (refer to appendix III for examples of the curve-fit spectral region 1750-750 cm^{-1} for untreated, 30 minutes, 1 hour, 2 hours and 5 hours treatment times). The amide I mode was resolved into three Gauss-shaped band assignments corresponding to α -helix (1655 cm^{-1}), β -sheet (1670 cm^{-1}) and random coil (1665 cm^{-1}) structure. The

literature [36] suggests that every chemical interference within a keratin fibre leads to a decrease in the share of α -helix as compared with a raw, untreated sample. There is a 27% decrease in the relative intensity area of the α -helix (from untreated to 5 hours treatment). The decrease in the α -helix structure is accompanied by an increase in the random-coil of almost 15% (from untreated to 5 hours treatment time). The β -sheet remains relatively stable. These results support the study by Pielesz et al [37] who found that treatment of wool fibres by azo dyes leads to a decrease in the α -helix structure, whilst the β -sheet is unaffected.

Nishikawa et al [38] studied the damage to hair caused by permanent waving treatment with nuclear magnetic resonance, wide angle X-ray diffraction, FT-IR and Raman methods. The authors found that the α -helix was partially changed to random-coil, rather than to β -sheet structure which remained unchanged by the treatment. In this study (table 3.5), the initial decrease in the content of the α -helix (amide I) occurred in the first 30 minutes of chemical treatment (23%), after which time no significant change could be observed (1 hour-24.8%, 2 hours-25.5% and 5 hours-26.9%). Nishikawa [38] proposed a 3% decrease to the content of the α -helix (amide I) after 20 minutes of permanent waving of hair. In their study, the authors suggested that the α -helix content decreased in the first 20 minutes of treatment and did not change during further treatment. The decrease of the α -helix estimated in the present study is much higher than the 3% decrease proposed by Nishikawa [38]. A possible explanation for the difference between the two studies could be due to the fact that bleaching is a severe chemical treatment and it will thus be expected to cause a greater damage on the secondary structure of a hair fibre than a less severe treatment

such as permanent waving. Furthermore, Nishikawa calculated the % decrease after 20 minutes of treatment, whilst in this study it was calculated after 30 minutes.

Amide II contains two vibrations in the FT-IR spectra of human hair fibres; that of an α -helix at 1550 cm^{-1} and that of a β -sheet at 1531 cm^{-1} . There is no random coil pattern associated with the amide II band (refer to table 3.2 for a list of the characteristic band assignments for the different types of protein conformations for amide I, II and III bands). Table 3.5 shows that the α -helix vibration of amide II decreases as a result of bleaching of the hair fibre. In particular, it was noted that a decrease of approximately 19% occurred after 30 minutes of bleaching. Table 3.5 also shows that the β -sheet vibration of amide II remains relatively stable, as it was noted in the case of the β -sheet vibration of the amide I. Since there is no random coil in the amide II vibration, the decrease observed in the α -helix is not accompanied by an increase in another structure of the amide II. What is interesting to note is that unlike the α -helix vibration of amide I, which partially changes to a random coil structure and is never re-formed as an α -helix, the α -helix of the amide II appears to be re-forming after 2 hours of treatment. In particular, there is an initial decrease in the first 30 minutes (19%) followed by a further decrease of a further 37%. However, after 2 hours of bleaching the α -helix re-forms 35% and after 5 hours there is an additional re-formation of approximately 21%. Therefore, out of a total of 56% of α -helix “lost” in the first 1 hour of bleaching, after 5 hours of bleaching time 56% of the α -helix is re-formed.

Amide III (β -sheet) remains relatively stable during chemical bleaching of the hair fibre. As a result of its stability during chemical treatment, amide III has found applications as an internal standard [14].

3.6.4.2. C-C Skeletal Backbone

The C-C skeletal backbone is conformationally sensitive and is found at approximately 1448 cm^{-1} in both IR and Raman spectra. As previously discussed in an earlier section of this chapter, this band can be used in conjunction with the amide bands for identification of various secondary structures [14]. According to Akhtar et al [10] changes to the S-S bond lead to alterations in the keratin skeletal conformations. Table 3.6 presents a summary of the results for the curve-fit area of the CH_2CH_3 band in the FT-IR spectra of untreated and treated hair fibres.

Table 3.6
Relative intensity curve-fitted areas of CH_2CH_3 for untreated and chemically treated hair fibres

Treatment Characteristics	CH_2CH_3
Untreated	0.33
½ hour treatment	0.29
1 hour treatment	0.26
2 hours treatment	0.24
5 hours treatment	0.20

Table 3.6 shows an initial decrease in the relative intensity of the CH_2CH_3 vibration of approximately 12% between the untreated and ½ hour treatment. Further decreases of an average of 10% are obtained between the 1, 2 and 5 hour treatments. The results obtained in the present study suggest that chemical bleaching of hair fibres has

Table 3.7.

Dihedral Angles of the two different proposed theories [38].

This table is not available online. Please consult the hardcopy thesis available from the QUT library

a direct affect on the CH_2CH_3 vibration, which indicates disruption of the polypeptide chain during chemical treatment.

3.6.4.3. Sulfur containing groups

In contrast to infrared spectra, where CS and especially SS modes of vibration are often inactive, Raman spectra provide a clear way of identifying the SS and CS modes and determining the conformations that produce them. Disulfide bonds are an important structural feature in proteins where they function as cross-links of cysteine along or between polypeptide chains. They provide stability without undue rigidity because each allows various conformations to take place (even though the S-S chemical bond generally insures a central dihedral angle of near 90 degrees rotation about each C-S bond with its adjacent β -carbon atom) [35, 36].

Sugeta et al [38] suggested that the stretching vibration of the disulphide bond is influenced by the conformation of carbon atoms in the disulphide bridge. The authors further proposed that the S-S stretching vibration is depended upon the internal rotation about the C-S and C-C bond of the C-C-S-S-C-C moiety. According to this theory, Raman spectroscopy can distinguish three types of disulfide-bond geometry, namely, *gauche-gauche-gauche*, *trans-gauche-gauche*, and *trans-gauche-trans* conformations. The position of the 510 cm^{-1} band for naturally occurring proteins and peptides indicates a preference to take the lowest potential energy conformation of the S-S bonds, corresponding to the *gauche-gauche-gauche* conformation. Other bands can also be observed at 525 and 540 cm^{-1} and correspond to *gauche-gauche-trans* and *trans-gauche-trans*, respectively. Table 3.7. presents the three different conformations along with the dihedral angles of the two different proposed rotations.

TABLE 3.8**Relative areas of S-S and S=O**

Treatment time	FT-IR (S=O)	Raman (S-S)
Untreated	0.0687±5.052e-05	4.0763±0.00856
30 minutes	0.0873±4.804e-05	3.821±0.00831
1 hour	0.1136±4.292e-05	3.743±0.00752
2 hours	0.1449±4.455e-05	3.575±0.00858
5 hours	0.1620±9.889e-05	2.7310±0.00517

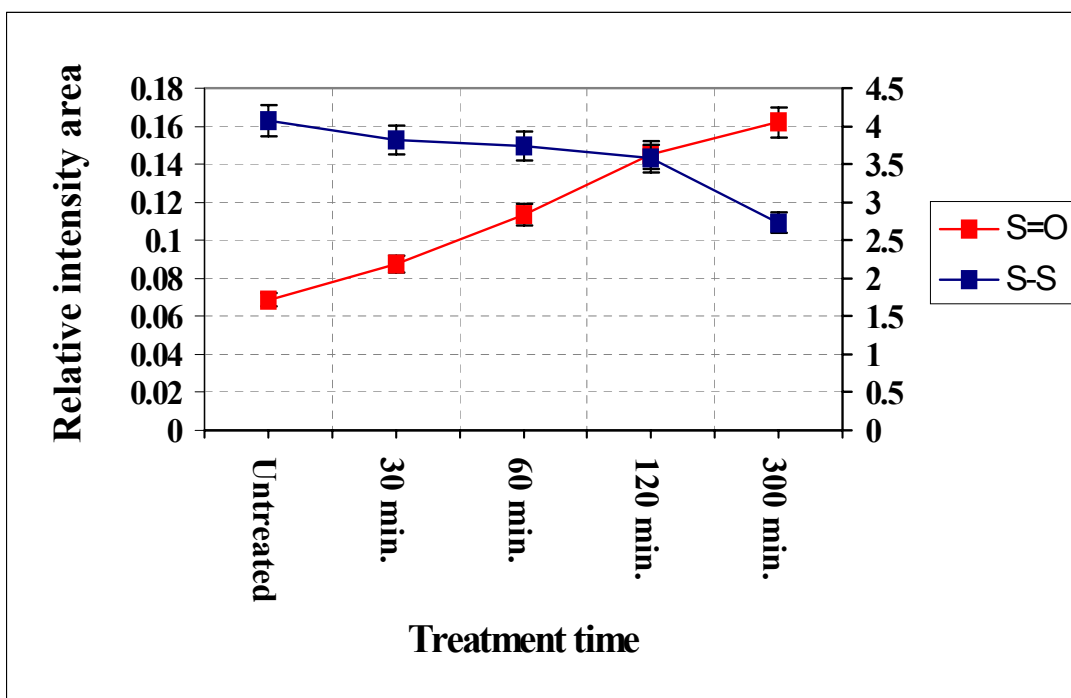


Figure 3.9. Relative areas of S-S and S=O versus treatment times.

Curve-fitting analysis of the Raman spectra collected from treated hair fibres shows a decrease in the intensity of S-S at 510 cm^{-1} . Analysis of the corresponding spectra using FT-IR shows an increase in the intensity of the (1040 cm^{-1}). These results are presented in Table 3.8 and figure 3.9.

Figure 3.9 indicates a nearly linear relationship between the relative intensities of S-S compared to the S=O band as a result of the peroxide treatment. These results agree with comments in the literature [3, 5] which state that oxidation of chemically modified hair results in increasing amounts of cysteic acid followed by decreasing amounts of cystine. The low levels of cysteic acid present in untreated hair fibres are possibly caused by harsh shampoos, abrasion, chlorinated pools and UV sunlight.

In the FT-IR spectra of hair fibres the C-S vibrational band originates from methionine, cysteine and cystine. In cysteine and cystine, the C-S stretching vibration is related to the internal rotation along the C-C axis of X-C-CH₂-S-S. The vibration depends upon the atom X at the trans site with respect to the sulfur atom adjacent to the C-C bond. For instance when X is a hydrogen atom, the C-S stretching vibration lies between 630 and 760 cm^{-1} , when X is a carbon it is present at 720 cm^{-1} , and when X is a nitrogen in present at 700 cm^{-1} [11, 13].

In the Raman spectrum there are no evident bands at 720 cm^{-1} and 700 cm^{-1} . The presence of the band at approximately 665 cm^{-1} suggests that the X atom at the trans-site with respect to the sulfur atom adjacent to the C-C bond is hydrogen.

3.6.4.4. Aromatic Hydrocarbon Groups

3.6.4.4.1. Tyrosine

In proteins, a number of Raman bands due to the tyrosine residue are readily visible and assignable, and have been used to mark tyrosine's several possible states and functions [13]. The phenolic OH of tyrosine is structurally important for the maintenance of overall conformation and kinetically important in enzymatic and other binding activities.

A pair of tyrosine bands near 830-850 cm^{-1} are known to vary in intensity in accordance with the state of the molecule [11, 13]. The 850/830 cm^{-1} doublet reflects the Fermi resonance between the ring-breathing vibration and an overtone of an out-of-plane ring breathing vibration of the para-substituted benzene [11,13]. The intensity ratio of 830 to 850 cm^{-1} is frequently used to determine whether the tyrosine residue is buried or exposed. The ratio is believed to depend on the manner of the hydrogen bonding of the tyrosine hydroxyl group. If the tyrosine is buried in the protein structure, it acts as a strong hydrogen-bond donor and the ratio of 850/830 cm^{-1} is quite low (≈ 0.5) resulting from the higher intensity of the 830 cm^{-1} band. However, when the tyrosine is on the surface of a protein (exposed) then the ratio is higher because of the higher intensity of the 850 cm^{-1} band. With this knowledge it is then possible to determine quantitatively the number of buried and exposed residues by using the following equation [11]:

$$xN_{\text{buried}} + xN_{\text{exposed}} = 1$$

$$0.5N_{\text{buried}} + 1.25N_{\text{exposed}} = I_{850}/I_{830} \quad \dots\dots\dots\text{Equation 3.1}$$

where N_{buried} and N_{exposed} refer to the mole fractions of buried and exposed tyrosine residues.

At the present time, the literature offers no detailed study on the microenvironment of tyrosine residues in human hair during chemical treatment. This is the first time a detailed research of the behaviour of tyrosine during hair bleaching at different time intervals has been investigated. In this study, it was observed that the intensity of the 850 cm^{-1} band was higher than that of the 830 cm^{-1} band, giving an I_{850}/I_{830} , which is indicative of an exposed tyrosine side chain i.e., the OH group acts as a hydrogen acceptor.

Tyrosine at the surface of a protein is most often exposed to the weak or moderate H-bonding of water as both donor and acceptor, and yields an intensity ratio in the intermediate range, near 1.0 [11, 13]. Analysis by curve-fitting of the untreated samples resulted in a ratio of $I_{850}/I_{830} = 1.12$. Therefore solving the above equations gave $N_{exposed} = 0.83$ and $N_{buried} = 0.17$. This suggests that in human hair fibres tyrosine acts as a hydrogen-bond acceptor. After 30 minutes of treatment the ratio decreases to 1.07 (approximate 4.5% decrease, $N_{exposed} = 0.76$ & $N_{buried} = 0.23$) and after one hour the ratio is 0.99 (approximate 7.5% additional decrease from 15 minutes, $N_{exposed} = 0.65$ & $N_{buried} = 0.34$). This indicates that oxidation results in modification of the tyrosine ring resulting in a decrease to the mole fraction of the exposed tyrosine, while there is a slight increase to the mole fraction of the buried tyrosine. After 2 and 5 hours of treatment similar results are obtained.

The decrease in the observed intensity of tyrosine from the present study, is consistent with the lower amounts of tyrosine residues of oxidative treated hair fibres reported in the literature [34]. However in a study by Zahn et al [42] the authors proposed that

tyrosine, although normally sensitive to oxidation, was not affected during bleaching and permanent waving.

3.6.4.4.2. Phenylalanine

Although a number of Raman bands can be attributed to phenylalanine residues and are therefore useful for identification, in practical terms all of their intensities are constant and are not useful for monitoring structural features [35].

The breathing vibration of the benzene ring of phenylalanine can be detected at 1005 cm^{-1} when the concentration of phenylalanine is above 1%. There appears to be no change in the intensity of phenylalanine as a result of chemical treatment. The present results are supported by Nishikawa et al [37] who also found that phenylalanine is unaffected by permanent waving treatment. Robbins [34] reported no changes in the amount of phenylalanine in bleached hair. However, Zahn et al [42] proposed that the content of phenylalanine decreases with increasing bleaching time.

3.6.4.4.3. Tryptophan

Tryptophan residues in proteins have a number of recognisable Raman bands that give useful information about the tryptophan environment. Tryptophan bands include vibrations near 544, 577, 761, 880, 1015, 1340, 1362, 1554, 1580 and 1622 cm^{-1} [35]. Of these, only the 1340 cm^{-1} and 1362 cm^{-1} pair are strongly influenced by protein structure and functioning. A sharp band at 1360 cm^{-1} is diagnostic of a buried tryptophan [35]. The Fermi interactions that provide environmental sensitivity stem from a skeletal stretching fundamental and one or two combination bands. A high ratio of intensity I_{1360}/I_{1340} , indicates a hydrophobic environment, whereas low values indicate that the particular tryptophan is involved in the H-bonding of a hydrophilic atmosphere [35]. Care is required in interpreting this doublet, because the bands overlap with each other, and the lower component is often overlapped by CH bending vibrations that occur in all protein spectra.

In this study, the 1340 cm^{-1} band overlapped with CH bending vibrations and it was therefore not possible to obtain a quantitative estimate of its intensity. The Raman spectra of the hair fibres do not show any indication of the presence of the 1360 cm^{-1} band, which suggests that the tryptophan is exposed and it therefore acts as a hydrogen acceptor.

3.6.4.5. Basic amino acids

3.6.4.5.1. Histidine

Histidine occurs in two tautomeric forms (Figure 3.10) characterised by two different Raman bands corresponding to breathing vibrations of the imidazole ring. Tautomer I at 1282 cm^{-1} represents the 1-N-protonated form, and tautomer II at 1260 cm^{-1} is for the 3-N-protonated form.

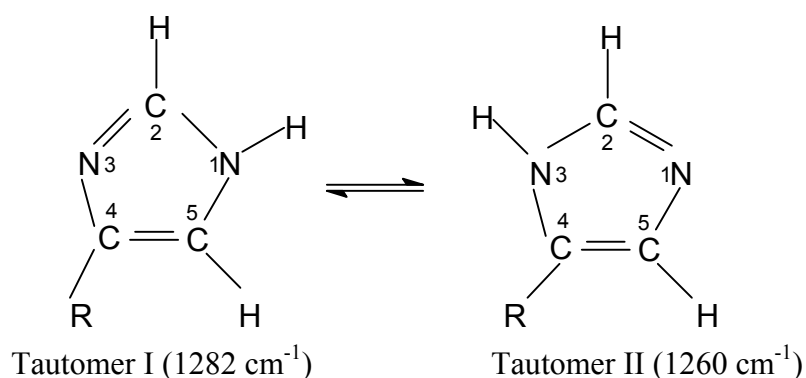


Figure 3.10. Tautomerism of the imidazole ring of histidine.

Tu [11] and Tensmeyer et al [13] have suggested that Tautomer I is more stable than tautomer II. The presence of the 1260 cm^{-1} band in the Raman spectra indicates that the 3-N-protonated form (Tautomer II) is the most likely form of histidine present in human hair. Even though Tautomer II is less stable there appears to be no effect on the histidine vibration as a result of the bleaching treatment. This agrees with comments by Tu [11] and Tensmeyer et al [13] who suggested that although a number of Raman bands can be attributed to histidine and phenylalanine residues and are therefore useful for identification, practically all of their frequencies are constant and do not discriminate structural features. Robbins [34] has also found that histidine remains unaffected during bleaching of the hair fibre.

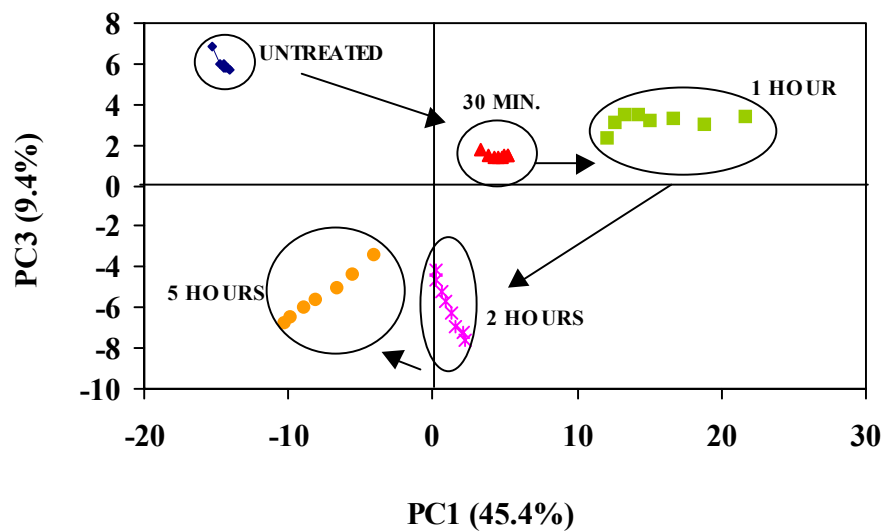


Figure 3.11. PC1 (45.4%) vs PC3 (9.4%) scores for the FT-IR spectra collected from untreated and chemically treated (bleached for 30 min., 1, 2 and 5 hours) in the region between 1750-750 cm^{-1} .

3.7. Chemometric Discussion

The FT-IR and Raman spectra were submitted to chemometrics methods of analysis such as PCA, SIMCA and FC. These chemometrics methods of analysis were used so as to obtain a quantitative and semi-quantitative estimate of the changes observed by curve-fitting methods of analysis.

3.7.1.1. PCA

The 40 FT-IR spectra collected from the untreated and treated human hair fibres were submitted to PCA in an attempt to discriminate the spectra collected from hair treated at different times. Five components were identified as significant and were sufficient to account for the total variance (99.5%) of the data set in the region between 1750 – 750 cm^{-1} . The PCA plot shown in figure 3.11 shows the best separation between the spectra on the basis of PC1 (45.4%) vs PC3 (9.4%).

Five clusters are present each corresponding to a different time of treatment. PC1 discriminates between the untreated samples (having high negative scores) from the 30 minute, 1 and 2 hours of treatment (all positive scores). The 5 hours treatment time has moderate negative scores along PC1 and appears to be separated on the PC with the untreated hair fibres. The grouping of the untreated and 5 hours treatment on the same PC could be due to the re-formation of the α -helix (in amide II) as discussed in section 3.6.4.1. A second separation is observed along PC3, which discriminates the untreated and low treatment times (30 minutes and 1 hour), from the higher treatment times (2 and 5 hours).

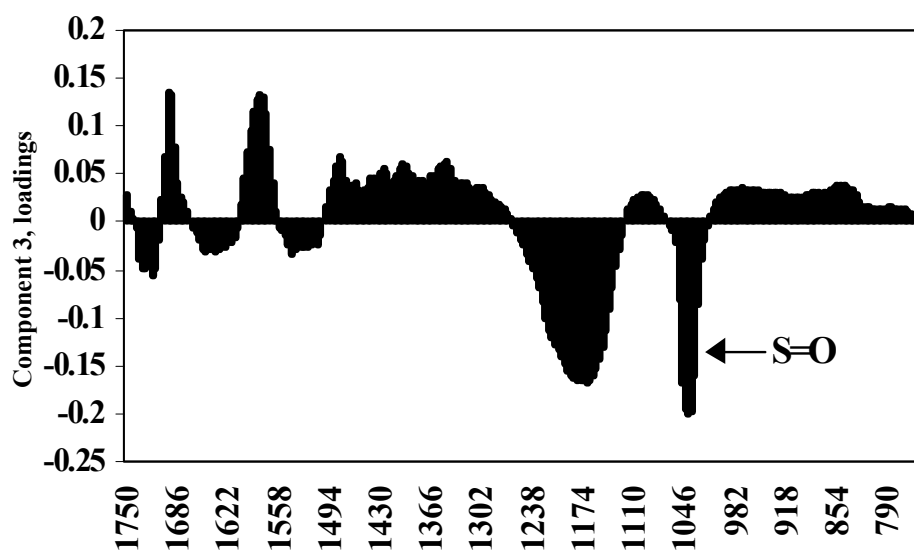


Figure 3.12. PC3 loadings plot against the variable for FT-IR spectra from untreated and chemically treated (bleached for 30 min., 1, 2 and 5 hours) in the region between 1750-750 cm^{-1} .

The PC1 loadings plot (not shown) contains very broad spectral regions and provides only limited information for the discrimination of the spectra. PC3 loadings plot (figure 3.12) clearly shows that hair samples with negative scores (treatment times of 2 and 5 hours) are mainly influenced by a sharp cysteic acid band at approximately 1040 cm^{-1} and a broad cystine oxide region between $1240\text{-}1120\text{ cm}^{-1}$ along with some minor contributions from COO^- at 1720 cm^{-1} .

3.7.1.2. SIMCA

PCA has indicated a difference between the FT-IR spectra collected from the untreated and treated hair samples. SIMCA was applied in an attempt to obtain a semi-quantitative indication of the extent of the separation observed in PCA. The spectra from the treated (1/2, 1, 2 and 5 hours) hair were defined as the model class because they contained the most number of objects (32). Four components were identified as significant by the leave-one-out method available in the SIRIUS version 2.3 software, with a 99.6% level of significance distributed between the four PCs (Table 3.9). The untreated samples were referenced to the model class.

TABLE 3.9.
SIMCA analysis with $\text{RSD}_{\text{crit}}=0.106$, $p=0.05$.

SIMCA results	Untreated	Treated
RSD, mean	1.089	0.085
N(number of spectra)	8	32
Distance between classes	-----	5.0

The objects separate into two groups: untreated and treated. FT-IR spectra obtained from the treated samples have RSD values (0.085) below the RSD_{crit} (0.106). FT-IR spectra collected from the untreated samples have RSD values (1.089) above the RSD_{crit} . In addition the class distance of 5.0 clearly indicates that the two sets of samples are different.

3.7.1.3. Fuzzy clustering

A two-cluster model was initially applied and the results for $p=2.5$ are shown in table 3.10. The untreated hair fibres have formed a single cluster with the rest of the treated fibres forming a second cluster.

TABLE 3.10.

FC membership values for a two-cluster model with a soft (2.50) weighting exponent value.

SAMPLE	CLUSTER 1	CLUSTER 2
UNTREATED	0.11	0.89
30 MINUTES	0.91	0.09
1 HOUR	0.90	0.10
2 HOURS	0.93	0.07
5 HOURS	0.88	0.12

The results of a FC analysis using a five cluster model - with a soft (2.50) weighting exponent value – are shown in table 3.11. Similar patterns were obtained when a hard (1.50) weighting exponent value was applied. In general, untreated hair fibres and chemically oxidised fibres from each treatment time formed their own clusters indicating a clear separation between each group and thus supporting the results obtained by PCA where each set of fibres had formed their own clusters.

TABLE 3.11.

FC membership values for a five-cluster model with a soft (2.50) weighting exponent value.

SAMPLE	CLUSTER 1	CLUSTER 2	CLUSTER 3	CLUSTER 4	CLUSTER 5
UNTREATED	0.00	0.92	0.05	0.03	0.00
30 MINUTES	0.03	0.05	0.07	0.85	0.00
1 HOUR	0.00	0.04	0.02	0.00	0.94
2 HOURS	0.01	0.05	0.89	0.03	0.02
5 HOURS	0.88	0.00	0.04	0.05	0.03

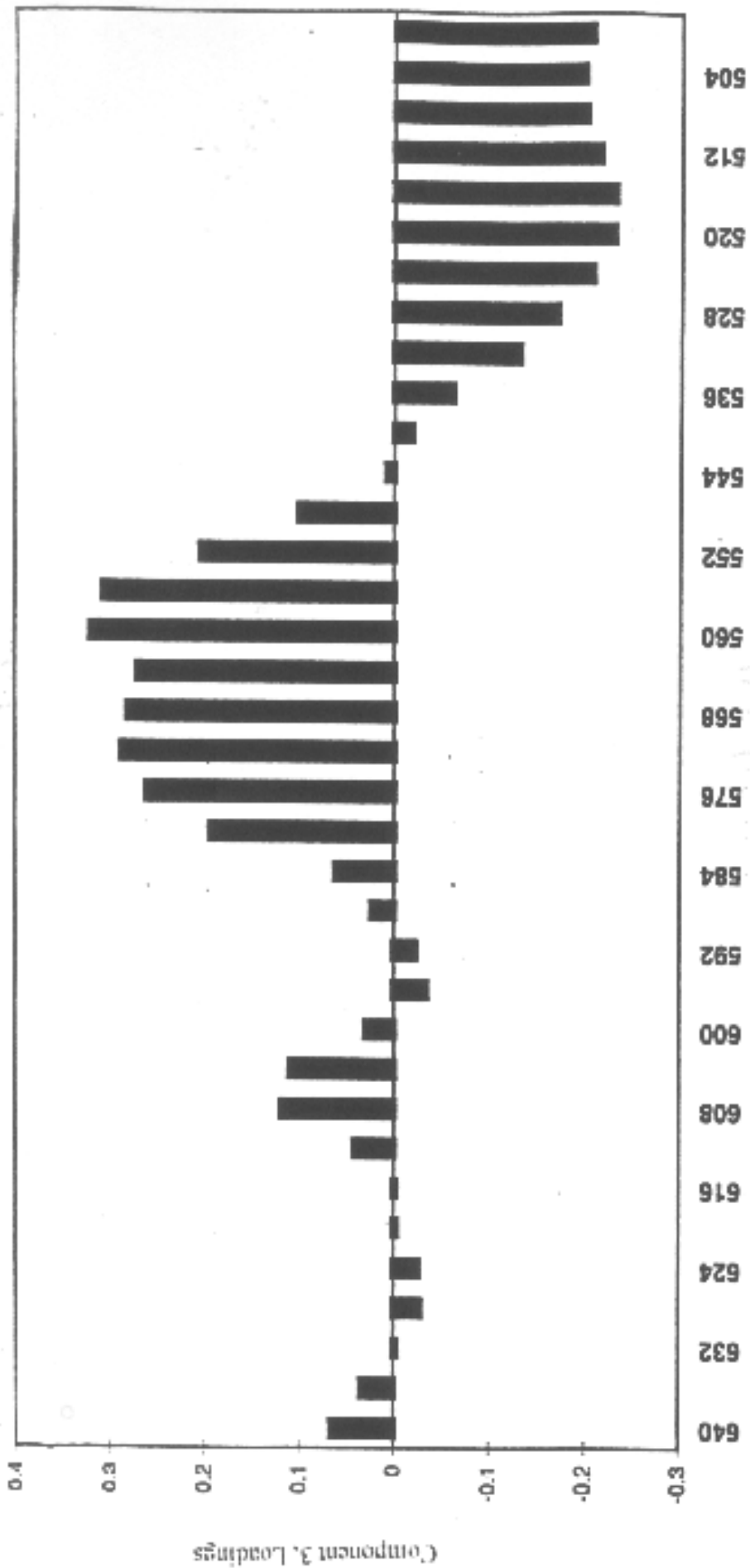


Figure 3.14. PC3 loadings plot (640-500 cm⁻¹)

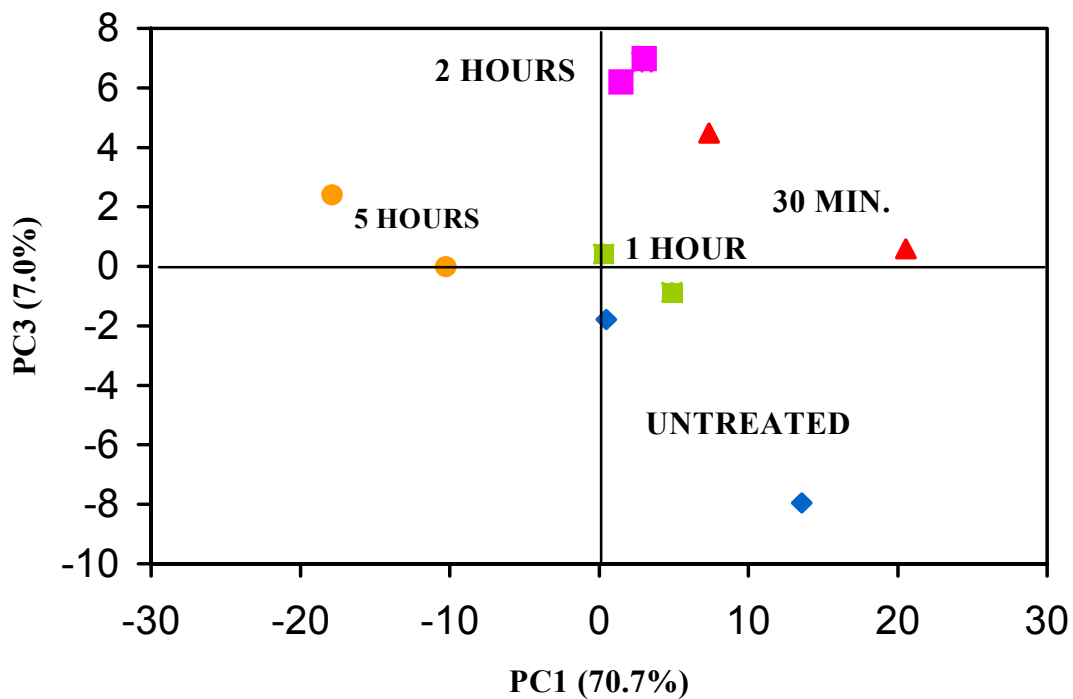


Figure 3.13. PC1 (70.7%) vs PC3 (7.0%) scores for the Raman spectra collected from untreated and chemically treated (bleached for 30 min., 1, 2 and 5 hours) in the region between 1750-750 cm^{-1} .

3.7.2. Raman Micro-spectroscopy

3.7.2.1. PCA

The PCA plot (PC1 vs PC3) of the Raman spectra collected from untreated as well as fibres treated at different time intervals is presented in figure 3.13. The separation in this plot is very similar to that of figure 3.11 (FT-IR spectra). Two spectra of each sample were obtained and a large scatter between the samples can be observed compared to FT-IR. Overall however, the trend in this plot is very similar to that from the PCA plot of the FT-IR spectra shown in figure 3.11. The main discrimination is observed along PC1 between the untreated and 30 minutes treated, while both the 1 hour and 2 hours treatment times appear to have zero to minimal contribution on this PC. Treatment time of 5 hours has negative scores along PC1. The second separation observed along PC3 is that between the untreated and treated hair. The PC3 loadings plot (figure 3.14) indicates that the separation of the spectral data collected from different treatment times is due to the presence of the cysteine vibration at approximately 510 cm^{-1} for the untreated hair fibres (negative scores on PC3).

3.7.2.2. SIMCA

In SIMCA analysis spectra from treated (1/2, 1, 2 and 5 hours) hairs were defined as the model class because they contained the most number of objects (8). Four components were identified as significant by the leave-one-out method available in SIRIUS version 2.3 software, with a 99.2% level of significance distributed between the four PCs (Table 3.12). The untreated samples were referenced to the model class.

TABLE 3.12.
SIMCA analysis with $RSD_{crit}=0.16$, $p=0.05$.

SIMCA results	Untreated	Treated
RSD, mean	0.42	0.12
N(number of spectra)	2	8
Distance between classes	-----	2.9

Overall the SIMCA results support the patterns obtained in PCA. The objects separate into two groups: untreated and treated. FT-IR spectra obtained from the treated samples have RSD values (0.12) below the RSD_{crit} (0.16). FT-IR spectra collected from the untreated samples have RSD values (0.42) well above the RSD_{crit} . In addition the class distance of 2.9 clearly refines the discrimination between the two classes.

3.7.2.3. Fuzzy clustering

Fuzzy clustering was also applied to the Raman spectra and an optimum number of two clusters was obtained. A summary of the FC results - with a soft (2.50) weighting exponent value - is presented in Table 3.13. Similar patterns were obtained when a soft (2.50) weighting exponent value was applied.

TABLE 3.13.
FC membership values for a two-cluster model with a soft (2.50) weighting exponent value.

SAMPLE	CLUSTER 1	CLUSTER 2
UNTREATED	0.06	0.94
30 MINUTES	0.88	0.12
1 HOUR	0.79	0.21
2 HOURS	0.84	0.16
5 HOURS	0.77	0.23

The results of a FC analysis using a five-cluster model - with a soft (2.50) weighting exponent value – are shown in table 3.14. Similar patterns were obtained when a hard (1.50) weighting exponent value was applied. In general, untreated hair fibres and chemically oxidised fibres from each treatment time formed their own clusters indicating a clear separation between each group and thus supporting the results obtained by PCA where each set of fibres had formed their own clusters.

TABLE 3.14.
FC membership values for a five-cluster model with a soft (2.50) weighting exponent value.

SAMPLE	CLUSTER 1	CLUSTER 2	CLUSTER 3	CLUSTER 4	CLUSTER 5
UNTREATED	0.79	0.02	0.10	0.07	0.02
30 MINUTES	0.06	0.04	0.87	0.04	0.00
1 HOUR	0.07	0.73	0.10	0.05	0.05
2 HOURS	0.00	0.02	0.08	0.83	0.07
5 HOURS	0.01	0.00	0.04	0.02	0.93

3.8. Chapter 3-Conclusions

The objective of the work presented in this study was to compare FT-IR and Raman micro-spectroscopic applications of human hair fibres and to determine through a number of essential experiments the preferred method for future forensic hair analysis. Despite its potential for reducing problems associated with water absorptions in the IR, Raman spectroscopy has until this time found only limited applications to pigmented hair and other natural pigmented fibres, because of background fluorescence, sample degradation in high-intensity, short-wavelength radiation and long scan times associated with the weakly scattering keratin species. In the Raman experiments, a comparison of the spectra collected using the 780 nm and 633 nm lasers, indicated no major reduction in fluorescence when using the 780 nm laser compared to the 633 nm. Taking into consideration the sensitivity factor between the two lasers it was proposed that the suitable laser wavelength to obtain a Raman spectrum of a white hair fibre is 633 nm. The quality of the Raman spectra collected from human hair fibres was to a large extent pigment dependent. White (non-pigmented hair) proving the only type of hair fibres that could be analysed through Raman micro-spectroscopy.

Curve-fitting of the relative intensity areas of the major bands in the FT-IR and Raman spectra collected from untreated and treated (bleached) hair fibres established that;

- (1) The fraction of the α -helix in amide I decreased with increase in bleaching time, whilst the β -sheet structure appears to be unaffected by treatment.
- (2) The decrease in the content of the α -helix (amide I) is accompanied by an increase in the content of the random coil. It is therefore proposed that the decrease in the

relative intensity of the α -helix is a result of its partial change to the random-coil structure.

- (3) There is a decrease in the content of the α -helix in amide II in the first hour of treatment. After 2 hours of bleaching there is an initial increase to the content of the helix which completely re-forms after 5 hours of treatment time. The β -sheet of the amide II remains relatively unaffected by treatment.
- (4) There is no significant change to the content of the amide III during chemical treatment and the band remains relatively stable during different bleaching times. The stable nature of the band during chemical treatments indicates that amide III is a good internal standard for any future work.
- (5) The present study has indicated a change in the content of CH_2CH_3 during chemical bleaching.
- (6) There is a nearly linear relationship between the formation of cysteic acid (as seen in the FT-IR spectra) in comparison to the disulfide bond of cysteine (as seen in the Raman spectra) with increase in treatment time.
- (7) Aromatic hydrocarbon groups such as tyrosine, phenylalanine and tryptophan are hydrogen acceptors and of these, oxidation agents affect only tyrosine.
- (8) Basic amino acid histidine is present in the 3-N-protonated form (Tautomer II) and it does not appear to be affected by chemical treatment.

The present study has demonstrated that the reported changes in amide I, II (both for α -helix) and largely attributed to alterations in the keratin skeletal conformations due to S-S bond scission during chemical treatment of the hair fibre.

Chemometrics has indicated a discrimination of untreated hair from treated hair fibers and similar results were obtained for both FT-IR and Raman spectral data. The loadings plots indicated that the separation between the untreated and treated hair fibres is a result of the formation of cysteic acid residues due to the chemical oxidation of the hair fibre which supports the curve fit results.

From a theoretical viewpoint, Raman micro-spectroscopy offers valuable information about the nature and distribution of compounds within the hair fibre. However, from a forensic aspect, Raman micro-spectroscopy is not applicable to coloured hair and thus is very limited in its application to real-life cases.

Furthermore, the work presented in this chapter established that bleaching of hair fibres is a complex process because it calls on a range of chemical reactions involving not only the pigment it is intended to lighten or bleach, but also the keratin fibre itself. It is therefore proposed that given the change in the chemical composition brought on by chemical treatment, a method of lightening hair that acts only on the pigment, and not on hair keratin, would be a great step forward in the cosmetic industry.

CHAPTER 3 - REFERENCES

1. Schraefer, B., *Infrared and Raman Spectroscopy: Methods and Applications*, VCH, N.Y., 1995.
2. Bradley, R. H., Mathieson, I., Chemical Interaction of Ultraviolet Light with Wool Fibre Surfaces, *Journal of Colloid and Interface Science*, **194**, pp. 338-343, (1997).
3. Brenner, L., Squires, P. L., Garry, M., Tumosa, C. S., A Measurement of Human Hair Oxidation by Fourier Transform Infrared Spectroscopy, *Journal of Forensic Sciences*, **13**, pp. 420-426, (1985).
4. Hopkins, J., Brenner, L., Tumosa, C. S., Variation of the Amide I and Amide II Peak Absorbance Ratio in Human Hair as Measured by Fourier Transform Infrared Spectroscopy, *Forensic Science International*, **50**, pp. 61-65, (1991).
5. Joy, M., Lewis, O. M., The Use of Fourier Transform Infrared Spectroscopy in the Study of the Surface Chemistry of Keratin Fibres, *J. Soc. Cosmet Chem.*, **13**, pp. 249-261, (1991).
6. Bramanti, E., Ronca, F., Teodori, L., Trinca, M-L., Papineschi, F., Benedetti, E., Spremolla, G., Vergamini, P., and Benedetti, E., A New Approach to the Study of Human Hair by means of FT-IR Microspectroscopy, *J. Soc. Cosmetic Chem.*, **43**, pp. 285-296, (1992).
7. Douthwaite, F. J., Lewis, D. M., Schumacher-Hamedat, U., Reaction of Cystine Residues in Wool with Peroxy Compounds, *Textile Res. J.*, **63**, pp. 177-183, (1993).
8. Hogg, L. J., Edwards, H. G. M., Farwell, D. W., and Peters, A. T., FT-Raman Spectroscopic Studies of Wool, *JSDC*, **110**, pp. 196-199, (1994).

9. Williams, A. C., Edwards, H. G. M., and Barry, B. W., Raman Spectra of Human Keratotic Biopolymers: Skin, Callus, Hair and Nail, *Journal of Raman Spectroscopy*, **25**, pp. 95-98, (1994).
10. Akhtar, W., Edwards, H. G. M., Farwell, D. W., Nutbrown, M., Fourier-Transform Raman Spectroscopic Study of Human Hair, *Spectrochimica Acta Part A.*, **53**, pp. 1021-1031, (1997).
11. Tu, A. T., **Raman Spectroscopy in Biology: Principles and Applications**, John Wiley and Sons, U.S.A., 1982.
12. Fraser, R. D. B., MacRae, T. P. and Rogers, G. E., **Keratins: Their Composition, Structure and Biosynthesis**, Charles C Thomas, U.S.A., 1972.
13. Tensmeyer, L. G., Wayne Kauffman, E., II., Chapter 5, Protein Structure as Revealed by Nonresonance Raman Spectroscopy in **Spectroscopic Methods for Determining Protein Structure in Solution**, edited by Havel, H. A., VCH Publishers, U.S.A., (1996).
14. Jurdana, L. E., Ghiggino, K. P., Nugent, K. W., and Leaver, I. H., Confocal Laser Raman Microprobe Studies of Keratin Fibres, *Textile Res. J.*, **65**, pp. 593-600, (1995).
15. Weston, G. J., The Infrared Spectrum of Paracetic acid-treated wool, *Biochimica et Biophysica Acta*, **17**, pp. 462-462, (1955).
16. Bit-Alkhas, M., and Alter, H., Infrared Analysis of Oxidised Keratin, *Textile Research Journal*, pp. 479-481, (1969).
17. Baddiel, C. B., Structure and Reaction of Human Hair: an Analysis by Infrared Spectroscopy, *J. Mol. Biol.*, **38**, pp. 181-199, (1968).
18. Low, M. J. D., Severdia, A. G., Infrared Spectra of a Single Human Hair, *Spectroscopy Letters*, **16**, pp. 871-877, (1983).

19. Strassburger, J., Quantitative Fourier Transform Infrared Spectroscopy of Oxidised Hair, *J. Soc. Cosmetic Chem.*, **36**, pp. 61-74, (1985).
20. Hilterhaus, S., Zahn, H., Influence of Permanent Waving on the Chemistry and Structure of Human Hair, Proceedings of the 7th International Wool Textile Conference, Tokyo, **IV**, pp. 392-401, (1985).
21. Signori, V and Lewis D. M., FT-IR Investigation of the Damage Produced on Human Hair by Weathering and Bleaching Processes: Implementation of Different Sampling Techniques and Data Processing, *J. Soc. Cosmet. Chem.*, **19**, pp. 1-13, (1997).
22. Kalasinsky, K. S., Magluilo, J. Jr., Schaefer, T., Study of Drug Distribution in Hair by Infrared Microscopy Visualisation, *Journal of Analytical Toxicology*, **18**, pp. 337-341, (1994).
23. Gniadecka, M., Faurskov Nielsin, O., Højgaard Christensen, D., and Christian Wulf, H, Structure of Water, Proteins and Lipids in Intact Human Skin, Hair and Nail, *Journal of Investigative Dermatology*, **110**, pp. 393-398, (1998).
24. Batrick, E. G., Tungol, M. W., and Reffner, J. A., A New Approach to Forensic Analysis with Infrared Microscopy: Internal Reflection Spectroscopy, *Analytica Chimica Acta*, **288**, pp. 35-42, (1994).
25. Clark, R. J. H., and Hester, R. E., **Advances in Infrared and Raman Spectroscopy**, John Willey, Chichester, 1975.
26. Kelemen, J., Moss, S., and Glitsch, S., Azo-Hydrazone Tautomerism of Adsorbed 1-Phenylazo-2-naphthylamine and 1-Phenylazo-2-naphthol Dyes, *Dyes Pig.*, **5**, pp. 83-108, (1984).

27. Kulshreshtha, A. K., and Dweltz, N. E., Analysis of Flame-retardant Finishes on Textiles using Laser-Raman Spectroscopy, *Ind. J. Textile. Res.*, **6**, pp. 135-138, (1981).
28. Hsu, S. L., Moore, W. H., and Krimm, S., Vibrational Spectrum of the Unordered Polypeptide Chain: A Raman Study of Feather Keratin, *Biopolymers*, **15**, pp. 1513-1528, (1976).
29. Shishoo, R., and Lundell, M., Investigation of Structural Changes in Wool Fibres due to Annealing, *J. Polym. Sci. Polym. Chem. Ed.*, **14**, pp. 2535-2544, (1976).
30. Pande, C. M., and Jachowicz, J., Hair Photodamage-Measurement and Prevention, *J. Soc. Cosmet. Chem.*, **44**, pp. 109-122, (1993).
31. Rintoul, L., Carter, E. A., Stewart, S. D., and Fredericks, P. M., Keratin Orientation in Wool and Feathers by polarised Raman Spectroscopy, *Biopolymers (Biospectroscopy)*, **57**, pp. 19-28, (2000).
32. Tobin, D. J., and Paus, R., Graying: gerontobiology of the hair follicle pigmentary unit, *Experimental Gerontology*, **36**, pp. 29-54, (2001).
33. Robbins, C. R., **Chemical and Physical Behaviour of Human Hair**, 3rd edition, Springer-Verlag, U.S.A., (1994).
34. Fraser, R. D. B., MacRae, T. P., **Conformation in Fibrous Proteins and related synthetic Polypeptides**, Academic Press, N. Y., (1973).
35. Zviak, C., Hair Bleaching in **“The Science of Hair Care”** edited by Zviak, C., Marcel Dekker, Inc, U.S.A. (1986).
36. Carey, P.R., and Salares, V.R., in **Advances in Infrared and Raman Spectroscopy**, edited by Clark, R.J.H., and Hester, R.R., vol 7, Heyden, London, (1980).

37. Pielesz, A., Weselucha-Birczynska, A. The Identification of Structural Changes in the Keratin of Wool Fibre Dyed with an Azo Dye Using Raman and Fourier Transform Infrared Spectroscopy Methods, *Journal of Molecular Structure*, **555**, pp. 325-334, (2000).
38. Nishikawa, N., Tanizawa, Y., Tanaka, S., Horiguchi, Y., and Asakura, T., Structural Change of Keratin Protein in Human Hair by Permanent Waving Treatment, *Polymer*, **39**, pp. 3835-3840, (1998).
39. Sugeta, H., Go, A., and Miyazawa, T., S-S and C-S stretching vibrations and molecular conformations of dialkyl disulfides and cystine, *Chem. Lett.*, pp. 83, (1972).
40. Van Wart, H. E., Lewis, A., Scheraga, H. A., and Saeva, F. D., Disulfide bond dihedral angles from Raman Spectroscopy, *Proc. Nat. Acad. Sci.*, **70**, pp. 2619, (1973).
41. Martin, R.B., Invariance of disulfide wave numbers to Disulfide Dihedral Angles, *J. Phys. Chem.*, **78**, pp. 855, (1974).
42. Scheraga, H. A, Van Wart, H. E. and Martin, R. B., Agreement concerning the nature of the variation of disulfide stretching frequencies with disulfide dihedral angles, *J. Phys. Chem.*, **80**, pp. 1832, (1976).
43. Zahn, H., Hilterhaus, S and Strüpomann, A., Bleaching and Permanent Waving Aspects of Hair Research, *J. Soc. Cosmet. Chem.*, **37**, pp. 159-175, (1986).

4

PRELIMINARY INVESTIGATION OF NATURALLY OCCURRING KERATIN FIBRES BY FT-IR SPECTROSCOPY AND CHEMOMETRICS

The objective of this study is to expand the forensic applications of FT-IR micro-spectroscopy to other types of related keratin fibres. FT-IR spectral data will be interpreted through the use of curve-fit, chemometrics and MCDM methods of analysis.

4.1. Introduction

Forensic scientists deal with both human and animal hairs. Human hairs tend to appear mostly on articles from robberies eg., balaclavas and stocking masks; from sexual assaults eg., bedding and clothing, and on blunt weapons from crimes of violence. Animal hair investigation, on the other hand, tends to be related to allegation of bestiality, theft of furs, and as an additional source of evidence linking one set of items with another on which there are hairs from the domestic pets [1].

The basic structure of a fibre, whether human or animal, is essentially the same. In general, both types of fibre consist of an outer protective layer - the *cuticle*; this encloses the *cortex*, which is the central core of the fibre and the *medulla*. The medulla is particularly important for distinguishing human from animal hairs and different types of animal hairs from each other. The basis of the differentiation is the relative width of the medulla, and the precise structure and arrangement of its component parts [1, 2]. Although

individual animals cannot normally be identified, finding of similar animal hairs on two items recovered during an investigation may be sufficient circumstantial evidence to suggest that these two items were in contact with each other or with a common source of animal hair.

In a study by D'Andrea et al. [3], morphological characteristics of cat and dog hair such as length, colour, scales of the cuticle, and medulla were measured. Two major points drawn from the study were that fibres taken from different places of the same animal were not significantly different and that gender does not lead to microscopically visible differences within a breed. The authors argued that discrimination between animals of different species such as the dog and cat, and also between breeds of the same species by morphological means is not straightforward. The study concluded that scale casts and cross-sections do not permit differentiation of the two mentioned species, while the structure of the medulla does allow such differentiation. The authors proposed that individualisation of animal hair might be achieved using methods similar to those already employed in human DNA typing. However, literature [3] has shown that estimation of the mtDNA amount in animal hair shafts has proven difficult with dark-coloured hair, suggesting that melanin is the interfering molecule. A purification process was attempted in order to remove this interference but the results were not improved.

In another study by Hendricks et al. [4] the amino acid composition of cat hair was investigated and it was found that it is comparable with that of a dog, horse, sheep and human hair although the proline content of cat hair appears to be lower than that in the other species. The authors proposed that there was no significant ($P > 0.05$) effect of hair colour on the amino acid composition of cat hair. This is in accordance with

measurements in sheep [5] and human hair [6] studies. In these two separate studies the amino acid composition and amide I/II ratio, respectively, indicated no significant difference between hair fibres of different melanin composition. However, in a study by Kuttin et al [7], black and white hair obtained from a cow were analyzed and differences were detected in the concentrations of alanine, cystine, methionine and glycine. Other studies have shown a variation in the mineral content of differently coloured fibres collected from dog [8], mink [9] and human hair [6].

4.2. Application of Vibrational Spectroscopy to Keratin Fibres

The application of vibrational spectroscopy to human hair and wool has been discussed in chapter 3, sections 3.4 and 3.5. The discussion in this chapter will focus on other types of naturally occurring keratin fibres.

Bendit [10], in 1966, published a paper discussing the application of transmission infrared spectroscopy to study microtomed horse fibres. Polarisation measurements were employed to distinguish crystalline (α - and β -) and non-crystalline phases. Hydration of the hair resulted in shifts of the amide A, I and II frequencies for the non-crystalline phase, indicating the formation of water bridges and consistent with the high swelling capability of this secondary structure. The two crystalline phases (α - and β -) showed much smaller shifts in the amide I and II, and no shift in the amide A band, indicating that hydrogen bonding strength was not affected by hydration. The author argued that the spectra indicated the existence of a weak interaction between water molecules and the carbonyl of the peptide group.

Vibrational spectroscopy and in particular Raman spectroscopy has been utilised in order to investigate the molecular structure of feather keratin. An example of such study is by Hsu et al [11], who discussed the Raman spectra of native and solubilised samples of feather keratin. The amide I and III spectral regions were analysed by band resolving techniques. The spectra of the native form were consistent with a protein containing 64% of antiparallel chain pleated sheet structure and 36% of a disordered component. In the solubilised form, the protein was found to be 100% disordered and its conformational distribution differed from the disordered component of the native state.

Edwards et al [12, 13], have discussed the application of FT-Raman spectroscopy to keratin samples. In these papers, the authors presented the wavenumber assignments and the vibrational modes related to a variety of keratotic samples namely human hair and feather. The authors proposed that due to the characteristic Raman vibrations of the amide I and III bands, feather exists predominantly in the β -sheet conformation, while human hair acquires an α -helix structure.

Rintoul et al [14] and Jurdana et al [15] in separate studies, employed a confocal laser Raman microprobe to monitor the degree of order/disorder in the secondary structure of wool, hair and feather keratin. Rintoul et al [14] determined the orientation of the structures in the wool and feather samples using polarised Raman spectroscopy. The authors proposed an alpha helix orientation for the amide I band of the wool structure, while the feather samples displayed a β -sheet conformation. Similar results were obtained by Jurdana et al [15] who calculated the ratio of the intensity of 1248 cm^{-1} band (amide III, β -sheet) to that of the relatively stable CH_2CH_3 bending mode (1447

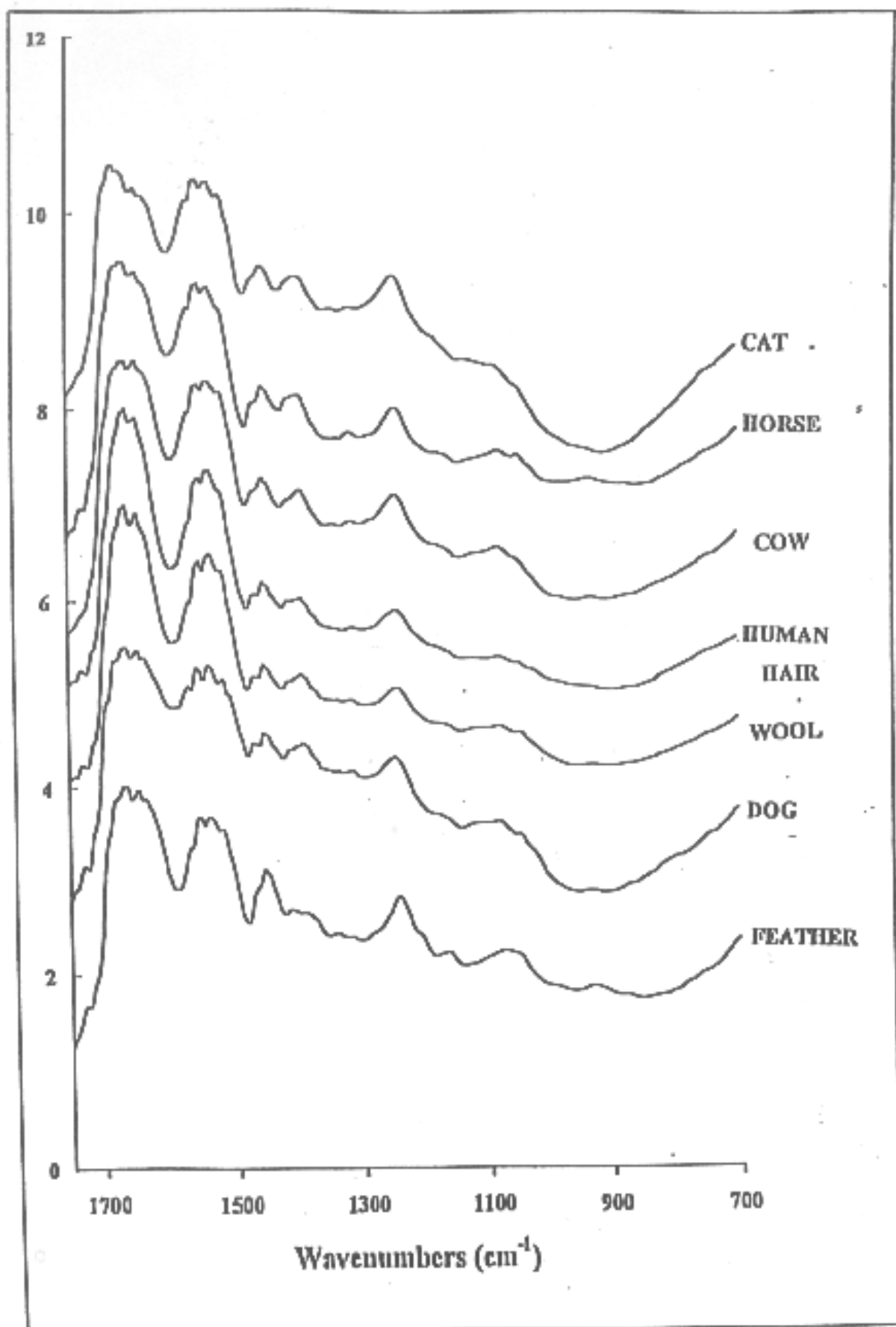


Figure 4.2. FT-IR spectra collected from the seven different keratin samples (1750-750 cm^{-1}) in absorbance.

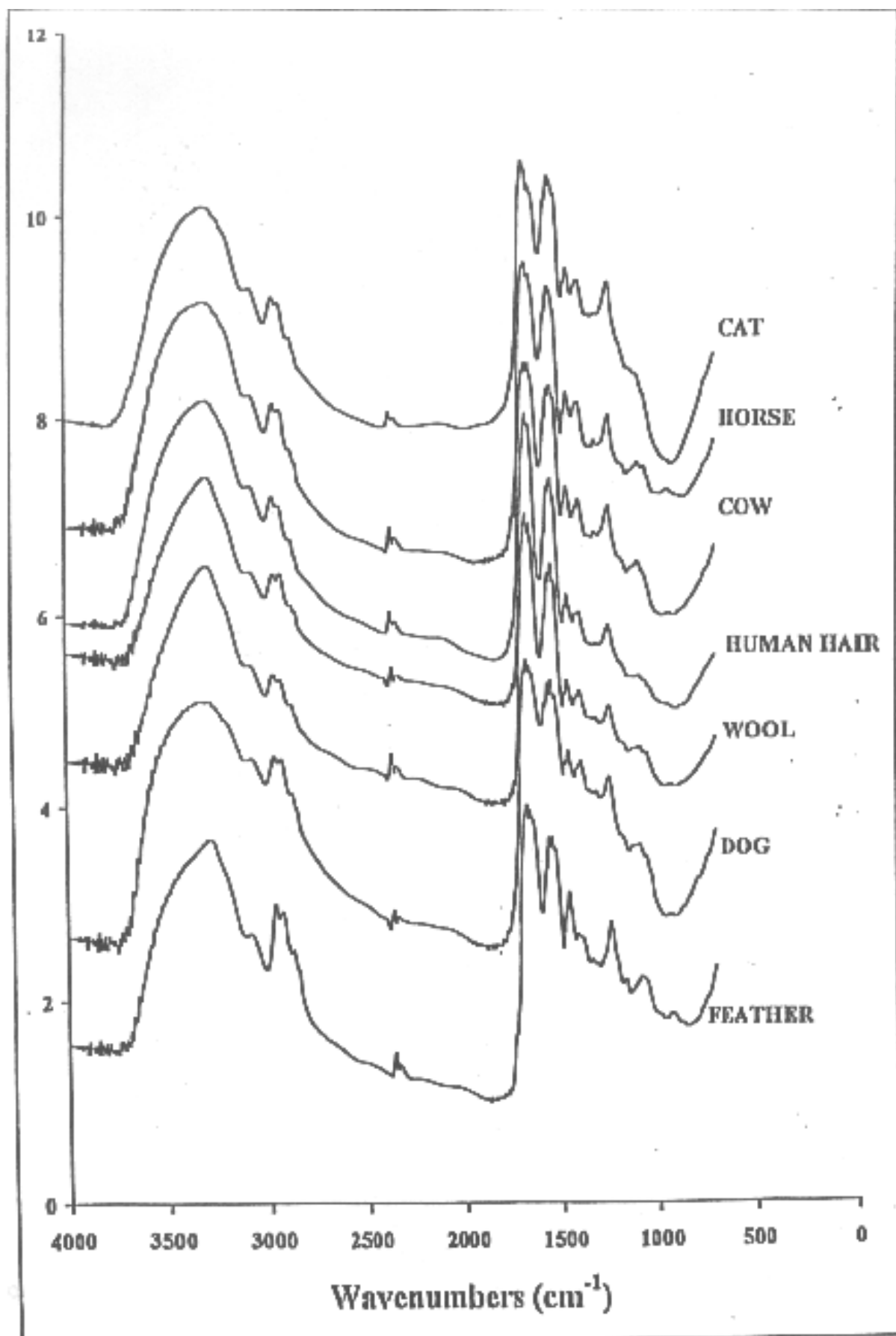


Figure 4.1. FT-IR spectra collected from the seven different keratin samples (4000-700 cm⁻¹) in absorbance.

cm^{-1}). The ratio indicated that feather samples are mainly found in the β -sheet orientation, while wool and human hair exhibit an α -helical structure.

4.3. General discussion of FT-IR keratin spectra

In the present work, representative samples of different keratotic tissues from mammals and birds were collected and FT-IR spectra were obtained; *cat's* fur, and *bird's* feather (parrot) represented the softer tissues, *cow* and *horse* hair represented the harder ones, while *human hair*, *wool* and *dog* hair represented tissues of intermediate thickness. This is the first time that a wide range of natural keratin fibres is investigated through the use of FT-IR micro-spectroscopy followed by chemometrics and MCDM methods.

All samples studied in this work showed similar vibrational modes in the spectral region between $4000\text{-}700\text{ cm}^{-1}$ (Figure 4.1). The region between $3300\text{-}3050\text{ cm}^{-1}$ corresponds to a Fermi resonance doublet and discussions in the literature suggest that these bands are sensitive to hydrogen bonding and, hence, α -helical or β -sheet keratin structural changes [16, 17]. The band at approximately 3400 cm^{-1} is due to the H-bonded OH stretch of water and appears as a broad band that masks less intense features in this region. Spectral features in the $3100\text{-}2700\text{ cm}^{-1}$ regions are assigned to the stretching modes of the C-H lipid alkyl chains. The methyl (CH_3) asymmetric and symmetric modes are observed at 2955 and 2933 cm^{-1} , respectively, and the methylene (CH_2) asymmetric and symmetric modes at 2875 and 2855 cm^{-1} . It has been suggested [17] that the 2930 and 2875 cm^{-1} bands form a Fermi resonance doublet through the interaction of the overtone of the CH_3 symmetric stretching mode for the methyl groups at the acyl chain termini.

The wavenumber region between 1750-750 cm^{-1} (Figure 4.2) contains the most intense features in the IR spectrum and provides valuable information concerning the nature of the secondary structures of the different keratotic biopolymers. This region contains vibrations arising from the $-\text{CONH}-$ grouping, predominantly from protein structures such as amide I and II bands at 1657 and 1547 cm^{-1} , respectively. A strong band was reported in the 1652 cm^{-1} region for all the keratin fibres except feather and was assigned to the $\nu(\text{C}=\text{O})$ stretching amide I band, indicating that the keratin in these samples exists predominantly in the α -helix conformation. Also the presence of a weaker band at approximately 1670 cm^{-1} indicates some presence of β -sheet conformation. Conversely, the feather samples exhibited a strong band at 1670 cm^{-1} characteristic of the β -sheet conformation of amide I with a weaker band at 1652 cm^{-1} characteristic of the α -helix.

Similarly, for amide II there are two characteristic vibrations; the first one at 1550 cm^{-1} corresponds to the N-H in-plane bending with contributions from the C-N stretching vibrations and is characteristic of the α -helix while the second vibration at 1531 cm^{-1} is related to the β -sheet conformation. The FT-IR spectra collected from the feather keratin exhibited a vibration at approximately 1531 cm^{-1} indicating that the secondary structure of the feather samples is predominantly that of a β -sheet. The FT-IR spectra collected from the rest of the samples showed a vibration at 1550 cm^{-1} characteristic of an α -helix secondary structure.

All samples exhibited a β -sheet conformation for the amide III band at $\approx 1244 \text{ cm}^{-1}$. The intensity of the amide III band for the feather keratin was stronger in comparison to the rest of the samples, which is consistent with the β -sheet preference of the feather

keratinisation process. This observation is consistent with comments made by Jurdana et al [15], who found that Raman spectra collected from feather keratin display a relatively intense amide III in comparison to spectra collected from wool and human hair. The authors further proposed that the intensity of the amide III band in the feather keratin is consistent with a significant contribution from the disordered β -sheet structure. In the present study, the relative amount of the β -sheet contribution to the amide III region for the different types of fibres was investigated and a detailed discussion is presented in a later section of this chapter.

The region at approximately 1040 cm^{-1} is related to the cysteic acid (S=O) vibration. Upon visual inspection, the FT-IR spectra collected from the feather samples have a broad cysteic acid band compared to the rest of the fibres. Cysteic acid will be further investigated through curve-fitting of the relative intensity area of the band and will be discussed in a later section of this chapter.

4.4. Curve-Fitting Analysis of Spectra

X-ray diffraction and infrared dichroic measurements reported in the literature have indicated the polypeptide chain conformations of natural keratins [18]. In its natural form feather contains proteins that exist predominantly in the β -sheet structure, whereas human hair and wool are mainly composed of an α -helix [18]. Visual inspection of the FT-IR spectra collected from the different types of keratin samples indicated certain variations in the band assignments of the amide conformations. The spectral region between $1750\text{-}750\text{ cm}^{-1}$ contains characteristic “fingerprint” vibrations for the keratin samples studied in this chapter. Due to the large amount of information that can be obtained from this spectral region, curve-fitting analysis of the bands in this region will enable a semi-quantitative assessment of the amide vibrations along with CH_2CH_3 and S=O vibrations present in the keratin fibres. The theoretical aspects of curve fitting have been discussed in detail in chapter 2, section 2.9. The model proposed for the curve-fit analysis is the Gaussian-Lorentzian model, a detailed discussion of which can be found in chapter 2, section 2.9.1. It is important to note that this is the first time a comprehensive curve-fit analysis of FT-IR spectra collected from a wide range of keratin fibres is presented.

In this study, FT-IR spectra were collected from three different fibres from each animal and human sample. For the purpose of this analysis, it was important to investigate the reproducibility of the curve-fit measurements in the FT-IR spectra. Table 4.1 (shown in page 144), shows the average (from three different fibres) curve-fitting error of the spectral area ($1750\text{-}750\text{ cm}^{-1}$) from each keratin sample. For example, the error of the curve-fit measurements for the three different fibres collected

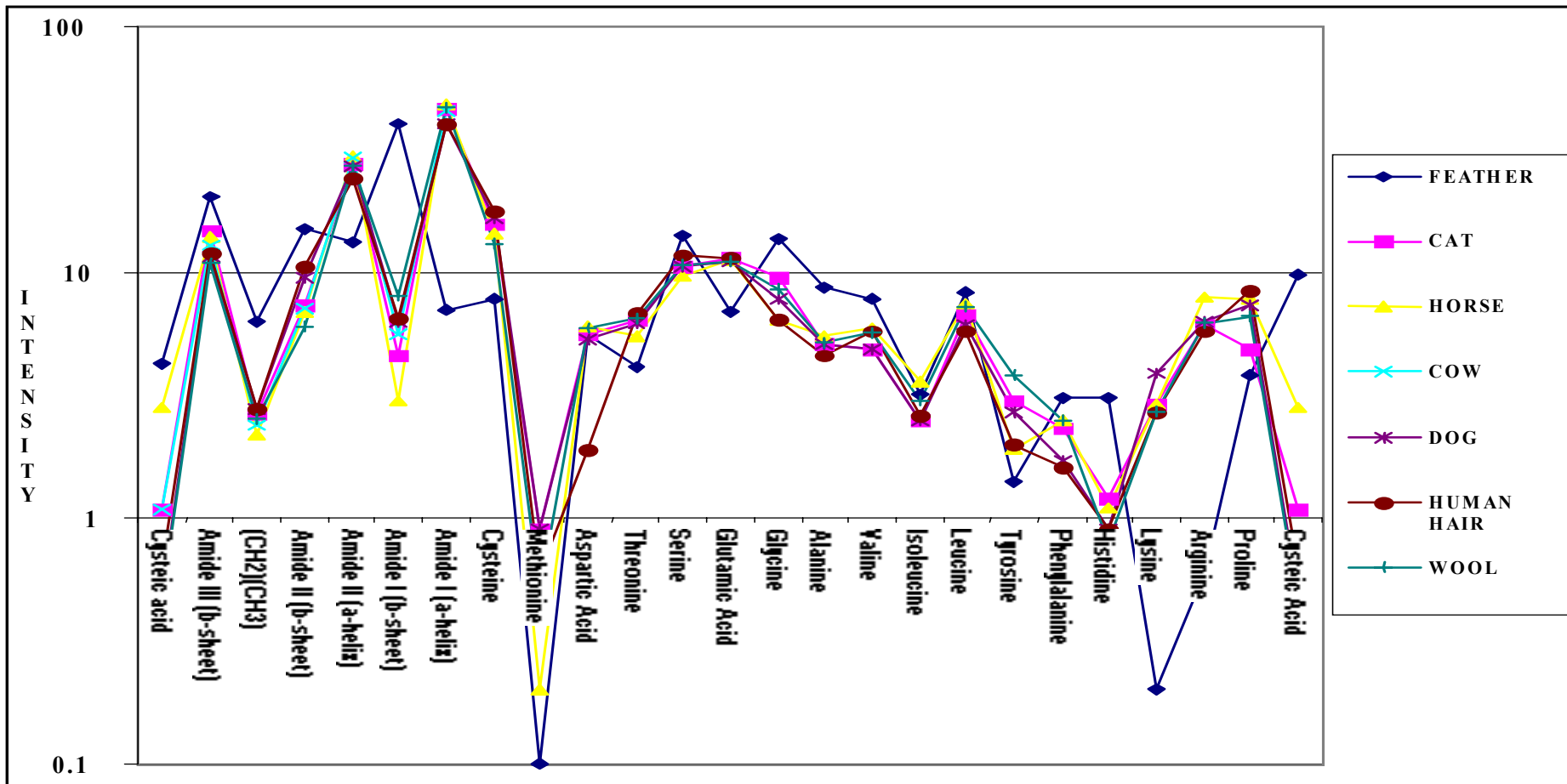


Figure 4.3 Fitted FT-IR relative intensity areas of FT-IR spectra.

Table 4.2.

Peak positions used in curve fitting for the keratotic samples of FT-IR spectra and their corresponding relative intensity areas and literature values (mol/100 mol of residue*).

	FEATHER	CAT	HORSE	COW	DOG	HUMAN HAIR	WOOL
Cysteic acid ¹	4.3	1.1	2.8	1.1	0.49	0.6	0.46
Amide III (β -sheet) ¹	20.4	14.7	13.8	12.9	11.6	11.9	10.9
(CH ₂)(CH ₃) ¹	6.3	2.7	2.2	2.4	2.8	2.8	2.5
Amide II (β -sheet) ¹	15	7.31	6.9	7.2	9.4	10.5	6
Amide I (α -helix) ¹	13.2	27.4	29.6	29.1	27.3	23.9	27.3
Amide I (β -sheet) ¹	40.3	4.6	3	5.61	6.3	6.5	8.10
Amide I (α -helix) ¹	7.01	45.9	48.3	45.2	40	40.2	46.6
Cysteine ²	7.1	15.8	14.4		16.7	17.8	13.1
Methionine ²	0.1	0.9	0.2		0.9	0.6	0.5
Aspartic acid ^{2,3}	5.6	5.6	6		5.3	1.9	5.9
Threonine ²	4.1	6.4	5.5		6.2	6.8	6.5
Serine ²	14.1	10.6	9.6		10.5	11.7	10.8
Glutamic acid ²	6.9	11.4	11.3		11.1	11.4	11.1
Glycine ²	113.7	9.5	6.4		7.8	6.4	8.6
Alanine ²	8.7	5.1	5.5		5.1	4.6	5.2
Valine ²	7.8	4.9	5.9		4.9	5.8	5.7
Isoleucine ²	3.2	2.5	3.6		2.5	2.6	3
Leucine ²	8.3	6.7	7.5		6.1	5.8	7.2
Tyrosine ²	1.4	3	1.9		2.7	2	3.8
Phenylalanine ²	3.1	2.3	2.5		1.7	1.6	2.5
Histidine ²	3.1	1.2	1.1		0.9	0.9	0.8
Lysine ²	0.2	2.9	2.9		3.9	2.7	2.7
Arginine ²	0.6	6.1	7.9		6.3	5.8	6.2
Proline ²	3.8	4.9	7.8		7.3	8.4	6.6

* Residue refers to the amino acid molecule as it is found within a protein.

¹ current study results

² literature results [4 (for cat, horse, dog, human hair and wool) and 13 (feather)]

from the feather sample was estimated to be 5.1×10^{-5} . This error is very small and it thus indicates that the curve-fit measurements of the spectral area investigated in this study are reproducible. Table 4.1 shows that the error in the curve-fitting measurements of each of the three¹ different FT-IR spectra collected from each subject was small to indicate any significant variation between the fibres from the same source.

Table 4.1.

Error in curve fitting measurements

Keratin	Error in curve fit measurements ($\times 10^{-5}$)
Feather	5.13
Dog	7.76
Wool	10.15
Human hair	14.9
Cow	13.8
Cat	14.6
Horse	8.36

The average area of each of the three fibres from each source was estimated by curve-fitting each of the major FT-IR spectral bands. The results are presented in table 4.2 and a graphical representation is shown in figure 4.3. The same table also presents results of some amino acids obtained from the literature [4, 13]. The amino acid amounts derived from the literature show that the feather samples contain high

¹ Even though this study did not include a detailed statistical analysis, the s^2 was calculated in an attempt to determine the optimum number of fibres necessary to establish the variance from a single animal. The s^2 for 3 spectra (Collected from different fibres from a single source) was 0.0518 and s^2 for 20 spectra (also collected from different fibres from a single source) was 0.494. At 95% confidence level the T-test indicates that 3 samples are not statistically significant (T-test for 3 samples = 0.950, $\therefore s^2 < 0.950$), whilst 20 samples are statistically significant (T-test for 20 samples = 0.433, $\therefore s^2 > 0.433$). Due to time constraints, only three fibres from each source were examined for the study in chapter 3.

amounts of hydrocarbon groups such as glycine, alanine, valine, isoleucine and leucine than the rest of the fibres [4, 13]. Out of the three basic amino acids, lysine and arginine are present in small quantities in feather compared to the other keratin fibres, whilst histidine is found in larger amounts.

According to table 4.2, curve-fitting of the 'fingerprint' region of the feather samples showed that this fibre contains the highest intensity of β -sheet for amide I, II and III in comparison to the rest of the keratins. In contrast, the feather keratin has the lowest intensity of α -helix for amide I and II. These results support previous studies in the literature [12-15], which proposed that feather keratin exhibits a β -sheet arrangement whilst keratin fibres such as human hair and wool indicate a preference for an α -helical structure.

The following is a detailed point form evaluation of the curve-fit analysis for the amide and cysteic acid vibrations obtained from the rest of the keratin fibres:

I. Amide I (α -helix):

1. Horse fibres were found to contain the highest α -helix at 48.3, followed very closely by wool (46.6).
2. The content of the α -helix estimated for fibres collected from cat and cow were very similar at 45.9 and 45.2, respectively.
3. Fibres collected from both dog and human hair showed similar content of α -helix at 40 and 40.2, respectively.

Conclusion: From the keratin samples studied, horse fibres contain the highest amount of α -helix, whilst human hair and fibres collected from dog contain the lowest amount of α -helix.

II. Amide I (β -sheet):

4. Horse fibres contained the lowest intensity value (3) for the β -sheet.
5. Fibres collected from the cat had a β -sheet value of approximately 4.6 followed by cow at 5.6.
6. The β -sheet content estimated for the fibres collected from the dog (6.3) was similar to that obtained from the human hair fibres at 6.5.
7. Wool contained the highest intensity of the β -sheet at 8.

Conclusion: From the keratin samples studied, wool fibres contain the highest β -sheet, whilst the horse fibres contain the lowest.

III. Amide II (α -helix):

8. Fibres collected from horse were found to have the highest α -helix at 29.6, followed by cow fibres (29.1).
9. Cat (27.4), dog (27.3) and wool (27.3) contained similar values for the α -helix.
10. Human hair contains the lowest amount of α -helix at approximately 23.9.

Conclusion: From the keratin samples studied, horse fibres contain the highest α -helix, whilst human hair fibres contain the lowest.

IV. Amide II (β -sheet):

11. Wool was found to contain the lowest amount of β -sheet at 6.
12. Fibres collected from horse were at approximately 6.9, followed by cow and cat at 7.2 and 7.3, respectively.
13. Fibres collected from dog and human hair had a high β -sheet content at 9.4 and 10.5, respectively.

Conclusion: From the keratin samples studied, human hair contains the highest amount of β -sheet, whilst wool fibres contain the lowest value.

V. Amide III (β -sheet):

14. Cat fibres were found to contain the highest β -sheet content at approximately 14.7.
15. Horse fibres contain the second highest amount of β -sheet at 13.8.
16. Cow fibres contain approximately 12.9, followed by human hair and dog fibres at 11.9 and 11.6, respectively.
17. Wool fibres contain the lowest intensity value for β -sheet at approximately 10.9.

Conclusion: From the keratin samples studied, cat fibres contain the highest amount of β -sheet, whilst wool fibres contain the lowest. Furthermore, the curve-fit results indicate that amide III is relatively more intense in hair than in wool. This is expected for a keratin high in α -helical content, which also has a higher proportion of disordered than ordered structure. These results support a previous study by Jurdana et al [15] who proposed that human hair fibres contain higher amounts of amide III (β -sheet) than wool fibres.

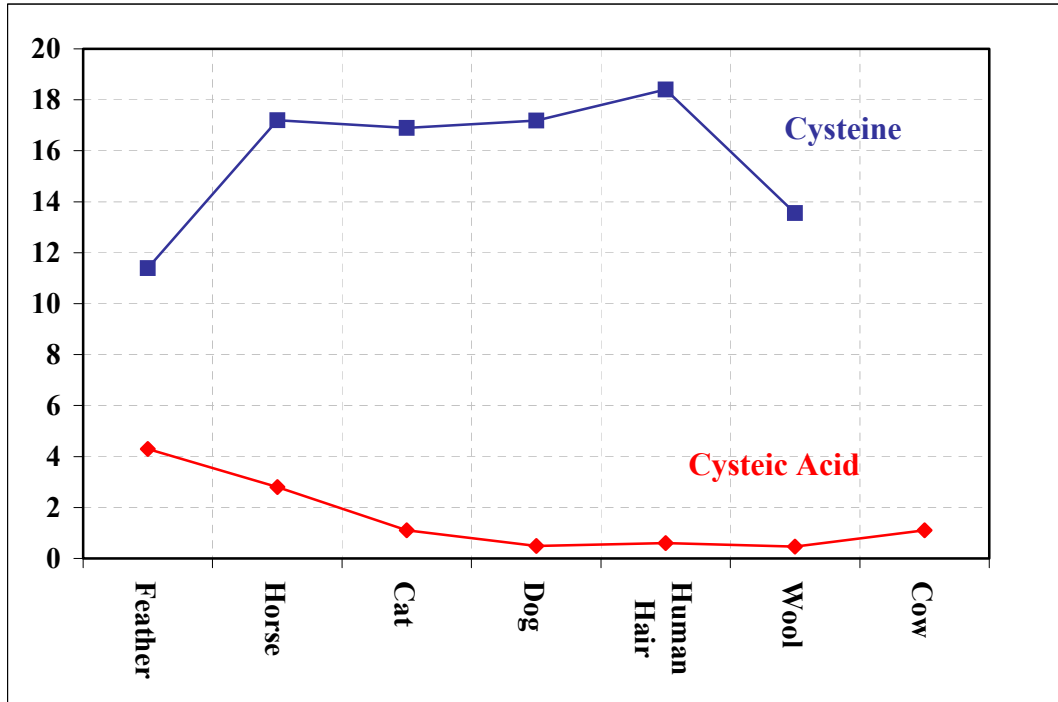


Figure 4.4. Relative areas of cysteic acid and cysteine of the different keratin fibres.

VI. Cysteic acid

Cysteine bonds are among the most important bonds in the molecular structure of keratin [18]. When cysteine bonds break, changes are introduced to the molecular structure of the keratin, which can lead to a disruption of the secondary structure of the fibre. FT-IR micro-spectroscopy has been successfully applied in chapter 3, section 3.6.4.3, to study the cysteic acid vibration during chemical treatment of human hair fibres. Raman spectroscopy was also applied in the same chapter to investigate the cysteine variation in the untreated and treated hair fibres. The study showed that an increase in the cysteic acid content is always accompanied by a decrease in the content of cysteine. In this study, Raman micro-spectroscopy could not be utilised to investigate the keratin fibres because of the limitations of the technique due to fluorescence problems. Therefore, values of cysteine were extracted from the literature for most of the keratin fibres studied. The literature did not offer any values of cysteine for the cow fibres.

Table 4.2 provides a the relative intensity area of cysteic acid obtained from the FT-IR spectra collected from the different keratin fibres and also the relevant cysteine content obtained from the literature [4, 13]. Figure 4.4. is a graphical representation of the cysteic acid and cysteine values plotted for each keratin fibre.

As shown in table 4.2, feather keratin contains the highest amount of cysteic acid at approximately 4.3. Horse fibres have the second highest value at 2.8. Fibres collected from cat and cow are found to contain low values of cysteic acid (≈ 1), whilst human hair had an even lower value at 0.6. The lowest amount of cysteic acid is found at

fibres collected from dog (0.49) and wool at 0.46. The amino acid results obtained from the literature [13] indicate that feather keratin contains the lowest cysteine content (7.08). Out of the mammalian fibres presented in the study human hair (17.8) and dog (16.7) contain the highest amount of cysteine, cat (15.8) and horse (14.4) are intermediate and wool (13.1) contains the lowest amount of cysteine. The literature did not provide any amino acid results for cow fibres. It is therefore evident that a fibre high in cysteine will contain low amounts of cysteic acid, whilst the opposite occurs for fibres with low cysteine values.

The work presented in chapter 3 highlighted the affect that chemical bleaching has on the secondary structure of human hair fibres. The study proposed that chemical oxidation leads to a decrease in the cysteine content of the treated fibre accompanied by an increase in the amount of cysteic acid. The study also showed that during chemical treatment, there is a decrease in the α -helix, which indicates disruption of the secondary structure of the fibre. The work carried out in the present chapter has shown that feather samples contain high amounts of β -sheet and cysteic acid, but low amounts of α -helix and cysteine. This further suggests that a fibre high in cysteic acid and low in cysteine will be characterised by a β -sheet secondary structure, whilst a fibre low in cysteic acid and high in cysteine will be characterised by a highly crystalline α -helical structure. **This study has therefore lead to the conclusion that the secondary structure of the keratin fibre is influenced by the amounts of cysteine and cysteic acid present in the fibre composition.**

Table 4.3.

Ratios of the relative area intensity for the keratotic FT-IR spectra.

Keratin	AmideIII (β)/(CH₂CH₃)	Amide I(α)/(CH₂CH₃)	Amide I (β)/(CH₂CH₃)
Feather	3.2	1.1	6.4
Dog	4.1	17	1.7
Wool	4.4	21.9	1.4
Human hair	4.3	18.8	2.3
Cow	5.4	14.3	2.2
Cat	5.5	14.4	2.3
Horse	6.3	18.6	3.2

4.5. Determination of secondary structure through FT-IR analysis

The best and most accurate way to determine protein conformation is by the combined use of both amide I and III bands [16]. Through these two bands it is possible to differentiate between the α -helix, β -sheet and random coil. In particular, the position of the amide I band has been reported [16] to be sensitive to changes in protein conformation and the variation in intensity and position of this band with sampling depth has been used as a means of estimating the position of the cuticle/cortex interface in keratin fibres using FT-IR/PAS spectroscopy. Jurdana et al [12] and Lippert et al [19] employed the ratio of amide III (1244 cm^{-1}) to CH_2CH_3 (1447 cm^{-1}) to estimate the secondary structure of keratin fibres. In particular, Jurdana et al used this ratio to estimate the β -sheet content in human hair, wool and feather. A similar procedure for estimating the secondary structure of keratin fibres was employed in the present study. Even though the amide III band is not as intense in the FT-IR spectra as it appears in the Raman spectra, similar trends are expected between the two techniques. The results presented in table 4.3 show the ratio of the relative area intensity of the amide III (β sheet)/(CH₂)(CH₃).

The results obtained from the ratio of amide III (β -sheet) to (CH₂)(CH₃) presented in table 4.3 do not agree with previous results by Jurdana et al [15]. In their study, the authors found the ratio of feather keratin (0.57) to be higher than that of Merino wool (0.47), whilst the ratio of human hair (0.50) was intermediate. In the present study, the ratio of amide III (β -sheet) to (CH₂)(CH₃) calculated for the feather sample resulted in the lowest value (3.2) for the β -sheet, which is inconsistent with the secondary structure of the fibre, which has been shown to contain the highest amount of β -sheet

[15]. A possible explanation for the disagreement between the present results and those obtained by Jurdana et al [15] could be due to the intensity of the amide III in the FT-IR spectra. As previously discussed, amide III is not as intense in the FT-IR spectra as it is in the Raman spectra. The study by Jurdana et al [15] employed Raman spectroscopy, whilst the present study used FT-IR. It therefore appears that the results obtained from the amide III (β -sheet)/(CH₂)(CH₃) ratio was not comparable for the FT-IR and Raman data.

Amides I and II have considerably high intensities in the FT-IR spectra and an attempt was made to use one or both of these bands to estimate the secondary structure of the keratin fibres. In particular, Surewicz et al [16] proposed that the amide I band is sensitive to changes in protein conformation and can therefore be used to monitor the molecular structure of keratins. The (CH₂)(CH₃) band was still used because it is not sensitive to changes in protein conformation [15].

The ratio of amide I(β -sheet)/(CH₂)(CH₃) was initially estimated and the results are presented in table 4.3. There is a clear separation of the keratin samples into four main groups; the first group contains the feather keratin with the highest ratio (6.4) indicative of the preference of the fibre for a β -sheet structure. The second group contains fibres collected from wool (3.2). The third group consists of fibres collected from three different types of keratin; dog, cow and human hair fibres (2.2, 2.3, 2.3, respectively). The final group contains fibres collected from cat and horse keratin, which contain the lowest amide I(β -sheet)/(CH₂)(CH₃) at 1.4.

The ratio of the α -helix (amide I) to CH_2CH_3 was also calculated in an attempt to obtain an estimate of the α -helix content in the keratin fibres. The results are presented in table 4.3 and as expected feather keratin (1.1) contains the lowest amount of α -helix. Horse fibres (21.9) were found to contain the highest amount of α -helix, in contrast to the amide I (β -sheet/ CH_2CH_3) ratio, which showed horse fibres to contain the lowest amount of β -sheet. Cow fibres (18.8) contained the second highest amount of α -helix, followed by wool fibres (18.6) and cat fibres (17). Human hair (14.4) had an intermediate value between wool (18.6) and feather (1.1) suggesting that wool fibres are made-up of a higher content of α helix than hair fibres. Finally, dog fibres formed part of the intermediate group at approximately 14.4.

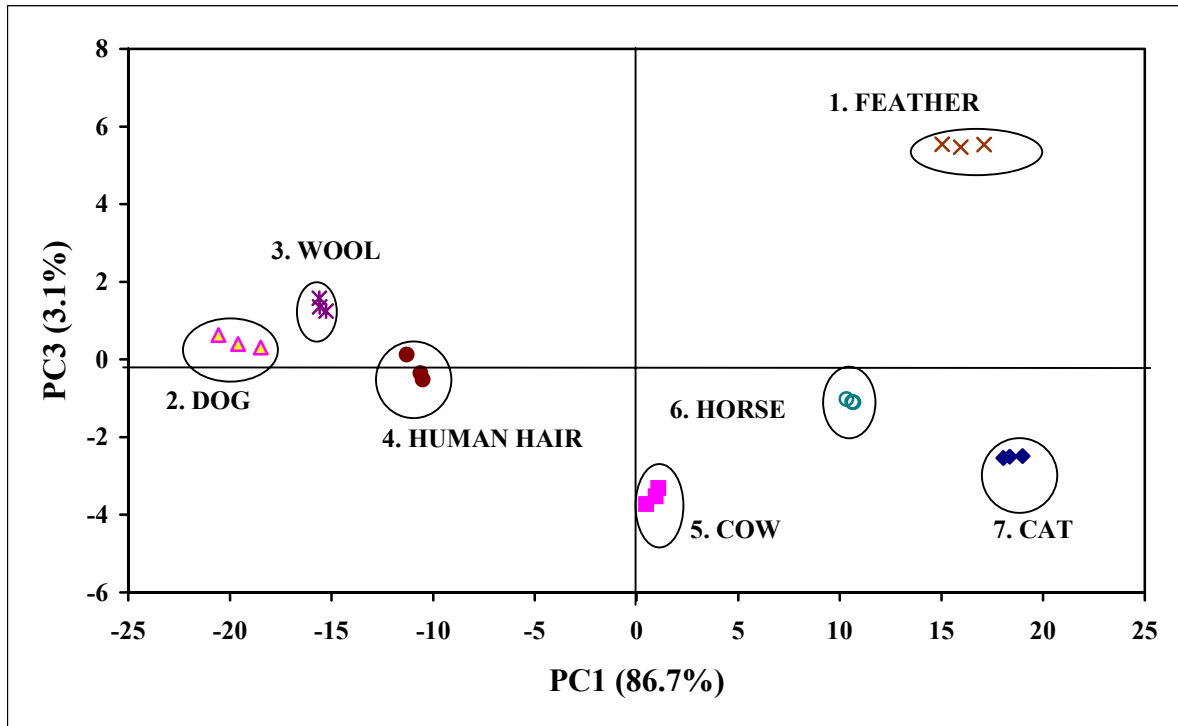


Figure 4.5. PC1 (86.7%) vs PC3 (3.1 %) scores plot of the FT-IR spectra collected from keratin hair samples (1750-750 cm^{-1}).

4.6. Chemometrics Analysis

A discussion regarding the theory and general applications of chemometrics methods of analysis has been presented in detail in chapter 2, section 2.5. In this work PCA, SIMCA and FC were applied in order to obtain further information to that of the curve-fitting experiments with regards to the conformational states present in the hard keratin samples.

The three FT-IR spectra obtained from each of the seven different keratotic samples; feather, cat, dog, horse, cow, wool and human hair, were submitted to PCA in order to match and discriminate the different keratin samples.

4.6.1. PCA

The PCA plot in figure 4.5 shows the best discrimination between the samples (PC1 (81.8%) vs PC3 (3.0%)). PC1 separates the feather, horse, cow and cat samples (positive scores) from the wool, dog and human hair (negative scores). The PC1 loadings plot (not shown) contains very broad spectral regions and provides only limited information for the discrimination of the spectra. PC3, on the other hand, highlights the discrimination between the feather samples (high positive scores) from the rest of the fibres (ranging from low positive to high negative scores on PC3).

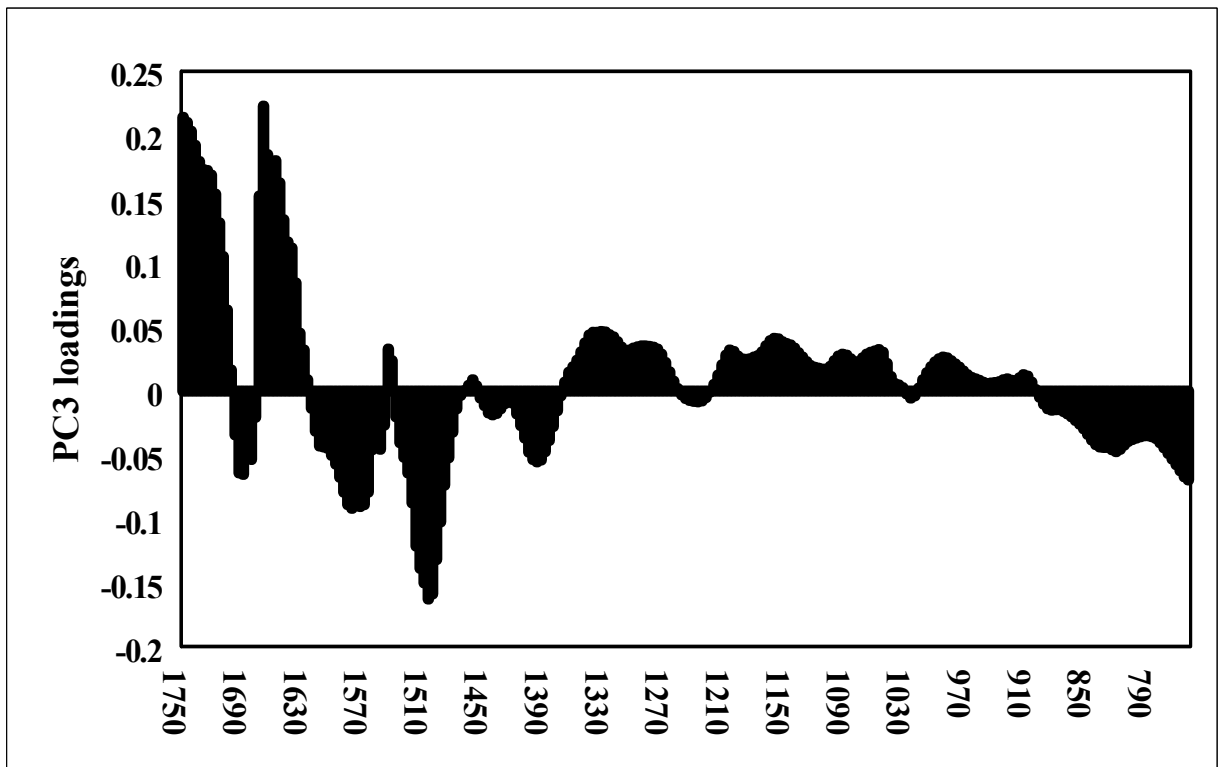


Figure 4.6. PC3 loadings plot (1750-750 cm^{-1}).

The PC3 loadings plot (figure 4.6) indicates that the feather samples are influenced by the following vibrations;

Assignment	Wavenumber (cm ⁻¹)
1. $\nu(\text{COO}^-)$	1733 cm ⁻¹
2. Amide I $\nu(\text{C=O})$ β -pleated sheet	1670 cm ⁻¹
3. Amide II $\delta(\text{N-H})$ $\nu(\text{C-N})$ β -pleated sheet	1531 cm ⁻¹
4. $\nu(\text{COO}^-)$	1387 cm ⁻¹
5. $\nu_s(\text{S-O})$ cystine dioxide	1300 cm ⁻¹
6. Amide III	1238 cm ⁻¹
7. $\nu_a(\text{S-O})$ cysteine-S-sulfonate	1194 cm ⁻¹
8. $\nu_a(\text{S-O})$ cysteic acid	1172 cm ⁻¹
9. $\nu_s(\text{S-O})$ cysteine dioxide	1125 cm ⁻¹
10. $\nu_s(\text{S-O})$ cysteine monoxide	1075 cm ⁻¹
11. $\nu_s(\text{S-O})$ cysteic acid	1041 cm ⁻¹

The rest of the fibres are influenced by the following vibrations:

Assignment	Wavenumber (cm ⁻¹)
1. Amide I $\nu(\text{C=O})$ α -helix	1670 cm ⁻¹
2. Amide II $\delta(\text{N-H})$ $\nu(\text{C-N})$ α -helix	1550 cm ⁻¹

The vibrational assignments obtained from the PC3 loadings plot confirm the results obtained from the curve-fitting experiments. In particular, the PC3 loadings plot indicates that the separation of the FT-IR spectra collected from the keratin fibres is

influenced by the amide I and II (α -helix) assignments for the dog, wool, cow, horse, cat and human hair fibres. The feather samples on the other hand are characterised by the amide I, II and III (β -sheet) as well as the cysteic oxide vibrations. It is therefore evident that the distribution of the vibrational assignments for the separation of the keratin fibres as seen in the loadings plot agree with the curve-fitting evaluations of the spectra.

The FT-IR spectra collected from feather keratin were removed, as it was the only keratin sample predominantly made-up of β -sheet, and a new PCA plot was constructed using the α -helix samples. Figure 4.7 is a representation of the separation (PC1 (88.8%) vs PC3 (1.7%)) between the α -helix keratin samples.

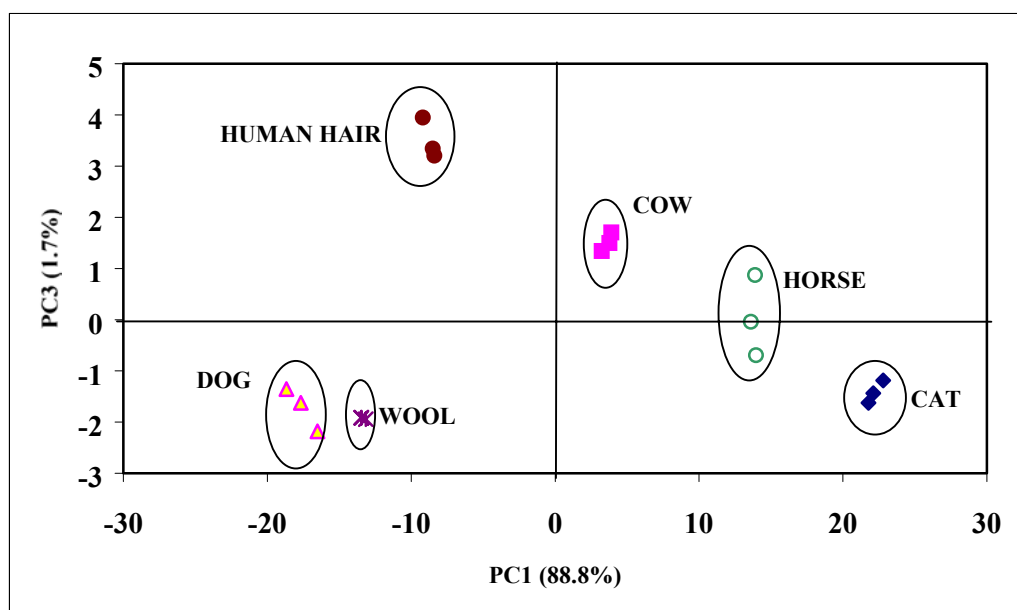


Figure 4.7. PC 1 (88.8%) vs PC3 (1.7%) scores plot of the six different types of mammal hard keratin samples ($1750\text{-}750\text{ cm}^{-1}$).

Table 4.4 shows a summary of the curve-fit results obtained for the amide I and II (α -, β -) spectral regions for the different keratin samples studied (except feather). The

separation of the FT-IR spectra collected from the different fibres along PC1 is very similar to the results obtained from the curve fit analysis. PC1 separates the fibres on the basis of their secondary structure; human hair, dog and wool fibres (all on negative scores on PC1) have a low α -helix and a high β -sheet, whilst fibres collected from cow, horse and cat (all on positive scores) have a high α -helix and a low β -sheet. According to table 4.4, on a scale of 1-6 (1 being the highest and 6 the lowest), horse fibres have a high α -helix (for both amide I and II) and a low β -sheet (for both amide I and II), whilst human hair fibres contain the opposite i.e., a high content of β -sheet and a low α helix (for both amide I and II).

Table 4.4.

Summary of the curve-fit results from the Amide I and II (α -, β -) spectral regions for the keratin samples (except feather)

Scale (1 is highest 6 is lowest)	Amide I (α -helix)	Amide I (β -sheet)	Amide II (α -helix)	Amide II (β -sheet)
1	Horse	Wool	Horse	Human Hair
2	Wool	Human Hair	Cow	Dog
3	Cat	Dog	Cat	Cat
4	Cow	Cow	Dog	Cow
5	Dog	Cat	Wool	Horse
6	Human Hair	Horse	Human Hair	Wool

4.6.2. SIMCA

The FT-IR spectra collected from keratin samples composed mainly of α -helix, which are all the samples except those of feather, were used to build a reference set and were compared to the feather samples. The model accounted for 99.4% of the variance and five components were identified as significant, by the leave-one-out method. SIMCA (Table 4.5) indicates a similar discrimination between the keratin samples as that seen in the PCA plot (figure 4.5). FT-IR spectra collected from the α -helix proteins have RSD values (0.0157) below the RSD_{crit} (0.0191), while feather proteins have RSD values (0.0837) well above the RSD_{crit} .

Table 4.5.

SIMCA analysis results with $RSD_{crit}=0.0191$, $p=0.05$

SIMCA results	α-helix proteins	β-sheet proteins
RSD, mean	0.0157	0.0837
N(number of spectra)	18	3
Distance between classes	----	3.3

As outlined in chapter 2, section 2.7.2, class distances greater than 3.0 illustrate that the classes are different, while values with less than approximately 1.0 indicate that the classes are very similar. In this study, a class distance of 3.3 was obtained for the above samples. The class distance indicates that the two classes are quite different.

4.6.3. FC

The FC results (Table 4.6) support the results obtained from PCA and SIMCA. A two-cluster model for both a hard (1.50) and soft (2.50) weighting exponent value was obtained. Feather samples have high membership values in class one, while the rest of the samples indicate a preference for class 2. Similar patterns are observed for both hard and soft weighting exponent values.

Table 4.6.

Fuzzy clustering membership values for a two-cluster model with a hard (1.50) and soft (2.50) weighting exponent value

Sample	W.E.=1.50		W.E.=2.50	
	Class 1	Class 2	Class 1	Class 2
β -sheet proteins (feather)	1.00	0.00	0.99	0.01
α -helix proteins (human hair, cat, cow, cat, horse, and dog)	0.00	1.00	0.02	0.98

Table 4.7 shows the membership values for a seven-cluster model. The decision to use seven clusters was based on the fact that there were seven different types of fibres examined. FC was used to test whether the different fibres will form their own unique groups.

Table 4.7.

Fuzzy clustering membership values for a seven-cluster model with a soft (2.50)

	<u>weighting exponent value</u>						
	Class 1	Class 2	Class 3	Class 4	Class 5	Class 6	Class 7
Cow	0.00	0.01	0.00	0.03	0.00	0.00	0.96
Dog	0.04	0.00	0.05	0.00	0.89	0.02	0.00
Cat	0.00	0.00	0.94	0.00	0.06	0.00	0.00
Feather	0.02	0.00	0.04	0.93	0.00	0.00	0.01
Wool	0.01	0.03	0.00	0.02	0.00	0.93	0.01
Human hair	0.00	0.78	0.00	0.10	0.00	0.07	0.05
Horse	0.82	0.00	0.05	0.00	0.03	0.04	0.06

Similar results are also obtained for a hard weighting component (1.50). The separation of each keratin sample in their individual class confirms the unique molecular structure of each keratin sample and supports the PCA discrimination of the fibres into their separate clusters.

As discussed in the introduction, MCDM methods are particularly suitable for assistance with multi-variate problems. PROMETHEE and GAIA, which are two of

well-regarded MCDM methods, were applied to investigate the different keratin fibres on the basis of their molecular structure as reflected by the IR spectra.

There are several possible MCDM methods, but as outlined in chapter 2, section 2.8, PROMETHEE and GAIA were selected to study the keratin fibres presented in this chapter. These two methods were chosen to explore the ranking and to investigate the relationships between the different keratin fibres. The data is aggregated via the utilization of multicriteria analysis software 'Promcalc' [20].

In this chapter, the focus is to introduce the setting up of a PROMETHEE model and its general application to fibre analysis. The work presented in this section is not specifically intended to obtain any additional information for the animal and human hair samples but appropriate attention will be drawn and comparisons will be made with the results from previous analyses by other chemometrics methods such as PCA, SIMCA and FC, so as to highlight the most important aspects of keratin characteristics.

The data matrix consists of seven objects, which include fibres collected from bird's feather, cow, cat, dog, wool, horse and human hair fibres. The criteria consist of four attributes, three of which (cysteic acid, amide I(α /CH₂CH₃) and amide I(β /CH₂CH₃)) were derived from the FT-IR spectral data and the band areas were estimated by curve fitting of the FT-IR spectra. The fourth criterion, cysteine, was obtained from the literature. The combination of a number of different variables obtained from different sources and methods in one matrix is one of the most important advantages of the PROMETHEE method.

As required by the PROMETHEE method, it is necessary to maximise or minimise each criterion i.e. to declare whether the largest values of a variable are preferred (maximized) or conversely the lowest ones (minimized). Such settings are an important aspect in defining the MCDM model and the scenario leading to the framework within which the results have to be interpreted. Thus, prior to analysing the PROMETHEE results, it is important to discuss the background of maximize/minimize settings in the context of the hair-keratin fibre composition.

The α - and β - amide I bands reflect the presence of two common but very different keratin structures. The α -helix is the common defining structural unit of fibrous keratins. A fibre with high amounts of α -helices is more crystalline and its physical properties are affected accordingly. In a hair keratin fibre, the content of the β -structure is expected to be relatively low, and any significant amounts of it would indicate a fibre that has been physically stressed or somehow treated to facilitate an $\alpha \rightarrow \beta$ keratin conversion. Similarly, only quite low amounts of cysteine and oxidized sulfur species are expected in a normal keratin fibre. Curve-fit analysis of the FT-IR spectra indicated that the ratio of the α -helix (amide I) to CH_2CH_3 is a good indication of the α -content present in the fibre, whilst the ratio of amide I (β -sheet/ CH_2CH_3) is a good indication of the β -sheet content. The ratio results presented in section 4.5 showed that feather keratin contains the lowest amount of α -helix, and the highest amount of β -sheet. The reverse was found to occur for the secondary structure for the rest of the keratin fibres.

TABLE 4.8.

Data matrix of Amide I ratios, Cysteine, and Cystelic acid band areas and PC1 and PC3 scores for the seven different keratins.

Objects	PC1	PC3	Cystelic acid	Amide I	Amide I	Cysteine
	(C1)	(C2)	(C3)	(β/CH_2CH_3) (C4)	(α/CH_2CH_3) (C5)	(C6)
Feather (A1)	16.5	5.7	4.3	6.4	1.1	7.1
Human Hair (A2)	-11.2	-0.2	0.6	2.3	18.8	17.8
Cat (A3)	18.9	-2.5	1.1	2.3	14.4	15.8
Dog (A4)	-19.7	1.2	0.49	1.7	17	16.7
Cow (A5)	1.8	-3.6	1.1	2.2	14.3	15.6
Horse (A6)	10.8	-0.9	2.8	3.2	18.6	14.4
Wool (A7)	-15.1	1.8	0.46	1.4	21.9	13.1

* P(a, b) is a V-shape function

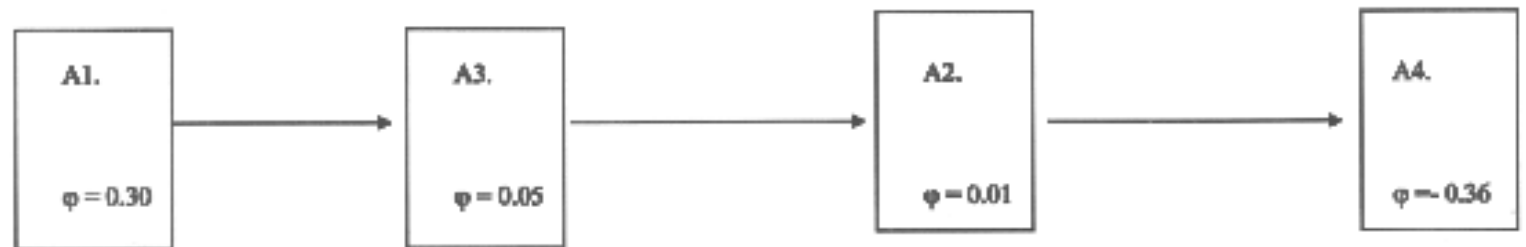


Figure 4.8. PROMETHEE II Complete Ranking for Scenario A.

TABLE 4.7.**Simulation Data matrix comparison of Amide I ratios, Cysteine, and Cysteic acid.**

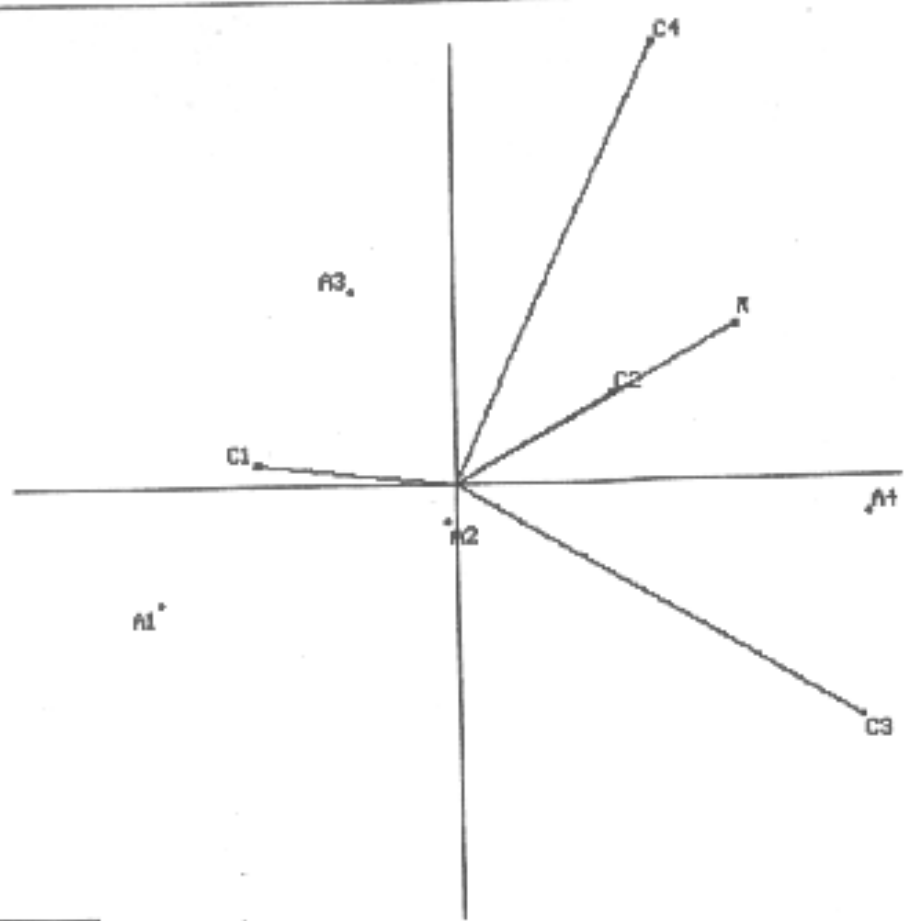
Criterion	Amide I (α/CH₂CH₃) (C1)	Amide I (β/CH₂CH₃) (C2)	Cysteine (C3)	Cysteic Acid (C4)
Scenario A (Min/Max)	Max	Min	Min	Min
Scenario B (Min/Max)	Max	Max	Max	Max
Type	3*	3*	3*	3*
Weight	1.00	1.00	1.00	1.00
P	10.00	3.00	4.00	3.00
Fibre 1 (A1)	10.00	1.00	1.00	1.00
Fibre 2 (A2)	8.00	2.00	2.00	2.00
Fibre 3 (A3)	9.00	2.00	1.00	1.00
Fibre 4 (A4)	6.00	3.00	4.00	3.00

* P(a, b) is a V-shape function

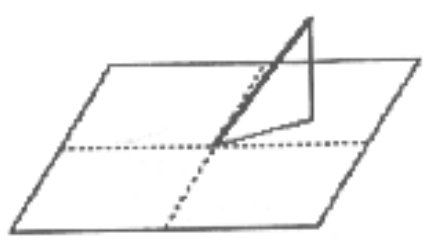
In the PROMETHEE study it is assumed that if the α -amide I ratio criterion is set to maximize, whilst the β -amide I ratio, cysteine and cysteic acid is set to minimize, then the PROMETHEE method is being set up to rank objects on the basis of a normal, undamaged and physically unstressed keratin fibre. In an ideal case, all four criteria vectors should roughly point to the objects highest in α -keratin and lowest in the other molecular constituents with the decision axis, π , being quite strong. On the other hand, if for example, all four molecular constituent criteria were set to maximize, the model is then defined to look for a compromise solution with the preferred keratin fibre having relatively high amounts of the four molecular constituents. The maximized criteria vectors will be scattered around the GAIA biplot, each pointing in the general direction of the best performing object-fibre. These theoretical scenarios are illustrated with a PROMETHEE analysis of a small 4x4 matrix simulation (Table 4.7).

The values in the matrix are of similar size to the real matrix presented in table 4.8 but have no direct connection to the actual entries. Objects A1-A4 may be thought of as fibre types 1-4. Both the net outranking flow ϕ diagrams and the GAIA biplots conform to the theoretical description of the two scenarios argued above. In Scenario A, where amide I ($\alpha/\text{CH}_2\text{CH}_3$) was maximised and the rest of the criteria were minimised, modelling the common α -keratin fibre composition, the ϕ outranking flows (figure 4.8) show that the A1 object is preferred (and has the highest value of ϕ of 0.15) while A4 (smallest ϕ value of -0.22) is least preferred. The GAIA plot (Figure 4.9) closely reflects the predicted outcome, with all the criteria vectors directed towards the most preferred object A1 with a strong decision axis pointing also towards this object. The data variance or information determined by the GAIA

GAIA Plane



C..1	: alpha	CI = 1.000	<
C..2	: beta	CI = 1.000	<
C..3	: cysteine	CI = 1.000	
C..4	: CA	CI = 1.000	



d = 100%

Figure 4.11. GAIA plane for Scenario B.

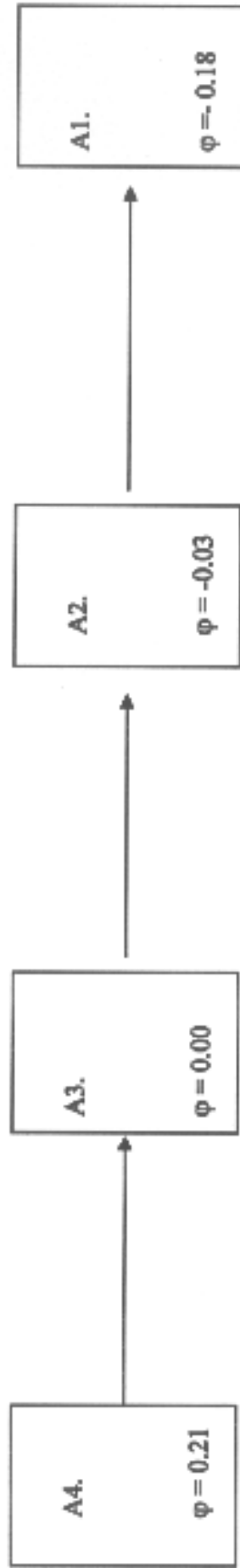
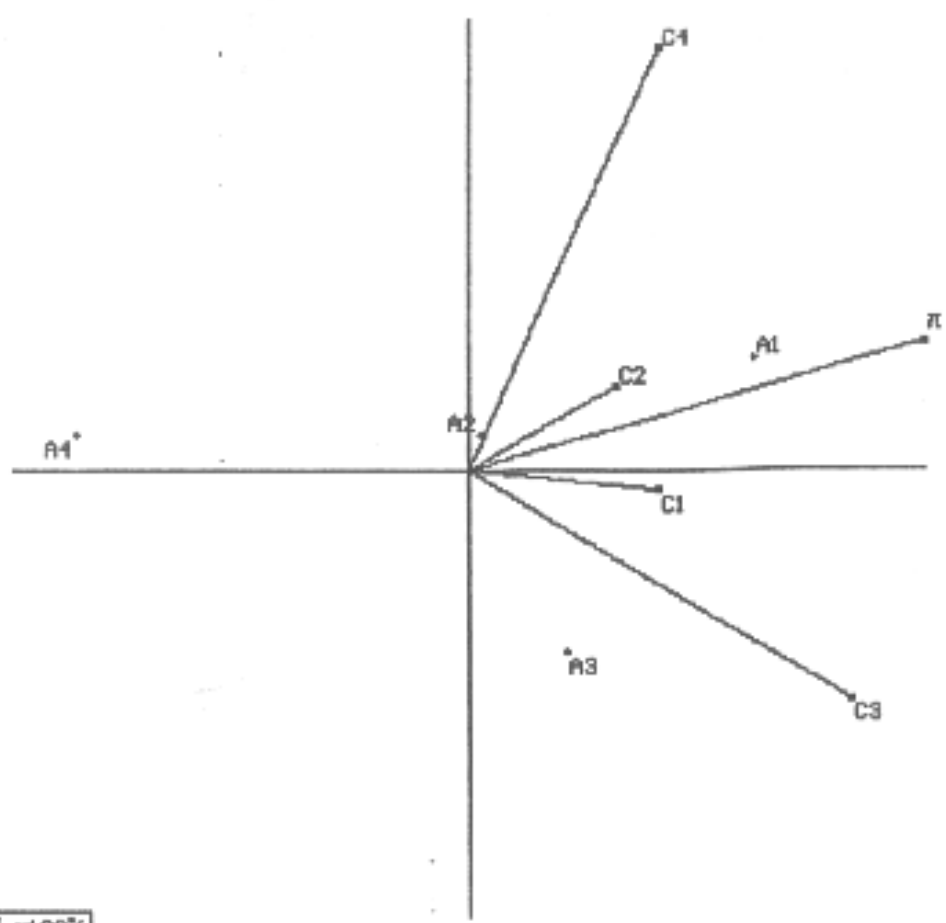


Figure 4.10. PROMETHEE II Complete Ranking for Scenario B.

GAIA Plane



C..1	: alpha	(W = 1.000 <
C..2	: beta	(W = 1.000
C..3	: cysteine	(W = 1.000
C..4	: CA	(W = 1.000

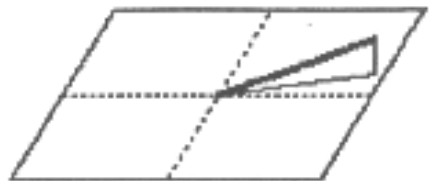


Figure 4.9. GAIA plane for Scenario A.

plane is 100%, which indicates that all of the information has been included in the analysis.

When all the criteria vectors are maximized (Scenario B) the net outranking flows (Figure 4.10), ϕ , changes; the four objects have ϕ values much closer together and object A4 ($\phi=0.07$) becomes the preferred compromise solution. The GAIA biplot (Figure 4.11) follows the general predictions of the discussed scenario with vectors generally pointing to objects consistent with the defined ranking sense-maximised or minimized. In addition, because there is no tendency to a unique solution but rather a compromise one, the π decision axis is relatively weak. The data variance determined by the GAIA plane is again at 100%, which indicates that all of the information has been included in the analysis.

4.7.1. PROMETHEE and GAIA Analysis of Animal Fibres

The analysis of a real matrix (shown in table 4.9) proceeded in a similar manner according to that of the discussion presented in section 4.7. At this point, it is important to note that the criteria presented in table 4.9 show a combination of spectral data and literature values. For instance the amide I ratios and cysteic acid values were obtained from the curve-fit results of the FT-IR spectra collected from the keratin fibres, whilst the cysteine values were obtained from the literature [4]. Prior to analysing the matrix it is also important to note that a search of the literature did not reveal the normal average content of cysteine in cow hair. Consequently, this created a missing value problem in the data matrix. The literature [21] has successfully dealt with missing values in the matrix. In this study, exploratory PROMETHEE and GAIA analysis showed that by inserting a zero value for the cysteine content of cow's hair, heavily biased the performance of the cow object. A scan of the α -keratin fibre cysteine values (table 4.9) shows that they range between about 13-18 mol/100 mols of residue. Thus, it was decided to replace the missing value with the average value of this range. While this must be kept in mind in the analysis of the cow hair, at least including the mean value of 15.6 is unlikely to significantly bias the cow object in respect to the others.

It is proposed that the analysis of the matrix presented in table 4.9 will be directed towards answering the following three hypotheses;

- 1.1. Different keratin fibres can be discriminated on the basis of the different criteria as indicated in table 4.9.
- 1.2 Individual features of the keratin fibres can be related to the total spectra by including PCs as criteria.

1.3. Keratin fibres can be ranked on the basis of changing the PROMETHEE modeling.

The above hypotheses will be explored through the application of different scenarios as represented in the following sections.

4.7.1.1. Scenario 1

In the first scenario, six α -keratin objects were submitted to PROMETHEE for analysis with the feather object being omitted. In this scenario, amide I ($\alpha/\text{CH}_2\text{CH}_3$) was maximised whilst the rest of the criteria were minimised. The objective of this scenario was to create a model of a common α -keratin fibre 'composition'. The criteria models and threshold parameters, p , are described in table 4.10.

TABLE 4.10.

Model Parameters

Sample	Cysteic acid (C3)	Amide I ($\beta/\text{CH}_2\text{CH}_3$) (C4)	Amide I ($\alpha/\text{CH}_2\text{CH}_3$) (C5)	Cysteine (C6)
Min/Max	min	min	max	min
Type	3*	3*	3*	3*
Weight	1.00	1.00	1.00	1.00
p	0.49	1.4	13.5	13.1

* $P(a, b)$ is V-shape function

The threshold, p , for amide I ($\alpha/\text{CH}_2\text{CH}_3$) was selected as 13.5. The threshold values for cysteic acid, amide I ($\beta/\text{CH}_2\text{CH}_3$) and cysteine were set as 0.49, 1.4 and 13.1, respectively. By maximising amide I ($\alpha/\text{CH}_2\text{CH}_3$) and minimising the rest of the

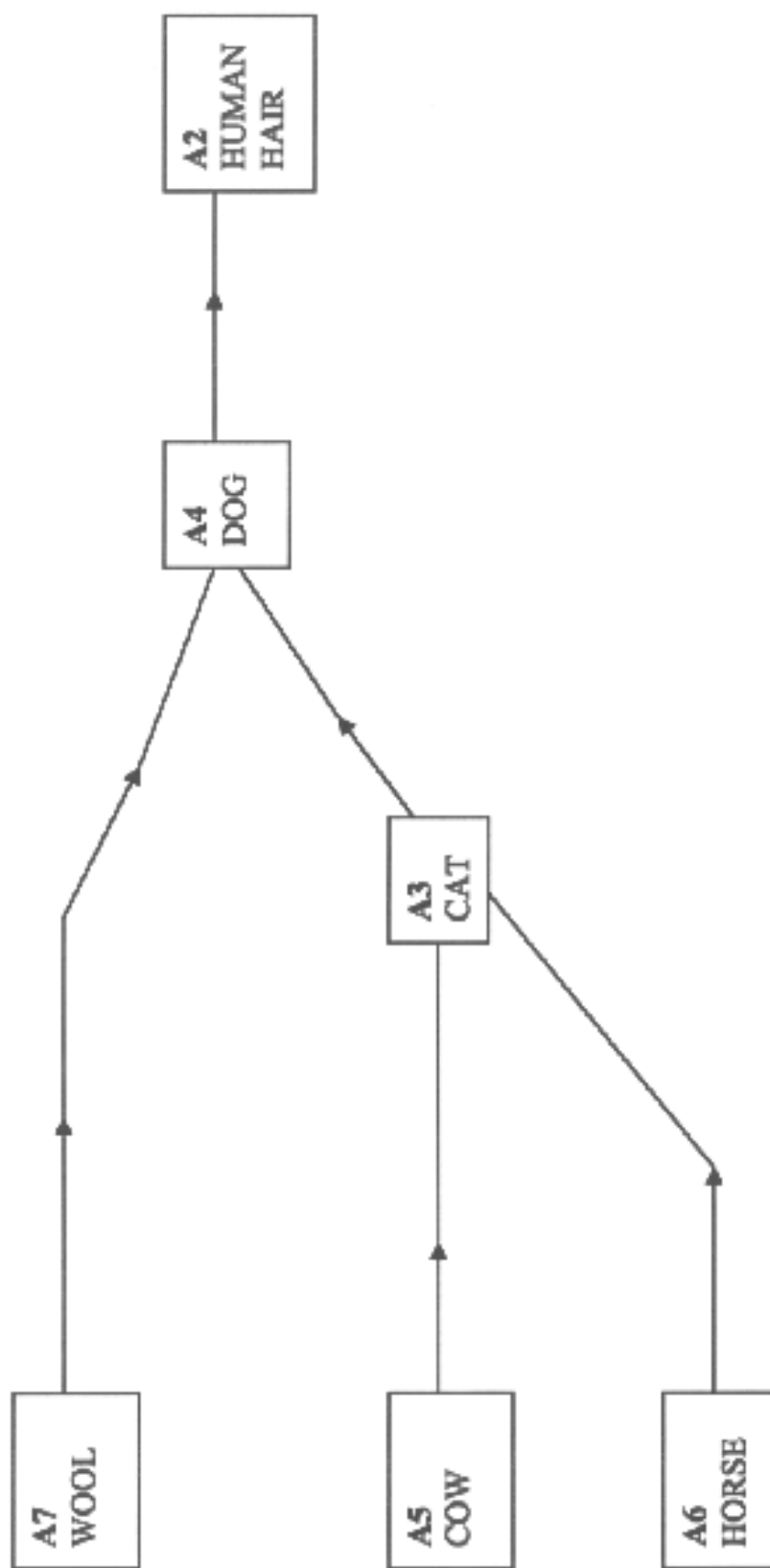


Figure 4.13. PROMETHEE I Partial Ranking for Scenario 1.

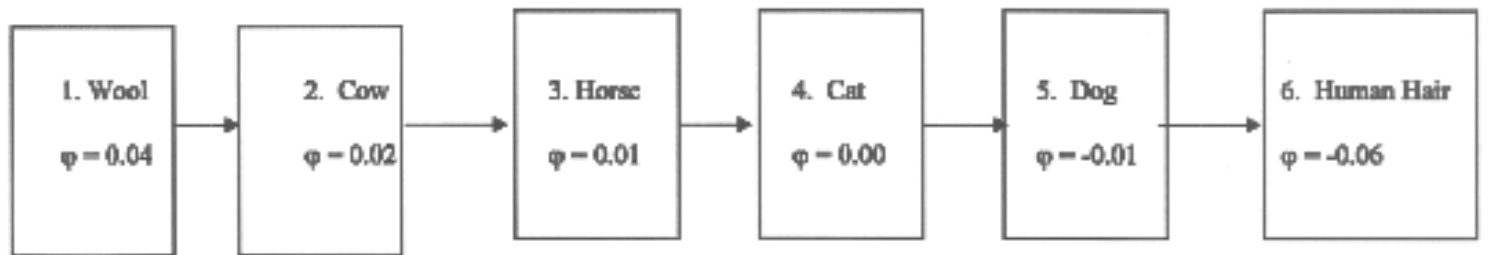


Figure 4.12. PROMETHEE II Complete Ranking for Scenario 1.

criteria, it is expected that PROMETHEE will rank the objects according to the most 'normal' α -keratin first and the least 'normal' α -keratin fibre last. The vectors of the criteria in the GAIA plot are expected to be pointing in the direction of the most 'normal' α -helix fibre.

The results of PROMETHEE II Complete ranking are presented in figure 4.12. The ϕ range of the six keratins is not very wide (0.04 to -0.06) indicating only a small variation between the six different keratin fibres. The complete ranking illustrates that wool, cow and horse fibres have very similar ϕ values, whilst cat fibres are close to zero. Dog and human hair fibres have negative values, with hair fibres having the highest negative ϕ value at -0.06 . The ranking of the wool, cow and horse fibres, indicates that these fibres are preferred on the basis of the above model in comparison to the other three fibres presented in this scenario. This is not surprising since it has previously been shown that the first three fibres also contain the highest α -helix content indicating a highly crystalline ordered fibre.

The PROMETHEE I Partial ranking (figure 4.13) shows that wool, cow and horse fibres are the best performing objects. These fibres have a high α -helix content, which indicates that they are more crystalline than the rest of the fibres. Although these are preferred to the other three, they cannot be compared presumably because they are derived from different sources. Human hair fibres were found to be the worst performing objects, principally because of their high level of cysteine and relatively low levels of amide I ($\alpha/\text{CH}_2\text{CH}_3$) in comparison to the rest of the fibres. The ranking of the human hair fibres as the least preferred fibre is possibly due to the wide range of chemical products, such as shampoos, conditioners, hair sprays etc applied to

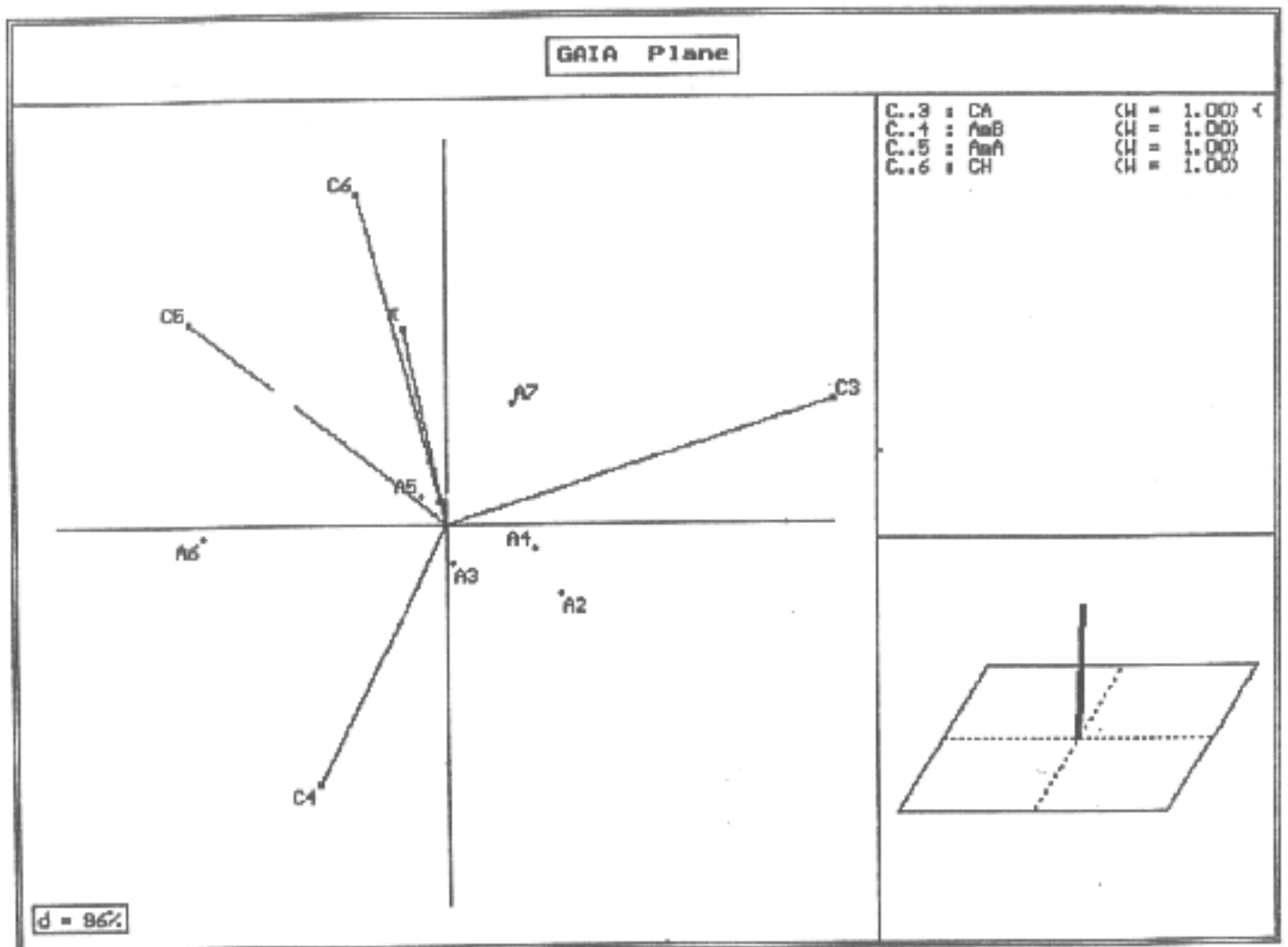


Figure 4.14. GAIA plane for Scenario 1.

human hair and also subject their hair to more hair grooming for example hair drying etc, than animal fibres.

The GAIA plot (figure 4.14) indicates that the GAIA plane is 96%, which suggests that most of the information has been included in the analysis. Human hair, dog and wool fibres are strong on minimal cysteic acid values, whilst horse and cow fibres are strong on amide I α -, β - and cysteine. The decision axis, π , is relatively strong, and is pointing in the same direction as the cysteine, α - and β - vectors. In this scenario, it has been shown that when cysteic acid is minimised, the α - vector is pointing in the same direction as that of cysteine and β - indicating a correlation between the three vectors. It therefore becomes apparent that since the direction of the α -helix vector is influenced by minimising or maximising the cysteic acid vector, it thus suggests that the α - helix is influenced by the amount of cysteic acid in human hair. This is excepted as it has already been shown that cysteic acid affects the stability of the α -helix secondary structure.

The results presented in this scenario have shown for the first time that the two MCDM methods, PROMETHEE and GAIA, can rank different keratin fibres on the basis of multivariate chemical information. This is essentially different from the more conventional chemometrics methods such as PCA, where ranking takes place on a univariate basis. In particular, PROMETHEE and GAIA enable the investigation of a combination of chemical information obtained from different sources i.e., FT-IR spectral bands and literature values.

In addition, PROMETHEE and GAIA analysis have shown that when a normal model is selected, by minimising the cysteic acid, horse, cow and to some extent wool fibres are the most preferred fibres. Human hair fibres are the least normal hair fibre. The decision axis in the GAIA plot along with the direction of the amide I ($\alpha/\text{CH}_2\text{CH}_3$), ($\beta/\text{CH}_2\text{CH}_3$) and cysteine vectors support the PROMETHEE I and II ranking by pointing in the same direction as that of the horse and cow fibres.

4.7.1.2. Scenario 2

In the second scenario, six α -keratin objects were submitted to PROMETHEE for analysis excluding the feather object. The objective of this scenario was to create a model, which represents a ‘damaged’ fibre, i.e. a fibre with a low crystalline order, and rank the fibres accordingly. The criteria models and threshold parameters, p , are described in table 4.11.

TABLE 4.11.

Model Parameters

Sample	Cysteic acid (C3)	Amide I ($\beta/\text{CH}_2\text{CH}_3$) (C4)	Amide I ($\alpha/\text{CH}_2\text{CH}_3$) (C5)	Cysteine (C6)
Min/Max	max	max	max	max
Type	3*	3*	3*	3*
Weight	1.00	1.00	1.00	1.00
P	2.8	3.2	13.5	17.8

* P(a, b) is a V-shape function

Amide I ($\alpha/\text{CH}_2\text{CH}_3$), amide I ($\beta/\text{CH}_2\text{CH}_3$), cysteine and cysteic acid were maximised and the threshold value, p , for each of the four criteria were set was selected as 13.5, 3.2, 17.8, and 2.8, respectively. By maximising the four criteria the model is then

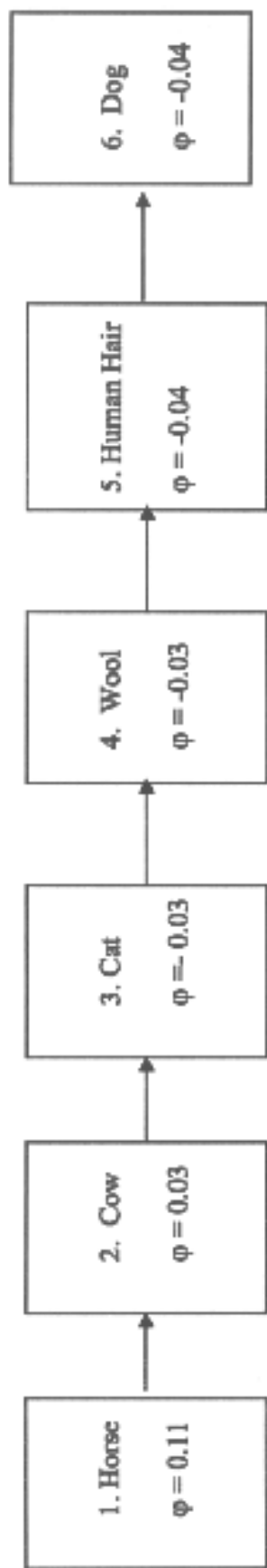


Figure 4.15. PROMETHEE II Complete Ranking for Scenario 2.

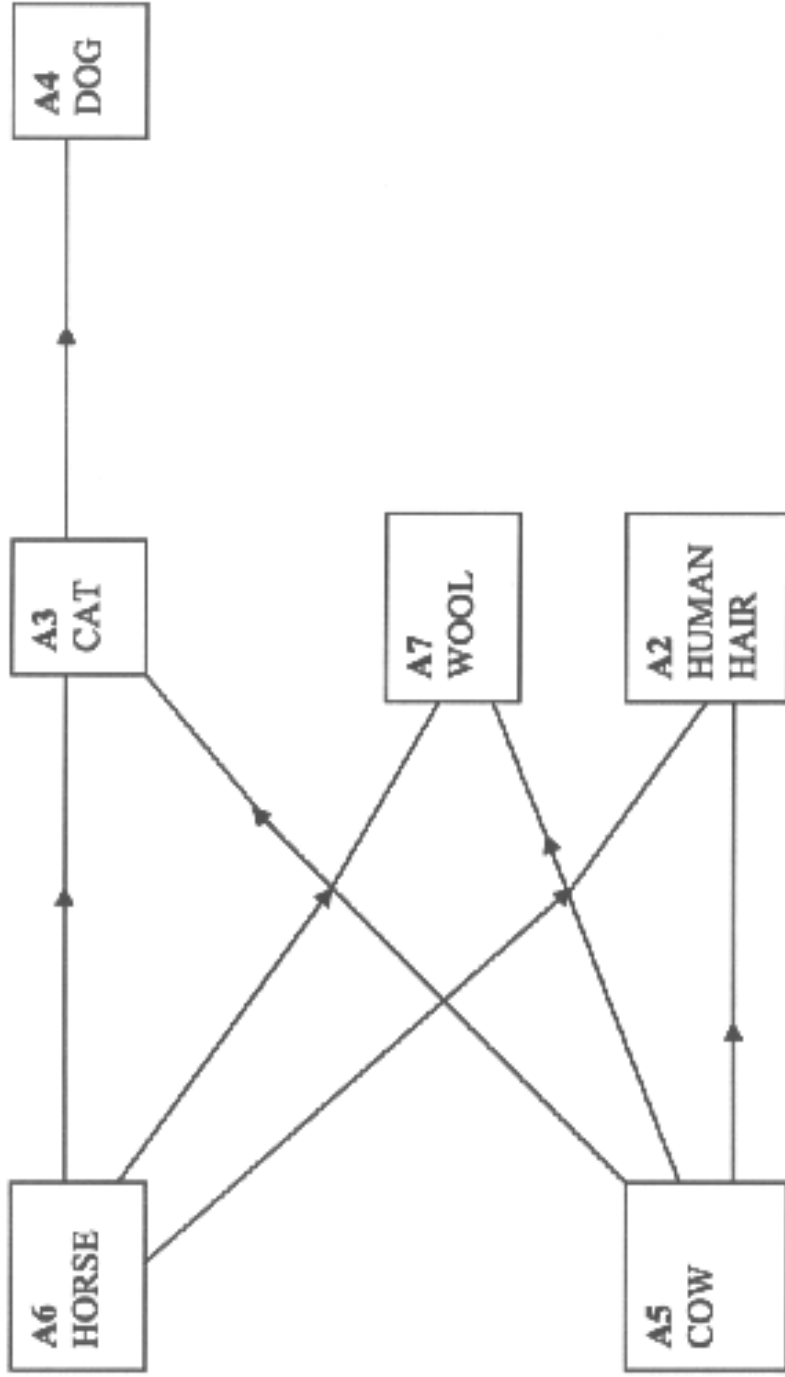


Figure 4.16. PROMETHEE I Partial Ranking for Scenario 2.

defined to look for a compromise solution with the preferred keratin fibre having relatively high amounts of the four molecular constituents. The maximized criteria vectors will be scattered around the GAIA biplot, each pointing in the general direction of the best performing object-fibre. The PROMETHEE ranking is expected to rank the lowest crystalline order fibre(s) first and the highly crystalline order fibre(s) last.

The total matrix, 6x4, was submitted to PROMETHEE II Complete ranking and the results are presented in figure 4.15. The ϕ range of the six keratins is not very wide (0.11 to -0.04) indicating only a small variation between the six different keratin fibres. The complete ranking illustrates that horse fibres (A6) are the preferred fibres with high positive ϕ values (0.11), while the dog fibres are the least preferred (-0.04). The rest of the fibres cow, cat, wool, human hair and dog all have practically the same negative ϕ values. The ranking of the keratin fibres is consistent with the fact that horse fibres have the second highest (after feather) content of cysteic acid and only intermediate cysteine values in comparison to the rest of the fibres. In addition, the amide I ($\alpha/\text{CH}_2\text{CH}_3$) ratio has shown that horse fibres contain the highest α -helix content in comparison to the rest of the fibres. The ranking of the horse fibres in PROMETHEE II, is therefore expected as horse fibres contain a highly crystalline α -helix order and are thus the preferred fibres.

The PROMETHEE I Partial ranking (figure 4.16) shows that horse and cow fibres are both the best performing fibres, but are not comparable. According to the amide I ($\alpha/\text{CH}_2\text{CH}_3$) ratio, horse and cow fibres have the highest and second highest amounts of α -helix, respectively, in comparison to the rest of the fibres. Therefore,

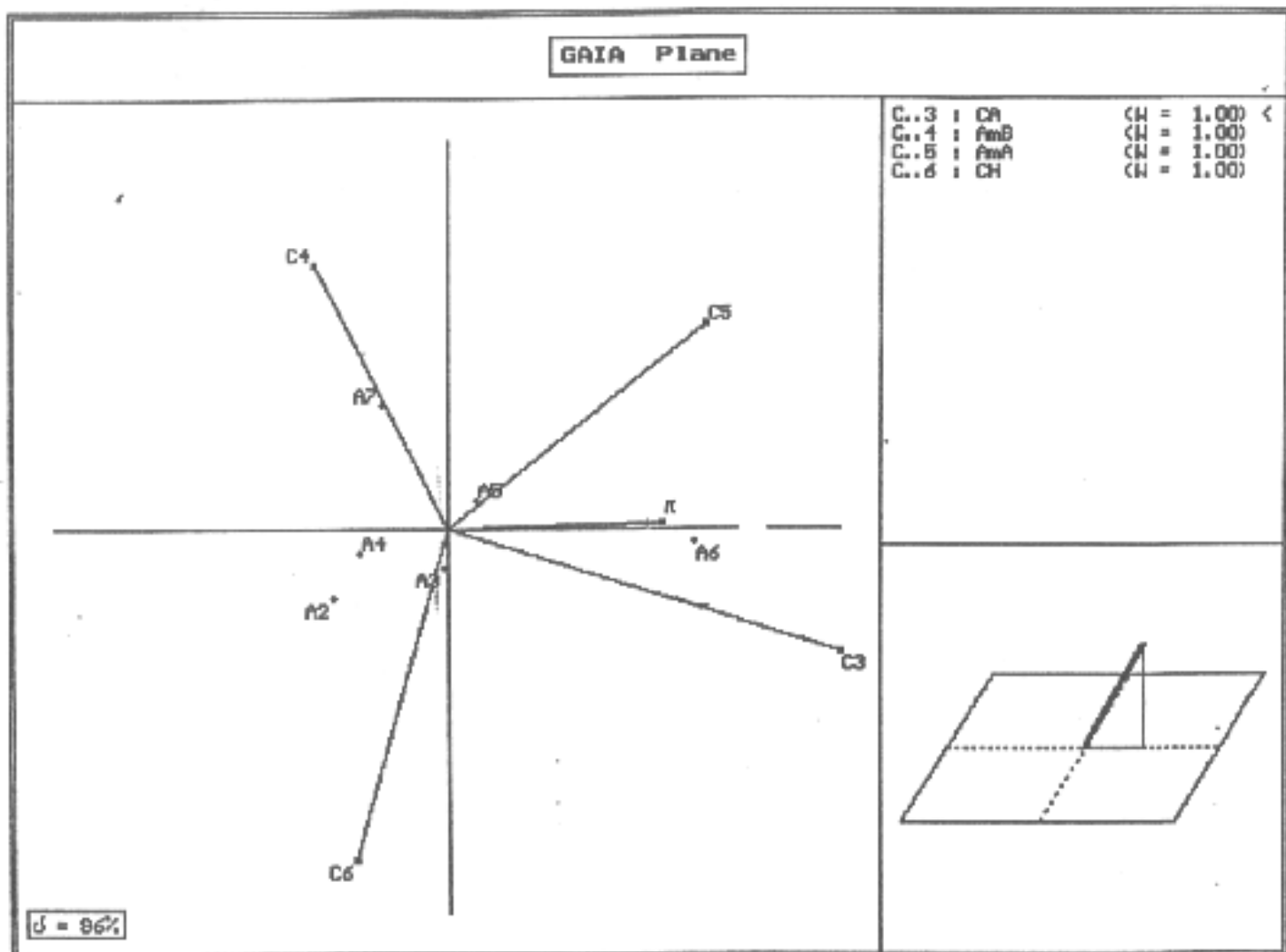


Figure 4.17. GAIA plane for Scenario 2.

PROMETHEE I suggests that these two fibres are both high in α -helix, but are not comparable because they are two different types of fibres. In addition, it can also be seen from figure 4.16 that cat, wool and human hair fibres have similar ranking but are also not comparable with each other. This is reflected in the amide I ($\alpha/\text{CH}_2\text{CH}_3$) ratio, where it was found that cat, wool and human hair fibres have very similar α -helix. However given that we are dealing with three fibres collected from three completely different sources, the fibres are not comparable. Dog fibres were found to be the worst performing fibres, which indicates that these fibres are low in α -crystalline order. This is supported by previous curve-fit studies (section 4.5) which have shown that dog fibres have very low amide I ($\alpha/\text{CH}_2\text{CH}_3$) ratio and cysteine values in comparison to the rest of the fibres.

The GAIA plot (figure 4.17) shows that the data variance determined by the GAIA plane is 96%, which indicates that most of the information has been included in the analysis. Overall, there is a clear separation of the preferred fibre (horse) with positive scores on PC1, from the rest of the fibres. The GAIA plot closely reflects the predicted outcome, with the decision axis, π , pointing towards the horse fibre, indicating that horse hair is the most preferred keratin under the chosen criteria. The vectors of cysteic acid and amide I α -helix are pointing towards the horse fibre, which indicates that these fibres are strong on these two criteria. The rest of the criteria, amide I β - and cysteine are pointing in the opposite direction suggesting that horse fibres are weak on these criteria.

The rest of the fibres are located some distance away from the decision axis, indicating that the fibres do not perform under the selected criteria. Apart from the

cow fibres (A5), which are located close to the amide I ($\alpha/\text{CH}_2\text{CH}_3$) vector, suggesting that the fibre is strong on α -helix, the rest of the fibres are located some distance away from the amide I ($\alpha/\text{CH}_2\text{CH}_3$) vector.

The results presented in this scenario have again demonstrated the ability of PROMETHEE and GAIA to rank different keratin fibres on the basis of multivariate chemical information. In particular, the PROMETHEE and GAIA analysis have shown that when a highly crystalline α -helix model is selected, horse fibres are the most preferred fibres. This is highlighted by both PROMETHEE I and II, which rank the horse fibres first. Dog fibres, on the other hand were the least preferred fibre, indicating that dog fibres have a relatively low α -crystalline order in their secondary structure. The decision axis in the GAIA plot along with the direction of the amide I ($\alpha/\text{CH}_2\text{CH}_3$) vector and cysteine acid vectors also support the PROMETHEE results and provide additional information with regards to the molecular structure of the horse fibre. The rest of the fibres are further differentiated on the basis of their preference for the amide I ($\beta/\text{CH}_2\text{CH}_3$) and cysteine. It therefore appears that PROMETHEE and GAIA are quite useful in the ranking of keratin fibres on the basis of their characteristic molecular structure.

4.7.1.3.Scenario 3

In the third scenario, the feather keratin was added to the matrix, which now consisted of 7 objects and the same four criteria as those previously described in scenarios 1 and 2. In this scenario, the ratio of amide I ($\beta/\text{CH}_2\text{CH}_3$) was maximised, whilst the rest of the criteria were minimised. This models a fibre that is high in β -keratin. The feather samples were added to the matrix, because as it was shown in the curve-fit studies in section 4.4, feather keratin contain high levels of β -sheet, in comparison to the remaining six fibres presented in this study. Since the amide I ($\beta/\text{CH}_2\text{CH}_3$) was maximised, it is therefore expected that PROMETHEE will rank the objects with the fibre(s) containing the highest β -sheet first, and those of the lowest β -structure last. The vectors in the GAIA plot are expected to be pointing towards the direction of highest β -keratin fibre. However, since cysteic acid was minimised and since it has been previously reported (section 4.4) that fibres high in β -sheet are also characterised by high amounts of cysteic acid, it is expected that the cysteic acid vector will be pointing in the opposite direction of the fibre highest in β -sheet. The new matrix (shown in table 4.12) was therefore submitted to PROMETHEE for analysis with the criteria models and threshold parameters set as discussed below.

TABLE 4.12.

Model Parameters

Sample	Cysteic acid	Amide I	Amide I	Cysteine
		($\beta/\text{CH}_2\text{CH}_3$)	($\alpha/\text{CH}_2\text{CH}_3$)	
	(C3)	(C4)	(C5)	(C6)
Min/Max	min	max	min	min
Type	3*	3*	3*	3*
Weight	1.00	1.00	1.00	1.00

* P(a, b) is V-shape function

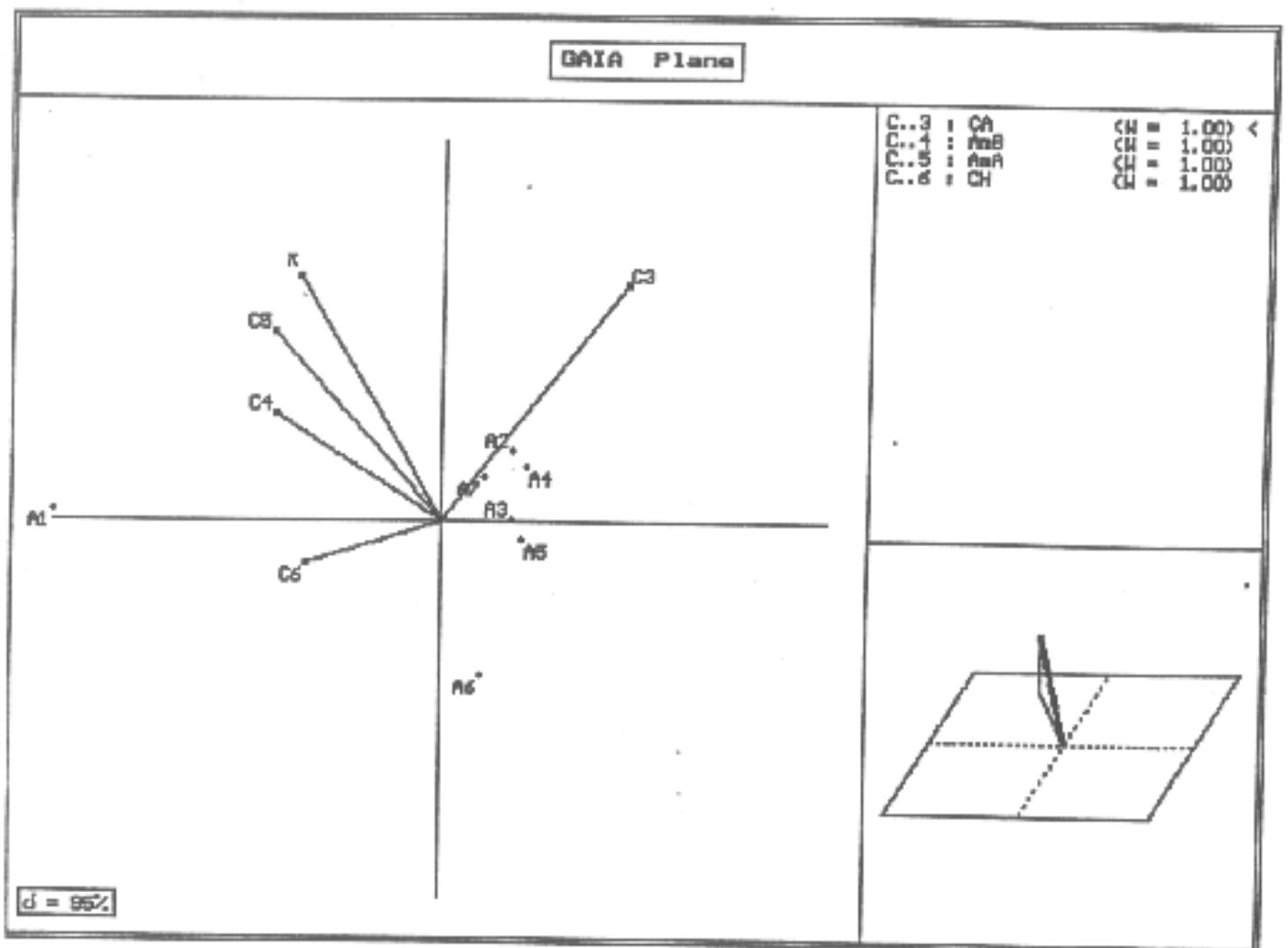


Figure 4.20. GAIA plane for Scenario 3.

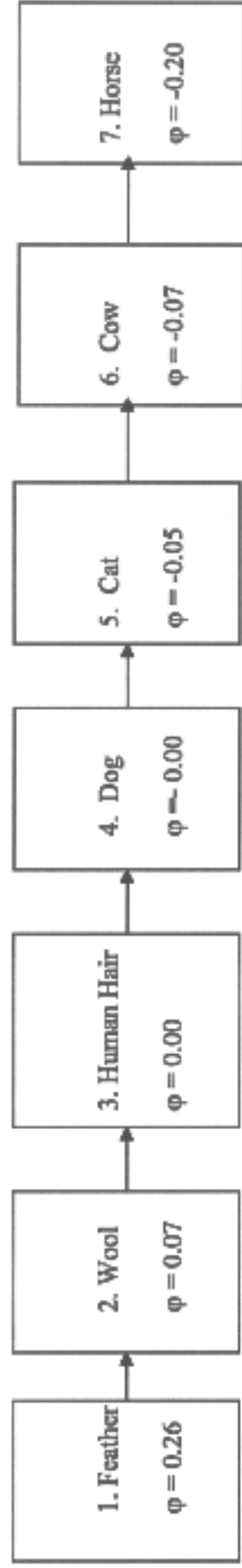


Figure 4.19. PROMETHEE II Complete Ranking for Scenario 3.

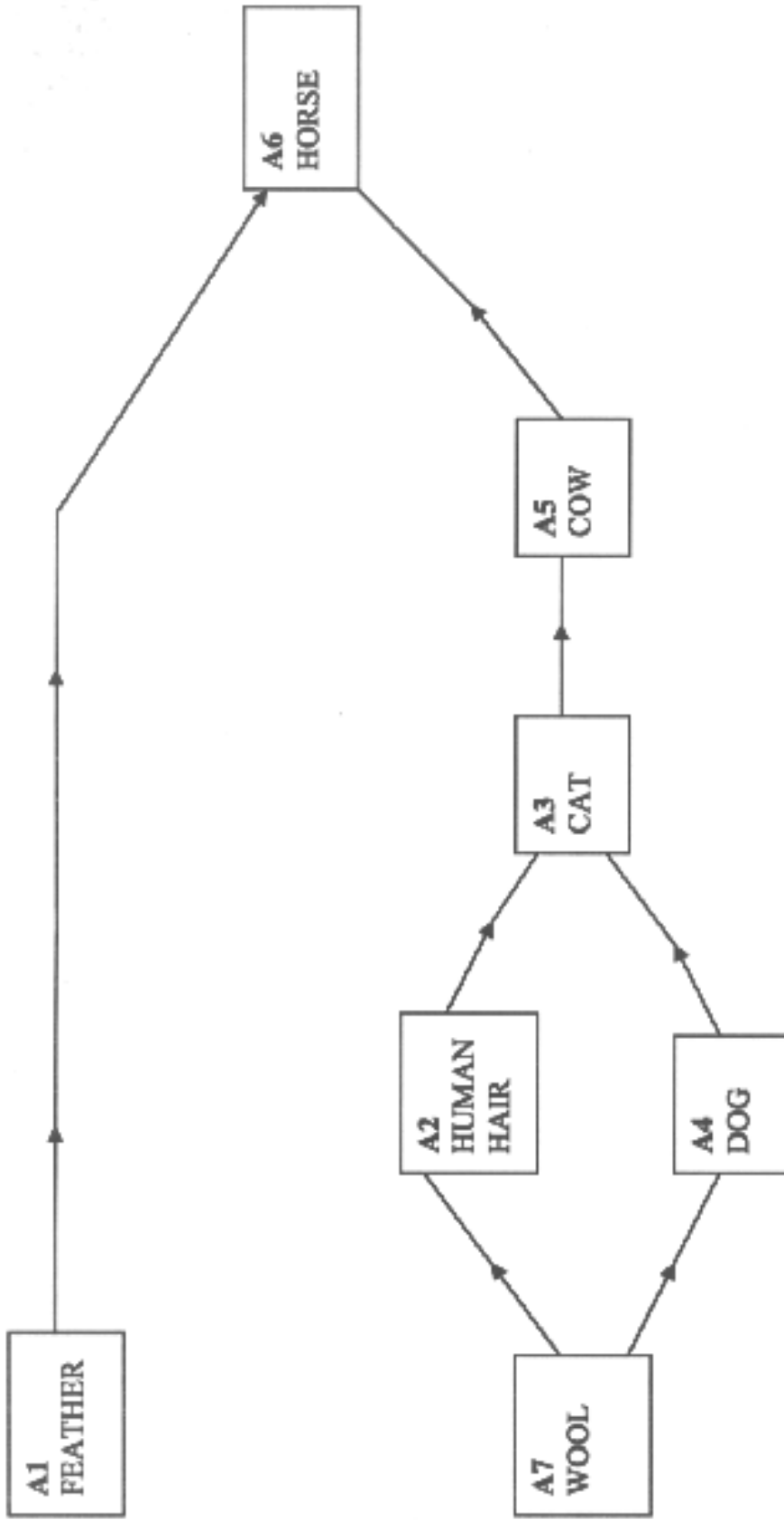


Figure 4.18. PROMETHEE I Partial Ranking for Scenario 3.

The threshold, p , for amide I ($\alpha/\text{CH}_2\text{CH}_3$), cysteine and cysteic acid were selected as 2.1, 7.1, and 4.3, respectively. The ratio of amide I ($\beta/\text{CH}_2\text{CH}_3$), was maximised, and the threshold, p , for this ratio was set as 6.4.

PROMETHEE I partial ranking results are shown in figure 4.18. The results indicate that the feather sample (A1) and wool keratin (A7) are the best performing fibres. However, the two fibres are not comparable. Indeed, the feather cannot be compared to any of the α -keratin fibres, since we are dealing with fibres of entirely different keratin composition. PROMETHEE has also shown that horse fibres are the least preferred objects, which indicates that they contain the least amount of β -sheet.

The PROMETHEE II complete ranking (figure 4.19) shows that the seven objects have a fairly wide range (0.15 to -0.11) of ϕ values, with the feather samples containing high positive ϕ values (0.55) on the ϕ scale and are therefore the preferred fibres under the conditions specified for the four criteria. Wool fibres have low positive scores (0.07), whilst most of the fibres have practically the same ϕ values, except the horse fibre which is the least preferred (and high in α -helix) with a ϕ value of 0.20. The wide range of ϕ values, further highlights the difference in the chemical composition of the fibres.

The GAIA plot (figure 4.20) provides valuable information additional to that of the PROMETHEE ranking. The data variance determined by the GAIA plane is 95%, which indicates that most of the information has been included in the analysis. The preferred keratin (feather) is separated on PC1 (negative scores) from the rest of the

fibres (positive scores). The GAIA plot closely reflects the predicted outcome, with the majority of the criteria vectors roughly directed towards the most preferred object i.e. feather (A1) with the strong decision axis, π , having a close relationship with criteria C5 (α -helix). The only criteria vector that is not pointing in the direction of the feather fibre is that of cysteic acid (C3), which is expected since cysteic acid was minimised.

This scenario has shown that apart from the expected difference between the feather and the other fibres, the α -keratin objects, such as wool, horse, cat, dog, cow, wool and human hair fibres would be ordered roughly according to their β -content. GAIA has also shown that other variables such as cysteic acid also contribute quite strongly to this ranking.

4.7.1.4. Scenario 4

Recently exploratory studies have commenced [22] to use PCs derived from spectral matrices as criteria to represent spectra in PROMETHEE matrices so as to enable a comparison of spectra with different other variables. An initial study [22] was recently presented where the IR spectra of kaolinite were compressed by PCA and scores represented spectra in a PROMETHEE matrix that also included criteria representing the chemical composition of kaolinites. As a result, it was possible to relate and display relationships (via the GAIA biplot) between the spectral PCs (and hence their corresponding loadings plots) and the elemental composition of the clays. Therefore, the application of GAIA in this study produced additional information that was otherwise lacking from the PCA results.

In this scenario, it is intended to use the same approach to examine the ordering and relationships of the animal and human hair in relation to their spectra as represented by their PC scores. This is intended as an exploratory study leading up to the more important one in chapter 5 where variables not directly related to spectra, such as age, gender, race etc, will be combined in one matrix, which will also include the corresponding spectral PC variables.

In the final scenario, the six α -keratins were analysed along with the two PCs (PC1 and PC3) obtained from the PCA plot shown in figure 4.7. The new matrix is now presented in table 4.13.

TABLE 4.13.

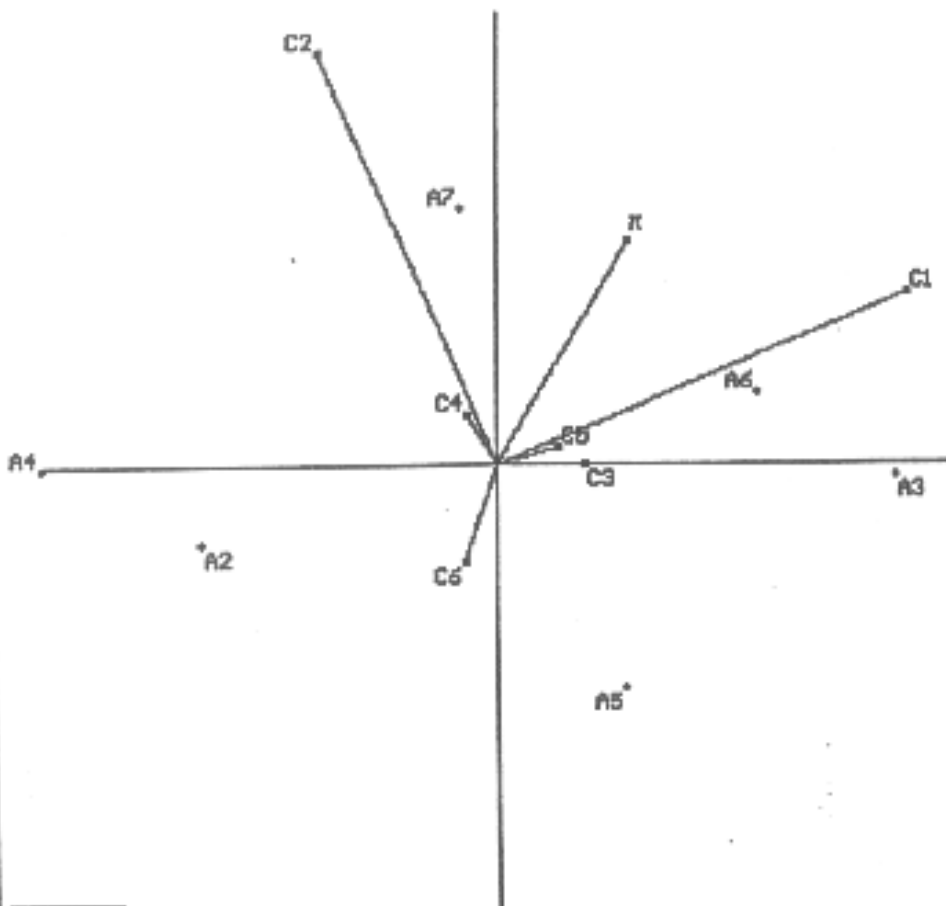
Model Parameters

Sample	PC1 (C1)	PC3 (C2)	Cysteic acid (C3)	Amide I (β/CH₂CH₃) (C4)	Amide I (α/CH₂CH₃) (C5)	Cysteine (C6)
Min/Max	max	max	max	max	max	max
Type	3*	3*	3*	3*	3*	3*
Weight	1.00	1.00	1.00	1.00	1.00	1.00
p	18.9	1.8	2.8	3.2	13.5	17.8

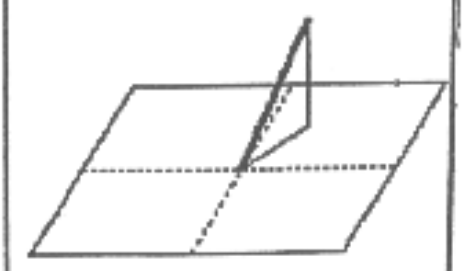
* P(a, b) is a V-shape function

The threshold, p, for all the criteria was maximised, so as to reflect a damaged fibre i.e. a fibre with a low crystalline order, similar to that obtained in scenario 2. By maximising the criteria, it is expected that the vectors relating to these criteria will be pointing towards a keratin fibre with a low crystalline order i.e. a keratin fibre low α -

GAIA Plane



0.000000	0.000000	1.000000	<
0.000000	0.000000	1.000000	
0.000000	0.000000	1.000000	
0.000000	0.000000	1.000000	
0.000000	0.000000	1.000000	
0.000000	0.000000	1.000000	



$\sigma = 92\%$

Figure 4.22. GAIA plane for Scenario 4.

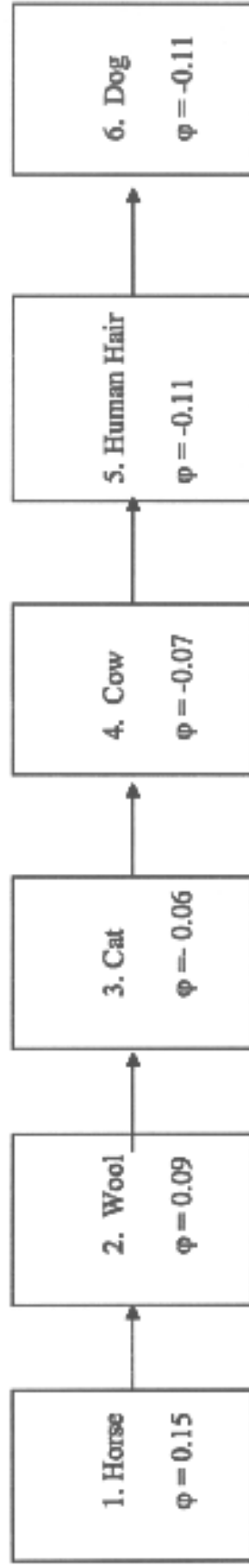


Figure 4.21. PROMETHEE II Complete Ranking for Scenario 4.

helix. The PROMETHEE ranking is expected to rank the lowest crystalline order fibre(s) first, and the highest crystalline order fibre(s) last.

PROMETHEE II Complete ranking results are presented in figure 4.21. The ϕ range is wide (0.15 to -0.11) indicating that there is a variation between the keratin fibres. Horse fibres are ranked first with the highest positive values (0.15), wool and cat fibres having close positive values, whilst cow, human hair and dog all having practically the same negative values. The ranking of the objects therefore indicates that the horse fibres are the most 'damaged' fibres in comparison to the rest of the keratin samples. This is consistent with the curve-fit measurements (presented in section 4.4), which showed that horse fibres are high in cysteic acid and also with the low cysteine values derived from the literature. The PROMETHEE ranking obtained from scenario 4 is similar with the ranking of the fibres obtained from scenario 2.

The GAIA plot (figure 4.22) shows that 92% of the data variance is determined by the GAIA plane, which indicates that most of the information has been included in the analysis. In this GAIA plot, the preferred fibres (horse, cat and cow fibres) have positive scores on PC1, and are separated from the wool, dog and human hair fibres, which have negative scores on PC1. The results obtained from the GAIA plot are in agreement with the PCA results shown in figure 4.7. In the PCA plot, PC1 was shown to discriminate the fibres on the basis of their secondary structure; human hair, dog and wool fibres (all on negative scores on PC1) have a low α -helix and a high β -sheet, whilst fibres collected from cow, horse and cat (all on positive scores) have a high α -helix and a low β -sheet. A similar trend for the location of the objects was also observed in the GAIA plot.

The vectors of amide I α -helix and cysteic acid are pointing in the direction of horse, cat and cow fibres suggesting that these fibres contain high α -helical structure and cysteic acid. The vectors of amide I β - and cysteine are pointing in the direction of dog, wool and human hair fibres indicating that these fibres contain higher levels of β -sheet and cysteine in comparison to horse, cat and cow fibres.

The vectors of amide I α -helix and cysteic acid are pointing in the opposite direction to that amide I β - and cysteine indicating that the two sets of vectors are in conflict. This is not surprising since higher levels of cysteine correspond to lower levels of cysteic acid and vice versa. In addition, a fibre high in α -helix contains lower values of β -sheet and vice versa.

In this scenario, the PROMETHEE and GAIA analysis have shown that when a highly crystalline α -helix model is selected, horse fibres are the most preferred fibres. The ranking of the fibres obtained from this scenario was almost identical to that seen in scenario 2. The PC1 vector is pointing in the same direction as that of the α -helix and cysteic acid vectors, which suggests that PC1 on the PCA plot discriminates the fibres on the basis of α -helix and cysteic acid. The PC2 vector is pointing in the same direction as that of β -sheet and cysteine vectors, which suggests that PC2 on the PCA is discriminating the spectra on the basis of β -sheet and cysteine. The direction of the PC vectors in relation to the other four vectors therefore confirms the previous chemometric results and indicates the grouping of the fibres on the basis of their characteristic molecular structure.

4.7.2. Conclusions for PROMETHEE and GAIA.

The objectives of the PROMETHEE and GAIA analysis presented in this chapter were successfully accomplished.

The four scenarios presented focused on illustrating the setting up of the data matrices for PROMETHEE modelling and interpreting the ranking and the GAIA biplot with emphasis on the importance of defining meaningful scenarios with respect to the objects in the data set. The discussion of PROMETHEE modeling included the consideration of selection of:

1. Preference functions $P(a, b)$;
2. Selection and importance of the ranking sense of a variable; and
3. Setting of any threshold parameters, p and q .

Two particular advantages of PROMETHEE and GAIA were highlighted;

1. The MCDM approach can provide similar information as curve-fitting. However, the MCDM approach is simpler, faster and more versatile; and
2. Results from FT-IR spectra can be readily compared with other values such as literature results in one matrix.

In accordance to the hypotheses proposed in section 4.7.1, the following conclusions are offered;

- 1.1. It is possible under the criteria chosen and the threshold values attributed to them, to rank the different objects, from the most preferred to the least preferred;

1.2. The combination of the PCs obtained from the FT-IR spectra along with additional information gathered from the curve-fit analysis of these spectra and literature material can be combined to successfully analyse keratin fibres. The literature extracted criteria have been shown to be related to the spectra and important information that was otherwise not available was readily available, and;

1.3. The selection (or preference) of the different seven types of fibres can be discriminated according to the different selection of maximum/minimum criteria.

It is particularly important to note that this is the first time PROMETHEE and GAIA have been applied to a wide range of keratin fibres. The results indicate the potential application of these methods for the exploration of a larger matrix of different keratin fibres and also different species of the same animal.

4.8. Chapter conclusions

This chapter has demonstrated that FT-IR spectra of keratotic specimens can be readily obtained. The molecular assignments highlighted the bands sensitive to skeletal backbone configuration, and identified spectral regions of characteristic spatial conformation. Examination of the amide bands provided secondary structural information and disclosed the difference in the biogenesis of the animal, human and feather keratin.

While only a limited number of samples were available for analysis, the error indicated by the variation between the replicate fibres from the same source was relatively small. Curve-fit analysis has indicated the following:

- good spectral fits with indications of low error;
- a quantitative analysis of the secondary structure of the keratins. Feather samples are predominantly made-up of a β -sheet structure, while mammalian keratins favour an α -helical arrangement; and
- each keratin fibre contains a characteristic secondary structure arrangement.
- Cysteic acid is an influential factor to the final arrangement of the secondary structure of the keratin fibre. The study has shown that high amounts of cysteic acid are indicative of a keratin fibre with low levels of α -helix and cysteine.

The results are consistent with those obtained using alternative methods such as x-ray diffraction and Raman spectroscopy.

Chemometrics methods of analysis such as PCA, SIMCA and FC supported the curve-fit results and provided statistical information regarding the conformation of the α -helix and β -sheet proteins. In particular the loadings plot has shown that the separation between the feather samples from the rest of the keratin samples is supported by the presence of the amide I (β -sheet) at 1670 cm^{-1} , amide II (β -sheet) at 1531 cm^{-1} , amide III (β -sheet) at 1238 cm^{-1} and cysteic acid at 1040 cm^{-1} for the feather samples. The rest of the keratin samples are influenced by the amide I and II (α -helix) vibrations at 1670 and 1550 cm^{-1} , respectively. SIMCA has shown that at a 95% confidence level the keratin samples composed of an α -helical structure are different from the samples containing a β -sheet conformation. FC further supported the separation of the keratin fibres into their individual classes. In addition, when two clusters were chosen, the keratin samples made up of predominantly the α -helix formed one class and the feather samples formed a second class.

PROMETHEE and GAIA have successfully demonstrated the simultaneous analysis of FT-IR spectral information and literature values for the ranking of α - and β - keratin fibres. PROMETHEE and GAIA further supported the theory that feather fibres are characterised by a high levels of amide I ($\beta/\text{CH}_2\text{CH}_3$) and cysteic acid in comparison to the rest of the fibres.

The work presented in this chapter has important forensic applications and these include;

(I) Based on the knowledge from the present study that each keratin fibre has a unique secondary structure, a prediction and thus classification of unknown keratin fibres can be made on the basis of their secondary structure.

(II) The study, although had a limited number of samples, clearly illustrated the possibility of discriminating keratin fibres and thus indicates the importance of a large database containing animal hair.

CHAPTER 4 - REFERENCES

1. Gallop, A., and Stockdale, R., Crime Scene to Court. The Essentials of Forensic Science, Chapter 3, in **Trace and Contact Evidence**, edited by White, P., The Royal Society of Chemistry, U.K., 1998.
2. Wildman, A. B., The Identification of Animal Fibres, *Journal of Forensic Science Society*, **1**, pp. 116-119, (1960).
3. D'Andrea, D., Fridez, F., Coquoz, R., Margot, P., Animal Hair as Trace, *Criminalistics*, pp. 68-70, (1997).
4. Hendriks, W. H., Tartelin, M. F., Moughan, P. J., The Amino Acid Composition of Cat (*Felis Catus*) hair, *Annual Science*, **67**, pp. 165-170, (1998).
5. Aitken, F. J., Cottle, D. J., Reid, T. C., and Wilkinson, B. R., Mineral and Amino Acid Composition of Wool from New Zealand Merino Sheep Differing in Susceptibility to Yellowing, *Australian Journal of Agricultural Research*, **45**, pp. 391-401, (1994).
6. Hopkins, J., Brenner, L., and Tumosa, C. S., Variation of the Amide I and Amide II peak absorbance ratio in human hair as measured by Fourier Transform Infrared Spectroscopy, *Forensic Science International*, **50**, pp. 61-65, (1991).
7. Kuttin, E. S., Alhanaty, E, Feldman, M., Chaimovits, M and Muller, J., Dermatophytosis of Camels, *Journal of Medical and Veterinary Micology*, **24**, pp. 341-344, (1986).
8. Mundt, H. C., and Stafforst, C., Productions and composition of dog hair. In nutrition, malnutrition and dietetics in the dog and cat, edited by Edney, A. T. B., Proceedings of an International Symposium, 3-4 September, 1987, pp. 62-65, British Veterinary Association and Waltham Centre for Pet Nutrition, U. K.,
9. Lohi, O., and Jensen, L. V., **Mineral Composition of mink feed and mink hair**, Beretning Foulum, Denmark, no.688.

10. Bendit, E. G., Infrared Absorption Spectrum of Keratin. I. Spectra of α -, β -, or supercontracted keratin, *Biopolymers*, **4**, pp. 539-559, (1966).
11. Hsu, S. L., Moore, W. H., and Krimm, S., Vibrational Spectrum of the unordered polypeptide chain: A Raman study of feather keratin, *Biopolymers*, **15**, pp. 1513-1528, (1976).
12. Edwards, H. G. M., Hunt, D. E., Sibley, M. G., FT-Raman Spectroscopic study of keratotic materials, horn, hoof and tortoiseshell, *Spectrochimica Acta, Part A*, **54**, pp. 745-757, (1998).
13. Akhtar, W., Edwards, H. G. M., Fourier-Transform Raman Spectroscopy of mammalian and avian keratotic biopolymers, *Spectrochimica Acta, Part A*, **53**, pp. 81-90, (1997).
14. Rintoul, L., Carter, E. A., Steward, S. D., and Fredericks, P. M., Keratin Orientation in wool and feathers by polarised Raman spectroscopy, *Biopolymers (Biospectroscopy)*, **57**, pp. 19-28, (2000).
15. Jurdana, L. E., Ghiggino, K. P., Nugent, K. W., and Leaver, I. H., Confocal laser Raman Microprobe studies of keratin fibres, *Textile Res. J.*, **65**, pp. 593-600, (1995).
16. Surewicz, W. K., and Mantsch, H. H., Infrared Absorption Methods for Examining Protein Structure, Chapter 7, in **Spectroscopic Methods for Determining Protein Structure in Solution**, edited by Havel, H. A., VCH, USA, 1996.
17. Harada, I., and Takeuchi, H., Raman and ultraviolet resonance Raman Spectra of Proteins and related compounds, Chapter 3, in **Spectroscopy of Biological Systems. Advances in Spectroscopy**, Volume 13, edited by Clark, R. J. H., and Hester, R. E., John Wiley and Sons, USA, 1986.
18. Fraser, R. D. B., MacRae, T. P., and Rogers, G. E., **Keratins: Their Composition, Structure and Biosynthesis**, Charles C Thomas, USA, 1972.

19. Lippert, J. L., Tyminski, D., and Desmules, P. J., Determination of the Secondary Structure of Protein by Laser Raman Spectroscopy, *J. Am. Chem. Soc.*, **98**, pp. 7075-7080, (1976).
20. Brans, J. P., PROMCALC (Version 3.1) Software, Centre for Statistics and Operational Research, Free University of Brussels, Brussels, 1991.
21. Grung, B., Manne, R., Missing values in principal component analysis, *Chemometrics and Intelligent Laboratory Systems*, **42**, pp. 125-139, (1998).
22. Carmody, O., Kokot, S., and Frost, R., Evaluation of Mecanochemically Activated Kaolinite using PROMETHEE and GAIA – Multi-criteria Decision making method, Presented at the 5th Australian Conference of Vibrational Spectroscopy, Melbourne, Australia, 2003.

5

A CRITICAL EVALUATION OF THE FORENSIC APPLICATION OF FT-IR MICRO-SPECTROSCOPY AND CHEMOMETRICS FOR SINGLE HUMAN SCALP HAIR FIBRES

Hair is extremely important as physical evidence. It must be collected in every case in which it occurs, and subjected to thorough study. The laboratory investigator who examines it must have a broad knowledge of the general nature of hair and a reasonable amount of detailed experience in its examination. Except for certain simple preliminary examinations...it is dangerous to depend on any but expert study of hair found in evidence [1].

The objective of this chapter is to propose an alternative method for the forensic analysis of single scalp human hair fibres through the use of FT-IR micro-spectroscopy and chemometrics. The research presented in this chapter will examine, through a systematic study, the potential application of FT-IR micro-spectroscopy for the discrimination and matching of a wide range of single scalp human hair fibres. Variables such as gender, race, treatment and black and white hair fibres will be investigated. FT-IR spectral data will be interpreted through the use of curve-fit and chemometrics methods of analysis.

5.1. Introduction

Even though we are quite familiar with the physical and chemical characteristics of human hair, the identification and comparison of hair fibres remains a complicated area. Upon initial observation, hair on a head of one person appears to be the same as those of the next, the most obvious difference being the colour change. However, at the molecular level, hair is expected to vary between individuals on the basis of

genetically related factors, diet, cosmetic treatment, and weathering [2, 3]. Studies have shown that drug intake of hair fibres varies between different ethnic groups, indicating possible variations between the chemical composition of hair fibres from people of different races [4].

In any struggle between victim and attacker, hairs and fibres from one are inevitably transferred to the other. The importance of hair in criminal investigation was realised at an early stage in the development of forensic science.

Hair can provide crime investigators with important clues. Unless it is burnt, hair is extremely durable. It remains identifiable on bodies in an advanced state of decomposition or attached to a murder weapon long after the crime is committed. Hair is composed of protein substances, chiefly keratin, and head hair grows at an average weekly rate of about 2.5mm, the beard growing faster and body hair more slowly. Growth ceases at death, but as the skin shrinks the hair, especially the beard, becomes more prominent, giving rise to the myth that hair grows after death. Hair can also be used in helping to reconstruct events. Collection of hair and fibres can indicate contact with surfaces or individuals and where individuals have been. Examination of the root structure can indicate whether hair has fallen out or been forcefully removed, indicating a struggle.

The recovery, subsequent examination and comparison of hair found at a crime scene with hair from the suspect and/or victim can provide valuable assistance in a criminal case. Possible identification of the hair fibre has as its purpose the determination of the physical or chemical identity of the evidence with as near absolute certainty as existing analytical techniques will permit.

Most efforts on hair analysis have been centered on morphological studies and the advantages and disadvantages of the technique have already been discussed in chapter 1, section 1.2.3.

Since the introduction of DNA into the forensic field, there have been several attempts to individualise human hair fibres on the basis of its DNA. The significance of DNA for the analysis of human hair has been discussed in chapter 1, section 1.2.5. Houck and Budolwe [5] in a paper discussing the correlation of microscopic and mtDNA hair comparisons concluded that mtDNA and microscopic analysis are both useful in forensic investigations because they both rely on independent types of information. The mtDNA sequence provides information about the genotype of the source individual, while the microscopic examination evaluates physical characteristics of an individual's hair in his/her environment. The authors proposed that both microscopic and mtDNA analysis should be used in conjunction with each other for hair analysis. Furthermore, the authors point out, that microscopy should not be seen as a "screening test" and mtDNA analysis as a "confirmatory test". Both methods, or either, the authors argue can provide probative information to an

investigation and one is not superior to another as both analyse different characteristics. The authors concluded their study by proposing that the two methods combined provide an additional level of information that provides greater accuracy than either alone.

The research presented in this chapter aims to investigate the possibility of an alternative technique for the forensic analysis of human hair fibres. FT-IR micro-spectroscopy has found wide practical applications in forensic science, some of which include the analysis of paint during hit and run accidents [6] and the discrimination of inks [7] and toners for colour photocopiers [8] during document examination. The application of FT-IR micro-spectroscopy to forensic samples can be attributed to the easy operation of the instrument, its quick response time during spectra collection and to the possibility of examining small amounts of sample.

The work presented in chapters 3 and 4 set out the FT-IR spectral collection parameters for the analysis of hair fibres as well as for other related types of keratin fibres. These chapters have also provided extensive analysis of the vibrational band assignments in the ‘fingerprint’ region, $1750\text{-}750\text{ cm}^{-1}$, of the FT-IR spectra. The research presented in this chapter will focus on the application of FT-IR micro-spectroscopy followed by chemometrics for the investigation of single scalp human hair fibres collected from different subjects with the ultimate scope of applying the technique to the individualisation of hair fibres in forensic cases. The conclusions drawn from this study will aim at establishing the fundamental role of the proposed technique in the field of forensic science, with the ultimate aim at developing an objective technique, which will assist police with their investigations.

5.1.1. Variations in Sample Collection and Preparation Methods

Prior to commencing any research, it is important to take into consideration the sample collection and preparation methods as they relate to the sample being investigated. In the case of hair analysis, there are a number of compounding variables that can limit the interpretation of the hair results. It is well reported in the literature [2, 3] that the rate of hair growth varies from person to person, with nutritional and disease states, with the presence of particular drugs, with gender, age, race, with site on the scalp and/or other body parts. While some of the factors may be known in an individual case, others are unknown, or cannot be known.

Hair analysis from a particular individual is fraught with a series of uncontrolled variables and unknown data. It should be obvious that uncontrolled variables and unknown data belie making any precise forensic analysis. The precision and standardization associated in the analysis of hair fibres is often related to the amount of hairs taken from any particular subject. Unless a uniform sample is taken from which all analyses are done, the validity of the analysis can be called into question. It is therefore very important to analyse a number of different hair fibres from the same head, in order to eliminate the variation differences within the single head.

The work presented in this chapter will initially focus on establishing the variations in hair sample collection and hair preparation methods for FT-IR analysis. For example attention will be directed towards the variation of multiple hair fibres from the same

scalp and variation of different hair fibres from different subjects, variation of black and white hair fibres from the same scalp, and also variations of treated hair fibres within the same scalp. The proposed experimental design is presented in the following section.

5.2. Experimental design

5.2.1. Purpose and scope

Previous work presented in chapters 3 and 4 of this thesis discussed the application of FT-IR micro-spectroscopy to the study of different types of keratin fibres. The research so far has indicated that FT-IR micro-spectroscopy is a rapid method of keratin fibre analysis, which offers valuable information on the basis of the molecular structure of the fibre. In this chapter, FT-IR micro-spectroscopy will be extended to single scalp human hair fibres and will be used to examine the potential forensic application of the technique for the discrimination and matching of single scalp human hair fibres. The objectives of the work presented in this chapter are:

1. To examine the possible application of FT-IR micro-spectroscopy followed by chemometrics for the discrimination and matching of single scalp human hair fibres in forensic cases.
2. To predict some characteristics of blind samples in an effort to understand the limits of the technique for application in the area of forensic science.
3. To investigate, with the aid of chemometrics and other statistical methods, the molecular basis for the discrimination of the hair fibres.
4. To investigate through chemometrics the matching and discrimination of black and white hair fibres from the same source and from different sources.

FT-IR spectra will be collected from single scalp human hair fibres from various subjects. The spectra will be analysed through chemometrics methods such as PCA, FC and SIMCA for qualitative as well as semi-quantitative analysis. In addition, curve fitting of the relative intensity areas in the spectral region between 1750-750 cm^{-1} will be applied in an attempt to identify and isolate the molecular characteristics of the different hair fibres. The analysis of the hair fibres will involve the discrimination and matching of unknown hair fibres to 'control' fibres as well as the identification of some variables for the unknown hairs. The variables to be examined are gender and race and treatment.

The experiments carried out in this chapter involved hair fibres randomly collected from different donors. This method of fibre sampling was based on the theory that each item in the population has an equal chance of selection. The database consisted of hair fibres collected from both genders (male and female) and Caucasian and Mongoloid subjects (it was found to be difficult to collect sufficient hair fibres from Negroid subjects). Gender and race were characterised as the major variables in the study. The literature [10] has suggested that age, hair colour and hair length do not have any effect on the results and were treated as minor variables. However, an attempt will be made to match unpigmented (white) hair fibres with pigmented hair fibres from the same subject.

5.2.2. Selecting samples from a population

Hair occurs frequently as physical evidence in non-violent as well as violent crimes [10]. The statistics presented by the Australian Institute of Criminology (AIC) provide a general picture of the different types of recorded crimes [11]. In 2003, the most commonly mentioned personal crimes were assault and theft. Males in the 25-44 age group and females between the ages of 15-24 were most at risk of being a homicide victim. Homicide offenders were more likely to be male than female, independent of age, and both males and females were most at risk of being a victim of assault while aged between 15 to 24. Females between the ages of 10-14 were more likely to be victims of sexual assault than males, but males aged between 15 and 24 were at least twice as likely to become a victim of armed robbery than persons in any other age category. In the case of unarmed robbery, males in the 15-19 age group were most likely to be victims.

Based on these statistics, the experiments in this chapter focused on hair fibres collected from people between 14 to 45 years old as they formed the age group most likely to be responsible for or be victims of a personal crime.

The subjects, whose hair fibres were analysed in this study, were randomly selected from the population of Brisbane. Random selection of samples ensures that every individual in the population has an equal chance of being selected [12]. Population statistics and its significance in forensic hair analysis will be discussed in a later section of this chapter.

5.3. Forensic Evaluation of Human Hair - Past Studies

The idea of exploring differences in the amino acid composition of human hair originated when Robbins and Kelly [2] proposed that genetic related factors, diet, cosmetic treatment and weathering of hair may produce variations in the actual contents of certain amino acids. Untreated hair samples from five different female Caucasians, ages 6 to 10 were analysed for a total of 18 amino acids. Analysis of variance indicated significant differences for 9 of the 18 amino acids (proline, glycine, alanine, valine, tyrosine, phenylalanine, cysteic acid, histidine and arginine) at the $\alpha=0.01$ level and for 3 more amino acids (half-cystine, isoleucine and leucine) at $\alpha=0.05$ level. The authors suggested that a larger number of samples will produce a better representation of the results. The reported variations in the amino acids of hair fibres collected from different subjects led to an FT-IR spectroscopic study by Hopkins et al [9]. The authors employed the amide I (1657 cm^{-1})/II (1547 cm^{-1}) band ratio method in an attempt to establish differences between the hair fibres that could be correlated to gender, age, hair colour, and chemical treatment. The conclusions drawn from this study were that the ratio of amide I/II does not provide reliable results that could differentiate hair fibres from different subjects. This ratio will be further discussed in a later part of this chapter. In another study [13], it was proposed that the only visual difference in the FT-IR spectra collected from hair fibres from different subjects is the presence of the cysteic acid band (1040 cm^{-1}) for the treated fibres.

There are two major differences between the two FT-IR investigations mentioned above and the work presented in this thesis;

1. The first difference is related to the fibre preparation procedure prior to IR analysis. Flattening of the hair fibre offers several advantages. Firstly, deviations from Beer's law are reduced, secondly the reduction in pathlength is important for fibres possessing high absorptivity and finally flattening increases the surface area of the sample available for analysis, thereby enhancing the signal to noise ratio while reducing diffraction effects at the fibre edges. There are various ways of flattening fibres prior to analysis some of which include the use of diamond anvil cell, ATR, and the metallic hand-held roller [14]. These methods have been discussed in chapter 3, section 3.4.
2. The application of chemometrics for a wide variety of fibrous and similar samples, other than hair, has shown that such analysis can provide information often unavailable by visual examination of the spectral data [15, 16]. Spectral data interpretation, in previous studies, was carried out by visual examination. However, in this work, apart from the S=O spectral region around 1040 cm^{-1} , there are no easily discernible peaks, which could be profitably used for matching and discrimination of the spectra. Thus, in the present work, chemometrics methods of analysis such as PCA, SIMCA and FC were applied in order to extract any differences between the different types of hair used in the study. Curve-fitting of the major bands in the FT-IR spectra was also applied so as to account for any differences between the spectra collected from various subjects.

5.4. Population statistics

The research published in this chapter deals with the discrimination and matching of FT-IR spectra collected from single scalp human hair fibres and is directed towards forensic applications. The hairs were collected from different subjects and variables such as gender, race and treatment were examined. Prior to the examination of the hair it is important to establish the ideal sample size that needs to be taken into account in order to achieve a reliable database for the hair fibre study. The discussion on population statistics presented in this thesis is not extensive and is only used as a general guideline for the sample collection parameters to be used in this work.

During any analysis, it is particularly important to know the size or amount of sample necessary to collect in order to have a reasonable chance of detecting an effect when such an effect exists [17]. The definition of a population relevant to a particular case is quite difficult. At the present time there are no obvious general set of guidelines available for choosing the “right” hair population. A population study will ideally include samples from the global population [17]. However, in the case of human hair, it will be impossible to sample every single head of the whole human population.

In a paper by Gaudette and Keeping [18], the authors attempted to discuss the issue of population statistics as they relate to human scalp hair comparisons by optical microscopic methods. In total, 100 different individuals submitted a sample of 80-100 hairs randomly collected from various regions of the scalp. From these,

depending on the homogeneity of the sample, 6 to 11 mutually dissimilar hairs were selected to represent the range of length, coarseness and colour present in the 80 to 100 hairs. The representative hairs were mounted individually on glass slides and compared to one another, utilising a comparison microscope. A total of 861 hairs from 100 individuals were compared in this manner. By the use of a card coding system, it was possible to record 366,630 hair comparisons between the 861 hairs. It was estimated that if one human head hair found at the scene of a crime is found to be similar to a representative hair from a suspect's head, the odds against it originating from another person are about 4500 to 1. Negroid and Mongoloid hairs exhibit less variation in many of their characteristics indicating that these odds would be somewhat less for persons of these racial origins.

A critical paper by Barnett et al [19] raised four arguments in relation to the study by Gaudette et al. Those were;

- (1) The validity of the application of the findings to real-life situations,
- (2) Possible examiner bias,
- (3) The use of non-individualising features in the sorting procedure, and
- (4) The statistical treatment of data.

In an attempt to provide answers to these questions, the authors collected 930 hairs from 97 different Caucasian subjects and two examiners independently examined, classified and prepared the final comparison list. Barnett et al, state that based on the results obtained by the two examiners the classifications of hair by both examiners were inconsistent and it thus leads to subjective conclusions.

Stafford Smith and Goodman [20] published a paper discussing the validity of Gaudette's hair comparison studies. In particular, the authors highlighted three important points;

- (1) Lack of blind samples. Gaudette had prior knowledge that he was comparing hairs, which came from different people. Stafford Smith and Goodman propose that the experiment should be replicated using examiners who are not told that any matches found will be false;
- (2) Subjective nature of hair examination; and
- (3) "Featureless hair". Gaudette groups hair as "featureless hair". The author argues that there is increased probability of false matches with "featureless" scalp hair and reports that such a false match occurred in his experiment twice. Gaudette did not define a "featureless hair".

Table 5.1 illustrates an approach in establishing the sample size necessary to obtain a representative sample of the total population. If we consider an infinite population in which the population variance of the characteristic of interest is σ^2 , sample size is n and sample mean has a variance σ^2/n , then with reference to Table 5.1 the sampling fraction can be estimated [17].

TABLE 5.1

Relationship between sample size and population size

Sample size	Population size	Sampling fraction
--------------------	------------------------	--------------------------

n	N	$\sqrt{\{(N-n)/N\}}$
100	2 000	0.9747
100	20 000	0.9975
100	200 000	0.9998

There is a 2.5% improvement in precision by using N=200 000 instead of N=2 000. The question however arises whether the relative merits of improvement in precision of 2.5% account for an increase of the cost and time of sampling a larger population. The study in this research project was carried out at the Queensland University of Technology, which is situated in Brisbane, Australia. The total population of Brisbane was, at the end of 2002, approximately 1.6 million [22] and the total population of Australia was estimated to be 19,813,742 [23]. In the present study, the hair fibres were collected from subjects living in Brisbane. Hair samples were collected from a total of 136 subjects. Therefore on the basis of the equation presented in table 5.1, a sample size of n=136, in a population size of N=1.6 million, provides a sampling fraction of 0.9999. Therefore, the sample size chosen for this work is sufficient for a reliable hair database for the Brisbane population.

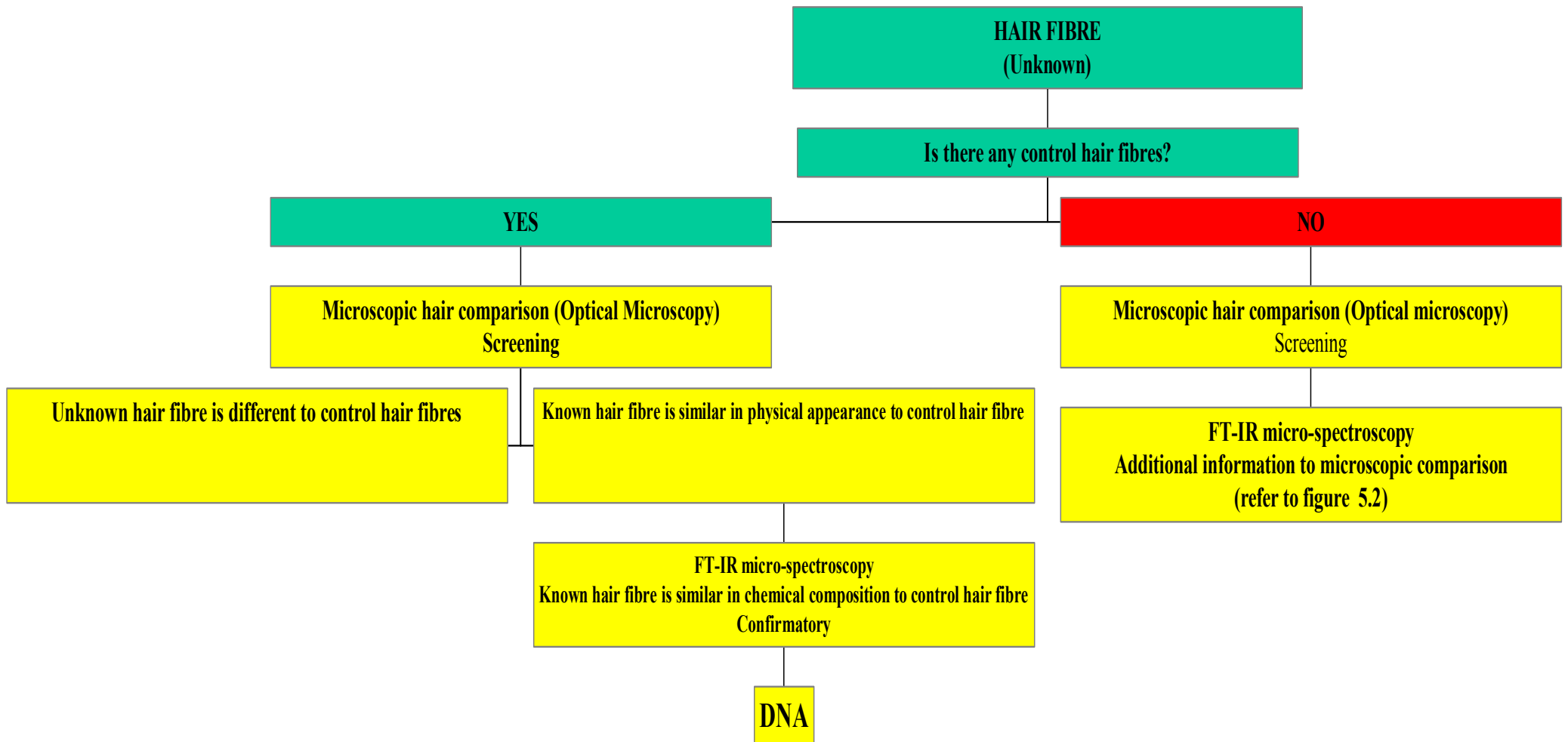


Figure 5.1. Schematic representation of the proposed application of microscopic, FT-IR and DNA techniques for the analysis of unknown hair fibres.

5.5. Hair Examination Protocol

The aim of the research presented in this chapter is to develop a technique that will offer additional information, which when used in conjunction with the common microscopic techniques and the more recent DNA advances, will provide better information for matching or discrimination of single scalp human hair fibres. It is proposed that a combination of the three techniques will enable an improved identification of a hair ‘profile’. A scheme is proposed (figure 5.1) in which the three techniques, in order of the screening step carried out by microscopic methods of analysis to the more confirmatory DNA are to be implemented in the hair methodology. FT-IR micro-spectroscopy is proposed to be implemented in between the two existing hierarchical methods of hair analysis. The hierarchical structure of the three techniques and the reasons behind the choice of the order of the techniques in the hierarchical model is discussed below.

Any hair investigation begins with the recovery of an unknown hair fibre(s) from the crime scene. The initial question to be addressed is whether there are any control hairs i.e., hair fibres from the victim and/ or suspect(s) that the unknown (or recovered) hair fibre(s) can be compared to. If there are control hair fibres then it is proposed that these hair fibres need to be initially microscopically examined for possible identification of race and treatment along with any other particular traits i.e.,

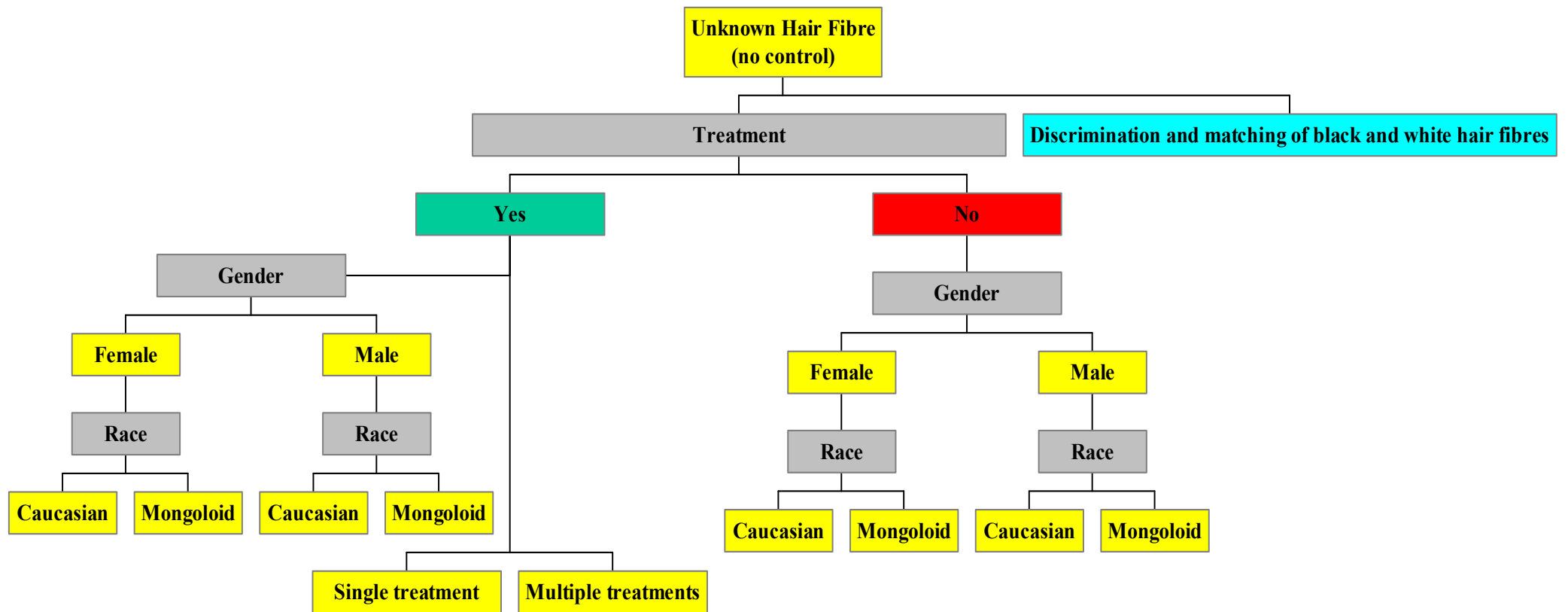


Figure 5.2. Schematic representation of the hypotheses proposed to investigate the origin of an unknown hair fibre found at the crime scene through FT-IR micro-spectroscopy and chemometrics.

whether the hair was forcibly removed or any other unique physical characteristics. If the fibres are found to be microscopically different then there is no need for further examination. If however, the hair fibres are found to be similar to the hair fibres collected from either the suspect or the victim, then further investigation is necessary so as to remove any subjective measurements from the microscopic comparisons that can be seen as providing a false positive match. FT-IR micro-spectroscopy and chemometrics can be used to compare the recovered hair fibres with the control hairs and determine any chemical similarities between the fibres. An example of hair comparison of recovered and control hair fibres is presented as cases (A) and (B) in the following sections of this chapter.

In cases where there are no control hair fibres submitted or where the recovered hair fibres do not match to any of the control then FT-IR micro-spectroscopy followed by chemometrics can be used to investigate variables such as gender, race and treatment in an attempt to provide the investigating police with a ‘profile’ identification of the person whose the hair belongs to. The investigation of such a hair fibre begins with the first variable, which is treatment, followed by gender and race as shown in figure 5.2. The ‘profile’ identification of the person from a single strand of hair is shown as case (C). Case (C) will involve the investigation of two ‘blind’ hair samples, which are hair fibres collected from a known subject but which are used to validate the proposed methodology of hair identification. The same two ‘blind’ hair samples will be used in a number of case studies presented in scenario C, so as to establish the origin of the hair fibre and to narrow its identity to variables such as treatment, gender and race. In cases where a positive identification has been established it will be

advantageous also to apply DNA for additional verification of the microscopic and FT-IR results.

Another important aspect of hair analysis, which cannot be achieved through microscopic examination, is the comparison of pigmented and white (unpigmented) hair fibres from the same subject. Case (D) will present an investigation into the matching and discrimination of pigmented and unpigmented hair fibres through the use of FT-IR micro-spectroscopy and chemometrics. In particular, attention will be given to the information provided in the FT-IR spectra and identifying the major spectral bands that could assist in providing a comparative analysis of pigmented and unpigmented hair fibres.

5.6. Validation of methodology

Hair samples from a number of different subjects (as shown in table 5.2) were used to validate the methodology by evaluating the success rate of the technique and for highlighting any limitations. The hair fibres were obtained from four different groups of people that donated their hair for this research. These groups visited the Queensland University of Technology over a period of 12 months. The results of the success rate are presented in table 5.2.

Initially, the identification of the validation hair fibres involved the formation of a reference set i.e. a set of known hair fibres similar to that shown in case (C). The validation samples were matched to the reference set in a similar way as that shown in the examples of gender and race identification presented as case C. Table 5.2 shows a 100% success rate for treatment, 80% success rate for gender and 88.5% success rate

Table 5.2

Summary of the Success Rate obtained for the Validation hair samples
(Variables examined; treatment, gender and race).

	Reference Samples	Significant PC's	Validation Samples	Success at p=0.05
Reference set-1				
Treatment	15	5	15	100%
Gender				80%
Race				80%
Reference set-2				
Treatment	20	5	20	100%
Gender				75%
Race				95%
Reference set-3				
Treatment	18	5	18	100%
Gender				83%
Race				89%
Reference set-4				
Treatment	25	6	12	100%
Gender				82%
Race				90%

for race. The incorrect results were obtained from fibres collected from subjects who have been taking long-term medication. It therefore appears that the analysis of the hair fibres that have been subjected to long-term medication is a major limitation of the technique as it can lead to incorrect results. These results suggest that long-term medication can lead to changes in the molecular structure of the hair fibres. Future research is warranted in this area in order to determine the exact affects of the long-term medication to the hair protein. This will in turn provide an insight into the incorrect results obtained during the FT-IR analysis of the hair fibre.

5.7. Results and Discussion

The application of FT-IR micro-spectroscopy and chemometrics for the analysis of single scalp human hair fibres obtained from the present study is presented as cases A, B, C and D.

5.7.1. Case A - Comparison of untreated hair fibres from two different subjects and an unknown source.

In forensic cases it is essential to receive a sample of known hairs from all relevant individuals in a case i.e., suspect, victim and all other relevant parties in the case. It is recommended that a 'control' head hair sample consists of at least 15-20 hairs from each of the five different areas of the scalp (center, front, back, left and right side) and that these hairs be obtained by both pulling and combing [1].

In order to investigate the variations between hair fibres collected from different individuals it is important to examine the variation of hairs within a single head. In this study, hair fibres were randomly collected from the hairbrushes of the two subjects, whilst in previous study [25] the hair fibres were collected from known positions on the head. The hairbrushes were only used by those subjects.

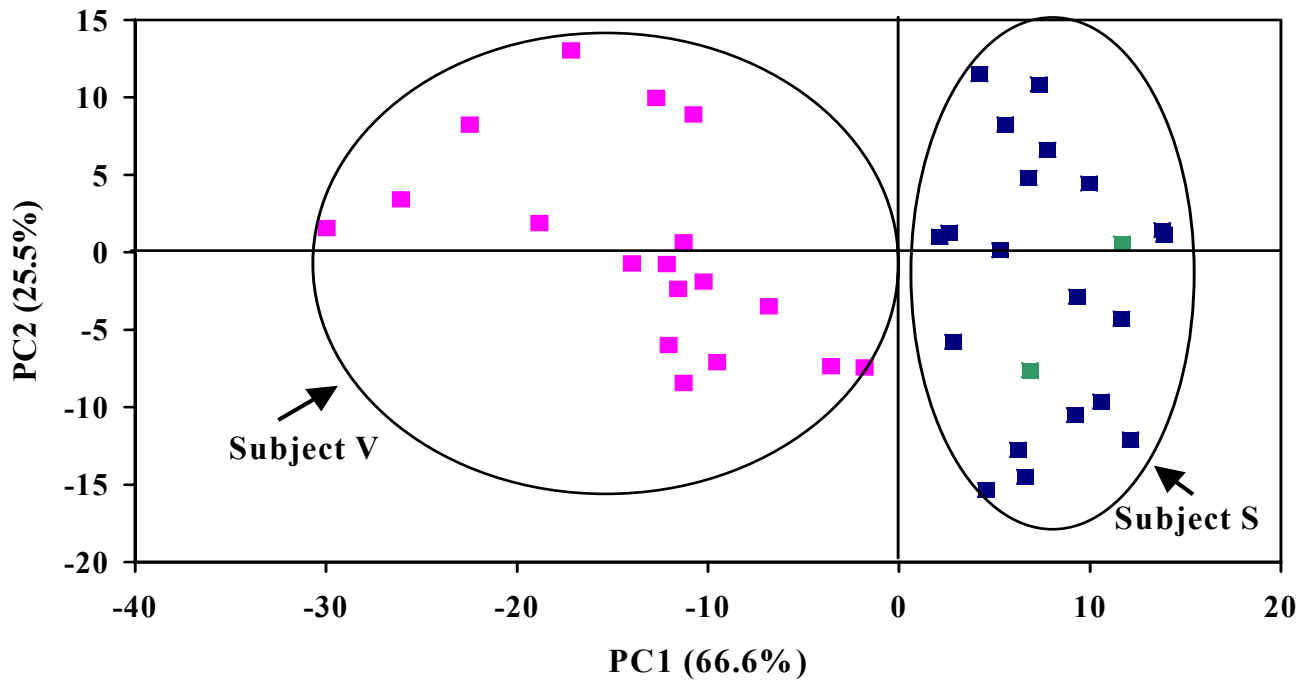


Figure 5.4. PC1(66.6%) vs PC2(25.5%) scores plot of subject V (■), subject S (■) and unknown (U1 and U2 (■)) hair

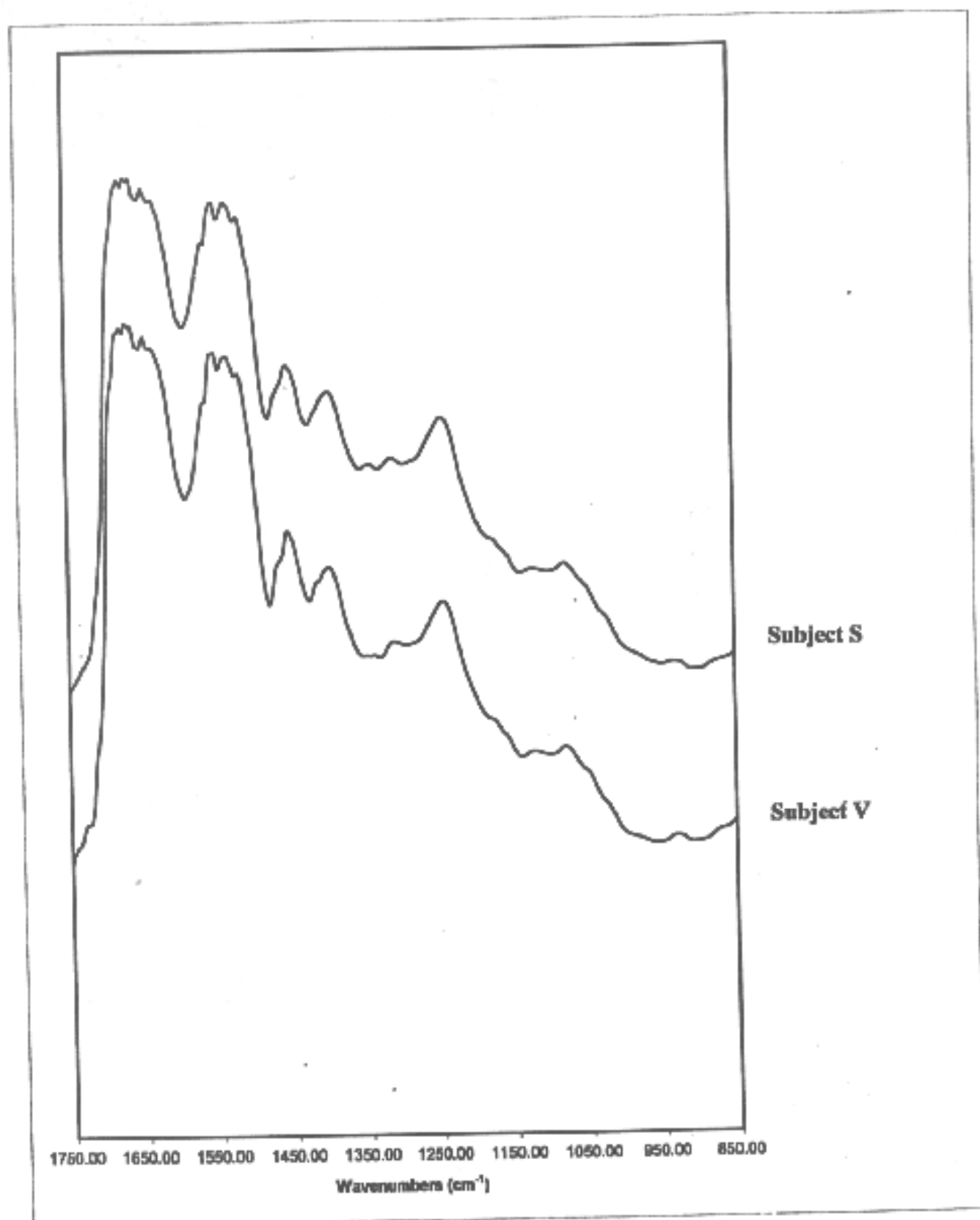


Figure 5.3. Examples of FT-IR spectra collected from subject S and subject V (1750-750 cm⁻¹) in absorbance.

5.7.1.1. PCA

In this case multiple hair fibres (at least 15 hair fibres) were randomly collected from two subjects (subject V and subject S). These hair fibres will be referred to as ‘control’ hairs. The subjects were Caucasian females in their late 20’s with no reported chemical treatment done on their hair. FT-IR spectra were collected from each fibre (Figure 5.3) and submitted to chemometrics for PCA. Visually, the FT-IR spectra collected from subject S and V appeared, apart from some slight changes to the lineshape for amides I and II, very similar. In addition to the ‘control’ fibres, two unknown hairs were also examined. The unknown hair fibres were randomly selected from subject S and were treated as ‘blind’ samples in an attempt to validate the PCA results. The results from PCA (PC1(66.6%) vs PC2 (25.5%)) are shown in figure 5.4. PC1¹, which accounts for most of the variance in the data set, discriminates subject V (negative scores) from subject S (positive scores). The two unknown hair fibres group with subject S.

The grouping of the two unknown hair fibres highlights the potential forensic application of the technique for the discrimination and matching of untreated hair fibres from known and unknown subjects.

¹ The PC1 loadings plot has a very broad spectral region with minimal information, and was therefore not included in this case.

5.7.1.2. SIMCA

The separation observed by PCA between the FT-IR spectra of the two subjects was further studied by SIMCA in order to obtain a semi-quantitative estimate of the separation. FT-IR spectra collected from subject S were used to build a model set because it contained the most number of objects in the data set. The results from SIMCA are presented in Table 5.3. Five components were identified as significant by the cross-validation approach and the model accounted for 97.3% of the variance. The F-test statistic at $P=0.05$ and $DF=13$ (subject V) and 15 (Subject S) was 1.35.

TABLE 5.3

SIMCA analysis results with $RSD_{crit}=0.21$, $p=0.05$

SIMCA results	Subject V	Subject S
RSD mean	0.65	0.17
n(number of spectra)	15	17
distance between classes	3.2	----

FT-IR spectra collected from subject S have RSD values (0.17) lower than the RSD_{crit} (0.21) while FT-IR spectra collected from subject V have RSD values (0.65) significantly higher than the RSD_{crit} . **Therefore, given the variation between the mean RSD values, there is a clear discrimination between the FT-IR spectra collected from subject V and subject S.**

As outlined in chapter 2, section 2.5(b), a class distance of around 3.0 indicates that the classes are different, while values with less than 1.0 indicate that the classes are similar. In this case, a class distance of 3.2 was obtained between the two classes, which indicates a variation between the FT-IR spectra collected from the two subjects.

Table 5.4.

Fuzzy clustering membership values for a two-cluster model with a hard (1.50) and soft (2.50) weighting exponent value

SOURCE	W.E.=1.50		W.E.=2.50	
	1	2	1	2
V1	1.00	0.00	0.91	0.09
V2	1.00	0.00	0.91	0.09
V3	1.00	0.00	0.94	0.06
V4	0.97	0.03	0.75	0.25
V5	0.99	0.01	0.83	0.17
V6	1.00	0.00	0.95	0.05
V7	0.96	0.04	0.72	0.28
V8	0.67	0.33	0.57	0.43
V9	0.97	0.03	0.75	0.25
V10	0.60	0.40	0.91	0.09
V11	1.00	0.00	0.93	0.07
V12	0.96	0.04	0.76	0.24
V13	1.00	0.00	0.84	0.16
V14	0.95	0.05	0.70	0.30
V15	0.95	0.05	0.70	0.30
V16	0.97	0.03	0.73	0.27
S1	0.02	0.98	0.23	0.77
S2	0.12	0.88	0.36	0.64
S3	0.03	0.97	0.30	0.70
S4	0.06	0.94	0.38	0.62
S5	0.14	0.86	0.13	0.87
S6	0.00	1.00	0.34	0.66
S7	0.09	0.91	0.12	0.88
S8	0.00	1.00	0.32	0.68
S9	0.07	0.93	0.13	0.87
S10	0.00	1.00	0.12	0.88
S11	0.00	1.00	0.13	0.87
S12	0.00	1.00	0.28	0.72
S13	0.04	0.96	0.19	0.81
S14	0.01	0.99	0.27	0.73
S15	0.03	0.97	0.07	0.93
S16	0.00	1.00	0.26	0.74
S19	0.02	0.98	0.28	0.72
S20	0.02	0.98	0.26	0.74
Unknown hair 1	0.00	1.00	0.08	0.92
Unknown hair 2	0.01	0.99	0.22	0.78

The previous analyses by PCA and SIMCA suggested a separation between subject V and S. FC is an independent non-parametric technique and acts as a confirmatory procedure for PCA. A summary of the FC results for a two-cluster model (for both a hard (1.50) and a soft (2.50) weighting exponent value) is shown in table 5.4. The membership criterion for a two-cluster model is 0.5. FT-IR spectra collected from subject V indicate a preference for class 1, while FT-IR spectra collected from subject S belong to class 2. In addition, the unknown hair fibres group with class 2, confirming the PCA results that the unknown hairs have originated from subject S. The FC results suggest a lack of fuzziness between the two classes, which indicates that the membership between the classes is robust.

5.7.1.4. Conclusions for case A

This study has shown that comparisons of the FT-IR spectra collected from hair fibres (of similar hair morphology and colour) obtained from two subjects of similar age, gender, race and treatment can lead to the discrimination of the spectra (on the basis of their origin) through chemometrics methods of analysis. Furthermore, unknown hair fibres can be compared and correctly matched to the ‘control’ hair.

5.7.2. Case B - Comparison of chemically treated hair fibres from two different subjects and an unknown source.

Treated hair can be readily distinguished from untreated hair by the visual comparison of their corresponding FT-IR spectra. In the case of treated hair, the presence of the band at 1040 cm^{-1} , which is attributed to cysteic acid vibrations, is an indication that the hair fibre has undergone some form of chemical treatment. Previous work [25] has established that FT-IR spectra collected from untreated hair can be readily discriminated from FT-IR spectra collected from treated hair with the use of chemometrics. Research presented in chapter 3 of this thesis has indicated that FT-IR spectra collected from untreated hair fibres can be readily discriminated from the FT-IR spectra collected from treated hair fibres.

In the example presented as case A, it was demonstrated that multiple untreated hair fibres from two different subjects of the same gender, race, hair morphology and colour can be readily discriminated according to their source and the unknown hair can be matched to their origin. In the following example, hair fibres were collected from two subjects of the same gender, race and chemical treatment. Both fibres had undergone the same treatment i.e., bleached and dyed. The aim of this study was to establish whether it is possible to discriminate hair, in a similar way as that of case A, even after the hair has undergone chemical treatment. **This is the first time FT-IR micro-spectroscopy and chemometrics have been collectively applied to the discrimination and matching of similarly treated human scalp hair fibres collected from different subjects.**

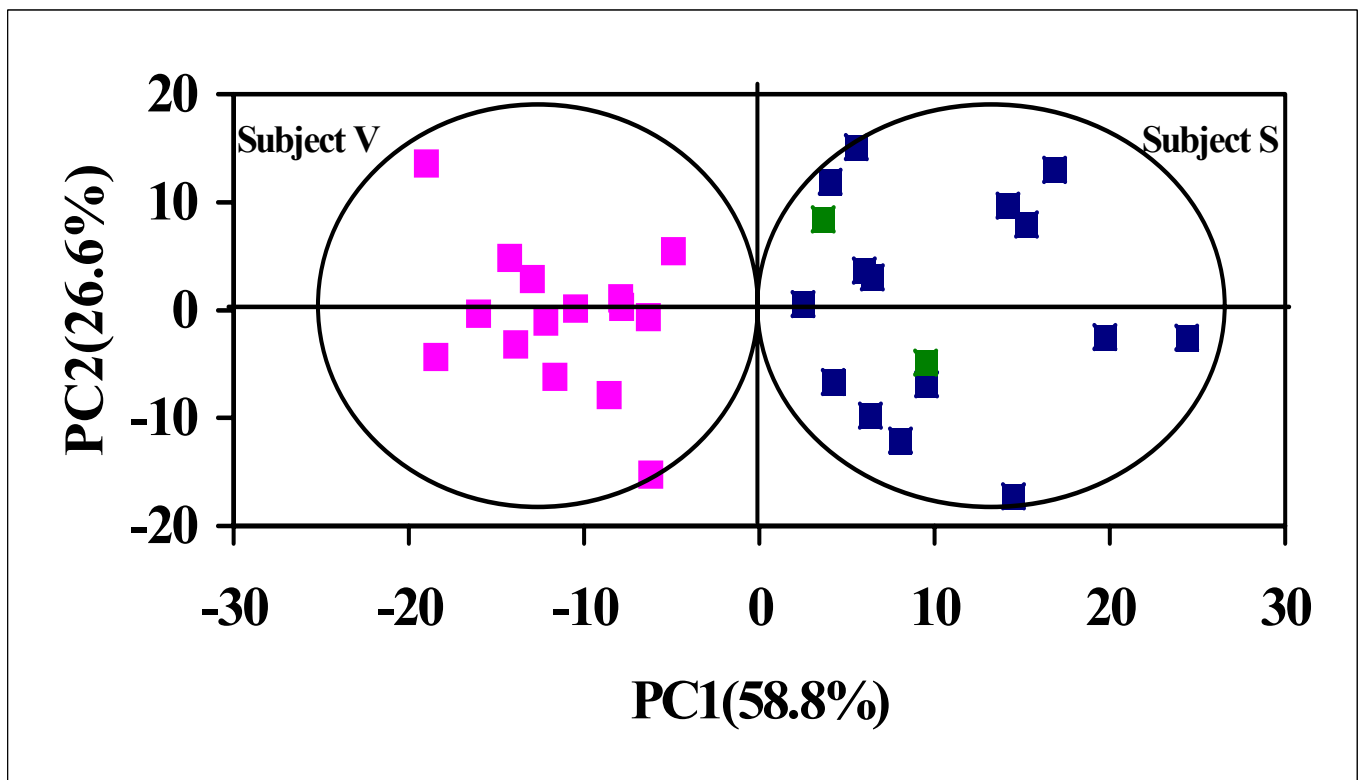


Figure 5.6. PC1(58.8%) vs PC2(26.6%) scores plot of subject V (■), subject S (■) and unknown (U1 and U2 (■)) hair

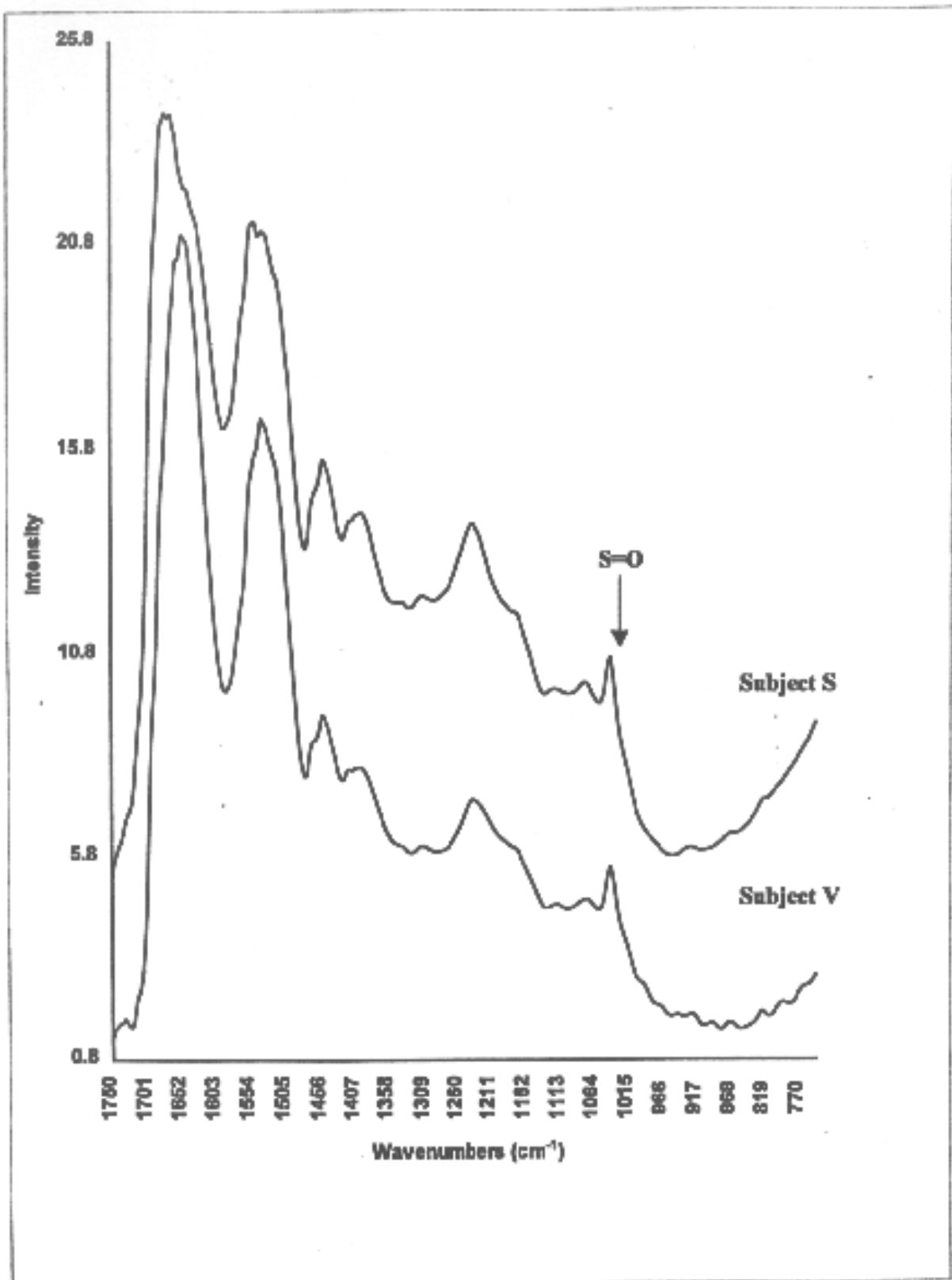


Figure 5.5. Examples of FT-IR spectra collected from subject S and subject V (1750-750 cm⁻¹).

5.7.2.1. PCA

A similar scenario is used as that previously shown in case A. Multiple hair fibres (at least 15 hair fibres) are collected from subject V and subject S. In addition to the ‘control’ fibres, unknown hair fibres were also collected. The unknown hair fibres were randomly selected from subject S and were treated as ‘blind’ samples in an attempt to validate the PCA results. An example of the FT-IR spectra collected from the hair of the two subjects is shown in figure 5.5. Visually, the FT-IR spectra collected from subject S and V appeared, apart from some slight changes to the lineshape for amides I and II, very similar. The PCA (PC1(58.8%) v PC2(26.6%)) plot shown in figure 5.6 clearly discriminates the FT-IR spectra of the hair fibres collected from subject V (negative scores) from the FT-IR spectra of the hair fibres collected from subject S (positive scores) along PC1. The two unknown hairs group correctly with subject S.

5.7.2.2. SIMCA

SIMCA was applied in an attempt to obtain a semi-quantitative indication of the extent of the separation observed in PCA. In SIMCA, the spectra from subject V were defined as the model class. Five components were identified as significant, by the leave-one-out method available in the SIRIUS version 2.3 software, with a 96.4% level of significance distributed between the five PCs. Even though five PCs were identified as significant, only two (PC1 and PC2) were applied as they explained 85.4% of the total variance and are therefore considered as the two significant PCs in the study. FT-IR spectra collected from subject S were referenced to the model class. Table 5.5 shows the results obtained from SIMCA.

TABLE 5.5

SIMCA analysis results with $RSD_{crit}=0.31$, $p=0.05$

SIMCA results	Source V	Source S
RSD, range	0.26	0.95
n(number of spectra)	17	15
distance between classes	-----	2.8

The SIMCA results obtained from fitting subject V to subject S support the patterns obtained by PCA. FT-IR spectra of hair fibres from the two subjects separate into two groups: subject V and subject S. FT-IR spectra obtained from subject V have RSD values (0.26) less than the RSD_{crit} (0.31), whilst FT-IR spectra collected from subject S have RSD values (0.95) higher than the RSD_{crit} .

In the current study, the class distance between subject V and subject S was found to be 2.8. Chapter 2, section 2.5.2, discussing the theoretical aspects of SIMCA,

indicated that class distance values less than one indicate a very small degree of difference, while values greater than three indicate that the classes are quite different. A class distance of 2.8 as the one obtained in this study therefore indicates that even though hair fibres collected from subject V and subject S are different, there is also a small degree of similarity between the two sets of hair samples. The similarity can be attributed to the fact that the hair fibres were collected from two very similar subjects of the same gender, race, age and treatment characteristics. The separation observed in SIMCA is consistent with the results obtained from the PCA study and supports the discrimination between the two sets of classes.

Table 5.6.

Fuzzy clustering membership values for a two-cluster model with a hard (1.50) and soft (2.50) weighting exponent value

SOURCE	W.E.=1.50		W.E.=2.50	
	1	2	1	2
V1	1.00	0.00	0.87	0.13
V2	1.00	0.00	0.91	0.09
V3	0.99	0.01	0.86	0.14
V4	1.00	0.00	0.84	0.26
V5	1.00	0.00	0.86	0.24
V6	0.99	0.01	0.79	0.21
V7	0.99	0.01	0.87	0.13
V8	0.96	0.04	0.74	0.26
V9	1.00	0.00	0.88	0.12
V10	0.94	0.06	0.70	0.30
V11	0.87	0.13	0.66	0.34
V12	0.98	0.02	0.80	0.20
V13	0.99	0.01	0.79	0.21
V14	0.82	0.18	0.62	0.38
V15	1.00	0.00	0.89	0.11
S1	0.17	0.83	0.38	0.62
S2	0.13	0.87	0.36	0.64
S3	0.17	0.83	0.39	0.61
S4	0.04	0.96	0.27	0.73
S5	0.12	0.88	0.35	0.65
S6	0.01	0.99	0.20	0.80
S7	0.08	0.92	0.33	0.67
S8	0.11	0.89	0.34	0.66
S9	0.02	0.98	0.22	0.78
S10	0.04	0.96	0.25	0.75
S11	0.01	0.99	0.15	0.85
S12	0.12	0.88	0.35	0.65
S13	0.03	0.97	0.26	0.74
S14	0.02	0.98	0.24	0.76
S15	0.17	0.83	0.39	0.61
Unknown hair 1	0.01	0.99	0.17	0.83
Unknown hair 2	0.12	0.88	0.36	0.64

5.7.2.3. FC

In order to further investigate the PCA and SIMCA results, a complementary evaluation was applied by the use of fuzzy clustering analysis. A summary of the FC results for the 32 spectra are shown for a two-cluster model in Table 5.6, and on the whole, support the previous observations from the exploratory PCA and SIMCA. Thus, for a two cluster model, with a hard weighting exponent (1.50), spectra from source V indicate a strong membership for class 2, while spectra from source S have a high membership for class 1. When a softer weighting exponent (2.50) is chosen, similar patterns were obtained. The membership criterion for a two-cluster model is 0.5.

A lack of fuzziness between the classes indicates that the membership between the classes is quite robust. The grouping of the two unknown hairs (U1 and U2) with subject V suggests that the unknown fibres could have originated from subject V, which agrees with the grouping by PCA.

5.7.2.4. Conclusions for case B

This study has illustrated through chemometrics methods of analysis a discrimination between FT-IR spectra collected from hair fibres from two different subjects of the same age, gender, race and treatment (bleached and dyed). The unknown hair fibres were successfully matched to the 'control' hair. It is therefore proposed that comparison of hair fibres of similar characteristics (even after the hair fibres have

been chemically treated in the same way) allows discrimination of the fibres on the basis of their origin.

The FC results established a clear separation of the hair samples on the basis of their origin, which supports the SIMCA results that showed a class distance of 2.8 between the samples. As discussed in the SIMCA results, this class distance indicates a difference between the hair samples from the two subjects but it also supports a certain degree of similarity. The FC results further strengthen the difference between the two sets of samples and therefore support the difference obtained in the SIMCA results.

Table 5.7.

Background information of the hair fibres used to build the reference and validation set for the gender and race variables

Source	Gender	Race	Treatment	Age	Hair Colour
F1	Female	Mongoloid	No	33	Black
F2	Female	Mongoloid	No	35	Black
F3	Female	Caucasian	No	15	Brown
F4	Female	Caucasian	No	15	Brown
F5	Female	Caucasian	No	15	Brown
F6	Female	Caucasian	No	15	Blonde
F7	Female	Caucasian	No	14	Brown
F8	Female	Mongoloid	No	15	Black
F9	Female	Caucasian	No	14	Brown
M1	Male	Caucasian	No	14	Brown
M2	Male	Caucasian	No	15	Brown
M3	Male	Mongoloid	No	14	Black
M4	Male	Mongoloid	No	35	Black
M5	Male	Caucasian	No	16	Black
M6	Male	Caucasian	No	14	Brown
M7	Male	Mongoloid	No	15	Black
M8	Male	Caucasian	No	17	Brown
M9	Male	Caucasian	No	15	Brown
U1	Female	Caucasian	No	14	Black
U2	Female	Caucasian	No	25	Blonde

5.7.3. Case C - Identification of gender and race variables of unknown hair fibres

In the two previous cases (A and B), the unknown hair found at the crime scene could be matched with hair fibres from one of the two known subjects. However, in cases where no match is possible or there is no ‘control’ set of hairs for the unknown hair to be compared to, then it becomes important to determine the origin of the hair fibre and to limit it to variables such as gender, race and treatment. As previously discussed, visual inspection of FT-IR spectra collected from a hair fibre can easily discriminate between untreated and chemically treated hair fibres. Chapter 3 has shown a discrimination of FT-IR spectra collected from untreated hair fibres and hair fibres subjected to chemical treatment at different time intervals through the use of chemometrics methods of analysis. It is therefore proposed that the initial variable responsible for the discrimination of hair fibres is chemical treatment.

In order to investigate an unknown hair fibre, it is essential to create a reference set, i.e. a set of known hair fibres and to compare the unknown fibre to that set. It is important to note that in the present work, only untreated hair fibres were used to build the reference set. Work carried out previously [24] used both untreated and treated hair fibres to build the reference set. In order to be able to study the

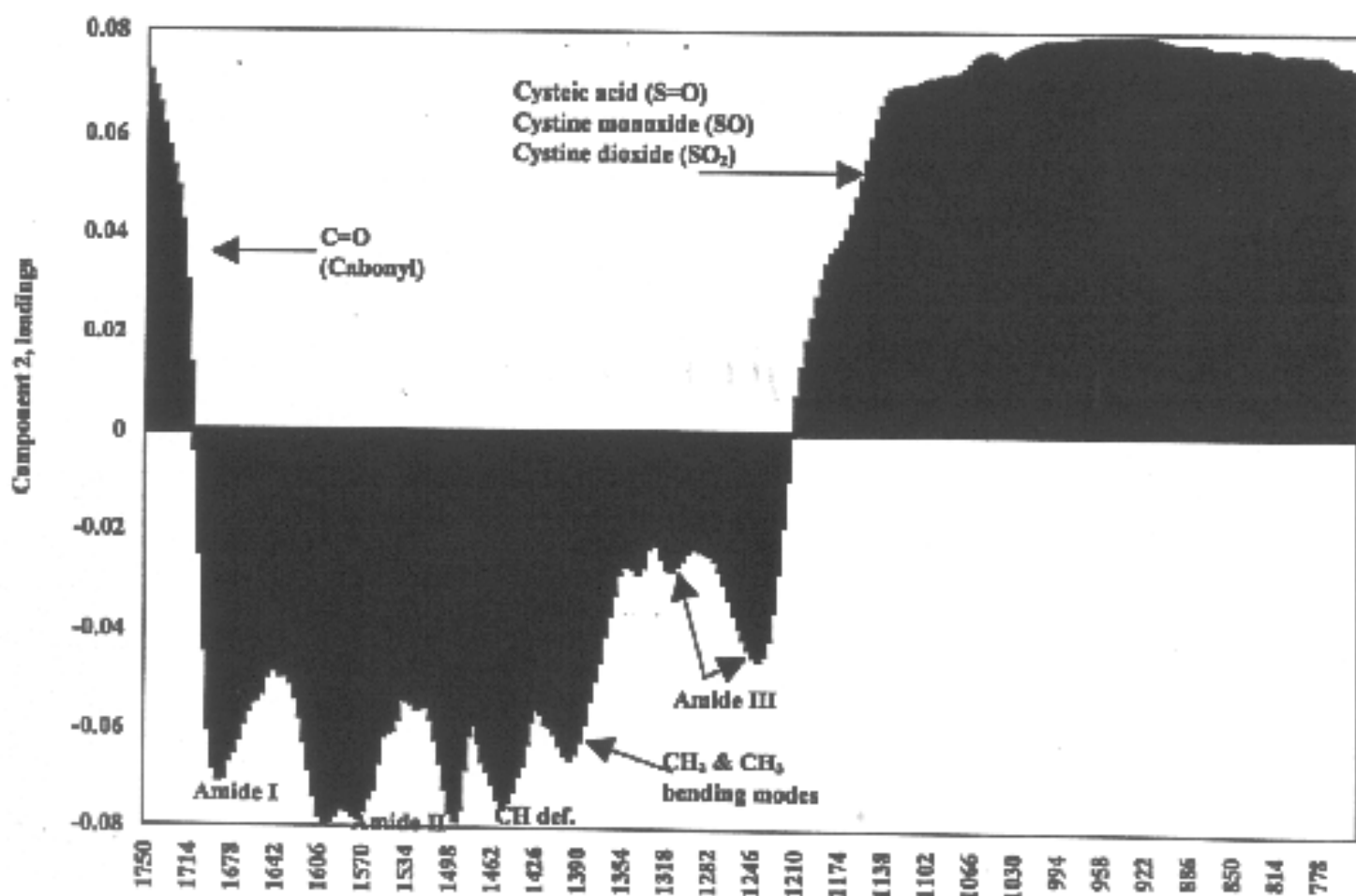


Figure 5.9. PC2 loadings plot (1750-750 cm^{-1}).

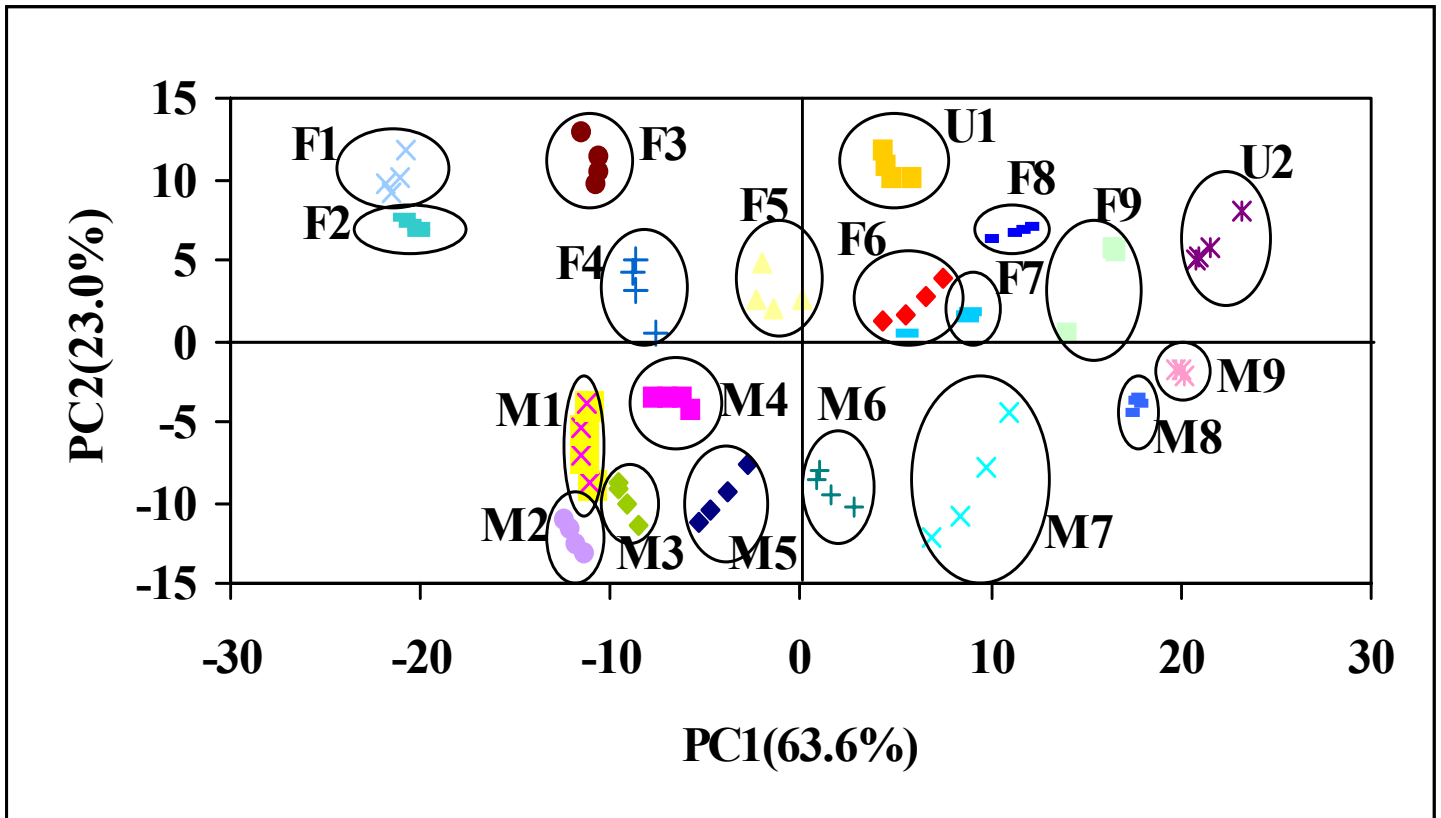


Figure 5.8. PC1(63.6%) vs PC2(23.0%) of the reference set (female (F1-9) and male (M1-9)) and validation samples U1 and U2.

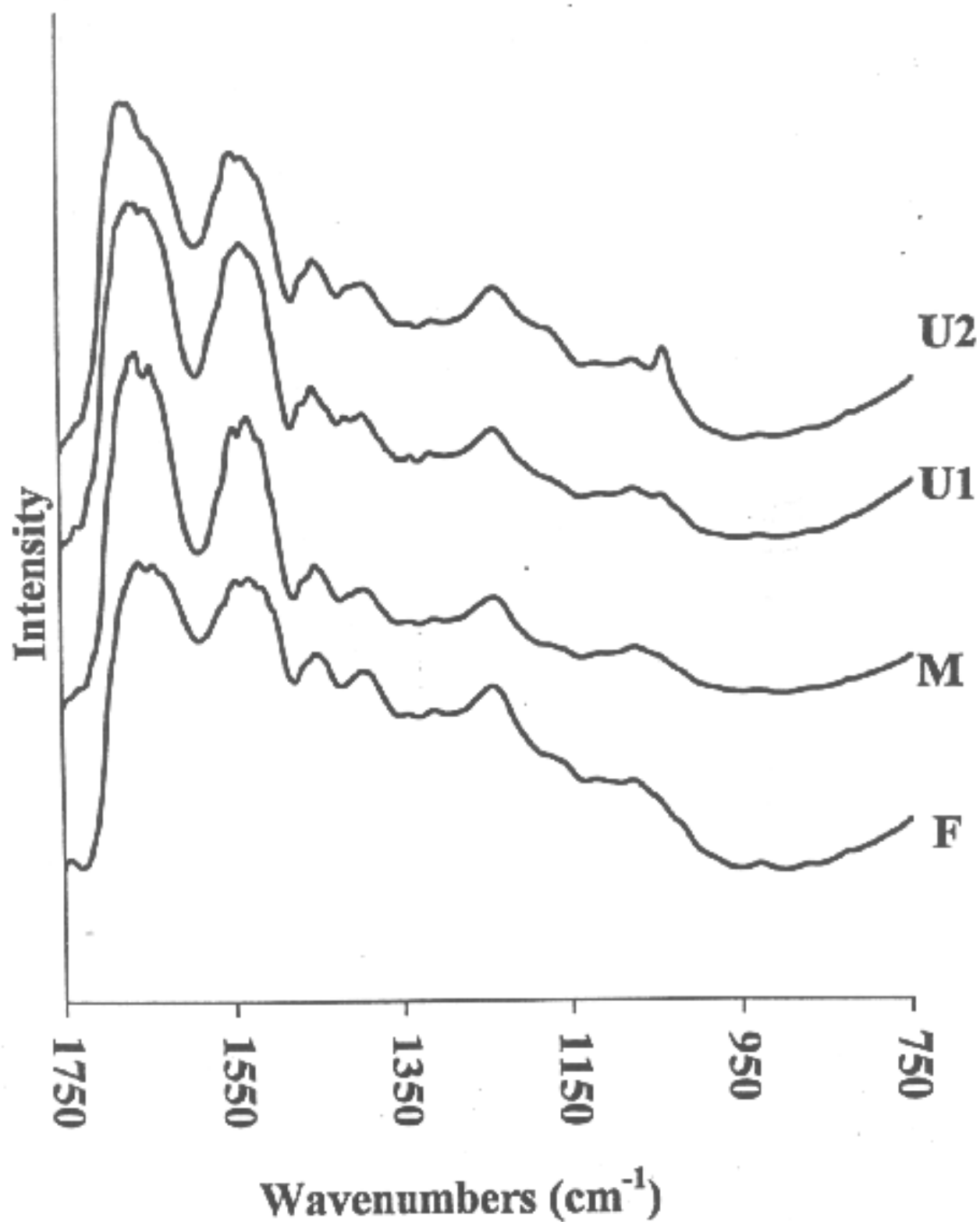


Figure 5.7. Examples of FT-IR spectra collected from Female (F), Male (M) and unknown hair fibres (U1 and U2) (1750-750 cm⁻¹) in absorbance.

fundamental chemical reasons for the discrimination of male and female subjects, it is necessary to eliminate the chemical treatment variable. In total 18 subjects (9 females, and 9 males) of known history (Table 5.7) were used to build the reference set. Four spectra were collected from each hair sample and submitted to chemometrics. In addition, two unknown hair fibres were selected to build a validation set. The validation hair samples were collected by another person and the history of each samples was withheld from the author, until the author completed predictions and these are summarised in Table 5.7. The collected FT-IR spectra are shown in figure 5.7 and they visually appear quite similar, apart from some slight changes in the lineshapes of the amide I and II bands.

5.7.3.1 The Gender Variable

5.7.3.1.1. PCA

In total 80 spectra were submitted to chemometrics for PCA analysis. Five PCs were sufficient to account for the total variance (97.4%) of the data set. The variance was distributed with 63.6% on the first PC, 23% on the second, 6.5% on the third and 4.3% distributed between the fourth and fifth PC. The PC1 (63.6%) vs PC2 (23.0%) plot (Figure 5.8) shows a discrimination between the spectra collected from female subjects (all F clusters with positive scores on PC2), from the spectra collected from the male subjects (all M clusters with negative scores on the same PC). The two unknown hair fibres (U1 and U2) group with the rest of the fibres collected from female subjects.

According to the PC2 loadings plot (Figure 5.9), the FT-IR spectra collected from the male subjects are influenced by the presence of the bands at 1679 and 1618 cm^{-1}

attributed to amide I β -pleated sheet and 1557 and 1515 cm^{-1} which relates to amide II δ (N-H) ν (C-N) α -helix and β -pleated sheet, respectively. The female samples are mainly influenced by C=O stretch (1710 cm^{-1}) with some contributions from the region between 1422-750 cm^{-1} which contains the amide III, CH_2 and CH_3 bending modes as well as cysteic acid, cystine monoxide and dioxide vibrations. The presence of the cysteic acid band in the case of the female hair samples is expected because females generally subject their hair to more cosmetic treatments than males.

PCA indicated a separation between the FT-IR spectra collected from female subjects from those collected from male subjects. SIMCA is applied in order to obtain a semi-quantitative estimate of the observed separation. The spectra collected from female subjects were used to build a model set because it contained the most number of objects in the data set. The results from SIMCA are shown in Table 5.8. Five components were identified as significant by the cross-validation approach. The model accounted for 97.6% of the variance. The F-test statistic at $P=0.05$ was 1.35.

TABLE 5.8

RSD values for SIMCA analysis, $\text{RSD}_{\text{crit}}=0.19$, $p=0.05$

SIMCA results	Female	Male
RSD mean	0.15	0.74
N(number of spectra)	44	36
Distance between classes	----	2.7

The female class has RSD values (0.15) below the RSD_{crit} (0.19), while the male class has RSD values (0.74) well above the RSD_{crit} . The variation in the RSD values clearly indicates that female fibres are different from male fibres. The class distance

Table 5.9.

Fuzzy clustering membership values for a two-cluster model with a hard (1.50) and soft (2.50) weighting exponent value

SOURCE	W.E.=1.50		W.E.=2.50	
	1	2	1	2
M1	1.00	0.00	0.97	0.03
M2	1.00	0.00	0.91	0.09
M3	0.99	0.01	0.96	0.04
M4	1.00	0.00	0.94	0.06
M5	1.00	0.00	0.86	0.14
M6	0.99	0.01	0.99	0.01
M7	0.99	0.01	0.87	0.13
M8	0.98	0.02	0.84	0.16
M9	1.00	0.00	0.88	0.12
F1	0.03	0.97	0.10	0.90
F2	0.03	0.97	0.15	0.85
F3	0.02	0.98	0.11	0.89
F4	0.01	0.99	0.01	0.91
F5	0.02	0.98	0.08	0.92
F6	0.00	1.00	0.11	0.89
F7	0.17	0.83	0.18	0.82
F8	0.13	0.87	0.16	0.84
F9	0.17	0.83	0.09	0.91
U1	0.04	0.96	0.05	0.95
U2	0.12	0.88	0.03	0.97

for the male and female samples was found to be 2.7. This class distance as previously explained in section 5.5.3.2 suggests that eventhough the two sets of classes are different, there is also a certain degree of similarity between the hairs. Overall, the separation observed in SIMCA is consistent with the results obtained from the PCA study and supports the discrimination between the two sets of classes.

5.7.3.1.3. FC

FC was employed as a complementary evaluation to the discrimination of the spectra observed by PCA and SIMCA. A summary of the FC results for the 32 spectra are shown for a two-cluster model in Table 5.9, and on the whole, support the previous observations from the exploratory PCA and SIMCA. The membership criterion for a two-cluster model is 0.5. Thus, for a two cluster model, with a hard weighting exponent (1.50), spectra collected from female fibres indicate a strong membership for class 2, while spectra collected from male fibres have a high membership for class 1. When a softer weighting exponent (2.50) is chosen, similar patterns were obtained. A lack of fuzziness between the classes indicates that the membership between the classes is quite robust. The two unknown (U1 and U2) hair fibres have a high membership for class 2, which indicates that the unknown fibres have originated from female subjects.

The FC results established a clear separation of the hair samples on the basis of their origin, which supports the SIMCA results that showed a class distance of 2.7 between the samples. As discussed in the SIMCA results, this class distance indicates a difference between the hair samples from the male and female subjects but it also supports a certain degree of similarity. The FC results further strengthen the difference between the female and male hair samples and therefore support the SIMCA results.

Table 5.10

Curve-fit of single hair of major spectral band areas in the "fingerprint" region of the FT-IR spectra collected from different subjects

Subject	1040 cm ⁻¹ ν _s (S-O) cysteic acid	1077 cm ⁻¹ ν _s (S-O) cystine monoxide	1125 cm ⁻¹ ν _s (S-O) cystine dioxide	1170 cm ⁻¹ ν _s (S-O) cysteic acid	1239 cm ⁻¹ Amide III β-sheet	1481 cm ⁻¹ (CH ₂)(CH ₂)	1531 cm ⁻¹ Amide II β-sheet	1550 cm ⁻¹ Amide II α-helix	1650 cm ⁻¹ Amide I β-sheet	1673 cm ⁻¹ Amide I α-helix
Male 1	0.62	2.42	0.95	2.61	8.66	3.27	12.68	23.89	9.15	4.00
Male 2	0.55	2.29	0.94	2.34	8.37	2.79	12.62	22.94	9.04	4.11
Male 3	0.85	2.08	1.16	2.39	7.60	2.74	11.13	22.69	11.61	4.26
Male 4	0.76	2.53	1.09	2.82	8.78	3.34	12.69	23.04	8.80	3.81
Male 5	0.79	2.09	1.16	2.91	8.83	3.80	11.03	21.22	10.16	2.99
Male 6	0.68	2.21	1.31	2.52	8.52	2.69	13.87	22.16	7.74	2.50
Male 7	0.74	2.57	1.02	2.33	8.04	2.61	12.35	23.22	9.64	4.61
Male 8	0.69	2.22	0.98	2.23	8.23	2.77	12.24	22.45	9.87	4.32
Male 9	0.72	2.19	1.13	2.11	8.32	2.98	12.73	22.98	10.05	3.78
Female 1	0.92	2.76	1.20	2.85	8.39	2.66	13.03	23.83	9.37	3.41
Female 2	0.99	2.89	1.26	2.77	8.48	2.93	12.92	23.53	9.19	3.19
Female 3	0.68	2.53	1.16	2.59	8.56	3.28	12.26	22.48	8.71	3.07
Female 4	0.98	2.44	1.56	3.38	9.50	3.11	12.16	21.95	7.38	2.65
Female 5	0.86	2.63	1.31	3.27	9.54	3.94	10.99	20.79	8.16	3.28
Female 6	0.90	2.72	1.13	2.69	8.52	2.94	12.98	24.09	9.43	3.05
Female 7	0.92	2.89	1.36	2.93	8.94	3.33	12.11	22.43	8.53	3.17
Female 8	0.93	2.77	1.44	2.89	8.78	3.54	13.15	22.64	8.65	3.23
Female 9	0.91	2.82	1.36	3.12	8.68	2.89	12.69	23.42	8.98	3.45
Unknown 1	0.81	2.52	1.29	2.81	8.76	2.79	13.21	21.00	8.89	3.81
Unknown 2	0.91	2.39	1.46	3.05	8.68	3.71	11.53	22.35	8.77	2.92

5.7.3.1.4. Curve-fit Analysis Discussion of the FT-IR spectra

The spectral (or “fingerprint”) region between $1750\text{-}750\text{ cm}^{-1}$ was curve-fitted as described in chapter 2, section 2.6, in an attempt to provide an insight into the molecular basis for the discrimination observed by chemometrics. This region contains bands such as amide I, II, III, CH_2CH_3 deformations and cysteic acid vibrations. If there is any variation between hair fibres collected from different subjects then this variation is likely to be reflected in the “fingerprint” region of the FT-IR spectra. Jackson and Mantsch [25] suggested that out of the three amide vibrations, amide II is often excluded from studies, whilst amide I has been employed in more than 90% of all IR investigations of protein secondary structure.

Overall 10 bands (the major bands of interest in the FT-IR spectra of a hair fibre) were curve-fitted and the results are presented in table 5.10. The positions (wavenumbers) of the FT-IR spectral bands were selected according to values from the literature [13, 14]. Curve-fit of the relative intensity area of the cysteic acid band (1040 cm^{-1}) indicates that hair fibres collected from female subjects contain higher levels of cysteic acid (0.68-0.99) in comparison to the male hair fibres (0.55-0.85). The higher levels of cysteic acid reported in the female hair fibres is expected as the females subject their hair to more cosmetic treatments i.e., hair conditioners, hair care products, than males. In addition, intensity values for the vibrations relating to cysteic acid monoxide (1077 cm^{-1}), cysteic acid dioxide (1125 cm^{-1}) and $\nu_a(\text{S-O})$ (1170 cm^{-1}) are also higher for the female subjects compared to the male subjects. This agrees with previous results obtained from the loadings plot (PC2, figure 5.9), which demonstrated that one of the factors that influences the separation of the hair fibres on the basis of gender is the

presence of the cysteic acid vibrations in the case of the fibres collected from female subjects.

The frequencies of the amides are sensitive to peptide conformation and hydrogen bonding and can be used to characterise the secondary structure of the peptide backbone. Analysis of the relative intensity area of amide I (α -helix at 1673 cm^{-1} and β -sheet at 1650 cm^{-1}), amide II (α -helix at 1550 cm^{-1} and β -sheet at 1531 cm^{-1}) and amide III (1239 cm^{-1}) did not indicate any significant differences in the secondary structure of the FT-IR spectra collected from female and male subjects. In addition, the intensity of the band at 1451 cm^{-1} , which corresponds to the (CH_2) (CH_3) vibration, did not vary between male and female hair fibres. It therefore follows that apart from a variation in the intensity of the cysteic acid band, the rest of the bands do not indicate any further variation in the hair fibres.

In Hopkins et al [10], it was suggested that the intensity of amide I and II relates to the quantities and types of amino acids present in the hair fibres and possibly to the different relative ratios of these amino acids in different proteins. The authors proposed that variations in these bands could be due to genetic differences, varying nutritional status or to the physiological state of the individual. The authors employed the ratio of amide I/II in an attempt to investigate variations between the FT-IR spectra on the basis of variables such as gender, hair colour and race. Hopkins et al [9] justified the use of amide I and II bands on the basis of the high absorbance of the bands, ease of detection, and probable sensitivity to variation within changing composition. The study indicated that in spite of the expectations of differences in hair protein composition detectable by infrared spectroscopy, the spectra showed little or no difference in the amide I/II band ratio that could be correlated to gender, age, hair colour or chemical treatment. The amide I and II bands in the FT-IR spectra published in the

paper appeared highly saturated. This was a major point of concern and in order to ensure that the results obtained from Hopkins et al were not influenced by the saturation of the bands, the amide I/II ratio was calculated for the FT-IR spectra collected from the present work.

In the present study, calculation of the ratio of amide I/II showed that the ratio for the male fibres (0.11-0.20) overlapped with the ratio of the female hair fibres (0.11-0.18). The overlap in the range values suggests that amide I/II does not discriminate human hair fibres on the basis of gender. Therefore, the results presented in the current study are in agreement with the results obtained by Hopkins et al. who also found that the ratio of amide I/II does not show any significant difference between the spectra collected from different subjects. In their study, 39 males with untreated hair and 59 females with both untreated (22) and treated (37) hair were examined. The ratio of the amide I to amide II peaks was found to be in the range of 0.9-1.0 for all the samples tested. A comparison of the means failed to show any difference between the treated and untreated hair samples from females. Similar testing failed to show differences in the absorbance ratios of hair samples from males and females. A possible explanation for not being able to discriminate FT-IR spectra on the basis of the amide I/II ratio could be due to the fact that there is a correlation between the changes of the two bands and that this correlation is too high to highlight any difference between the fibres. It therefore becomes important to investigate the application of other bands that could differentiate the hair fibres on the basis of gender and race variables.

Previous work presented in chapter 3 has shown that by calculating the ratio of amide I(β -sheet)/(CH₂CH₃) an estimate of the beta-sheet composition present in a keratin

fibre could be obtained. In this study, the ratio was calculated in an attempt to establish any differences between the secondary structure of the keratin fibres from female and male subjects. In addition to the ratio of amide I(β -sheet)/(CH₂CH₃), the ratio of amide I(α -sheet)/(CH₂CH₃) was also calculated in order to obtain an estimate of the alpha-helical arrangement in the hair fibres.

The ratio of amide I (α -helix) to CH₂CH₃ did not show any significant difference between the FT-IR spectra collected from the male and female subjects. There was an overlap in the range obtained from the male hair fibres (2.63-4.24) and that obtained from the female hair (2.07-3.52). This indicates that hair fibres collected from subjects of both genders do not differ significantly on the basis of the alpha-helical structure.

Curve-fitting analysis of the FT-IR spectra collected from the various subjects indicated considerably higher levels of amide I (β -helix) to CH₂CH₃ did not show any significant difference between the FT-IR spectra collected from the male and female subjects. There was an overlap in the range obtained from the male hair fibres (0.78-1.77) and that obtained from the female hair (0.679-1.28). This indicates that hair fibres collected from subjects of both genders do not differ significantly on the basis of the β - structure.

It therefore appears that there is no variation in the secondary structure of the hair fibres on the basis of the gender variable.

5.7.3.2. The Race variable

Once the gender variable has been determined the next step is to build a second reference set, this time of hair fibres collected from subjects of same gender, in this case hair fibres were collected from females of different race origin. In this study, two sets, each of Asian and Caucasian single hair samples, were used to build a reference set (Table 5.11). The same two unknown hair fibres were used to determine the race. FT-IR spectra are shown in figure 5.10 and overall appear visually similar making it difficult to draw any conclusions about the origin of the spectra.

Table 5.11

Background information of the hair samples used to build the reference and validation set for Hypotheses (a) and (b)

Subject	Gender	Race	Treatment	Age	Hair Colour
C1	Female	Caucasian	No	15	Brown
C2	Female	Caucasian	No	15	Brown
C3	Female	Caucasian	No	14	Brown
M1	Female	Asian	No	33	Black
M2	Female	Asian	No	35	Black
M3	Female	Asian	No	15	Black
U1	Female	Caucasian	No	14	Black
U2	Female	Caucasian	No	25	Blonde

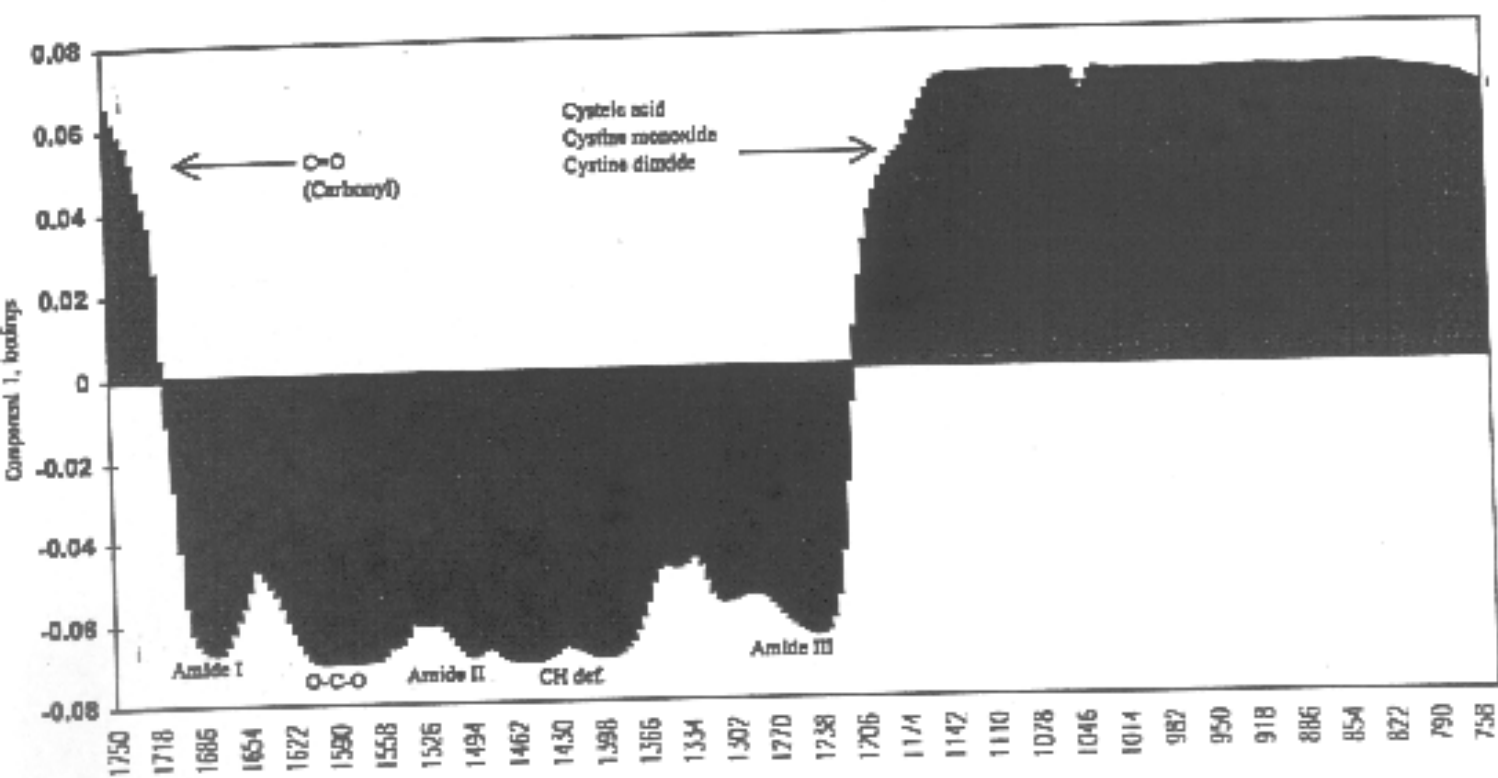


Figure 5.12. PC1 loadings plot (1750-750 cm^{-1}).

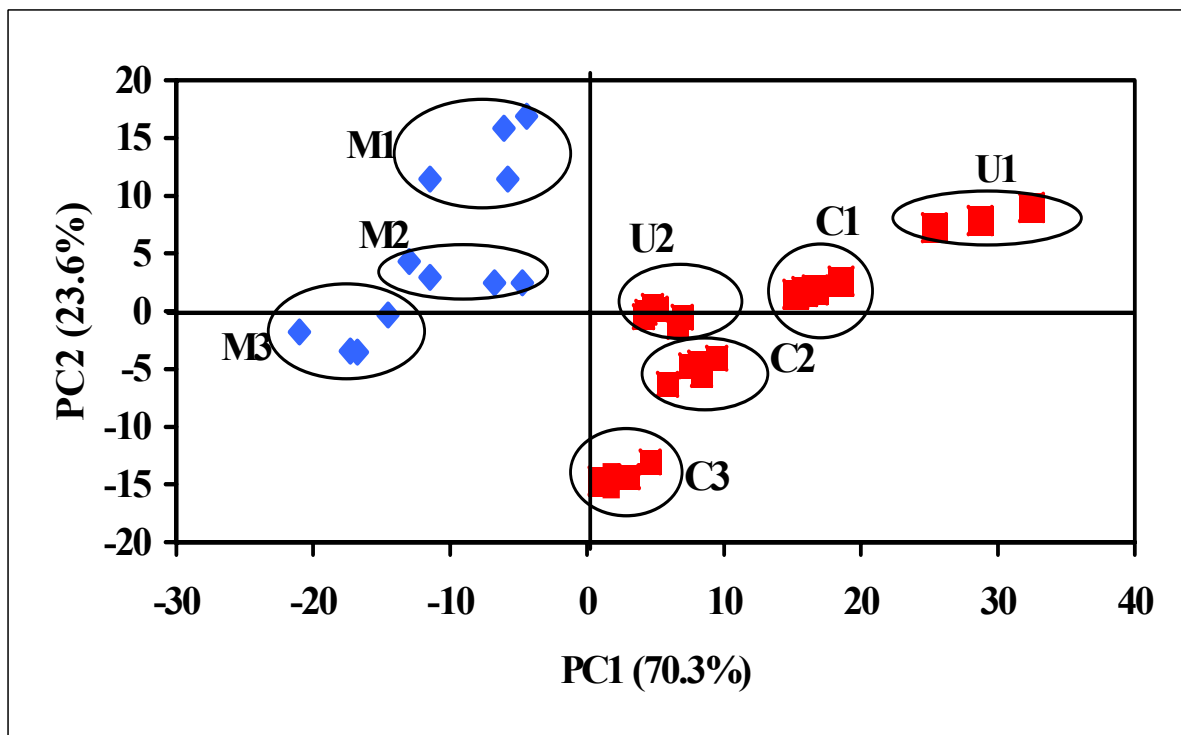


Figure 5.11. PC1 (70.3%) vs PC2 (23.6%) of the FT-IR spectra collected from Caucasian (C1-C3), Mongoloid (M1-M3) and unknown hair fibres (U1 and U2) ($1750\text{-}750\text{ cm}^{-1}$).

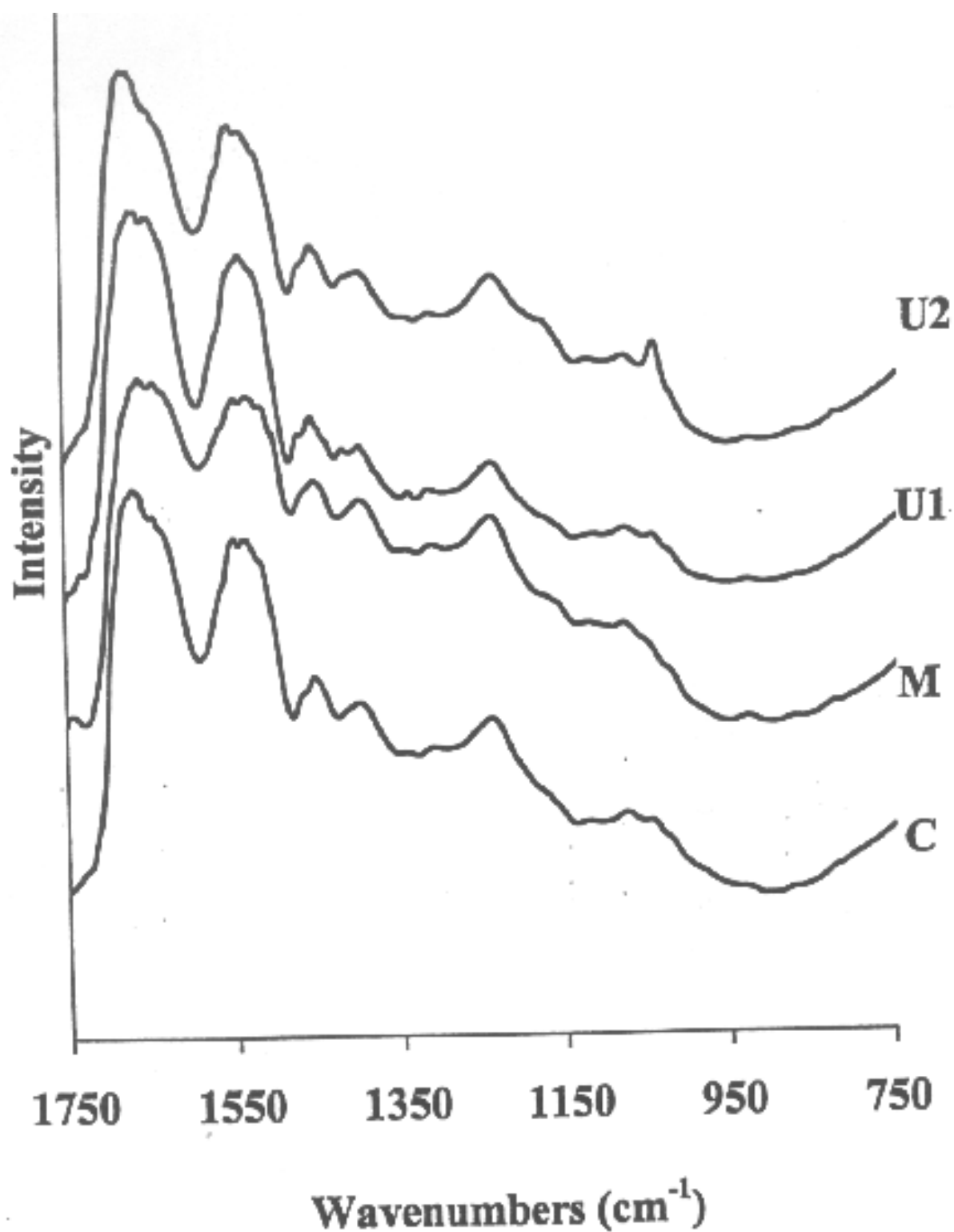


Figure 5.10. Examples of FT-IR spectra collected from Caucasian (C), Mongoloid (M) and unknown hair fibres (U1 and U2) (1750-750 cm⁻¹) in absorbance.

5.7.3.2.1. PCA

PCA was applied in an attempt to discriminate between FT-IR spectra collected from hair fibres that are dark and visually similar. The results of the exploratory PCA are presented in figure 5.11. Four PCs were sufficient to account for most of the variance (99.0%). The PC1 (70.3%) versus PC2 (23.6%) scores plot of the FT-IR spectra reveals eight clusters. PC1 discriminates the FT-IR spectra on the basis of the two different races. Mongoloid hair fibres (M1-M3) have negative scores on PC1, whereas the Caucasian hair fibres (C1-C3) have positive scores on the same PC. A plot of PC1 loadings against variable (Figure 5.12) indicates the underlying spectral features for the observed discrimination. FT-IR spectra collected from Mongoloid females are characterised by the bands at 1690 cm^{-1} (amide I), with minor contributions from $1614\text{-}1550\text{ cm}^{-1}$ (O-C-O), 1500 cm^{-1} (amide II), $1470\text{-}1390\text{ cm}^{-1}$ (C-H deformation), and $1310\text{-}1225\text{ cm}^{-1}$ (amide III). Caucasian females are characterised by bands at $1710\text{-}1742\text{ cm}^{-1}$ (C=O) and the frequency range containing the sulphur-oxygen bands possibly, indicating some type of oxidation. According to the hair history provided by the Caucasian subjects, the hair fibres had not undergone any chemical treatment, therefore the oxidation is thought to be a result of natural weathering of the fibre. All of the sampled subjects reported spending approximately the same amount of time in the sun. It has been reported in the literature that Mongoloid hair fibres contain more melanin pigment than Caucasian hair [26]. The higher contain of melanin in Mongoloid hair fibres suggests that the hair will be less susceptible to photo-oxidation in comparison to the less pigmented fibres from the Caucasian samples. It therefore follows that the higher levels of cysteic acid reported

in the FT-IR spectra collected from Caucasian hair fibres can be related to the melanin pigmentation of the fibre. In this case has therefore demonstrated that the PCA results support comments in the literature, that Caucasian hair are somewhat more susceptible to oxidation than Mongoloid hair.

The previous example established the gender variable of the unknown samples to be that of female subjects. The present hypothesis has shown both of the unknown hair fibres to group together with the Caucasian reference group, suggesting that the unknown hair could have most likely originated from Caucasian subjects.

5.7.3.2.2. SIMCA

The separation between the Caucasian and Mongoloid samples was further investigated on a semi-quantitative basis by the use of SIMCA (Table 5.12). The Caucasian spectra were used to construct a class model, because they contained the most number of objects (19). Four components were identified as significant with the use of cross-validation approach. The model accounted for 99.0% of the variance. The FT-IR spectra collected from the Mongoloid samples were then fitted to the model. The results indicate that the spectra from the Caucasian females hair have RSD value lower than the RSD_{crit} (0.2284). The distance between the classes (3.2) also indicates that there is a significant difference between the spectra from the Caucasian and Mongoloid hairs.

Table 5.12

SIMCA analysis results with $RSD_{crit}=0.2284$, $p=0.05$

SIMCA results	Caucasian	Mongoloid
RSD, mean	0.1627	4.434

n (number of spectra)	19	12
Distance between classes	----	3.2

5.7.3.2.3. FC

Fuzzy clustering was performed on the FT-IR spectra collected from Caucasian and Mongoloid subjects for both a hard (1.50) and soft (2.50) weighting exponent value for a two-cluster model (table 5.13).

Table 5.13

Fuzzy clustering membership values for a two-cluster model with a hard (1.50) and soft (2.50) weighting exponent value

SUBJECT	W.E.=1.50		W.E.=2.50	
	1	2	1	2
C1	1.00	0.00	0.91	0.09
C2	1.00	0.00	0.95	0.05
C3	1.00	0.00	0.92	0.08
M1	0.03	0.97	0.25	0.75
M2	0.02	0.98	0.17	0.83
M3	0.02	0.98	0.05	0.95
U1	0.96	0.04	0.72	0.28
U2	0.97	0.03	0.77	0.23

The results indicate that FT-IR spectra collected from Caucasian samples have high membership values for class 1, while FT-IR spectra from Mongoloid samples have high membership values for class 2. The unknown hair fibres (U1 and U2) have high

membership for class 1, which indicates that the fibres most likely belong to Caucasian female subjects. It is therefore proposed that FC analysis supports the PCA and SIMCA results that the FT-IR spectra collected from Caucasian female hair fibres are different from the FT-IR spectra collected from the Mongoloid female samples.

It was also observed that cysteic acid was significantly higher for the Caucasian hair (average 8.9) in comparison to those found in the hair fibres collected from Mongoloid subjects (average of 8.1). Light coloured hair fibres (as well as skin) have been found to be more susceptible to photo-oxidation than darker coloured fibres [25]. Clinical experiments have shown [26] that there is a higher incidence of skin cancer and increased photosensitivity in people with red and light skin compared to those with dark hair and skin. This is generally attributed to the lower amounts of melanin present in the skin of the former group and/or differences in the type of melanin in these individuals. It is widely accepted that light coloured hair has predominantly pheomelanin, in contrast to the eumelanin usually present in dark hair [26]. Eumelanin is chemically different from pheomelanin, the most obvious difference being the higher sulfur content of pheomelanin compared to eumelanin [25]. The higher levels of sulfur present in pheomelanin will therefore indicate that the melanin pigment will be more oxidised than eumelanin, which has lower sulfur content.

Therefore, the variation in the cysteic acid levels between hair fibres collected from the two different racial groups is expected given that Mongoloid hair fibres are more densely pigmented [27] and are therefore less susceptible to photo-oxidation compared to less pigmented fibres such as those collected from Caucasian subjects

which are more susceptible to photo-oxidation and thus will contain higher levels of cysteic acid.

5.8. Case D - Discrimination and matching of black and white (unpigmented) hair fibres from the same source and from different sources.

5.8.1. Introduction

Melanins are among the most frequently occurring pigments in nature [28]. They are responsible for tegumentary pigmentation in chordates, coloration of insect cuticles and the colour of hair. Hair cells, which form the hair shaft, do not produce melanin. Melanin is synthesised in melanosomes which are discrete organelles located within melanocytes. Cells that form the cortex and medulla contain melanosomes and melanin, whereas cuticular cells contain little or no melanin [29].

Colour is perhaps the most obvious characteristic of hair, but as far as we know it has no biological function in humans. It does not protect the hair from the harmful effects of sunlight (although hair itself protects the scalp, of course). As we have seen, the colour of hair is due to the presence in the cortex of granules of a pigment called melanin, which is formed in special pigment-producing cells (melanocytes) in the hair bulb during the growing phase (anagen) of each hair. The melanin granules lie along the amino acid chains of the proteins. Melanin is found in two forms. **Eumelanin** is the dark pigment, which predominates, in black and brunette hair. **Pheomelanin** is a lighter pigment, which is found in red and blond hair. Many people's hair contains a

mixture of the two: the more eumelanin there is in the mixture, the darker is the hair. The mixture (and the shade) varies not only from one person to another, but also across one person's head. The combination of pigments in the mixture is determined by the individual's genes. Differences between dark-haired people are due to differences in the overall quantities of melanins in their hair. Eumelanin granules are oval (elliptical) in shape, fairly uniform in their make-up and quite hard, with sharply defined edges. Pheomelanin granules are smaller, partly oval and partly rod-shaped. The range of colours produced by melanins is limited to shades of yellow, brown, red and black. Grey hairs contain only a few melanin granules, spread out through the hair. White hairs contain no melanin at all: their whiteness is an optical effect, due to the way they reflect the light. Surprisingly, however, unpigmented hairs look yellow (the 'color' of keratin) when they first grow, and only later turn white.

Bilinska et al [30] has illustrated that melanins show characteristic IR bands at 1540, 1650, and 3300 cm^{-1} . However, the two bands at 1540 and 1650 cm^{-1} interfere with the protein bands and it makes the identification of the melanin bands very difficult. Therefore, in this work the two regions; 1750-750 cm^{-1} and 3100-2800 cm^{-1} will be examined separately.

Table 5.14

A summary of the structural components of the melanins indicated by the infrared spectra.

Band frequency (cm^{-1})	Structural components
3600-3100	Due to water, phenols or amines aromatics
~2950 and ~2850	Stretching of methyl and methylene
2700-2600	NH+

1740-1720	CO, COOH, COO ⁻ , and also possible 5 membered ketone ring
1680	α - β unsaturated ketone
1620	Pyrone ring, γ -thiopyrone indole ring, quinone
1460	Bending of active methylene group (-CH ₂ CO) or CH ₂ adjacent to the electrons attracting N ⁺ or cyclopentane/cyclohexane ring
1438 and 1380	Methyl and methylene bending
1580 and 1450	Phenyl skeletal and methyl asymmetric bending

The three stages of hair growth as discussed in chapter 1, section 1.3, include the early anagen stage (which in terms of melanin pigmentation involves the period of melanocyte proliferation), followed by catagen (maturation of the hair follicle) and telogen (melanocyte death via apoptosis) [31]. It has been proposed [31] that on the basis of the three stages of hair growth, each hair cycle is associated with the reconstruction of an intact hair follicle pigmentary unit, at least for the first 10 cycles. Thereafter, gray and white hair appears, suggesting age-related, genetically regulated exhaustion of the pigmentary potential of each individual hair follicle. In this study, an attempt will be made to match white and black hair fibres from the single subject and to discriminate those of different subjects. The hypothesis to be tested in this study is that if white hair fibres have the same molecular structure as black hair fibres (with the only difference being the colour change) then white hair fibres can be matched with the black hair fibres collected from the same subject.

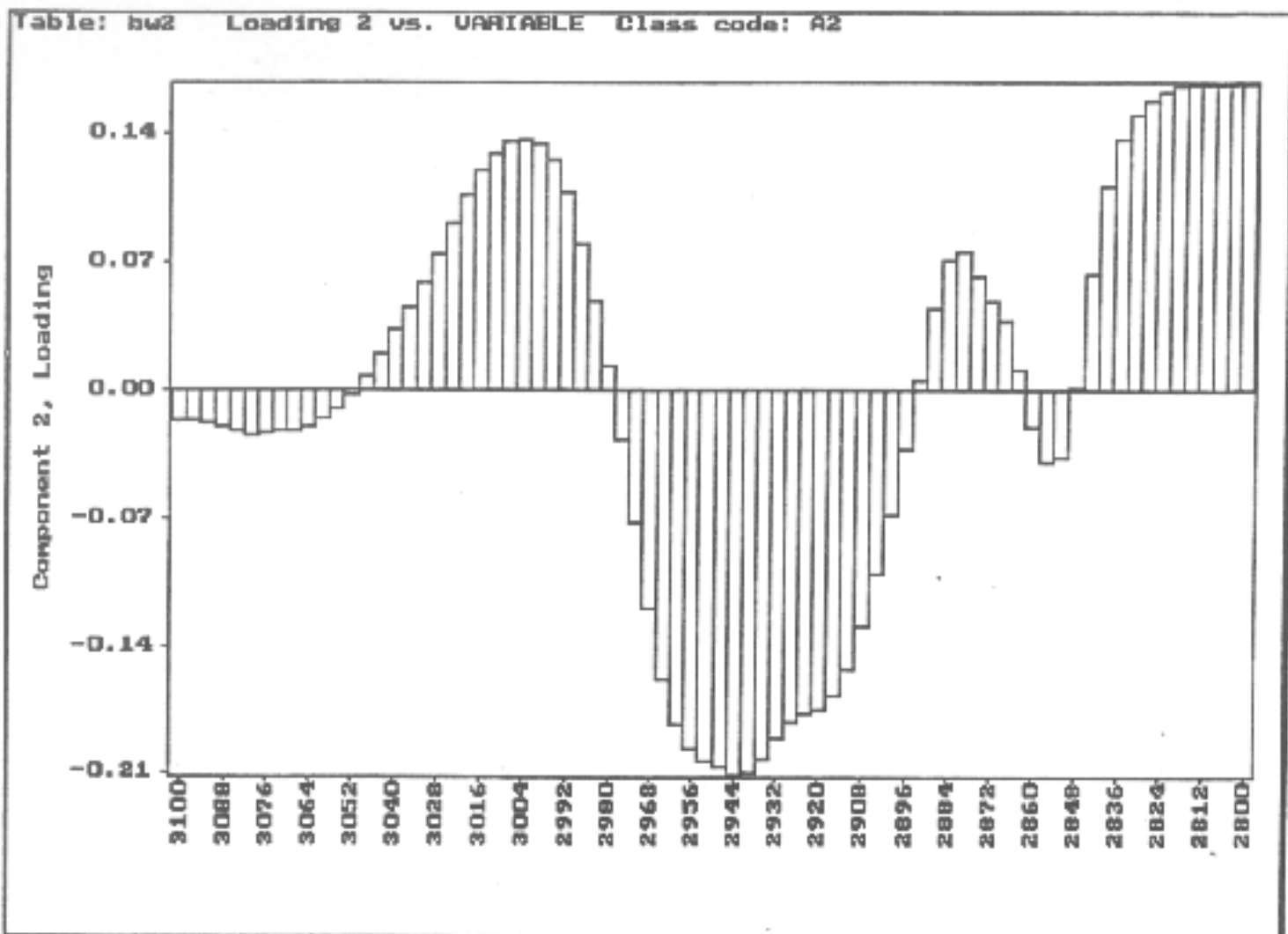


Figure 5.15. PC2 loadings plot (3100-2800 cm⁻¹).

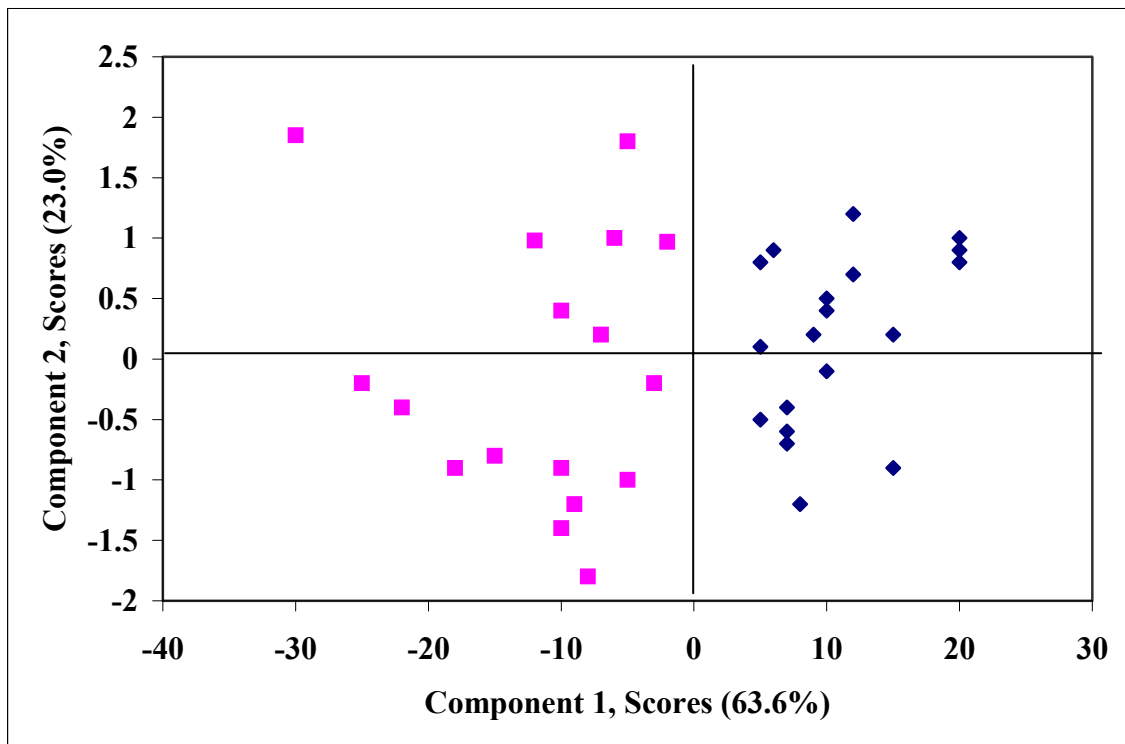


Figure 5.14. PC1 (63.6%) vs PC2 (23.0%) scores plot of the FT-IR spectra collected from black and white hair fibres from two different subjects (both subjects were Caucasian males in their early 60's) ($3100\text{-}2800\text{ cm}^{-1}$).

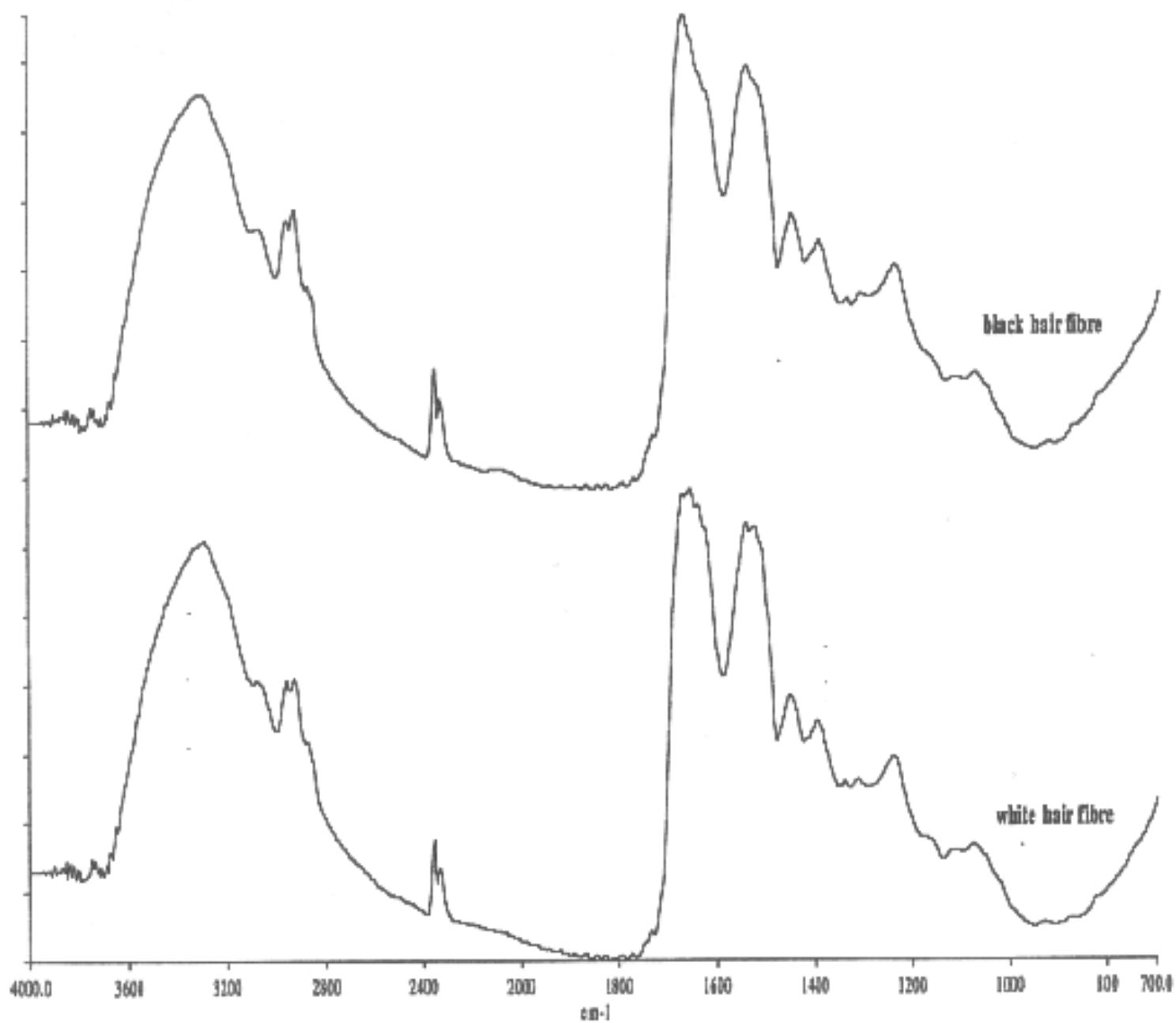


Figure 5.13. Examples of FT-IR spectra collected from black and white hair fibres.

5.8.2. Discussion of results

Black and white hair fibres were collected from eight different subjects. FT-IR spectra were collected over the 4000-400 cm^{-1} spectral region. Out of this region, two different spectral regions were investigated;

- (a) 3100-2800 cm^{-1} , and
- (b) 1750-750 cm^{-1} .

The first region contains mainly the melanin pigment, whilst the second region contains a mixture of protein and melanin. Both spectral regions were double centred and standardised.

5.8.2.1. PCA

Examples of FT-IR spectra collected from black and white hair fibres are shown in figure 5.13. The spectra region between 3100-2800 cm^{-1} was initially investigated and a simple PCA example of the matching and discrimination of black and white hair

fibres from two different subjects is presented in figure 5.14. Five components were identified as significant with the use of the cross-validation approach with 98.9% accounted for the total variation. The PC1 (63.6%) vs PC2 (23.0%) (figure 5.14) shows a discrimination along PC1 between the black and white hair fibres collected from subject 25 (positive scores), from the black and white hair fibres collected from subject 24 (negative scores) on the same PC. The PC1 loadings plot is presented in figure 5.15. The PC1 loadings plot indicates that stretching of methyl and methylene residues at approximately 2950 cm^{-1} and 2850 cm^{-1} is responsible for the separation of hair fibres from the different subjects.

5.8.2.2. SIMCA

The separation between the unpigmented and pigmented hair fibres collected from the two separate was further investigated on a semi-quantitative basis by the use of SIMCA (Table 5.15). The spectra collected from subject 1 were used to construct a class model, because they contained the most number of objects (19). Five components were identified as significant with the use of cross-validation approach. The model accounted for 98.9% of the variance. The FT-IR spectra collected from subject 2 were then fitted to the model. The results indicate that the spectra from subject 1 have RSD value lower than the RSD_{crit} (0.2284). The distance between the classes (3.8) also indicates that there is a significant difference between the spectra from subject 1 and 2.

Table 5.15

SIMCA analysis results with $RSD_{crit}=0.1684$, $p=0.05$

SIMCA results	Subject 1	Subject 2
RSD, mean	0.1135	2.896
n (number of spectra)	19	12
Distance between classes	----	3.8

5.8.2.3. FC

In order to further investigate the PCA and SIMCA results, a complementary evaluation was applied by the use of fuzzy clustering analysis. A summary of the FC results for the double-centred data matrix of the 20 spectra are shown for a two-cluster model in table 5.16, and on the whole, support the previous observations from the exploratory PCA and SIMCA. Thus, for a two cluster model, where values of approximately close to 0.5 indicate roughly equal membership, with a hard weighting exponent (1.50), spectra from FT-IR spectra collected from black and white hair fibres belonging to subject 24 indicate a strong membership for class 1, while spectra collected from black and white fibres collected from subject 25 have a high membership for class 1. When a softer weighting exponent (2.50) is chosen, similar patterns were obtained.

Table 5.16

Fuzzy clustering membership values for a two-cluster model with a hard (1.50) and soft (2.50) weighting exponent value

Subject	Class 1	Class 2	Class 1	Class 2
	(W.E.=1.50)	(W.E.=1.50)	(W.E.=2.50)	(W.E.=2.50)
24W1	0.01	0.99	0.18	0.82
24B1	0.00	1.00	0.24	0.76
25W1	1.00	0.00	0.78	0.22
25B2	0.98	0.02	0.69	0.31

Table 5.18.

Fuzzy clustering membership values for an eight-cluster model with a soft (2.50) weighting exponent value in the 1750-750 cm⁻¹ spectral region.

	Class 1	Class 2	Class 3	Class 4	Class 5	Class 6	Class 7	Class 8
1B	0.10	0.02	0.00	0.46	0.00	0.04	0.20	0.18
1W	0.22	0.20	0.00	0.11	0.00	0.00	0.34	0.13
2B	0.05	0.18	0.31	0.02	0.06	0.15	0.06	0.19
2W	0.09	0.00	0.15	0.10	0.38	0.00	0.08	0.20
3B	0.20	0.25	0.00	0.26	0.00	0.15	0.00	0.14
3W	0.12	0.00	0.00	0.27	0.01	0.28	0.03	0.33
4B	0.02	0.22	0.12	0.04	0.41	0.00	0.23	0.01
4W	0.00	0.05	0.22	0.34	0.00	0.00	0.26	0.13
5B	0.23	0.17	0.33	0.03	0.00	0.24	0.00	0.00
5W	0.12	0.16	0.14	0.00	0.28	0.12	0.00	0.18
6B	0.10	0.00	0.17	0.11	0.14	0.34	0.14	0.00
6W	0.15	0.32	0.12	0.00	0.13	0.02	0.20	0.00
7B	0.17	0.10	0.14	0.23	0.00	0.14	0.22	0.00
7W	0.00	0.13	0.20	0.20	0.00	0.32	0.00	0.20
8B	0.01	0.14	0.22	0.01	0.11	0.10	0.13	0.30
8W	0.10	0.00	0.03	0.30	0.33	0.00	0.24	0.00

Table 5.17.

Fuzzy clustering membership values for an eight-cluster model with a soft (2.50) weighting exponent value in the 3100-2800 cm⁻¹ spectral region.

	Class 1	Class 2	Class 3	Class 4	Class 5	Class 6	Class 7	Class 8
1B	0.00	0.01	0.00	0.96	0.00	0.03	0.00	0.00
1W	0.00	0.01	0.00	0.87	0.03	0.00	0.04	0.03
2B	0.95	0.02	0.00	0.02	0.01	0.00	0.00	0.00
2W	0.92	0.00	0.00	0.00	0.02	0.00	0.01	0.00
3B	0.00	0.00	0.91	0.00	0.04	0.00	0.03	0.02
3W	0.00	0.00	0.82	0.07	0.01	0.03	0.03	0.03
4B	0.00	0.01	0.00	0.04	0.92	0.00	0.02	0.01
4W	0.00	0.00	0.00	0.00	0.97	0.00	0.00	0.03
5B	0.00	0.01	0.03	0.02	0.00	0.04	0.00	0.91
5W	0.02	0.03	0.04	0.01	0.00	0.02	0.00	0.88
6B	0.00	0.89	0.00	0.01	0.04	0.04	0.02	0.00
6W	0.00	0.93	0.02	0.00	0.03	0.02	0.00	0.00
7B	0.00	0.01	0.00	0.03	0.00	0.94	0.02	0.00
7W	0.00	0.03	0.05	0.03	0.00	0.87	0.00	0.02
8B	0.01	0.00	0.02	0.01	0.01	0.00	0.95	0.03
8W	0.00	0.00	0.01	0.02	0.03	0.00	0.94	0.00

5.8.2.4. FC

Fuzzy clustering was also applied to larger sample of black and white hair fibres collected from different subjects. The two different spectral areas $3100\text{-}2800\text{ cm}^{-1}$ and $1750\text{-}750\text{ cm}^{-1}$ were investigated in order to demonstrate the capability of each region to differentiate black and white hair fibres from each source. The $1750\text{-}750\text{ cm}^{-1}$ (Table 5.17) did not show any specific grouping of the spectra, whilst the $3100\text{-}2800\text{ cm}^{-1}$ (Table 5.18) spectral region provided a 100% success rate for the matching and discrimination of black and white hair fibres between different sources. For both the spectral region, the FC results for an eight-cluster model used a soft (2.50) weighting component. Similar results were obtained for a hard (1.50) weighting component.

This is expected as the melanin is affected by the protein bands in the 1750 to 750 cm^{-1} spectral region, while the $3100\text{-}2700\text{ cm}^{-1}$ region is not affected by proteins conformations and thus is considered a more reliable region for melanin studies. It therefore follows that the matching and discriminating of black and white hair fibres needs to be investigated in the $3100\text{-}2700\text{ cm}^{-1}$ so as to minimise the affect of the protein bands in the hair fibres.

5.9. Chapter conclusions

The research presented in this chapter has provided an alternative approach to the characterisation of single scalp human hair fibres, which is rapid, easy to operate and provides objective results that can be readily produced and explained in the courts of law. The rapid detection and analysis of results has not previously been possible with the lengthy and quite laborious microscopic comparison techniques and DNA analysis. Although the proposed technique is not aimed at displacing the two existing methods of hair analysis, it has given a new dimension to the characterisation of hair fibres on a molecular level, providing a powerful tool for forensic investigations and the analysis of the complex hair fibres. Interpretations of each technique should be presented separately, with a statement that the results of the three methods substantiate each other, leading to an overall increase of the evidential value and therefore providing more convincing evidence in the courts of law.

The research has shown that it is possible to model and predict properties on the molecular level through the use of FT-IR and chemometrics methods of analysis. Blind samples were successfully applied both to validate available experimental data and extend the current database of experimental determinations.

In the first two cases (case A and case B), the discrimination of hair fibres of similar characteristics was made possible through the use of PCA, SIMCA and FC. Furthermore, unknown hair fibres can be readily matched to their corresponding 'control' hair through PCA and FC. An important aspect of this work, illustrated as case B, is that the treatment variable does not have an effect on the discrimination

capabilities of chemometrics when comparisons are made between similarly treated hair fibres of different subjects.

The research has proposed that in cases where ‘control’ hair fibres are not readily available or in cases where the unknown fibres cannot be matched to either hair from the victim or suspect(s), it is then possible, through FT-IR micro-spectroscopy and chemometrics to establish the characteristics of a hair fibre and to narrow it down to variables such as treatment, gender and race.

FT-IR spectra obtained from black and white (unpigmented) hair fibres collected from the same source could be matched by chemometrics methods of analysis. Two different spectral regions were investigated; 3100-2800 cm^{-1} , and 1750-750 cm^{-1} . The latter region is mainly dominated by the amide and CH_2CH_3 vibrations, and it was not possible to match black and white fibres from the same source using this region. The spectral region between 3100-2800 cm^{-1} was proven to be more successful and it was possible to match black and white hair fibres from the same source and discriminate those of different sources.

CHAPTER 5 – References

1. Kirk, P. L. and Thornton, J. I. *Crime Investigation*. Wiley, New York, p. 143, 1994.
2. Robbins, C. R., and Kelly, C. H., Amino Acid Composition of Human Hair, *Textile Research Journal*, pp. 891-896, (1970).
3. Marshall, R.C., and Gillespie, J.M., Variations in the Protein of Wool and Hair, in “The biology of wool and hair”, edited by Rogers, G.E., Reis, P.J., Ward, K.A., and Marshall, R.C., Chapman and Hall, London, 117-125, (1989).
4. Cone, E. J., and Joseph, R. E., Jr., The potential for drug bias in hair testing for drugs of abuse, Chapter 3, in **Drug Testing in Hair**, edited by Kintz, P., CRC Press, U.S.A., (1996).
5. Houck, M. H., and Budowle, B., Correlation of Microscopic and Mitochondrial DNA Hair Comparisons, *J Forensic Sci*, **47**, pp. 964-967, (2001).
6. Ryland, S., Bishea, G., Brun-Conti, L., Eyring, M., Flanagan, B., Jergovich, T., MacDougall, D., and Suzuki, E., “Discrimination of 1990s Original Automotive Paint Systems: A Collaborative Study of Black Nonmetallic Base Coat/Clear Coat Finished Using Infrared Spectroscopy”, *J Forensic Sci*, **46**, pp. 31-45, (2001).
7. Wang, J., Luo, G., Sun, S., Wang, Z., and Wang, Y., “Systematic Analysis of Bulk Blue Ballpoint Pen Ink by FTIR Spectrometry”, *J Forensic Sci*, **46**, pp. 1093-1097, (2001).
8. Mizrachi, N., Aizenshtat, Z., Levy, S., and Elkayam, R., “Classification and Identification of Color Photocopiers by FT-IR and GC/MS”, *J Forensic Sci*, **43**, pp. 353-361, (1998).

9. Hopkins, J., Brenner, L., and Tumosa, C. S., Variation of the Amide I and Amide II Peak Absorbance Ratio in Human Hair as Measured by Fourier Transform Infrared Spectroscopy, *Forensic Science International*, **50**, pp. 61-65, (1991).
10. Broad, J., Science and Criminal Detection, MacMillan Education Ltd, London, (1988).
11. <http://www.aic.org.au>
12. Fienberg, S, **The Evolving Role of Statistical Assessments as Evidence in the Courts**, Springer-Verlag, New York, 1989.
13. Brenner, L., Squires, P.L., Garry, M., and Tumosa, C.S., A Measurement of Human Hair Oxidation by Fourier Transform Infrared Spectroscopy, *Journal of Forensic Sciences*, **13**, pp. 420-426, (1985).
14. Lewis, D. M., and Signori, V., FTIR investigation of the damage produced on human hair by weathering and bleaching processes: implementation of different sampling techniques and data processing, *J. Cosmet. Science*, **19**, pp. 1-13, (1997).
15. Gilbert, C., and Kokot, S., Discrimination of Cellulosic Fabrics by Diffuse Reflectance Infrared Fourier Transform Spectroscopy and Chemometrics, *Vibrational Spectroscopy*, **9**, pp. 161-167, (1995).
16. Gilbert, S., Kokot, S., and Meyer, U., Application of DRIFT Spectroscopy and Chemometrics for the comparison of Cotton Fabrics, *Appl. Spectr.*, **47**, pp. 741-747, (1993).
17. Aitken, C. G. C., "Populations and Samples", in **The Use of Statistics in Forensic Science**, edited by Aitken, C.G.C., and Stoney, D.A., pp. 51-82, Ellis Horwood, England.
18. Gaudette, B. D., and Keeping, E. S., An Attempt at Determining Probabilities in Human Scalp Hair Comparison, *J. Forensic Sc.*, **19**, pp. 599, (1974).

19. Barnett, P. D., and Ogle, R. R., Probabilities and Human Hair Comparison, *J. Forensic Sci.*, **29**, pp. 272, (1982).
20. Stafford Smith C. A., and Goodman P. D., Forensic Hair Comparison Analysis: Nineteenth Century Science or Twentieth Century Snake Oil?, *Columbia Human Rights Law Review*, **27**, pp. 227-291, (1996).
21. <http://www.ourbrisbane.com/brisbane/brisinbrief/population.htm>
22. <http://www.population.org.au>
23. Swift, J. A., and Brown, A. C., Scanning Electron Microscope Observations of Human Hair Weathering in “The first human hair symposium”, edited by Brown, A. C., Medcom Press, U.S.A., p. 332-345, (1974).
24. Panayiotou, H., **Vibrational Spectroscopy of Human Hair Keratin Fibres**, Master’s thesis, Queensland University of Technology, 1998.
25. Jackson, M., and Mantsch, H. H., The use and misuse of FT-IR of FTIR Spectroscopy in the determination of Protein Structure, *Crit. Rev. Biochem. Mol. Biol.*, **30**, pp. 95-120, (1995).
26. Aravindakshan Menon, I., Persad, S., Haberman, H., and Kurian, C., A Comparative Study of the Physical and Chemical Properties of Melanins Isolated from Human Black and Red Hair, *The Journal of Investigative Dermatology*, **80**, pp. 202-206, (1983).
27. Prota, G., Thompson, R.H., Melanin Pigmentation in mammals, *Endeavour*, **35**, pp. 32-38, (1976).
28. Fitzpatrick, T.B., Brunet, P., and Kukita, A., The nature of hair pigment, in **The Biology of Hair Growth**, edited by Montagna, W and Ellis, R.A., Academic Press, New York, pp.255, (1958).

29. Ortonne, J.P. and Prota, G., Hair melanins and hair colour: ultrastructural and biochemical aspects, *J. Invest. Dermatol.*, 101, pp. 825, (1993).
30. Bilinska, B., Progress of Infrared Investigation of Melanin Structures, *Spectrochimica Acta Part A* 52, pp.1157-1162, (1996).
31. Tobin, D. J., and Paus, R., Graying: Gerontobiology of the Hair Follicle Pigmentary Unit, *Experimental Gerontology*, **36**, pp. 29-54, (2001).
32. Robbins, C. R., **Chemical and Physical Behaviour of Human Hair**, Springer-Verlag, New York, (1994).

6

CONCLUSIONS AND FUTURE WORK

The overall aim of this thesis was to investigate the potential of some vibrational spectroscopy techniques for matching and discrimination of single keratin hair fibres in the context of forensic evidence.

Spectral comparison of fibres was facilitated with the use of chemometrics methods such as PCA, SIMCA, fuzzy clustering, and the less common approach of multi-criteria decision making methodology (MCDM).

The primary objectives of the present study as set out in chapter 1, section 1.1.2, were successfully achieved as follows:

Objective 1: To investigate the forensic application of FT-IR and Raman micro-spectroscopy and some common methods of multivariate methods of analysis such as chemometrics for the investigation of the molecular structure of untreated and chemically treated hair fibres.

Curve-fitting of the relative intensity areas of the major bands in the FT-IR and Raman spectra collected from untreated and treated (bleached) hair fibres established that bleaching of hair fibres is a complex process which results in a range of chemical reactions involving not only the pigment it is intended to lighten, but also the keratin fibre itself. The study showed that the secondary structure of the hair fibre is greatly

affected by bleaching with the α -helix (amide I) undergoing a significant decrease in intensity with increase in treatment time. Furthermore, an increase in the intensity of the random coil (amide I) was also noted and this was proposed to be due to the α -helix being “lost” during chemical oxidation and being converted to the random-coil structure. The beta-sheet (amide I) was found to remain unaffected by treatment. Investigation of the cysteine band indicated a steady decrease of the band during chemical treatment. This decrease was accompanied by an increase in the intensity of the cysteic acid residues, which are characteristic by-products of chemical treatment. Aromatic hydrocarbon groups and in particular tyrosine, phenylalanine and tryptophan were also investigated and it was shown that all of these amino acids are hydrogen acceptors. Chemical treatment of the hair fibres indicated that oxidation agents affect only tyrosine, which decreases with increase in treatment time. One of the basic amino acids, histidine, was also examined and it was established that the acid is present in the 3-N-protonated form and it is not affected by chemical treatment.

Chemometrics methods of analysis showed a discrimination of untreated hair from treated hair fibers and similar results were obtained for both the FT-IR and Raman spectral data. The loadings plots indicated that the separation between the untreated and treated hair fibres is a result of the formation of cysteic acid residues due to the chemical oxidation of the hair fibre. Furthermore, the work presented in this chapter established that bleaching of hair fibres is a complex process because it calls on a range of chemical reactions involving not only the pigment it is intended to lighten, but also the keratin fibre itself.

Conclusions for objective 1

This work demonstrates that with the aid of chemometrics, it is possible to investigate simultaneously FT-IR and Raman micro-spectroscopic information from oxidised hair fibres collected from one subject and treated at different times. The discrimination and matching of hair fibres on the basis of treatment has potential forensic applications.

Objective 2: To examine the limitations of Raman micro-spectroscopy for the analysis of single human hair directed towards forensic applications.

Despite its potential for reducing problems associated with water absorptions in the IR, Raman spectroscopy has until this time found only limited applications to pigmented hair and other natural pigmented fibres, because of background fluorescence, sample degradation in high-intensity, short-wavelength radiation and long scan times associated with the weakly scattering keratin species. A comparison between the 780 nm and 633 nm lasers for the Raman experiments indicated no major reduction in fluorescence when the higher laser power was used. Taking into consideration the sensitivity factor between the two lasers it was proposed that the suitable laser wavelength to obtain a Raman spectrum of a white hair fibre is 633 nm. The quality of the Raman spectra collected from human hair fibres was to a large extent pigment dependent. White (non-pigmented hair) proving the only type of hair able to be analysed through Raman micro-spectroscopy. In addition, the approximate collection time of Raman spectra is 25 minutes (including burning out of fluorescence), compared to the faster collections times associated with FT-IR spectra (approximately 2 minutes and 20 seconds per spectra).

Conclusions for objective 2.

From a theoretical viewpoint, Raman spectroscopy offers valuable information about the nature and distribution of compounds within the hair fibre. However, from a forensic aspect, Raman spectroscopy is not applicable to all the hair and thus is very limited in its application to real-life cases. FT-IR micro-spectroscopy, on the other hand, offers the rapid collection of spectra from a wide range of hair fibres.

Objective 3: To examine the limitations of the FT-IR micro-spectroscopy technique for the discrimination of single scalp human hair fibres and to predict some characteristics of blind samples in an effort to understand the limits of FT-IR micro-spectroscopy for application in forensic science.

The research presented in this objective highlighted the possible forensic application of FT-IR micro-spectroscopy to the analysis of single scalp human hair fibres. The study established through essential experiments that even though FT-IR spectra of single human scalp hair fibres collected from different subjects visually appear the same, once the spectra are submitted to chemometrics methods of analyses such as PCA, SIMCA and FC, they are significantly different. In particular, chemometrics analysis has demonstrated discrimination of FT-IR spectra collected from hair fibres from different subjects and matching of FT-IR spectra collected from hair fibres from the same subject. This discrimination was based on the treatment, gender and race variables.

The FT-IR spectra collected from hair fibres belonging to male and female subjects were analysed through the use of curve-fit methods in an attempt to investigate the secondary structure of the fibres and to account for any differences between the fibres on the basis of gender. The results indicated female hair fibres were found to contain higher concentrations of cysteic acid than male hair. This is attributed to the fact that females subject their hair to more hair grooming such as hair sprays, conditioners etc, than males.

Curve-fit analysis was also applied to the FT-IR spectra collected from Caucasian and Mongoloid female subjects. The results suggested that Caucasian hair contain higher

levels of cysteic acid than Mongoloid hair. This is in accordance with comments in the literature, which suggest that dark coloured hair fibres are densely pigmented and are less susceptible to photo-oxidation than less pigmented light coloured fibres. Mongoloid fibres are darker than Caucasian fibres and are therefore more densely pigmented. The lower levels of cysteic acid reported in this study for the Mongoloid hair is expected, as the hair fibres are less likely to suffer from photo-oxidation. On the other hand, photo-oxidation is more likely to affect the Caucasian fibres as they are less pigmented, and therefore higher levels of cysteic acid are observed.

In total 75 blind samples were used in this study as a validation measure and the results indicated a 100% success rate on treatment, 80% on gender and 88.5% on race. The false negative results (for the gender and race variables) were obtained when subjects who are taking long-term medication were used as blind samples. This limitation of the technique highlights the importance of future work to involve such types of hair fibres so as to investigate the underlying chemical reasons for the false negative results.

Conclusions for objective 3.

This is the first time that a substantial, systematic FT-IR study of forensic hair identification has been presented. The research has shown that it is possible to model and correlate individual's characteristics with hair properties at molecular level with the use of chemometrics methods. A number of different, important forensic variables of immediate use to police in a crime scene investigation such as gender, race, treatment, black and white hair fibres were investigated. Blind samples were successfully applied both to validate available

experimental data and extend the current database of experimental determinations. Protocols were posed for the application of this methodology in the future.

Objective 4: To investigate the validity of the proposed methodology with some more complex forensic applications which include the matching and discrimination of black and white hair fibres from the same source and from different sources, the matching and discrimination of untreated and treated hair fibres from the same source and from different sources.

Chemometrics methods of analyses discriminated and matched FT-IR spectra obtained from black and white (non-pigmented) hair fibres collected from different subjects. Two different spectral regions were investigated; 3100-2800 cm^{-1} , and 1750-750 cm^{-1} . The latter region was found to be influenced by mainly the amide and CH_2CH_3 vibrations, which made the investigation of black and white hair fibres difficult. The spectral region between 3100-2800 cm^{-1} was proven more successful and it was possible using this region, to match black and white hair fibres from the same source and discriminate those of different sources.

Untreated hair fibres obtained from two different subjects can be readily discriminated from each subject by the use of chemometrics methods of analyses. Similarly, treated hair fibres obtained from two different subjects could also be discriminated from each other through the use of chemometrics.

Conclusions for objective 4.

The technique successfully demonstrated the matching of black and white hair fibres from the same source and the discrimination of black and white hair fibres from different sources. This is the first time FT-IR and chemometrics methods of analysis have been simultaneously used to investigate the matching and discrimination of black and white hair fibres. More importantly, the work has

shown that when two similarly chemically treated hair fibres are found at the crime scene, the FT-IR spectra of these fibres can be readily discriminated from each other by the use of chemometrics methods of analysis.

Objective 5: To extend the forensic application of the FT-IR micro-spectroscopy to other types of keratin fibres.

This objective established that FT-IR micro-spectroscopy allows the rapid collection of spectra from different keratotic specimens. The molecular assignments highlighted the bands sensitive to skeletal backbone configuration, and identified spectral regions of characteristic spatial conformation. Examination of the amide bands provided secondary structural information and disclosed the difference in the biogenesis of animal, human and feather keratin.

This study proposed that feather keratin is predominantly made-up of a β -sheet structure, while mammalian keratins favour an α -helical arrangement. Using the ratio of amide I (α -helix) to CH_2CH_3 it was possible to determine the characteristic α -helical composition of keratin fibres. In addition, the ratio of amide I (β -helix) to CH_2CH_3 was calculated to estimate the beta-sheet content. The results clearly indicate the preference of the feather keratin for a beta-sheet structure with less contribution from the alpha helix. Furthermore, it was also established that feather keratin contains very high levels of cysteic acid. The study in objective 1 established that disruption of the cystine amino acid leads to the formation of cysteic acid residues as well as to the disruption of the secondary structure of the fibre in particular the alpha-helix. The feather keratin study further supported these results and proposed that a fibre high in cysteic acid is characterised by low levels of alpha helix.

Chemometrics methods of analyses such as PCA, SIMCA and FC supported the curve-fit results and discriminated the keratin fibres on the basis of their secondary

structure. In particular chemometrics showed a discrimination between the fibres composed of beta-sheet from those predominantly made-up of an α -helix.

PROMETHEE and GAIA have successfully demonstrated the simultaneous analysis of FT-IR spectral information and literature values for the ranking of α - and β - keratin fibres. PROMETHEE and GAIA further supported the theory that feather fibres are characterised by a high levels of amide I (β /CH₂CH₃) and cysteic acid in comparison to the rest of the fibres.

Conclusions for objective 5.

The work presented here is the first detailed FT-IR micro-spectroscopic study, utilising chemometrics as well as MCDM methods, for a wide range of keratin fibres, which are commonly, found as forensic evidence. Furthermore, it was demonstrated with the aid of the rank ordering MCDM methods PROMETHEE and GAIA, that it is possible to rank and discriminate keratin fibres according to their molecular characteristics obtained from direct measurements together with information sourced from the literature.

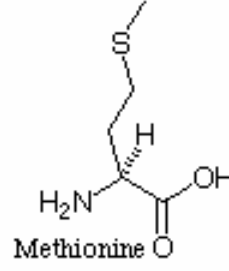
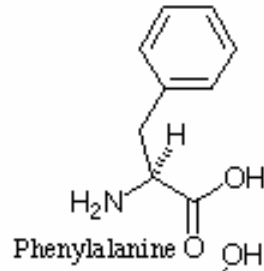
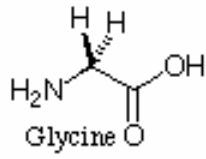
The forensic potential of the work presented in this objective was two-fold:

- (I) Based on the knowledge from the present study that each keratin fibre has a unique secondary structure, a prediction and thus classification of unknown keratin fibres can be made on the basis of their secondary structure. It is therefore proposed that a study of keratin fibres should be carried out to include a larger volume of different animals, animals within different species, and within different breeds of the same species.**

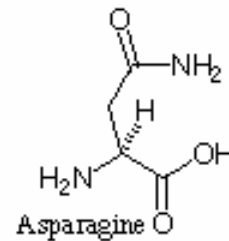
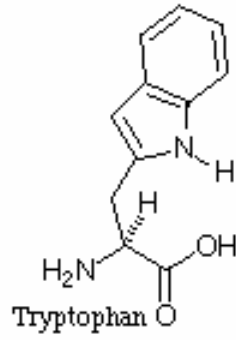
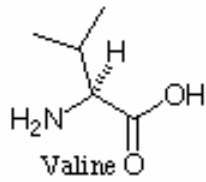
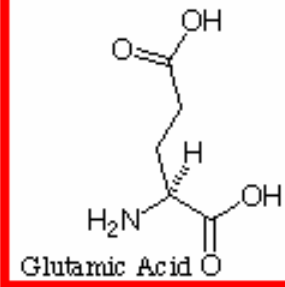
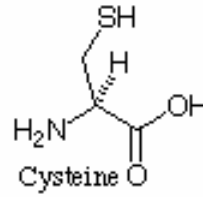
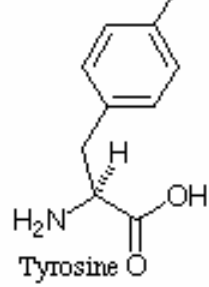
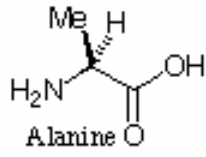
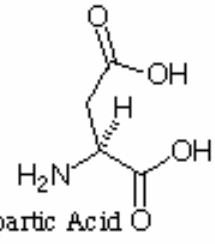
- (II) The study, although had a limited number of samples, clearly illustrated the possibility of discriminating keratin fibres and thus indicates the importance of a large database containing animal hair.**

OVERALL CONCLUSIONS FROM PhD THESIS

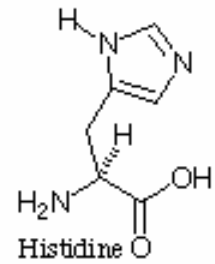
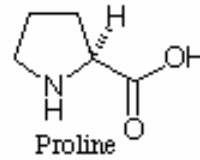
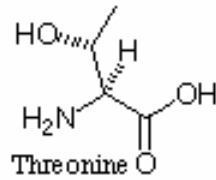
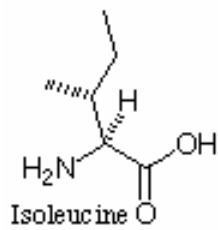
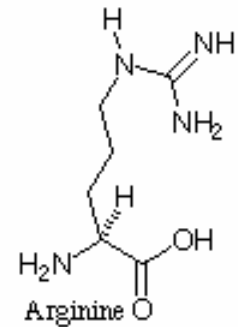
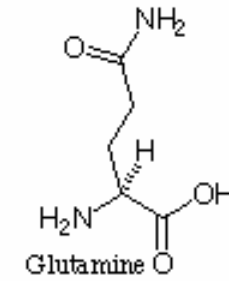
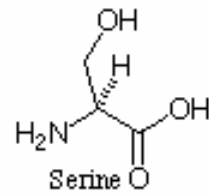
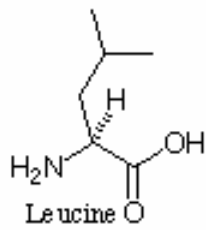
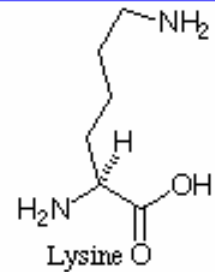
The proposed FT-IR methodology presented in this thesis has provided an alternative approach to the characterisation of single scalp human hair fibres. **The technique enables the rapid collection of spectra, followed by the objective analytical capabilities of chemometrics to successfully discriminate animal fibres, human hair fibres from different sources, treated from untreated hair fibres, as well as black and white hair fibres, on the basis of their molecular structure.** The results can be readily produced and explained in the courts of law. Although the proposed relatively fast FT-IR technique is not aimed at displacing the two slower existing methods of hair analysis, namely comparative optical microscopy and DNA analysis, it has given a new dimension to the characterisation of hair fibres at a molecular level, providing a powerful tool for forensic investigations.



Acidic



Basic



Reference Number	Gender	Race	Age	Treatment
1	Male	Caucasian	23	No
2	Female	Caucasian	32	No
3	Male	Caucasian	21	No
4	Female	Caucasian	32	No
5	Male	Caucasian	59	Yes-Dyed
6	Male	Caucasian	23	No
7	Female	Caucasian	52	Yes-Tint
8	Female	Caucasian	52	Yes-Dyed and Permed
9	Male	Caucasian	23	No
10	Male	Caucasian	24	No
11	Female	Mongoloid	26	Permed
12	Male	Caucasian	15	No
13	Female	Caucasian	14	Yes-Streaks
14	Female	Caucasian	14	No
15	Male	Caucasian	14	No
16	Male	Caucasian	15	No
17	Male	Caucasian	14	No
18	Male	Caucasian	15	No
19	Male	Caucasian	14	No
20	Male	Mongoloid	15	No
21	Female	Caucasian	14	No
22	Male	Mongoloid	15	No
23	Female	Caucasian	15	No
24	Male	Caucasian	62	No
25	Male	Caucasian	52	No
26	Male	Caucasian	37	No
27	Female	Caucasian	62	No
28	Male	Caucasian	52	No
29	Male	Caucasian	52	No
30	Male	Caucasian	45	No
31	Male	Caucasian	51	No
32	Male	Caucasian	50	No
33	Male	Caucasian	52	No
34	Male	Caucasian	48	No
35	Male	Caucasian	46	No
36	Male	Caucasian	50	No
37	Male	Caucasian	73	No
38	Female	Caucasian	23	No
39	Female	Caucasian	14	No
40	Male	Caucasian	14	No
41	Female	Caucasian	15	No
42	Female	Caucasian	14	No
43	Female	Caucasian	14	No
44	Female	Caucasian	15	No
45	Female	Caucasian	15	No
46	Female	Caucasian	15	No
47	Male	Caucasian	15	No

Reference Number	Gender	Race	Age	Treatment
48	Female	Mongoloid	32	No
49	Male	Caucasian	15	No
50	Male	Mongoloid	14	No
51	Female	Caucasian	14	No
52	Female	Caucasian/ Mongoloid	14	No
53	Female	Caucasian	15	No
54	Male	Caucasian	43	No
55	Male	Caucasian	21	No
56	Female	Caucasian	45	Yes-Dyed
57	Male	Caucasian	16	No
58	Female	Caucasian	21	Yes-Bleached and Dyed
59	Female	Caucasian	27	Yes-Bleached and Dyed
60 (a) Right hand side	Male	Caucasian	27	No
60 (b) Left hand side	Male	Caucasian	27	No
61 (a) Right hand side	Male	Caucasian	29	No
61 (b) Left hand side	Male	Caucasian	29	No
62	Female	Caucasian	28	Yes-Dyed and Permed
63	Female	Mongoloid	61	Yes-Dyed
64	Female	Mongoloid	35	No
65	Male	Mongoloid	65	No
66 (a) Right hand side	Female	Caucasian	32	Yes-Dyed
66 (b) Left hand side	Female	Caucasian	32	Yes-Dyed
67	Male	Caucasian	26	Yes-Dyed
68	Female	Caucasian	35	Yes-Dyed and Permed
69 (a) Right hand side	Female	Caucasian	32	Yes-Dyed
69 (b) Left hand side	Female	Caucasian	32	Yes-Dyed
70 (a) Right hand side	Female	Caucasian	20	Yes-Rinse
70 (b) Left hand side	Female	Caucasian	20	Yes-Rinse
71	Female	Caucasian	28	Yes-Dyed
72	Male	Caucasian	16	No
73	Female	Caucasian	38	Yes-Dyed
74	Female	Caucasian	27	No
75	Female	Caucasian	41	Yes-Bleached
76	Female	Mongoloid	45	Yes-Bleached and Dyed
77	Female	Caucasian	26	No
78	Male	Caucasian	29	No
79	Female	Mongoloid	38	No
80	Male	Mongoloid	55	No
81	Male	Caucasian	21	No
82	Female	Caucasian	29	Yes-Dyed
83 (a) Right hand side	Male	Caucasian	16	No
83 (b) Left hand side	Male	Caucasian	16	No
84 (a) Right hand side	Female	Caucasian	22	No
84 (b) Left hand side	Female	Caucasian	22	No
85 (a) Right hand side	Female	Caucasian	20	Yes-Bleached and Dyed
85 (b) Left hand side	Female	Caucasian	20	Yes-Bleached and Dyed
86	Male	Caucasian	16	No

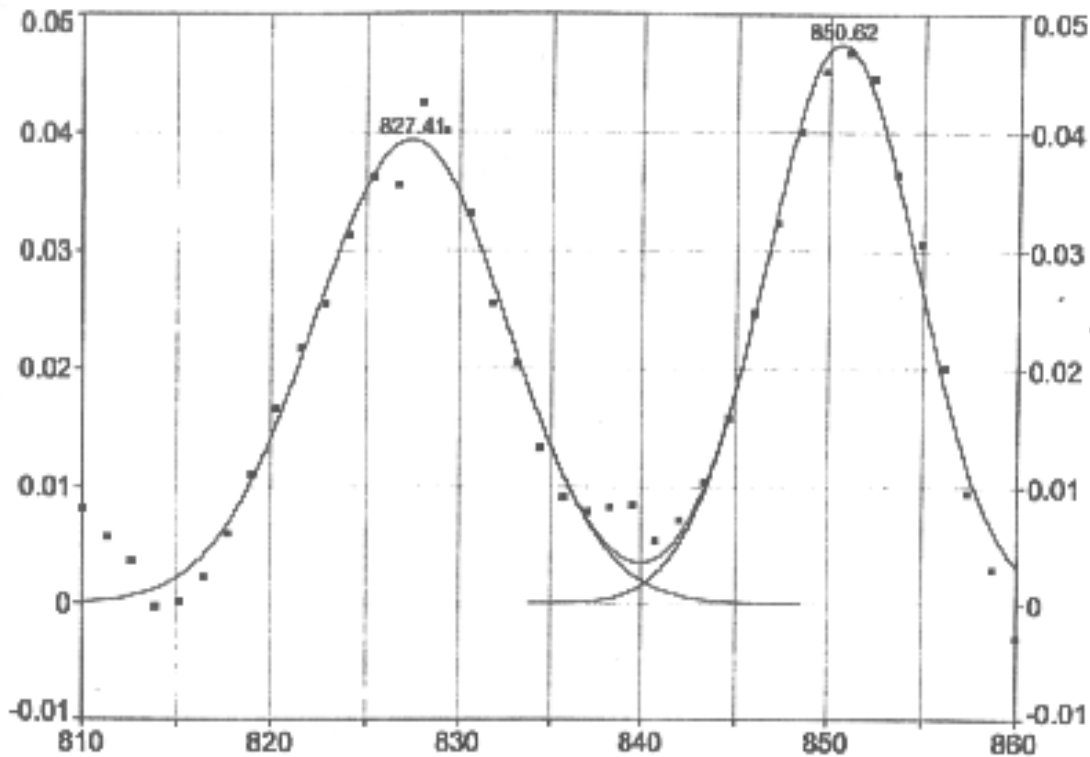
Reference Number	Gender	Race	Age	Treatment
87	Female	Samoaan	29	Yes-Dyed
88	Female	Caucasian	38	No
89	Female	Caucasian	23	Yes-Bleached
90 (a) Right hand side	Female	Caucasian	20	No
90 (b) Left hand side	Female	Caucasian	20	No
91 (a) Right hand side	Female	Caucasian	16	No
91 (b) Left hand side	Female	Caucasian	16	No
92 (a) Right hand side	Female	Caucasian	28	No
92 (b) Left hand side	Female	Caucasian	28	No
93 (a) Right hand side	Female	Caucasian	24	Yes-Bleached and Dyed
93 (b) Left hand side	Female	Caucasian	24	Yes-Bleached and Dyed
94	Female	Caucasian	42	Yes-Permed and Dyed
95	Male	Caucasian	41	No
96	Female	Caucasian	25	No
97	Female	Caucasian	24	No
98	Female	Mongoloid	25	No
99	Female	Mongoloid	22	No
100	Female	Mongoloid	34	No
101	Male	Mongoloid	25	No
102	Male	Mongoloid	32	No
103	Male	Caucasian	35	No
104	Female	Caucasian	15	No
105	Female	Caucasian	15	No
106	Female	Caucasian	15	No
107	Female	Caucasian	16	Yes-Dyed
108	Female	Caucasian	15	Yes-Dyed
109	Female	Caucasian	16	No
110	Female	Caucasian	16	No
111	Female	Caucasian	15	Yes-Dyed
112	Female	Caucasian	16	Yes-Dyed
113	Female	Caucasian	15	No
114	Female	Caucasian	15	Yes-Bleached
115	Male	Caucasian	43	No
116	Male	Caucasian	14	No
117	Female	Caucasian	14	No
118	Male	Mongoloid	15	No
119	Male	Caucasian	15	No
120	Male	Caucasian	15	No
121	Male	Caucasian	14	No
123	Female	Caucasian	15	No
124	Male	Caucasian	15	No
125	Male	Caucasian	15	No
126	Male	Caucasian	15	No
127	Male	Mongoloid	15	No
128	Female	Caucasian	14	No
129	Female	Caucasian	14	No
130	Female	Caucasian	15	No
131	Male	Caucasian	14	No

Reference Number	Gender	Race	Age	Treatment
132	Male	Caucasian	15	No
133	Female	Caucasian	15	No
134	Female	Mongoloid	15	No
135	Female	Caucasian	41	No
136	Female	Caucasian	27	No

Curve-fitting results for Raman (Tyrosine) at 15 minutes treatment time.

Pk=Gauss*Lor 2 Peaks

$r^2=0.967842$ SE=0.00291479 F=165.528



Description: C:\Users\helenp\onenote\1503c.wk1
 File Source: c:\users\helenp\onenote\1503c.wk1

Fitted Parameters

r^2	Coef Det	DF	Adj r^2	Fit Std Err	F-value
0.96784164		0.96060687		0.00201479	165.528065
Peak	Type	a_0	a_1	a_2	a_3
1	Gauss*Lor	0.03940222	827.409910	5.16323982	0.00000000
2	Gauss*Lor	0.04746533	850.618285	4.05573366	0.00000000

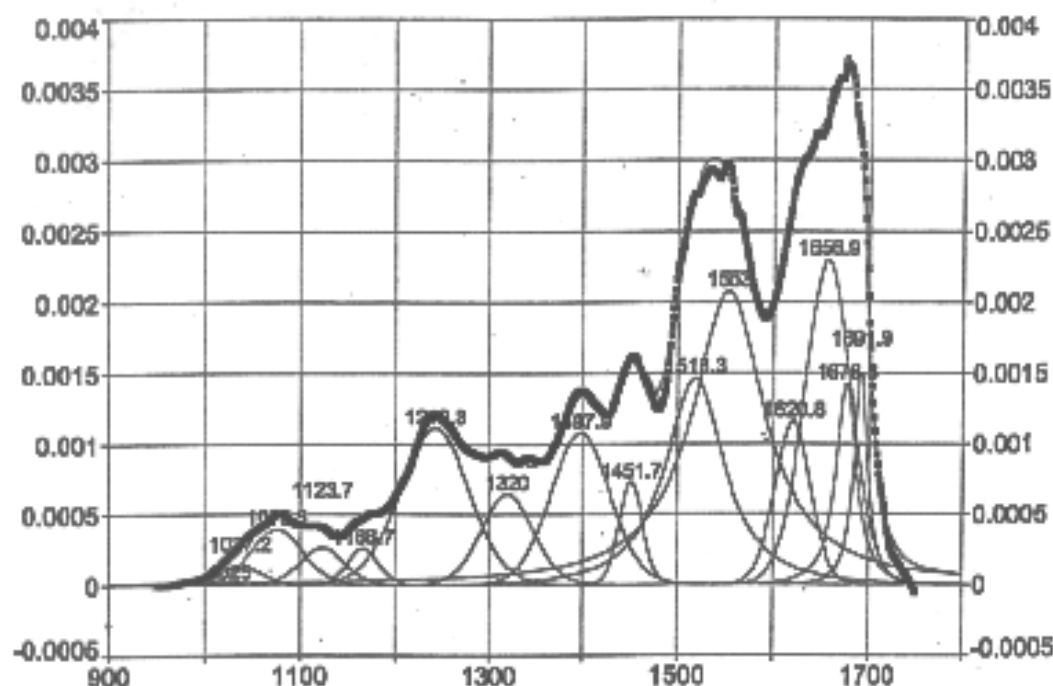
Measured Values

Peak	Type	Amplitude	Center	FWHM	Asym50	Int Area	% Area
1	Gauss*Lor	0.03940222	827.409910	12.1585002	0.99900007	0.50676374	51.8393263
2	Gauss*Lor	0.04746533	850.618285	8.65052368	1.00000000	0.47739813	48.3606737
Total						0.98716188	100.000000

Curve-fitting results for FT-IR (untreated hair fibre).

Pk=Gauss*Lor 15 Peaks

$r^2=0.997609$ SE=5.08863e-05 F=7528.62



Description: C:\Users\haleipich\24u2a\wk1
File Source: c:\users\haleipich\24u2a\wk1

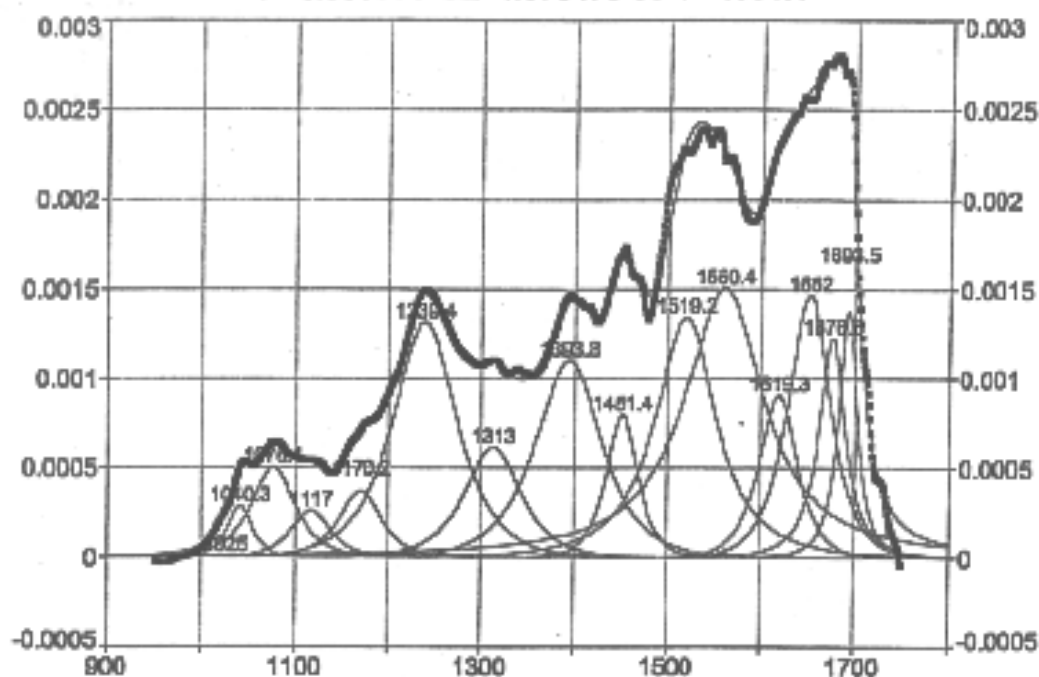
Measured Values

Peak	Type	Amplitude	Center	FWHM	Asym80	Int Area	% Area
1	Gauss*Lor	7.9072e-08	1026.00000	14.7480019	0.00000007	6.00618893	0.01683737
2	Gauss*Lor	0.00012553	1037.23888	31.7143760	1.00000001	0.00701076	0.00873488
3	Gauss*Lor	0.00039488	1076.64888	63.8258541	1.00000000	0.02713942	2.7048243
4	Gauss*Lor	0.00025829	1123.67674	54.5270095	1.00000000	0.01644888	1.63879878
5	Gauss*Lor	0.00029801	1183.73849	37.8571808	1.00000000	0.01033864	1.00004743
6	Gauss*Lor	0.00111138	1242.31350	85.5029677	1.00000000	0.10284828	10.2303815
7	Gauss*Lor	0.00064412	1319.66534	68.2880618	1.00000000	0.04642092	4.52748940
8	Gauss*Lor	0.00107818	1387.93940	73.8303828	1.00000024	0.06579168	6.54854340
9	Gauss*Lor	0.00072572	1451.67845	28.3907814	1.00000002	0.02304447	2.28678419
10	Gauss*Lor	0.00148034	1518.28258	71.9876985	1.00000000	0.13385468	13.4490338
11	Gauss*Lor	0.00078658	1593.04878	91.1140564	1.00000000	0.25883728	25.7838893
12	Gauss*Lor	0.00118203	1620.78608	43.4988889	1.00000000	0.05445913	5.42773400
13	Gauss*Lor	0.00229810	1698.87575	37.0912779	0.99988889	0.14188402	14.1211085
14	Gauss*Lor	0.00142717	1678.77507	24.8905847	1.00000008	0.04773877	4.74784177
15	Gauss*Lor	0.00149852	1621.63883	17.0859427	1.00000003	0.03480625	3.43800870
Total						1.00334625	100.000000

Curve-fitting results for FT-IR (15 minutes treatment time).

Pk=Gauss*Lor 15 Peaks

$r^2=0.996354$ SE=4.87847e-05 F=4931.4



Description: C:\Users\helen\p\ch424154a.wt1
File Source: c:\users\helen\p\ch424154a.wt1

Measured Values

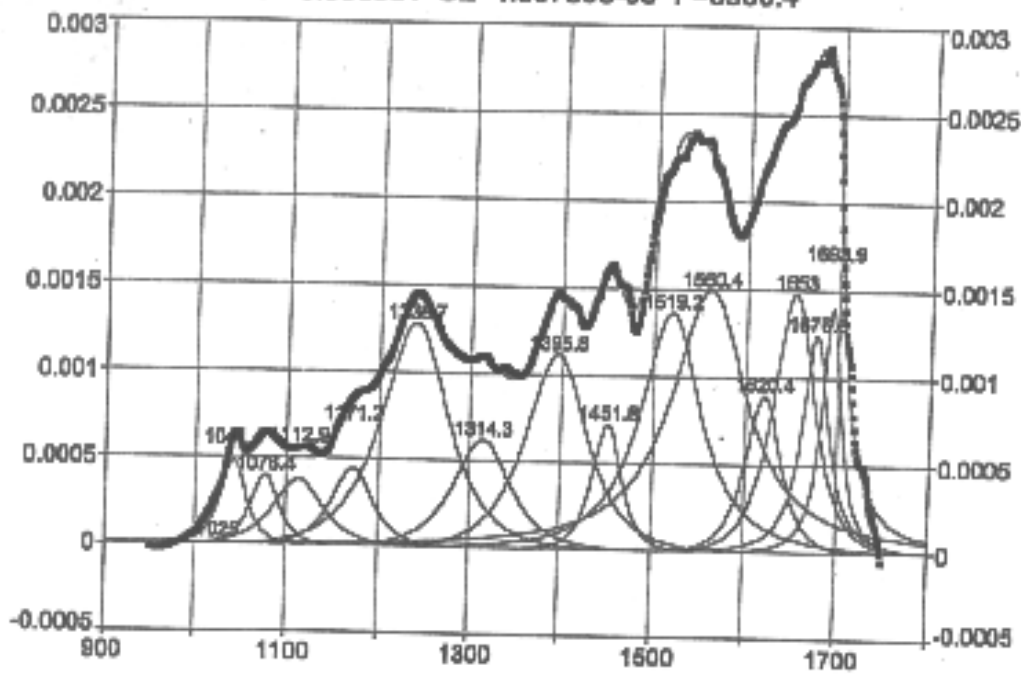
Peak	Type	Amplitude	Center	FWHM	AsymB1	Int Area	% Area
1	Gauss*Lor	7.7056e-06	1025.0000	135.099954	1.0000000	0.00117980	0.11784753
2	Gauss*Lor	0.00028479	1040.27339	31.0861819	1.0000000	0.01088989	1.08322691
3	Gauss*Lor	0.00050274	1078.00014	55.0306925	1.0000000	0.03307001	3.30897089
4	Gauss*Lor	0.00025331	1116.98381	48.5981779	1.0000000	0.01644395	1.54040733
5	Gauss*Lor	0.00037038	1170.20072	53.2759525	1.0000000	0.02379911	2.37082068
6	Gauss*Lor	0.00131571	1299.40173	80.7318362	1.0000000	0.12793031	12.7802470
7	Gauss*Lor	0.00061482	1312.98714	70.7974218	1.0000000	0.06238289	5.23486482
8	Gauss*Lor	0.00110143	1363.50002	82.7442938	1.0000000	0.10979803	10.9484733
9	Gauss*Lor	0.00079799	1481.44748	39.8345481	1.0000008	0.03807337	3.79780019
10	Gauss*Lor	0.00134410	1519.18629	75.9145623	1.0000000	0.13428488	13.3980824
11	Gauss*Lor	0.00150791	1560.36995	102.368960	1.0000000	0.21853000	21.4877885
12	Gauss*Lor	0.00090848	1519.34314	47.2171133	1.0000040	0.05187356	5.18411336
13	Gauss*Lor	0.00146724	1662.01895	82.8544893	0.9999992	0.06298894	6.27305963
14	Gauss*Lor	0.00122918	1675.57307	33.8932054	1.0000000	0.05339001	5.32831919
15	Gauss*Lor	0.00137710	1803.48383	22.7408293	0.9999991	0.04183362	4.17287100
Total						1.00296026	100.000000

This graph is not available online. Please consult the hardcopy thesis available from the QUT library

Curve-fitting results for FT-IR (2 hours treatment time).

Pk=Gauss*Lor 15 Peaks

$r^2=0.996981$ SE=4.30736e-05 F=5960.4



Description: C:\User\halep\ch42628a.wk1
File Source: c:\user\halep\ch42628a.wk1

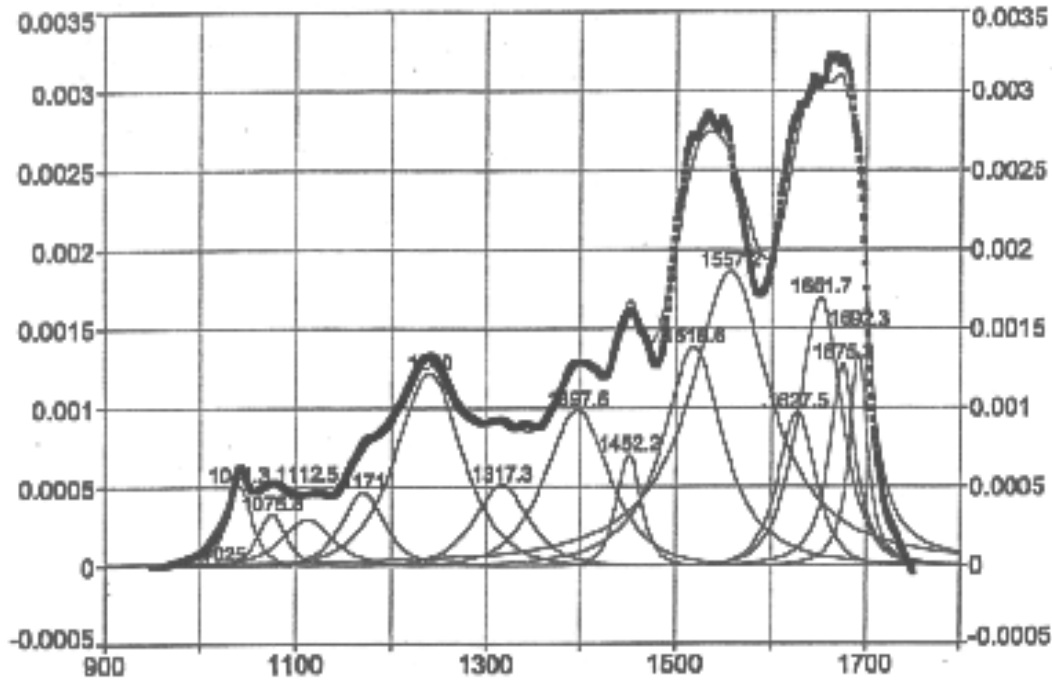
Measured Values

Peak	Type	Amplitude	Center	FWHM	Asym50	Int Area	% Area
1	Gauss*Lor	1.5329e-05	1025.00000	36.8937132	1.00000000	0.00073370	0.07344198
2	Gauss*Lor	0.00045497	1041.44715	33.2259851	1.00000000	0.01932714	1.93639823
3	Gauss*Lor	0.00036478	1076.41997	38.2103804	1.00000001	0.01732591	1.72952910
4	Gauss*Lor	0.00037475	1112.89043	52.4494298	1.00000000	0.02605593	2.60164818
5	Gauss*Lor	0.00044078	1171.19451	32.5559044	0.99999998	0.02790264	2.77268272
6	Gauss*Lor	0.00128130	1238.74530	45.5966948	1.00000000	0.13167738	13.1346615
7	Gauss*Lor	0.00083007	1314.33743	73.5260019	1.00000000	0.06488938	6.48987013
8	Gauss*Lor	0.00111752	1366.79957	74.4738450	1.00000000	0.10874274	10.8559478
9	Gauss*Lor	0.00372100	1401.79142	36.4485482	1.00000076	0.03189818	3.19132632
10	Gauss*Lor	0.00136448	1519.18439	79.7700139	1.00000000	0.13786160	13.7998209
11	Gauss*Lor	0.00149038	1590.36826	97.4710810	1.00000000	0.20466367	20.4882654
12	Gauss*Lor	0.00089792	1620.39131	44.5323381	1.00000000	0.04798080	4.79882686
13	Gauss*Lor	0.00168393	1652.96179	52.1498832	0.99999997	0.08244790	8.22943000
14	Gauss*Lor	0.00124746	1676.64013	33.5378965	1.00000000	0.05663429	5.65362790
15	Gauss*Lor	0.00140094	1693.89485	24.7039482	1.00000094	0.04806483	4.80837291
Total						1.00179498	100.000000

Curve-fitting results for FT-IR (5 hours treatment time).

Pk=Gauss+Lor 15 Peaks

$r^2=0.988366$ SE=0.000100901 F=1459.68



Description: C:\Users\helenpich\2463aa.wk1
 File Source: c:\users\helenpich\2463aa.wk1

Measured Values

Peak	Type	Amplitude	Center	FWHM	Asym%	Int Area	% Area
1	Gauss+Lor	4.7479e-06	1025.00000	36.5448776	1.0000000	0.00005790	0.0396894
2	Gauss+Lor	0.00000783	1041.28488	31.7141963	1.0000000	0.01900468	1.8878821
3	Gauss+Lor	0.00032782	1075.81884	34.0728252	1.0000002	0.01318808	1.30673010
4	Gauss+Lor	0.00029878	1112.81914	62.5848722	1.0000000	0.02184860	2.17627987
5	Gauss+Lor	0.00046491	1171.02227	52.2095349	0.9999997	0.02665488	2.84625342
6	Gauss+Lor	0.00121838	1240.09680	81.8006825	1.0000000	0.11743309	11.8844228
7	Gauss+Lor	0.00001239	1317.27494	67.8833336	1.0000000	0.04198139	4.09054014
8	Gauss+Lor	0.00088403	1387.61867	80.0644891	1.0000000	0.09290789	9.23731388
9	Gauss+Lor	0.00099982	1452.29121	39.8316082	1.0000000	0.02447009	2.43067909
10	Gauss+Lor	0.00138043	1518.59547	73.4679802	1.0000000	0.13353410	13.2837915
11	Gauss+Lor	0.00186184	1557.19631	100.522553	1.0000000	0.28238411	28.0631924
12	Gauss+Lor	0.00098704	1627.48822	48.7428218	1.0000000	0.05221452	5.18838884
13	Gauss+Lor	0.00169515	1651.68196	52.5348418	0.99999984	0.10482870	10.4131914
14	Gauss+Lor	0.00127880	1676.27814	32.0886132	1.0000000	0.05453732	5.41716552
15	Gauss+Lor	0.00139094	1692.28285	32.4802482	0.99999997	0.04029023	4.00194489
	Total					1.00878121	100.000000